

# **Formation of *N*-nitrosodimethylamine during water disinfection with chloramine: Insights into reaction mechanisms from isotope fractionation analyses**

THÈSE N° 7196 (2016)

PRÉSENTÉE LE 14 OCTOBRE 2016

À LA FACULTÉ DE L'ENVIRONNEMENT NATUREL, ARCHITECTURAL ET CONSTRUIT  
LABORATOIRE POUR LE TRAITEMENT ET LA QUALITÉ DE L'EAU  
PROGRAMME DOCTORAL EN GÉNIE CIVIL ET ENVIRONNEMENT

ÉCOLE POLYTECHNIQUE FÉDÉRALE DE LAUSANNE

POUR L'OBTENTION DU GRADE DE DOCTEUR ÈS SCIENCES

PAR

**Stephanie SPAHR**

acceptée sur proposition du jury:

Prof. A. J. Wüest, président du jury  
Prof. U. von Gunten, Dr T. Hofstetter, directeurs de thèse  
Prof. H. Gallard, rapporteur  
Prof. T. Schmidt, rapporteur  
Prof. S. Takahama, rapporteur



ÉCOLE POLYTECHNIQUE  
FÉDÉRALE DE LAUSANNE

Suisse  
2016



# Dank

Als Erstes möchte ich mich ganz herzlich bei Thomas Hofstetter und Urs von Gunten für die tolle Betreuung meiner Dissertation bedanken. Danke, dass ihr mir die Möglichkeit geschenkt habt an der Eawag zu doktorieren, in die Trinkwasser- und Isotopenchemie einzutauchen und an verschiedensten Konferenzen teilzunehmen. Ich habe in den letzten vier Jahren unheimlich viel von euch gelernt und danke euch für das Vertrauen, die Unterstützung und die zahlreichen Diskussionen aus denen immer neue, kreative Ideen für Experimente und Manuskripte hervorgingen. Thomas danke ich ganz besonders dafür, dass mir seine Tür immer offen stand und ich alle Angelegenheiten offen mit ihm diskutieren konnte. Durch seine enthusiastische Art hat er mich nicht nur sehr für die Isotopenchemie und englischsprachige Podcasts begeistert, sondern mich auf allen Ebenen der Wissenschaft und des Lebens gecoacht. Urs hat mit seinem enormen Wissensschatz erheblich zur Qualität dieser Arbeit beigetragen und mich nebenbei mit Artikeln aus der NZZ über das Verhältnis zwischen den Schweizern und den Deutschen zum Schmunzeln gebracht. Thomas, Urs, d Ziit mit eu isch genial gsi!

I would like to thank Alfred J. Wüest, Satoshi Takahama, Hervé Gallard, and Torsten Schmidt for coming to Dübendorf, being part of my exam committee, and having a great discussion about my work.

Olaf Cirpka danke ich für die Diskussionen über meine Arbeit, sei es via skype oder in Person, die Modellierung (Schweizerdeutsch: Modelliärig) meiner Daten und die Kommentare zu den Manuskripten. Olaf hat zu jeder Zeit die richtigen Fragen gestellt und mich animiert meine Daten von anderen Blickwinkeln aus zu betrachten, was sehr erfrischend war und mir bei der Interpretation meiner Ergebnisse geholfen hat. Zudem danke ich ihm und Stefan Haderlein für die Einladung nach Tübingen ins GeoEnviron Seminar!

Des Weiteren möchte ich mich bei all denjenigen bedanken, die mich im Labor unterstützt haben. Allen voran danke ich Jakov Bolotin, der es wie kein anderer schafft analytische Probleme anzugehen und im Nu zu lösen. Rebekka Gulde danke ich für ihre Hilfe

bei den LC-HR-MS/MS Messungen, Fabian Soltermann für die Einführung ins MIMS und den Support, sogar von zu Hause aus! Zudem möchte ich mich bei Birgit Beck, Philipp Longrée, Andreas Maccagnan und Lisa Sahli bedanken für die kleinen, aber doch so wichtigen Hilfestellungen im Labor. Jürgen Schleucher und Ina Ehlers danke ich für NMR Messungen. Mein Dank gilt auch meinen Masterstudentinnen Carolin Öhl und Christine Egli. Christine hat mich mit ihrem Engagement, Interesse und sonnigen Gemüt beeindruckt und ich hatte sehr viel Spaß so intensiv mit ihr zusammenzuarbeiten.

Den aktuellen und ehemaligen Doktoranden und Postdocs der Thomas-Gruppe (Sarah Pati, Reto Wijker, Marita Skarpeli-Liati, Marco Ratti, Iris Schilling, Rani Bakkour, Ashley Brown) sowie der Urs-Gruppe (Frank Leresche, Sung Eun Lim, Fabian Soltermann, Michèle Heeb, Minju Lee, Peter Tentscher, Tony Merle, Marc Bourgin, Linda Oennby, Amisha Shah) danke ich für die motivierende und unterstützende Gruppenatmosphäre, spannende Diskussionen, Feedback für Konferenzvorträge und tolle Ausflüge. Besonders danken möchte ich Michèle Heeb für die zahlreichen Telefonate und Gespräche! Sie hatte durchweg die richtige Antwort auf Fragen bezüglich der EPFL-Administration und immer ein offenes Ohr für Neuigkeiten aus der Welt des NDMA Bildungsmechanismus. Besonderer Dank gebührt auch Sarah Pati. Sie war das perfekte "Labor-Gspänli" und von ihr habe ich nicht nur viel über Sauerstoff- und Isotopenchemie gelernt, sondern sie war in jeder Lebenslage die perfekte Gesprächspartnerin. Jennifer Schollée und Emma Schymanski danke ich für die Beantwortung meiner unzähligen Fragen zur englischen Grammatik und Rechtschreibung.

Ebenfalls bedanken möchte ich mich bei Juliane Hollender. Sie hat mir schon im Jahr 2011 die Chance gegeben meine Masterarbeit in Uchem zu machen (großes Dankeschön auch an Sebastian Huntscha) und mir dadurch ermöglicht an die Eawag zu kommen. Und natürlich geht ein riesiges DANKE an ganz Uchem! Die zahlreichen Aperos, Gruppenausflüge und Partys haben meine Zeit an der Eawag unvergesslich werden lassen.

Lenny Winkel danke ich für unsere Gespräche über die Wissenschaft und das Leben. Mit ihrer außergewöhnlich motivierenden und positiven Art hat sie mich darin bestärkt meinen Weg zu gehen. Johanna Otto und Judith Rothardt danke ich für viele leckere gemeinsame Abende und Känguru-mäßig viel Spaß auf dem T-bow Brett - auf dass der "Buuuch nüm usse blobbt"!

Special thanks to all book club ladies, namely Aurea Chiaia, Jennifer Schollée, Eva Manova, Barbara Stötzer, Luba Kovalova, and Louise Camenzuli. My world broadened so much through being exposed to all the different types of literature and our discussions - not only about books, but all aspects of life.

Hannah Waitzinger, Marietta Lindenmaier, Kathrin Folger, Isabelle Kessler, Madlen Nrecaj und Eva Fella danke ich von Herzen für unsere einzigartige, langjährige Freundschaft. Auch wenn wir meist an verschiedenen Orten auf der Welt leben und oft nicht mal auf demselben Kontinent sind - wir sind immer im Herzen vereint. Der Erinnerungsschatz, den ich mit euch habe, ist durch nichts in der Welt zu ersetzen. Wie könnte ich nur ohne unsere zahlreichen, von Freude erfüllten Erlebnisse, die ich alle tief im Herzen trage, ein so glücklicher Mensch sein.

Nicht genug danken kann ich Kaspar Rohrer, der gleich zu Beginn meiner Dissertation in mein Leben trat und seitdem alle Höhen und Tiefen mit mir gemeinsam durchlebt. Kaspar hat die letzten 4 Jahre zu etwas ganz Besonderem werden lassen, indem er mir die schönsten Seiten der Schweiz von Nidwalden bis Basel gezeigt hat, mir geduldig Schwiizerdütsch beibringt, meine Leidenschaft für Spiele und das Reisen teilt und mir mit seiner Liebe wie ein Fels in der Brandung ist. Ich hoffe, dass wir noch viele gemeinsame Abenteuer erleben werden - bis zur Unendlichkeit und noch viel weiter!

Zu guter Letzt möchte ich den wichtigsten Personen in meinem Leben, meiner Familie Peter, Marianne und Timo Spahr danken. Danke, dass ihr immer für mich da seid und mich mit so großer Liebe beschenkt, auch wenn wir räumlich oft voneinander getrennt sind. Ihr habt mir nicht nur diese tolle Ausbildung ermöglicht, sondern mir die Freiheit gegeben das Leben nach meinen eigenen Vorstellungen und Wünschen zu gestalten. Zu wissen, dass ihr immer hinter mir steht und mich bei allem unterstützt, ist unendlich kostbar und es gibt mir die Kraft und das Vertrauen auch weiterhin spannende Themenfelder zu erforschen, Abenteuer zu erleben und meine Träume zu erfüllen.



# Table of contents

<b>Summary</b>	<b>ix</b>
<b>Zusammenfassung</b>	<b>xi</b>
<b>1 Introduction</b>	<b>1</b>
1.1 Drinking water disinfection by-products (DBPs) . . . . .	2
1.2 <i>N</i> -Nitrosodimethylamine in drinking water . . . . .	3
1.2.1 Toxicity, occurrence, and mitigation . . . . .	3
1.2.2 NDMA precursors and proposed formation pathways . . . . .	4
1.3 Assessing NDMA formation with compound - specific isotope analysis . .	7
1.3.1 Stable isotope analysis - fundamentals and application . . . . .	7
1.3.2 CSIA to assess DBP formation . . . . .	9
1.4 Objectives and approach . . . . .	10
<b>2 Compound-Specific Carbon, Nitrogen, and Hydrogen Isotope Analysis of <i>N</i>-Nitrosodimethylamine in Aqueous Solutions</b>	<b>13</b>
Abstract . . . . .	14
2.1 Introduction . . . . .	15
2.2 Experimental Section . . . . .	17
2.2.1 Safety considerations . . . . .	17
2.2.2 Solid-phase extraction (SPE) . . . . .	17
2.2.3 Chemical analysis . . . . .	18
2.2.4 Stable isotope analysis . . . . .	19
2.2.5 NDMA formation experiments . . . . .	21
2.3 Results and Discussion . . . . .	22
2.3.1 C, N, and H isotope analysis of <i>N</i> -nitrosamines . . . . .	22
2.3.2 C, N, and H isotope analysis of <i>N</i> -nitrosamines after solid-phase extraction (SPE) from aqueous samples . . . . .	28
2.3.3 Tracking NDMA isotope signatures during water chloramination .	28
2.4 Conclusion . . . . .	31

<b>Supporting Information to Chapter 2</b>	<b>33</b>
S2.1 Chemicals . . . . .	34
S2.2 GC/IRMS chromatogram of <i>N</i> -nitrosamines . . . . .	35
S2.3 Reproducibility of C, N, and H isotope analysis of <i>N</i> -nitrosamines . . . . .	36
S2.4 Conversion efficiency of <i>N</i> -nitrosamines to analyte gases for IRMS analysis	37
S2.5 Method quantification limits for accurate isotope analysis of <i>N</i> -nitrosamines	38
S2.6 C, N, and H isotope analysis of <i>N</i> -nitrosamines after solid-phase extrac- tion (SPE) from aqueous samples . . . . .	39
S2.7 NDMA formation during chloramination of ranitidine . . . . .	40
 <b>3 Formation of <i>N</i>-Nitrosodimethylamine during Chloramination of Sec- ondary and Tertiary Amines: Role of Molecular Oxygen and Radical Intermediates</b>	 <b>41</b>
Abstract . . . . .	42
3.1 Introduction . . . . .	43
3.2 Experimental Section . . . . .	45
3.2.1 Chemicals . . . . .	45
3.2.2 Chloramination experiments . . . . .	45
3.2.3 Oxygen isotope fractionation experiments . . . . .	46
3.2.4 Chemical analyses . . . . .	47
3.2.5 Stable oxygen isotope analysis . . . . .	48
3.3 Results and Discussion . . . . .	49
3.3.1 Chloramination of amines: Kinetics, reaction products, and stoi- chiometry of $\text{NH}_2\text{Cl}$ and $\text{O}_2$ consumption . . . . .	49
3.3.2 Oxygen isotope fractionation during the reaction of aqueous $\text{O}_2$ .	55
3.3.3 Impact of radical scavengers on NDMA formation . . . . .	57
3.3.4 Potential NDMA formation mechanisms involving radical inter- mediates . . . . .	58
3.4 Implications for water treatment . . . . .	61
 <b>Supporting Information to Chapter 3</b>	 <b>63</b>
S3.1 Safety considerations . . . . .	64
S3.2 Chemicals . . . . .	64
S3.3 Quantification of ranitidine, DFUR, and NDMA . . . . .	65
S3.4 Transformation product identification . . . . .	65
S3.5 Quantification of $\text{NH}_2\text{Cl}$ . . . . .	66
S3.5.1 Membrane introduction mass spectrometry (MIMS) . . . . .	66
S3.5.2 Colorimetric methods . . . . .	68
S3.5.3 Comparison of different $\text{NH}_2\text{Cl}$ quantification methods . . . . .	69
S3.6 Aqueous vs. methanolic DFUR spike solution . . . . .	71



S3.7	Reactivity of DFUR with chloramine quenchers: Sulfite vs. thiosulfate . . . . .	72
S3.8	Impact of the tertiary amine to chloramine ratio on NDMA formation . . . . .	73
S3.9	Chloramination of secondary and tertiary amines . . . . .	74
S3.9.1	Reaction kinetics and stoichiometry of $\text{NH}_2\text{Cl}$ and $\text{O}_2$ consumption . . . . .	74
S3.9.2	Transformation products . . . . .	81
S3.10	Chloramination of furfuryl alcohol . . . . .	84
S3.11	Oxygen isotope analyses of aqueous $\text{O}_2$ . . . . .	85
S3.12	Experiments with radical scavengers . . . . .	87
S3.12.1	<i>tert</i> -Butanol . . . . .	87
S3.12.2	ABTS . . . . .	88
S3.12.3	Trolox . . . . .	89
S3.13	Quantification of $\text{H}_2\text{O}_2$ through transformation to $\text{O}_2$ by catalase . . . . .	91
<b>4</b>	<b>Stable Isotope Fractionation Trends in <i>N</i>-Nitrosodimethylamine as Proxy for Its Formation Pathway During Chloramination of Tertiary Amines</b>	<b>93</b>
Abstract	. . . . .	94
4.1	Introduction . . . . .	95
4.2	Experimental Section . . . . .	98
4.2.1	Chemicals . . . . .	98
4.2.2	NDMA formation experiments . . . . .	98
4.2.3	Chemical analyses . . . . .	99
4.2.4	Stable isotope analyses . . . . .	99
4.2.5	Data evaluation . . . . .	100
4.3	Results and Discussion . . . . .	102
4.3.1	Observable C, H, and N isotope fractionation trends in NDMA . . . . .	102
4.3.2	Isotope ratios of NDMA reveal the origin of C, H, and N atoms in NDMA . . . . .	104
4.3.3	Isotope fractionation trends in tertiary amines and NDMA reflect the multistep NDMA formation pathway . . . . .	105
4.3.4	Isotope fractionation trends in NDMA as proxy for its formation pathway and precursors . . . . .	109
4.4	Implications for CSIA as a tool to identify NDMA precursors . . . . .	113
	<b>Supporting Information to Chapter 4</b>	<b>115</b>
S4.1	Safety considerations . . . . .	116
S4.2	Chemicals . . . . .	116
S4.3	Stable isotope analysis . . . . .	117
S4.3.1	Reference isotope signatures . . . . .	117

S4.3.2	Method quantification limits (MQLs) for C and N isotope analysis of DMTA . . . . .	117
S4.4	Isotope fractionation in tertiary amines during chloramination . . . . .	118
S4.4.1	Isotope fractionation in DMTA and DMBA . . . . .	118
S4.4.2	Bulk isotope enrichment factors . . . . .	119
S4.4.3	$^{15}\text{N}$ equilibrium isotope effect associated with the deprotonation of DMTA . . . . .	119
S4.4.4	Isotope enrichment factors and kinetic isotope effects associated with the reaction of DMTA and DMBA . . . . .	120
S4.5	C, H, and N isotope ratios of NDMA during chloramination of four tertiary amines . . . . .	120
S4.6	Impact of buffer concentration and type on NDMA formation kinetics and N isotope fractionation . . . . .	122
S4.6.1	Phosphate buffer concentration . . . . .	122
S4.6.2	Buffer type . . . . .	123
S4.6.3	Impact of buffer concentration and buffer type on N isotope fractionation in NDMA . . . . .	124
S4.7	Chloramination of 2-thiophenemethanol . . . . .	125
S4.8	pH-dependence of NDMA formation . . . . .	126
S4.9	N isotope signatures versus NDMA yield . . . . .	129
<b>5</b>	<b>Conclusions and Outlook</b>	<b>131</b>
5.1	CSIA for investigating NDMA formation pathways . . . . .	132
5.2	Potential variability of isotope fractionation trends in NDMA . . . . .	133
5.3	Isotope fractionation trends as fingerprints for NDMA formation pathways and precursors . . . . .	134
5.4	Roadmap for the application of CSIA to identify NDMA precursors in natural waters . . . . .	136
	<b>Bibliography</b>	<b>139</b>
	<b>Curriculum Vitae</b>	<b>161</b>

# Summary

Disinfection processes such as chlorination, chloramination, and ozonation are a crucial measure to provide safe drinking water because they effectively inactivate pathogenic microorganisms. However, these processes can also lead to the formation of harmful disinfection by-products (DBPs) such as the carcinogen *N*-nitrosodimethylamine (NDMA). NDMA is primarily formed during chloramination of wastewater and wastewater-impacted surface waters, where natural organic materials and anthropogenic pollutants serve as NDMA precursors. A better understanding of NDMA precursors and various formation pathways is vital for developing appropriate mitigation strategies. Compound-specific isotope analysis (CSIA) can be used to both allocate sources of organic contaminants in the environment and elucidate their (trans)formation pathways. The goal of this dissertation was to explore the use of CSIA for assessing NDMA formation mechanisms and identifying reactive precursor moieties from stable isotope fractionation trends.

In laboratory model systems, NDMA formation was studied during chloramination of secondary and tertiary amines, which are relevant precursor compounds in natural waters. Reaction kinetics and stoichiometries were determined to elucidate poorly characterized reaction steps of the NDMA formation pathway involving chloramine, molecular oxygen, and intermediate species. Although molar NDMA yields from the selected precursors differed significantly (1%-90%), one O<sub>2</sub> molecule was consumed per N(CH<sub>3</sub>)<sub>2</sub> moiety of the precursor. This observation indicates that the reaction of O<sub>2</sub> with secondary and tertiary amines proceeded via the same mechanism, but did not control the molar NDMA yield. NDMA formation coincided with the disappearance of the precursor, demonstrating that (oxygen) intermediates were highly reactive and short-lived. Changes of <sup>18</sup>O/<sup>16</sup>O isotope ratios in aqueous O<sub>2</sub> revealed that oxygen reacted with radical species, which was confirmed by additional experiments with radical scavengers (*tert*-butanol, ABTS, and trolox). Based on these results, a NDMA formation mechanism was proposed involving N-centered aminyl radicals.

To investigate whether changes of the natural isotopic composition of NDMA can provide additional insights into the NDMA formation mechanism, an analytical method for the accurate determination of C, H, and N isotope ratios of NDMA was developed using solid-phase extraction coupled to gas chromatography isotope ratio mass spectrometry (SPE-GC/IRMS). During chloramination of tertiary amines, C and H isotope ratios of NDMA remained widely unaltered. Along with quantitative deuterium nuclear magnetic resonance spectroscopy, this result demonstrated that the  $\text{N}(\text{CH}_3)_2$  moiety of NDMA originated from the tertiary amine precursor. In contrast, the N atom of the nitroso group of NDMA stemmed from  $\text{NH}_2\text{Cl}$  as inferred from experiments with  $^{15}\text{N}$ -enriched  $\text{NH}_2\text{Cl}$ . N isotope ratios of NDMA increased significantly during its formation meaning that  $^{14}\text{N}$  reacted preferentially to NDMA. Several steps of the reaction sequence leading to NDMA can be responsible for this observable N isotope fractionation. Trends in correlated C and N isotope ratios of NDMA were nevertheless characteristic for chloramination of four tertiary amines and might serve as probes for this class of precursors. This important proof-of-concept work is a first step towards applying CSIA to reveal relevant NDMA precursors in water treatment processes.

**Keywords:** water disinfection, chloramination, disinfection by-products, *N*-nitrosodimethylamine (NDMA), compound-specific isotope analysis (CSIA), stable isotope fractionation

# Zusammenfassung

Die Desinfektion von Trinkwasser mit beispielsweise Chlor, Chloramin, oder Ozon ist einer der wichtigsten Schritte der Trinkwasseraufbereitung, da pathogene Mikroorganismen abgetötet werden und die Bevölkerung mit sauberem Trinkwasser versorgt werden kann. Jedoch führt der Einsatz chemischer Desinfektionsmittel häufig zur Bildung potentiell gesundheitsschädlicher Desinfektionsnebenprodukte. Eines dieser zahlreichen Nebenprodukte ist *N*-Nitrosodimethylamin (NDMA), welches als krebs-erregend eingestuft wird. Einer der Hauptwege zur Bildung von NDMA ist die Reaktion von Chloramin mit natürlichem organischen Material oder mit Mikroverunreinigungen, die vor allem durch gereinigtes kommunales Abwasser in natürliche Gewässer gelangen. Um die Bildung von NDMA im Trinkwasser zu vermeiden, wird ein umfassendes Verständnis der NDMA Bildungswege benötigt. Hierbei ist es von essentieller Bedeutung diejenigen Vorläufersubstanzen zu identifizieren, die für die NDMA Bildung während der Trinkwasseraufbereitung verantwortlich sind. Substanzspezifische Isotopenanalyse (engl. compound-specific isotope analysis, CSIA) ist ein etabliertes Verfahren der Umweltanalytik, mit dem sowohl Schadstoffquellen identifiziert, als auch abiotische und biotische Abbauwege von Schadstoffen charakterisiert und in der Umwelt nachgewiesen werden können. Da CSIA bisher nur selten im Trinkwasserbereich angewendet wurde, war es das Ziel dieser Dissertation zu evaluieren, ob CSIA (a) neue Einblicke in NDMA Bildungswege eröffnet und (b) die Identifikation wichtiger Vorläufersubstanzen ermöglicht.

Nach heutigem Wissensstand fungieren vor allem aminhaltige Substanzen, die oftmals in natürlichen Gewässern auftreten, als bedeutende NDMA Vorläufer während der Chloraminierung. Jedoch sind die Reaktionsmechanismen noch wenig verstanden. Um bisher unbekannte Reaktionsschritte, die vor allem Chloramin und gelösten Sauerstoff betreffen, besser zu charakterisieren, wurden sekundäre und tertiäre Amine in Laborexperimenten mit Chloramin versetzt, um die resultierende NDMA Bildung sowie Reaktionskinetiken und Reaktionsstöchiometrien zu bestimmen. Obwohl die unter-

suchten Substanzen zu verschiedenen molaren NDMA Ausbeuten führten (1% - 90%), wurde das Verschwinden eines Sauerstoffmoleküls pro  $\text{N}(\text{CH}_3)_2$ -Gruppe der Vorläufersubstanz beobachtet. Dieses Ergebnis deutet darauf hin, dass molekularer Sauerstoff auf dieselbe Weise mit sekundären und tertiären Aminen reagierte, diese Reaktion jedoch nicht bestimmend für die molare NDMA Ausbeute war. Die Bildung von NDMA fand zeitgleich mit dem Verschwinden der Vorläufersubstanz statt, was zeigt, dass Reaktionszwischenprodukte sehr reaktiv und kurzlebig waren. Änderungen im  $^{18}\text{O}/^{16}\text{O}$  Isotopenverhältnis von gelöstem  $\text{O}_2$  wiesen auf eine Reaktion von Sauerstoff mit Radikalen hin, was in Experimenten mit Radikalfängern (*tert*-Butanol, ABTS, und Trolox) bestätigt wurde. Basierend auf diesen Ergebnissen wurde ein Reaktionsmechanismus für die NDMA Bildung vorgeschlagen, in dem N-zentrierte Aminyl Radikale eine bedeutende Rolle spielen.

Um zu untersuchen, ob Änderungen in der natürlichen Isotopenzusammensetzung von NDMA zusätzliche Einblicke in den Reaktionsmechanismus ermöglichen, wurde eine analytische Methode entwickelt, mit der mittels Festphasenextraktion gekoppelt an Gaschromatographie und Isotopenverhältnismassenspektrometrie (SPE-GC/IRMS) eine präzise und genaue Bestimmung der C, H, und N Isotopenverhältnisse von NDMA realisiert wurde. Während der Reaktion von Chloramin mit tertiären Aminen blieben C und H Isotopenverhältnisse im gebildeten NDMA weitgehend konstant. Gemeinsam mit Deuterium-Kernspinresonanzspektroskopie zeigte dieses Ergebnis, dass die  $\text{N}(\text{CH}_3)_2$ -Gruppe in NDMA aus dem tertiären Amin stammt. Hingegen hat das N-Atom der Nitroso-Gruppe seinen Ursprung in Chloramin. Während der NDMA Bildung wurde eine signifikante Anreicherung von  $^{15}\text{N}$  Isotopen im NDMA beobachtet. Mehrere Reaktionsschritte des NDMA Bildungsmechanismus können für diese N Isotopenfraktionierung verantwortlich sein. Dennoch lieferte die Korrelation von C und N Isotopenverhältnissen in NDMA charakteristische Trends für die Reaktion von Chloramin mit vier ausgewählten tertiären Aminen. Diese Isotopenfraktionierungstrends könnten dazu dienen bestimmte Vorläufersubstanzen oder funktionelle Gruppen in Gewässern zu identifizieren. Durch die vorgestellte Arbeit wird aufgezeigt, dass CSIA neue Wege eröffnen kann, um essentielle Informationen über NDMA Bildungswege und Vorläufersubstanzen zu gewinnen.

**Schlagwörter:** Wasserdeshinfektion, Chloraminierung, Desinfektionsnebenprodukte, N-Nitrosodimethylamin (NDMA), substanzspezifische Isotopenanalyse (CSIA), Isotopenfraktionierung

# Chapter 1

## Introduction

## 1.1 Drinking water disinfection by-products (DBPs)

The disinfection of drinking water and the ensuing reduction of waterborne disease outbreaks is one of the greatest public health achievements of the twentieth century.<sup>1</sup> Chemical disinfectants are routinely used to inactivate environmental and enteric pathogens in drinking water, but also serve as oxidants to remove color, taste and odor compounds as well as micropollutants and to control microbial regrowth in water distribution systems.<sup>2</sup> However, chemical oxidation/disinfection is associated with unintentional health hazards through the formation of potentially toxic oxidation/disinfection by-products (DBPs).<sup>3–5</sup>

DBPs are formed when oxidants such as chlorine, chloramines, ozone, or chlorine dioxide react with natural organic matter, bromide, iodide, or anthropogenic contaminants.<sup>3,4,6</sup> Since the discovery of trihalomethanes (THMs; e.g., chloroform, bromoform) in chlorinated drinking water in the mid-1970s,<sup>7,8</sup> there has been increasing concern about adverse health effects caused by DBPs. Toxicological and epidemiological studies showed that certain THMs as well as haloacetic acids (HAAs; e.g., dichloroacetic acid) are genotoxic and potentially carcinogenic and that lifetime exposure to chlorinated drinking water is associated with an increased risk for cancer, especially of the bladder.<sup>9–11</sup> As a consequence, many countries introduced regulations for selected THMs and HAAs in drinking water.<sup>12,13</sup> To meet new and stringent drinking water quality standards, many utilities discontinued chlorination and applied alternative disinfectants.<sup>5</sup> Ozone, chlorine dioxide, and chloramine have numerous advantages over chlorination in that they significantly reduce THM and HAA formation, eliminate pathogens, and remove a range of toxic organic (micro)pollutants.<sup>4,14–17</sup> However, the efforts to reduce regulated DBPs have had unintended consequences, that is the formation of new and unregulated by-products of concern.<sup>16,18,19</sup>

To date, more than 600 organic and inorganic DBPs have been reported and new classes of DBPs are continuously identified.<sup>20–23</sup> While only few suspected human carcinogens such as bromate are regulated, the vast majority of DBPs are poorly characterized in terms of formation, occurrence, and potential chronic health effects. *In vitro* cellular bioassays have demonstrated that nitrogen-containing DBPs (N-DBPs) such as halonitromethanes, haloacetamides, haloacetoneitriles, and *N*-nitrosamines are significantly more cytotoxic and genotoxic than the regulated THMs and HAAs.<sup>24–26</sup> Increased levels of N-DBPs have especially been found in chloraminated drinking water, which has caused great concern, because many water utilities switched from chlorination to chloramination.<sup>27</sup> Moreover, wastewater-impacted source waters containing high



levels of dissolved organic nitrogen promote the formation of N-DBPs.<sup>28</sup> In times of increasing water demand and increasing reliance on impacted surface waters and water reuse processes, knowledge about DBP formation pathways is needed to develop appropriate DBP mitigation strategies.<sup>29,30</sup>

## 1.2 *N*-Nitrosodimethylamine in drinking water

### 1.2.1 Toxicity, occurrence, and mitigation

This study focuses on *N*-nitrosodimethylamine (NDMA), which belongs to a family of non-halogenated N-DBPs that is *N*-nitrosamines. Although other nitrosamines such as *N*-nitrosodiethylamine, *N*-nitrosomorpholine, and *N*-nitrosopyrrolidine have been identified in drinking water,<sup>31,32</sup> NDMA is the most commonly detected species. Within the framework of the Unregulated Contaminant Monitoring Rule (UMCR 2, 2008-2010) of the United States Environmental Protection Agency (U.S. EPA), NDMA accounted for 95% of the total *N*-nitrosamine detections in drinking water.<sup>33,34</sup> In addition, NDMA is among the most mutagenic and genotoxic *N*-nitrosamines and has been classified as probably carcinogenic to humans by the International Agency for Research on Cancer (IARC) as well as by the U.S. EPA.<sup>35-37</sup> For oral exposure, the cancer potency of NDMA is approximately 600 times greater than that of regulated THMs and the U.S. EPA lists a concentration of 0.7 ng L<sup>-1</sup> NDMA in drinking water associated with a 10<sup>-6</sup> lifetime cancer risk.<sup>30,37</sup>

Prior to the first detection of NDMA in drinking water in Ontario, Canada,<sup>38</sup> concern about NDMA stemmed primarily from its widespread occurrence in food, beverages, personal care products, and tobacco smoke.<sup>39,39-42</sup> In contrast to initial assumptions, NDMA in drinking water did not originate from anthropogenic sources such as rocket fuels, polymers, or plasticizers, but was formed when chemical disinfectants react with natural organic matter or anthropogenic pollutants present in source waters.<sup>31,43-46</sup> Despite public and regulatory concern about potential long-term chronic health effects, NDMA and other *N*-nitrosamines remain widely unmonitored and unregulated. Currently they are under evaluation for regulation by the U.S. EPA. The World Health Organization (WHO) as well as many industrialized countries have established guidance values allowing for maximum NDMA concentrations of 9-100 ng L<sup>-1</sup> in drinking water.<sup>43,47-49</sup> A nationwide survey of NDMA in U.S. drinking waters revealed that the average concentration of NDMA was 9 ng L<sup>-1</sup> and thus within this acceptable range.<sup>33</sup> However, exceedingly high concentrations of up to 600 ng L<sup>-1</sup> were detected in chloram-

inated drinking water, which could pose increased human health risks to consumers.<sup>33</sup>

Once NDMA has been formed in drinking water, its physical removal is challenging, especially because NDMA can continue to form in chlor(am)inated drinking water distribution systems.<sup>50</sup> While NDMA is not efficiently retained by reverse osmosis and only partially removed through biodegradation in sand or activated carbon filtration,<sup>41,51</sup> UV treatment is an effective method to destroy NDMA.<sup>43,52</sup> However, owing to the high UV doses required, it is an expensive approach that can, in addition, not prevent the formation of NDMA in distribution systems.<sup>43,52</sup> To avoid drinking waters with elevated NDMA concentration reaching the consumers tap, the best strategy is to mitigate the formation of NDMA and other DBPs. However, even though considerable efforts have been devoted to identify NDMA precursor compounds, reaction pathways leading to NDMA remain poorly understood.

### 1.2.2 NDMA precursors and proposed formation pathways

Generally, NDMA can be formed during chlorination, chloramination, ozonation, and chlorine dioxide treatment.<sup>41,45,46,53,54</sup> However, the most important pathway to NDMA is likely the chloramination of wastewater and wastewater-impacted surface waters that contain a variety of nitrogenous NDMA precursor compounds.<sup>30,55</sup> Most mechanistic research has been done with dimethylamine (DMA) as model precursor because DMA and tertiary amines containing DMA-functional groups have been identified as frequently occurring NDMA precursors in raw waters.<sup>28,44,55</sup> Figure 1.1 depicts three proposed mechanisms for NDMA formation from DMA.

Pathway (i) suggests the reaction of DMA with a nitrosating agent such as  $\text{N}_2\text{O}_4$  that might be produced in the reaction of nitrite ( $\text{NO}_2^-$ ) with chlorine, ozone, or hydroxyl radicals.<sup>56,57</sup> However, NDMA yields during chlorination and ozonation in the presence of  $\text{NO}_2^-$  were low ( $<0.5\%$ ) indicating that these pathways are of minor relevance.<sup>45,56,57,60</sup> Pathway (ii) shows the nucleophilic substitution reaction of the neutral DMA with monochloramine ( $\text{NH}_2\text{Cl}$ ) leading to unsymmetrical dimethylhydrazine (UDMH), which is subsequently oxidized to NDMA.<sup>44,61</sup> This pathway was revised because the reaction of dichloramine ( $\text{NHCl}_2$ ) with DMA formed two orders of magnitude more NDMA than  $\text{NH}_2\text{Cl}$ . Pathway (iii) illustrates the proposed reaction of DMA with  $\text{NHCl}_2$  leading to chlorinated UDMH.<sup>58</sup> Experiments with  $^{18}\text{O}$ -labeled water did not show an incorporation of  $^{18}\text{O}$  into NDMA, but molar NDMA yields from DMA increased with increasing concentration of dissolved molecular  $\text{O}_2$  demonstrating that the latter plays an important role for NDMA formation.<sup>58</sup>

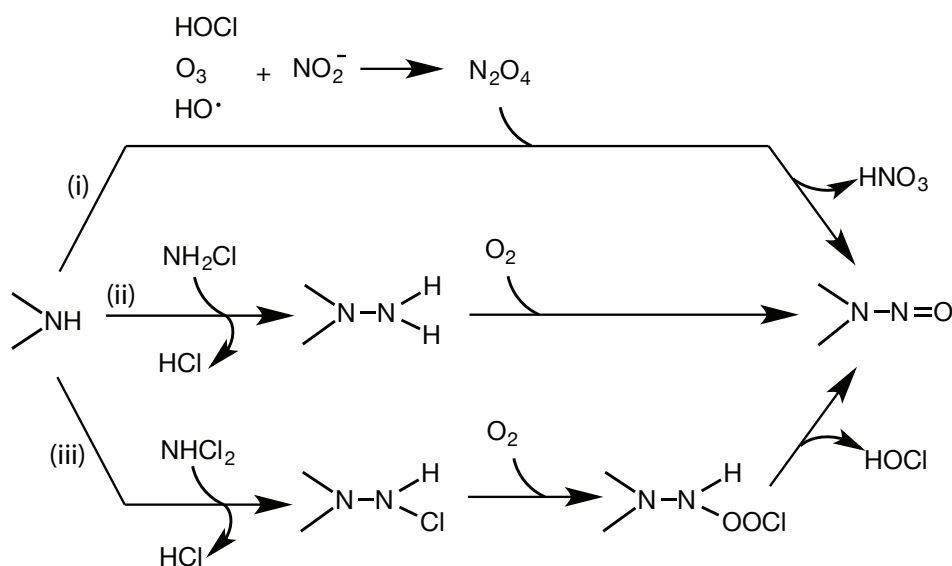


**Figure 1.1:** Proposed NDMA formation pathways for ozonation, chlorination, and chloramination of dimethylamine (DMA) leading to NDMA yields of  $<5\%$ .<sup>44,56–59</sup> The scheme depicted here illustrates the most important reactions only.

As molar NDMA yields from chlor(am)ination of DMA are low ( $<0.5\text{--}5\%$ ), it has been concluded that the DMA concentrations in wastewater treatment plant effluents and surface waters in the low  $\mu\text{g/L}$  range cannot be responsible for the formation of significant concentrations of NDMA in drinking water.<sup>28,55,62</sup> Since then, numerous other NDMA precursors have been identified including natural organic matter,<sup>63,64</sup> algae,<sup>65</sup> soluble microbial products,<sup>66</sup> trimethylamine,<sup>67,68</sup> amine-containing water treatment polymers (e.g., polyDADMAC),<sup>40,55,69,70</sup> and anthropogenic micropollutants such as pharmaceuticals, personal care products, and pesticides.<sup>40,71–74</sup> Although reaction mechanisms leading to NDMA have not been studied separately for each of these compounds, many NDMA precursors have one common structural feature: they contain secondary, tertiary, or quaternary amine functional groups. Tertiary alkylamines have been shown to degrade to secondary amines during chloramination so that NDMA formation pathways in Figure 1.1 might apply.<sup>75</sup> Indeed, molar NDMA yields from most tertiary amines are low ( $<6\%$ ) and comparable to those of secondary amines.<sup>50,72</sup>

However, one subset of tertiary amines exhibits much higher NDMA yields of  $>60\%$  during chloramination.<sup>67,72,76</sup> These potent NDMA precursors possess a dimethylamine functional moiety bound via a methylene group to an aromatic ring.<sup>67</sup> This structure can be found in certain pharmaceuticals such as ranitidine.<sup>77</sup> Owing to the high molar NDMA yield from these tertiary amines, NDMA formation is unlikely to proceed through

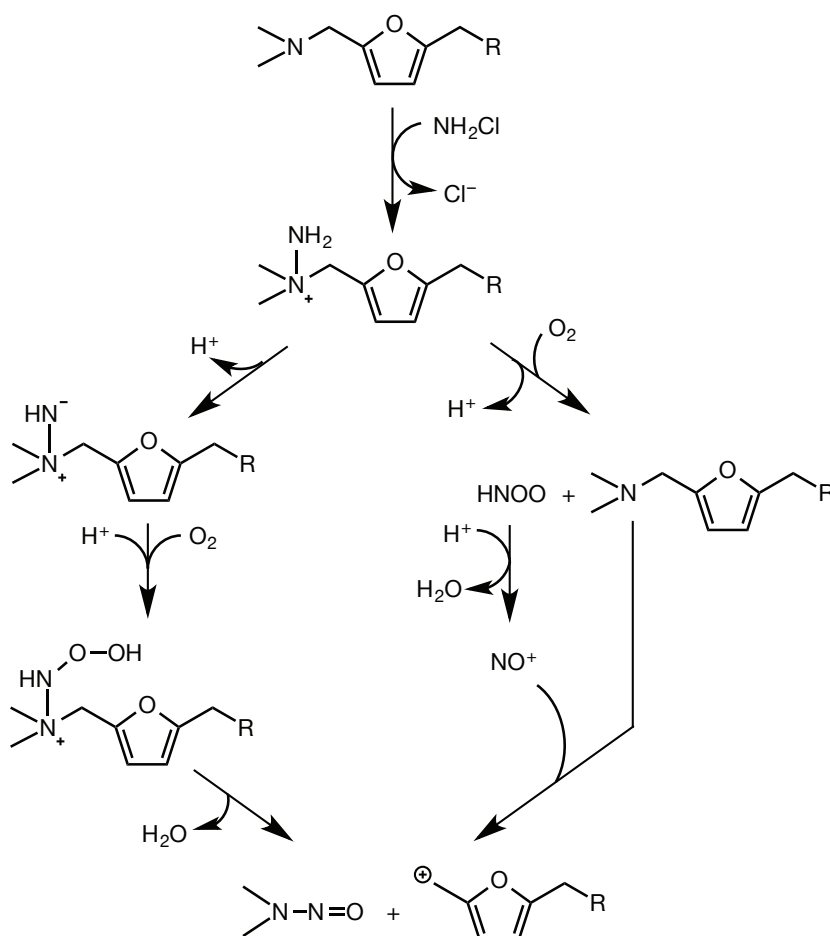


**Figure 1.2:** Proposed NDMA formation pathways for chloramination of ranitidine derivatives leading to >60% molar NDMA yield.<sup>79,80</sup>

secondary amine or UDMH intermediates.<sup>78,79</sup> Instead two different NDMA formation pathways have been proposed as illustrated in Figure 1.2.<sup>79,80</sup> Both pathways suggest a common initial reaction step that is a nucleophilic substitution reaction between the tertiary amine and  $\text{NH}_2\text{Cl}$  leading to a dimethylhydrazone-type intermediate.<sup>79,80</sup> Furthermore, both pathways suggest the formation of NDMA and a carbocationic leaving group whose stability has been pointed out as key feature for high NDMA yields.<sup>67,80</sup> NDMA formation was significantly inhibited under anoxic conditions demonstrating the crucial role of dissolved  $\text{O}_2$  for NDMA formation.<sup>76</sup> However, reaction mechanisms involving molecular  $\text{O}_2$  and reactive intermediates remain speculative owing to the difficulty to detect short-lived (oxygen) intermediates.

Although NDMA is one of the best studied DBPs, knowledge about NDMA formation pathways remains incomplete. This situation complicates the prediction and

prevention of NDMA formation. Owing to the large number of structurally diverse NDMA precursor compounds, new tools are needed to identify relevant precursors in raw waters.

## 1.3 Assessing NDMA formation with compound - specific isotope analysis

Assessing the formation of NDMA during water treatment is a challenging task, because precursor compounds and formation pathways cannot be inferred solely from measurements of NDMA concentrations. Compound-specific isotope analysis (CSIA) is a promising approach to elucidate NDMA formation pathways and to obtain a reaction-related characterization of specific precursors in raw waters, because changes in the isotopic composition of NDMA might reflect reaction mechanisms leading to its formation.

### 1.3.1 Stable isotope analysis - fundamentals and application

CSIA is an effective tool to (i) allocate and distinguish sources of organic compounds and (ii) identify and quantify abiotic and biotic transformation reactions on scales ranging from laboratory batch experiments to contaminated field sites (see reviews).<sup>81–85</sup> Using gas or liquid chromatography coupled to isotope ratio mass spectrometry (GC/- or LC/IRMS), the natural isotopic composition of organic compounds is determined as the ratio of heavy to light isotopes of an element E ( $^h\text{E}/^l\text{E}$ ). Stable isotope ratios are expressed as isotope signatures,  $\delta^h\text{E}$ , that reflect the relative difference between the isotope ratio of the compound and the isotope ratio of an internationally accepted reference material.<sup>86,87</sup>  $\delta^h\text{E}$  values are expressed in per mil (‰).

$$\delta^h\text{E} = \frac{(^h\text{E}/^l\text{E})_{\text{compound}}}{(^h\text{E}/^l\text{E})_{\text{reference}}} - 1 \quad (1.1)$$

Organic compounds often have characteristic isotope signatures that are defined by the isotopic composition of the precursor material as well as by industrial or biogenic formation processes.<sup>82,85,88</sup> If isotope signatures of a compound remain constant during time or space, they can be used as fingerprint for source apportionment.<sup>83,89,90</sup> It is generally assumed that physical processes (i.e., transport, dilution, and phase-transfer) only cause minor changes in the isotopic composition of an organic compound.<sup>82</sup> In contrast, isotope signatures exhibit significant changes (so called isotope fractionation)

if chemical bonds in a compound are broken or formed in rate-determining steps of a reaction. Isotope fractionation is a consequence of kinetic isotope effects (KIEs) that arise when molecules containing a light or heavy isotope in the reactive position react with different rates.

$$\text{KIE}_E = \frac{l_k}{h_k} \quad (1.2)$$

where  $l_k$  and  $h_k$  are the rate constants for molecules containing the light and heavy isotope, respectively. KIEs are caused by differences in the activation energies of molecules carrying light or heavy isotopes, which in turn depends on energy differences between the reactant and the transition state.<sup>83</sup> KIEs thus provide insights into transition state structures and are characteristic for elementary reactions and the chemical bonds and functional groups involved therein.<sup>82,83,91</sup> To determine KIEs, the observable isotope fractionation is quantified by bulk isotope enrichment factors,  $\varepsilon_E^{\text{bulk}}$ , using the Rayleigh equation.

$$\frac{\delta^h E + 1}{\delta^h E_0 + 1} = \left( \frac{c}{c_0} \right)^{\varepsilon_E^{\text{bulk}}} \quad (1.3)$$

where  $\delta^h E_0$  and  $\delta^h E$  are isotope signatures measured at the beginning and at certain time points of the reaction in the remaining fraction of the reactant ( $c/c_0$ ). If a reactant contains more than one atom of element E, the  $\varepsilon_E^{\text{bulk}}$  value reflects the average, bulk isotope fractionation in the reactant. Consequently, the KIE at the reactive position will be diluted. To interpret observable isotope fractionation in terms of the underlying reaction mechanism,  $\varepsilon_E^{\text{bulk}}$  values need to be converted to position-specific apparent kinetic isotope effects (AKIEs) at reacting bonds. This conversion requires a priori knowledge of the total number of atoms of an element E in a molecule ( $n$ ), the number of atoms in reactive positions ( $x$ ), and the number of atoms in intramolecular competition ( $z$ ).<sup>83,84</sup>

$$\text{AKIE} = \frac{1}{1 + (n/x) \cdot z \cdot \varepsilon_E^{\text{bulk}}} \quad (1.4)$$

In elementary reactions, the AKIE reflects the *intrinsic* KIE pertinent to a specific bonding change. However, enzymatic and chemical reactions are often multi-step processes in which several reaction steps can be (partially) rate-determining. In such cases, the AKIE derived from observable isotope fractionation can significantly deviate from the *intrinsic* KIE of the chemical elementary reaction step of interest, which complicates mechanistic interpretations.<sup>83,83,92</sup> If reaction steps that mask the *intrinsic* KIE are non-fractionating, multi-dimensional isotope analysis allows to discern transformation pathways because all elements are affected by masking in the same way.<sup>83</sup> In this

approach, measured isotope signatures of two elements,  $\delta^h E_1$  and  $\delta^h E_2$ , are correlated. The slope of the linear correlation,  $\Lambda$ , is approximately equal to the ratio of the bulk enrichment factors,  $\varepsilon_{E_1}^{\text{bulk}}$  and  $\varepsilon_{E_2}^{\text{bulk}}$ .<sup>83</sup>

$$\Lambda = \frac{\delta^h E_1}{\delta^h E_2} \approx \frac{\varepsilon_{E_1}^{\text{bulk}}}{\varepsilon_{E_2}^{\text{bulk}}} \quad (1.5)$$

Such dual isotope slopes are in many cases indicative for reaction mechanisms.<sup>83,93</sup> However, if several reaction steps cause isotope fractionation, these slopes might not longer be constant and the analysis of multiple isotope ratios of the reactants, reaction intermediates, and products can be instrumental in gaining insights into the reaction mechanism.<sup>83,92,94</sup>

To date, the investigated spectrum of compounds comprises mainly hazardous priority pollutants<sup>81</sup> such as chlorinated organic solvents,<sup>94–97</sup> benzene,<sup>98,99</sup> toluene,<sup>100,101</sup> ethylbenzene, and xylene (BTEX),<sup>102</sup> fuel additives,<sup>103,104</sup> nitroaromatic explosives,<sup>93,105</sup> or aromatic amines.<sup>106</sup> However, there is increasing interest in the application of CSIA to study the sources and fate organic micropollutants such as pharmaceuticals,<sup>107,108</sup> herbicides,<sup>109,110</sup> or corrosion inhibitors<sup>111,112</sup> in the environment.

### 1.3.2 CSIA to assess DBP formation

Given the potential of isotope fractionation analysis to allocate sources of organic compounds and to provide unique insights into reaction mechanisms, CSIA might be a promising tool to assess DBP formation. An initial exploratory study by Arnold et al. indeed demonstrated that changes in  $^{13}\text{C}/^{12}\text{C}$  ratios of chloroform can be used as probes for reactive precursor moieties in NOM and chloroform formation pathways.<sup>113</sup> Various model compounds representing NOM functional groups produced chloroform upon chlorination. However, C isotope ratios of chloroform changed in distinctly different manner depending on the type of precursor. While chloroform from resorcinol and (di)ketones was enriched in  $^{13}\text{C}$ , it was enriched in  $^{12}\text{C}$  when produced from (chloro)phenols. Chloroform produced during chlorination of Lake Zurich water was as well enriched in  $^{12}\text{C}$ , indicating that phenolic moieties in NOM were responsible for chloroform formation. While C isotope fractionation trends could be successfully used for the identification of chloroform precursors, a mechanistic interpretation was more challenging. The variability of C isotope fractionation in chloroform hinted at differences in the chloroform formation pathways from different NOM functional groups. Reactions leading to the observed C isotope fractionation trends in chloroform could, however, not be identified as chloroform

formation is a complex multi-step process that likely involves isotope-sensitive branching of competing reaction pathways. Trends in C isotope ratios were nevertheless indicative for chloroform formation pathways from specific precursor compounds.

Likewise, isotope ratios of NDMA might be indicative for its formation pathway and could be used to link NDMA formation to the presence of specific precursor compounds or functional groups therein. Similar to chloroform, NDMA is formed in a series of reaction steps, which are poorly understood to date (Figures 1.1 and 1.2). Together with the study of reaction kinetics and the identification of reactive intermediates, CSIA might provide unique insights into reaction mechanisms leading to NDMA.

## 1.4 Objectives and approach

The objective of this dissertation was to explore the use of CSIA for (i) elucidating NDMA formation mechanisms and (ii) identifying reactive precursor moieties from stable isotope fractionation trends. To this end, the formation of NDMA during chloramination of secondary and tertiary amines was studied in laboratory model systems using conditions similar to those in water treatment. The specific goals of this work were:

1. To develop and validate an analytical method for the accurate determination of the isotopic composition of NDMA and four additional *N*-nitrosamines in aqueous water samples including the identification of optimal extraction efficiencies and quantification limits.
2. To gain new insights into central reaction steps leading to NDMA during chloramination of the selected amine model precursors with special emphasis on reactions of molecular oxygen and radical intermediates.
3. To evaluate changes in the C, N, and H stable isotope ratios of NDMA during chloramination of tertiary amines as proxies for NDMA formation pathways and precursors responsible for NDMA formation.



Chapter 2 presents the newly developed method for the analysis of  $^{13}\text{C}/^{12}\text{C}$ ,  $^{15}\text{N}/^{14}\text{N}$ , and  $^2\text{H}/^1\text{H}$  ratios of NDMA and four *N*-nitrosamines using solid-phase extraction coupled to gas chromatography isotope ratio mass spectrometry (SPE-GC/IRMS). To test the applicability of this method, C, N, and H isotope ratios of NDMA were determined during chloramination of the pharmaceutical ranitidine. The comparison of H isotope ratios in NDMA with site-specific H isotope ratios of the  $\text{N}(\text{CH}_3)_2$  moiety of ranitidine measured with quantitative deuterium nuclear magnetic resonance spectroscopy demonstrated the accuracy of the developed SPE-GC/IRMS method.

Chapter 3 focuses on the elucidation of central reaction steps of the NDMA formation mechanism involving molecular oxygen, monochloramine, and transient intermediate species. In laboratory experiments, NDMA formation was studied during monochloramination of amine-containing model precursors. To evaluate the relevance of short-lived reactive (oxygen) intermediates, the reaction was characterized in terms of reaction kinetics and stoichiometries. To this end, concentrations of the precursor, NDMA,  $\text{NH}_2\text{Cl}$ , and  $\text{O}_2$  were quantified. The presence or absence of various radical species was revealed by oxygen isotope analysis of aqueous  $\text{O}_2$  and experiments with various radical scavengers. Based on these results, potential NDMA formation pathways involving N-centered radical species are proposed.

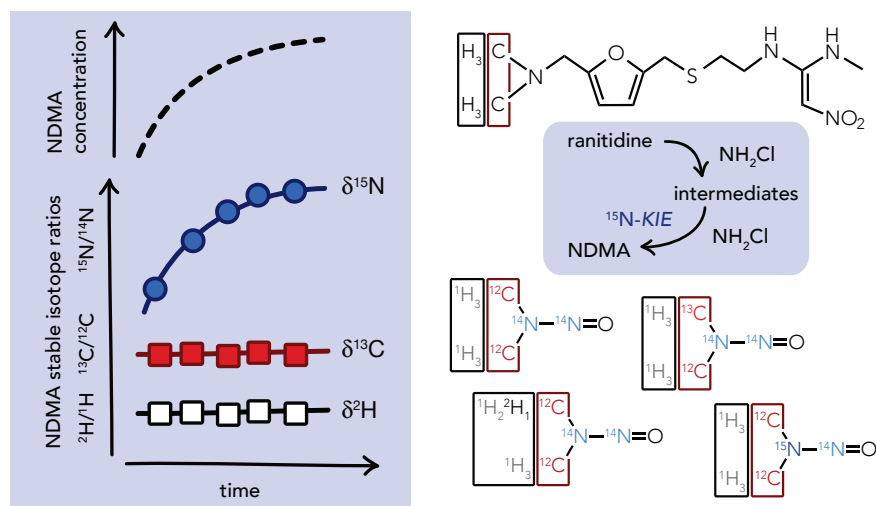
Chapter 4 addresses the question whether changes in isotope ratios of NDMA can provide insights into the NDMA formation mechanism and can function as proxies for NDMA precursors. The origin of the atoms in NDMA was inferred by determining the initial isotope ratios of the precursors and by studying isotope fractionation in NDMA and selected precursors. With this approach, reaction steps that could be responsible for the observed N isotope fractionation in NDMA and precursors were revealed. Irrespective of the molar NDMA yield, linear trends in  $\delta^{15}\text{N}$  versus  $\delta^{13}\text{C}$  values of NDMA were characteristic for the chloramination of four tertiary amines and robust even under varying reaction conditions. This indicates the potential diagnostic power of CSIA to identify NDMA precursor compounds during water disinfection.

In a general conclusion section, open questions and directions for future research are discussed (Chapter 5).



## Chapter 2

# Compound-Specific Carbon, Nitrogen, and Hydrogen Isotope Analysis of *N*-Nitrosodimethylamine in Aqueous Solutions



Reprinted with permission from Stephanie Spahr, Jakov Bolotin, Jürgen Schleucher, Ina Ehlers, Urs von Gunten, and Thomas B. Hofstetter. *Anal. Chem.*, **2015**, 87 (5), 2916-2924. Copyright 2015 American Chemical Society.

*Spahr, S. conducted GC/IRMS measurements, designed and performed NDMA formation experiments, analyzed data, and wrote the paper. Schleucher, J. and Ehlers, I. performed quantitative deuterium NMR spectroscopy and wrote the corresponding part in the experimental section. Von Gunten, U. and Hofstetter, T. B. supervised the project, contributed to the discussion of the results and revision of the manuscript.*

## Abstract

Mitigation of *N*-nitrosodimethylamine (NDMA) and other hazardous water disinfection by-products (DBP) is currently hampered by a limited understanding of DBP formation mechanisms. Because variations of the stable isotope composition of NDMA can potentially reveal reaction pathways and precursor compounds, we developed a method for the compound-specific isotope analysis (CSIA) of  $^{13}\text{C}/^{12}\text{C}$ ,  $^{15}\text{N}/^{14}\text{N}$ , and  $^2\text{H}/^1\text{H}$  ratios of NDMA by gas chromatography coupled to isotope ratio mass spectrometry (GC/IRMS). Method quantification limits for the accurate isotope analysis of NDMA, *N*-nitrosodiethyl-, -dipropyl-, and -dibutylamine as well as *N*-nitrosopyrrolidine were between 0.18 to 0.60 nmol C, 0.40 to 0.80 nmol N, and 2.2 to 5.8 nmol H injected on column. Coupling solid-phase extraction to GC/IRMS enabled the precise quantification of C, N, and H isotope ratios of NDMA in aqueous samples at concentrations of 0.6  $\mu\text{M}$  (45  $\mu\text{g L}^{-1}$ ). We validated the proposed method with a laboratory experiment, in which NDMA was formed with stoichiometric yield ( $97 \pm 4\%$ ) through chloramination of the pharmaceutical ranitidine (3  $\mu\text{M}$ ).  $\delta^{13}\text{C}$  and  $\delta^2\text{H}$  values of NDMA remained constant during NDMA formation while its  $\delta^{15}\text{N}$  value increased due to a reaction at a N atom in the rate-limiting step of NDMA formation. The  $\delta^2\text{H}$  value of NDMA determined by SPE-GC/IRMS also corresponded well to the  $\delta^2\text{H}$  value of the  $\text{N}(\text{CH}_3)_2$ -group of ranitidine measured by quantitative deuterium nuclear magnetic resonance spectroscopy. This observation implies that the  $\text{N}(\text{CH}_3)_2$ -moiety of ranitidine is transferred to NDMA without being chemically altered and illustrates the accuracy of the proposed method.

## 2.1 Introduction

*N*-nitrosamines are of public and regulatory concern because these potent carcinogens can be formed as unintentional by-products during drinking and waste water disinfection. Among the typically surveyed *N*-nitrosamines, *N*-nitrosodimethylamine (NDMA) is the most frequently detected disinfection by-product in drinking water.<sup>50,114,115</sup> Because of its mutagenicity, maximum NDMA concentrations in drinking water should not exceed guidance values in the range of 9 to 100 ng L<sup>-1</sup>.<sup>49,116,117</sup> Preventing NDMA formation is, however, a challenging task. Numerous compounds have been identified as precursors that lead to NDMA when source waters are disinfected by chlorine, chloramine, or ozone.<sup>118</sup> NDMA precursors typically contain aliphatic amine functional groups and include natural organic materials<sup>66,119</sup> as well as compounds of anthropogenic origin such as additives for water treatment,<sup>69</sup> pesticides,<sup>41,54,73,120</sup> pharmaceuticals,<sup>72,76,79</sup> and potential CO<sub>2</sub>-capture systems.<sup>121,122</sup> Depending on the precursor compound, NDMA yields vary by orders of magnitude. Whereas chloramination of dimethylamine gives rise to molar NDMA yields of a few percent,<sup>55,60,123</sup> yields increase to up to 90% for chloramination of a dimethyl-aminomethyl furfuryl alcohol.<sup>123</sup> It is evident that in addition to the presence of an alkylamine moiety, other structural features impact the NDMA formation potential.<sup>124</sup> Unfortunately, understanding the mechanisms of *N*-nitrosamine formation is challenging. It remains very difficult to predict NDMA formation potentials of different water constituents and to develop efficient mitigation strategies.

We have shown previously that the formation pathways of disinfection by-products can be inferred from changes of their stable isotope ratios.<sup>113</sup> The <sup>13</sup>C/<sup>12</sup>C ratio of chloroform produced upon chlorination of natural organic matter in lake water evolved in a way that chloroform was depleted in <sup>13</sup>C. This inverse C isotope fractionation of chloroform was typical for a reaction of phenolic precursor moieties due to a characteristic <sup>13</sup>C kinetic isotope effects (<sup>13</sup>C-KIE). As in many applications of compound-specific isotope analysis (CSIA) for contaminant degradation assessment, KIEs are specific measures of a reaction mechanism<sup>82-84,125</sup> and thus also reflect the reactions of the precursor material. CSIA-based methodology works at natural isotope abundances and can be applied to track reaction products in general, for example, to infer the origin of naturally produced chloroform from soil organic matter.<sup>126-129</sup> However, elucidation of NDMA formation pathways during disinfection processes by CSIA has not been attempted to date, because procedures for isotopic analysis of *N*-nitrosamines at natural isotope abundances are still missing.

It is currently unclear which of the four chemical elements of NDMA is accessible by stable isotope ratio measurements and whether this information reveals the identity of precursor moieties and reaction mechanisms. Current hypotheses suggest that the *N,N*-dimethylamine moiety of NDMA originates from the organic precursor molecule.<sup>43,55,79,123</sup> The nitroso group of NDMA, in contrast, stems from nitrite or from different processes including reaction of the disinfectant and molecular O<sub>2</sub> with the precursor compounds. On the basis of such a simplistic assumption, one could speculate that the two *N*-methyl groups are not involved in the NDMA formation reaction and its <sup>13</sup>C/<sup>12</sup>C and <sup>2</sup>H/<sup>1</sup>H ratios function as isotopic fingerprints of *N*-methyl groups of the organic precursor molecule. In contrast, <sup>15</sup>N/<sup>14</sup>N and <sup>18</sup>O/<sup>16</sup>O ratios are expected to change during NDMA formation and convey information on the reaction mechanism.

In this study, we present a method for the analysis of C, N, and H isotope ratios of NDMA in aqueous samples in the micromolar concentration range. Note that chemically pure NDMA, which could be used as isotopic reference material for method development, is not available commercially in Europe. Therefore, we used four alternative *N*-nitrosamines, namely *N*-nitrosodiethylamine (NDEA), *N*-nitrosodipropylamine (NDPA), *N*-nitrosodibutylamine (NDBA), and *N*-nitrosopyrrolidine (NPYR), to establish sensitive procedures for accurate, that is true and precise C, N, and H isotope analysis by coupling solid-phase extraction to gas chromatography / isotope ratio mass spectrometry (SPE-GC/IRMS).<sup>105,111,130–132</sup>

We validated our method by studying a model reaction, in which NDMA is formed stoichiometrically upon chloramination of the pharmaceutical ranitidine. This compound is a frequently detected micropollutant in sewage treatment plants and surface waters<sup>28,133,134</sup> and shows one of the highest NDMA formation yields reported for chloramination reactions.<sup>76,79</sup> Moreover, ranitidine exhibits a *N,N*-dimethylamine functional group that has been suggested to lead to NDMA.<sup>79</sup> Here, we applied quantitative deuterium nuclear magnetic resonance (NMR) spectroscopy to determine the <sup>2</sup>H/<sup>1</sup>H ratio of the *N,N*-dimethylamine functional group of ranitidine for comparison with the corresponding H isotope ratios measured in NDMA by SPE-GC/IRMS.

## 2.2 Experimental Section

A list of all chemicals including suppliers and purities is provided in the Supporting Information (SI).

### 2.2.1 Safety considerations

*N*-nitrosamines are potent carcinogens. The pure substances and concentrated solutions should be handled with great care. Work should be done in a well-ventilated chemical fume hood and appropriate protective clothing, goggles, and gloves should be worn. They should be kept away from heat, sparks, and flame.

### 2.2.2 Solid-phase extraction (SPE)

We compared the performance of two different SPE methods for the extraction and enrichment of *N*-nitrosamines from 1 L of aqueous solution. For SPE method 1 (modified from Yoon et al.<sup>135</sup>), SepPak Aminopropyl Plus Short cartridges (360 mg, Waters) were placed on top of SepPak AC-2 Plus Short cartridges (400 mg, Waters). Cartridges were conditioned with 5 mL dichloromethane, 5 mL methanol, and 5 mL NANO-pure water or phosphate buffer (1 mM, pH 7.0). A volume of 1 L of aqueous sample was passed through at a flow rate of 2-3 mL/min. AC-2 cartridges were dried for 2 h and eluted with 10 mL dichloromethane. For SPE method 2 (modified from Krauss and Hollender<sup>136</sup>), Oasis HLB cartridges (6 mL, 200 mg, Waters) were conditioned with 10 mL pentane, 10 mL ethyl acetate, 10 mL methanol, and 15 mL tap water or phosphate buffer (10 mM, pH 7.0). Coconut activated carbon cartridges (EPA method 521, Charcoal for NDMA, 6 mL, 2 g, Restek, BGB) were conditioned with 15 mL pentane, 20 mL ethyl acetate, 15 mL methanol, and 20 mL tap water or phosphate buffer. A volume of 1 L of aqueous sample was passed through both connected cartridges (Oasis HLB on top, charcoal in bottom) at a flow rate of 2-3 mL/min. Cartridges were washed with 5 mL tap water or buffer and dried separately for 2 h by applying vacuum. Cartridges were reconnected and analytes were eluted with 5 mL ethyl acetate. The Oasis HLB cartridge was removed and analytes were eluted from the charcoal cartridge with 10 mL of ethyl acetate. Both ethyl acetate extracts were combined in the same collection tube and evaporated at 30°C under a gentle stream of N<sub>2</sub> to 10 mL for analysis by GC/MS or to 1 mL for isotope ratio measurements with GC/IRMS.

We evaluated SPE methods 1 and 2 in terms of *N*-nitrosamine recovery. We prepared a methanolic stock solution containing 10 mM NDMA, NDEA, NDPA, NDMA, and

NPYR with which we made 1 L aqueous solutions (tap water or phosphate buffer) containing 0.5 - 3  $\mu\text{M}$  of each analyte. Blank samples did not contain any *N*-nitrosamines. Samples and blanks were processed identically as described above. *N*-Nitrosamine concentrations in dichloromethane (method 1) or ethyl acetate (method 2) were analyzed by GC/MS after dilution to the concentration range calibrated on our instrument. Owing to higher recoveries, method 2 was further evaluated to rule out SPE-induced isotope fractionation. According to the linear range for C, N, and H isotope analysis (Figure 2.2 and Figure S2.4), we prepared three methanolic stock solutions with different concentrations of NDMA, NDEA, NDPA, NDBA, and NPYR. Note that for N isotope analysis, the methanolic stock solution contained all five analytes in equal concentration (10 mM), whereas C and H isotope analysis required different concentrations for each analyte because of differing number of C and H atoms. Subsequently, we spiked 1 L of tap water and 1 L of 10 mM phosphate buffer (pH 7.0) to achieve final NDMA concentrations of 0.5 - 1.2  $\mu\text{M}$ , 1 - 3  $\mu\text{M}$ , and 1.5 - 2.5  $\mu\text{M}$  for C, N, and H isotope analysis, respectively. All samples were processed with SPE method 2. To achieve a 1000-fold analyte enrichment, we evaporated the ethyl acetate extracts to 1 mL. Solvent evaporation to less than 1 mL led to a decrease in *N*-nitrosamine recovery of up to 30% (Table S2.2).

### 2.2.3 Chemical analysis

Concentrations of NDMA, NDEA, NDPA, NDBA, and NPYR in organic solvents were quantified using a GC/MS system (TRACE GC Ultra and TRACE DSQ EI 250, Thermo). A sample volume of 1  $\mu\text{L}$  in ethyl acetate or dichloromethane was injected with a CombiPAL autosampler (CTC) in a split/splitless injector operated at 200°C for 1 min in splitless and thereafter in split mode. The split flow was 50 mL/min. Helium carrier gas was used at constant pressure of 150 kPa. Chromatographic separation was achieved with a 1 m DPTMDS (methyl/phenyl) deactivated fused-silica guard column (530  $\mu\text{m}$  i.d., BGB Analytik), a 60 m x 0.32 mm RTX-VMS column (1.8  $\mu\text{m}$  df, Restek), and a DPTMDS (methyl/phenyl) deactivated fused-silica postcolumn (180  $\mu\text{m}$  i.d., BGB Analytik). The temperature program started at 40°C (5 min) and increased with 20°C/min to 220°C (6 min). The mass spectrometer ran in the full scan mode within a mass-to-charge ( $m/z$ ) range of 50 - 205. *N*-nitrosamines were quantified with an external calibration in the range of 0.8 - 16  $\mu\text{M}$ .

Concentrations of NDMA and ranitidine in aqueous samples from NDMA formation experiments were quantified without analyte enrichment by reverse phase HPLC (Dionex UltiMate 3000) with UV-vis detection at wavelengths corresponding to the absorption



maxima of the analytes (228 nm for NDMA and 320 nm for ranitidine). The limit of quantification was 0.1  $\mu\text{M}$  for both analytes. For NDMA analysis, an aqueous sample volume of 50  $\mu\text{L}$  was analyzed using a Supelcosil LC-18 column (25 cm x 4.6 mm, 5  $\mu\text{m}$ , Supelco) with a LC-18 guard column. The eluent mixture consisted of 90% phosphate buffer (1 mM, pH 7.0) and 10% methanol at a flow rate of 1 mL/min. For quantification of ranitidine, 40  $\mu\text{L}$  of aqueous sample were analyzed using a XBridge column (LC-18, 5 cm x 3 mm, 2.5  $\mu\text{m}$ , Waters) equipped with a XBridge guard column (C18, 2.5  $\mu\text{m}$ , Waters). Ranitidine analysis was carried out with an eluent mixture of 65% phosphate buffer (1 mM, pH 11.5) and 35% methanol at a flow rate of 0.5 mL/min.

Monochloramine ( $\text{NH}_2\text{Cl}$ ) stock solutions (30 mM) were prepared daily by mixing hypochlorite and ammonium chloride at pH 9.5 (molar Cl/N ratio of 1:1.05) with a dual syringe pump (T-mixing system).<sup>137</sup> A Varian Cary 100 Bio UV-visible spectrophotometer was used to quantify HOCl at  $\lambda = 292 \text{ nm}$  ( $\varepsilon_{292\text{nm}} = 350 \text{ M}^{-1}\text{cm}^{-1}$ ) and  $\text{NH}_2\text{Cl}$  at  $\lambda = 245 \text{ nm}$  ( $\varepsilon_{245\text{nm}} = 445 \text{ M}^{-1}\text{cm}^{-1}$ ) and to check for the absence of  $\text{NHCl}_2$  at  $\lambda = 295 \text{ nm}$  ( $\varepsilon_{295\text{nm}} = 267 \text{ M}^{-1}\text{cm}^{-1}$ ), which could alter the transformation kinetics of ranitidine.<sup>137,138</sup> In reaction mixtures containing ranitidine or NDMA,  $\text{NH}_2\text{Cl}$  was quantified photometrically with 2,2'-azino-bis(3-ethylbenzothiazoline-6-sulfonic acid) di-ammonium salt (ABTS) using potassium iodide (KI) as catalyst. Prior to reagent addition, samples were diluted to  $\text{NH}_2\text{Cl}$  concentrations of 1 - 10  $\mu\text{M}$ .  $\text{NH}_2\text{Cl}$  oxidizes iodide to hypoiodous acid, which reacts with ABTS. The colorless ABTS is oxidized to a stable, green colored radical ( $\text{ABTS}^{\bullet+}$ ), which was quantified photometrically at  $\lambda = 405 \text{ nm}$  ( $\varepsilon_{405\text{nm}} = 28500 \pm 950 \text{ M}^{-1}\text{cm}^{-1}$ ).<sup>139</sup>

## 2.2.4 Stable isotope analysis

C, N, and H isotope measurements of NDMA, NDEA, NDPA, NDBA, and NPYR in ethyl acetate were conducted with a TRACE GC coupled to an isotope ratio mass spectrometer (GC/IRMS) via a GC Combustion III interface (Thermo). GC setup and temperature program were identical to GC/MS analysis except for a larger inner diameter of the postcolumn (320  $\mu\text{m}$ ). For all  $\delta^{13}\text{C}$  and  $\delta^{15}\text{N}$  measurements, a self-made Ni/Ni/Pt reactor<sup>111</sup> was operated at 1000°C and reoxidized for 20 min with a continuous  $\text{O}_2$  stream after every measurement. For N isotope analysis, a standard reduction reactor (Thermo) was operated at 650°C and liquid  $\text{N}_2$  was used for cryogenic trapping of  $\text{CO}_2$ . Isotope ratio analysis of H was achieved by pyrolysis using a non-porous alumina tube reactor heated to 1440°C. A GC/IRMS chromatogram for C isotope analysis is shown in Figure S2.1.

$\delta^{13}\text{C}$ ,  $\delta^{15}\text{N}$ , and  $\delta^2\text{H}$  values are reported relative to Vienna PeeDee Belemnite, air, and Vienna standard mean ocean water, respectively.

$$\delta^h\text{E} = \frac{R(^h\text{E}/^l\text{E})_{\text{sample}}}{R(^h\text{E}/^l\text{E})_{\text{standard}}} - 1 \quad (2.1)$$

where  $\delta^h\text{E}$  is the isotope signature of the respective element, and  $R(^h\text{E}/^l\text{E})$  are the isotope ratios of heavy ( $h$ ) and light ( $l$ ) isotopes in sample or standard.<sup>140</sup> If not stated otherwise, isotope signatures are reported as arithmetic mean of triplicate measurements. The trueness of isotope measurements is expressed as  $\Delta^h\text{E}$ , which is the deviation of isotope signatures measured by GC/IRMS ( $\delta^h\text{E}_{\text{GC/IRMS}}$ ) from reference isotope signatures of in-house standards (NDEA, NDPA, NDBA, NPYR) determined independently by elemental analyzer IRMS ( $\delta^h\text{E}_{\text{EA/IRMS}}$ ).

$$\Delta^h\text{E} = \delta^h\text{E}_{\text{GC/IRMS}} - \delta^h\text{E}_{\text{EA/IRMS}} \quad (2.2)$$

The deviation of isotope signatures measured after solid-phase extraction (SPE-GC/IRMS) is reported from isotope signatures of *N*-nitrosamine in-house standards measured by GC/IRMS ( $\Delta_{\text{Std}}^h\text{E}$ ).

We used a series of 14 different compounds with known isotopic composition (TableS2.1) from A. Schimmelmann (Indiana University, USA) to calibrate C, N, and H isotope ratios in the following ranges:  $\delta^{13}\text{C}$  from  $-55\text{‰}$  to  $+8\text{‰}$ ;  $\delta^{15}\text{N}$  from  $-6\text{‰}$  to  $+41\text{‰}$ ;  $\delta^2\text{H}$  from  $-230\text{‰}$  to  $+500\text{‰}$  (TableS2.1). Method quantification limits (MQLs) for accurate isotope analysis of *N*-nitrosamines were defined with the moving mean method using uncertainty intervals of  $\pm 0.5\text{‰}$ ,  $\pm 1\text{‰}$ , and  $\pm 5\text{‰}$  for C, N, and H isotope analysis, respectively.<sup>87,111,141</sup> We calculated operational conversion efficiencies of *N*-nitrosamines to the analyte gases ( $\text{CO}_2$ ,  $\text{N}_2$ , and  $\text{H}_2$ ) in the combustion interface between GC and IRMS. For this reason, we established linear regressions of peak areas in Vs at the respective  $m/z$  ratios (44, 28, and 2) vs. the nominal amount of injected mass of C, N, and, H, respectively.<sup>111</sup>

## Quantitative deuterium NMR spectroscopy

The site-specific deuterium abundance of the  $\text{N}(\text{CH}_3)_2$ -group of ranitidine was determined by quantitative deuterium nuclear magnetic resonance (NMR) spectroscopy. The NMR sample was prepared by dissolving ranitidine hydrochloride (150 mg) in a water-ethanol mixture (1:2, v:v, 600  $\mu\text{L}$ ) containing 0.8 M sodium bicarbonate. The  $^2\text{H}/^1\text{H}$

ratio of the methyl group of the ethanol was calibrated by comparison of its NMR signal to tetramethylurea (Joint Research Centre of the European commission, Geel, Belgium,  $^2\text{H}/^1\text{H}$  ratio =  $153.7 (\pm 0.8) \times 10^{-6}$ ). A  $\text{C}_6\text{F}_6$  capillary was added for locking. Deuterium NMR spectra with proton decoupling were recorded at 323 K on an Avance III 850 spectrometer (Bruker, Fällanden, Switzerland) equipped with a cryogenic probe optimized for deuterium detection and with  $^{19}\text{F}$  lock. A recycle time of 7.4 s ( $7 T_1$ ) was chosen to ensure complete relaxation. Spectra were processed in the program Topspin (version 3.2; Bruker) using exponential line-broadening; signal integrals were determined by deconvolution. To determine the  $^2\text{H}/^1\text{H}$  ratio of the  $\text{N}(\text{CH}_3)_2$  group, the integral of its  $^2\text{H}$  signal was compared to the methyl group of ethanol, taking into account the compounds' molar ratio determined by  $^1\text{H}$  NMR on the same sample. Error estimates include standard errors of the ethanol calibration and of the ranitidine measurements. The  $^2\text{H}/^1\text{H}$  ratio of the  $\text{N}(\text{CH}_3)_2$  group was expressed as  $\delta^2\text{H}$  value relative to Vienna standard mean ocean water.

### 2.2.5 NDMA formation experiments

Experiments were carried out in 14 amber glass bottles containing 1 L of 10 mM phosphate buffer (pH = 8.0), to which we added 100  $\mu\text{L}$  of a 30 mM methanolic stock solution of ranitidine. Initial ranitidine concentrations were 3  $\mu\text{M}$ . To initiate the NDMA forming reaction, we added 1.5 mL of a 30 mM aqueous solution of  $\text{NH}_2\text{Cl}$  to each reactor to obtain a final concentration of 45  $\mu\text{M}$ . At predefined time points, we measured the  $\text{NH}_2\text{Cl}$  concentration with ABTS as well as the solution pH. Reactions were quenched by adding 1 g of  $\text{Na}_2\text{S}_2\text{O}_3$ . All samples were stored in the dark at 4°C until concentration and isotope analysis. Two types of control experiments were set up identically except for addition of  $\text{NH}_2\text{Cl}$  and ranitidine. In the absence of  $\text{NH}_2\text{Cl}$ , we quantified the recovery of ranitidine. The second control experiment enabled us to quantify the pseudo-first order decay rate constant of  $\text{NH}_2\text{Cl}$  over a time period of 30 h ( $0.004 \text{ h}^{-1}$ ) in the absence of ranitidine. All  $\text{NH}_2\text{Cl}$  concentrations measured in NDMA formation experiments were corrected by taking into account the self-decay of  $\text{NH}_2\text{Cl}$ . From the disappearance kinetics of ranitidine, we calculated the second-order rate constant for its reaction with  $\text{NH}_2\text{Cl}$ .

## 2.3 Results and Discussion

### 2.3.1 C, N, and H isotope analysis of *N*-nitrosamines

We developed a procedure for stable C, N, and H isotope analysis of *N*-nitrosodimethylamine (NDMA) and four additional *N*-nitrosamines, namely *N*-nitrosodiethylamine (NDEA), -dipropylamine (NDPA), -dibutylamine (NDBA), and -pyrrolidine (NPYR). The latter four *N*-nitrosamines are available in Europe in chemically pure form and were used as isotopic reference materials, whereas NDMA can only be purchased as dilute solution. As we will show in the following sections, C, N, and H isotope signatures ( $\delta^{13}\text{C}$ ,  $\delta^{15}\text{N}$ , and  $\delta^2\text{H}$ ) of NDMA could be determined with high precision from solutions containing at least 0.1, 0.4, and 0.6 mM of NDMA, respectively.

#### Carbon isotope analysis

C isotope ratio measurements of *N*-nitrosamines by GC/IRMS were very reproducible over a time period of 8 months (Figures 2.1a and S2.2). The  $\delta^{13}\text{C}$  values of *N*-nitrosamines ranged from  $-25.8 \pm 0.3\text{‰}$  to  $-40.6 \pm 0.3\text{‰}$  and showed good precisions (expressed as  $\pm$  one standard deviation) of  $\leq \pm 0.3\text{‰}$  ( $n = 161$ , Table 2.1). As shown in Figure 2.1b,  $\delta^{13}\text{C}$  of NDEA, NDPA, NDBA, and NPYR measured with GC/IRMS were slightly larger than  $\delta^{13}\text{C}$  reference signatures determined by EA/IRMS.  $\delta^{13}\text{C}$  of NDEA, NDPA, and NPYR showed a small and reproducible offset ( $\Delta^{13}\text{C}$ ) of  $+0.8 \pm 0.2\text{‰}$ ,  $+1.1 \pm 0.4\text{‰}$ , and  $+1.5 \pm 0.3\text{‰}$ , respectively (Table 2.1). The trueness of C isotope measurements of NDBA was within the typical total uncertainty of  $\pm 0.5\text{‰}$ .<sup>142</sup>

We calculated operational conversion efficiencies of *N*-nitrosamines to  $\text{CO}_2$  in the IRMS as area of the  $m/z$  44 signal per nominally injected mass of C.<sup>111</sup> Conversion efficiencies of NDMA, NDEA, NDPA, and NDBA ranged from 7.5 to 10.2 Vs/nmol C (Figure S2.3). A lower value of 5.6 Vs/nmol C was found for NPYR what might be due to less efficient combustion of the heterocyclic ring to  $\text{CO}_2$ . Conversion efficiencies of all *N*-nitrosamines were higher than those of four benzotriazole derivatives (3.7 to 5.0 Vs/nmol C) and dodecane (5.9 Vs/nmol C) determined recently with the same type of Ni/Pt combustion reactor.<sup>111</sup> This comparison suggests that *N*-nitrosamines can be efficiently transformed into analyte gases enabling a sensitive measurement by IRMS. High conversion efficiencies were, however, not necessarily a measure for greater accuracy of isotope ratio measurements. For example, the  $\Delta^{13}\text{C}$  of NPYR ( $+1.5 \pm 0.3\text{‰}$ ) exceeded that of benzotriazole ( $+0.5 \pm 1.0\text{‰}$ <sup>111</sup>) despite a  $\approx 50\%$  more efficient combustion (5.6 vs. 3.7 Vs/nmol C).

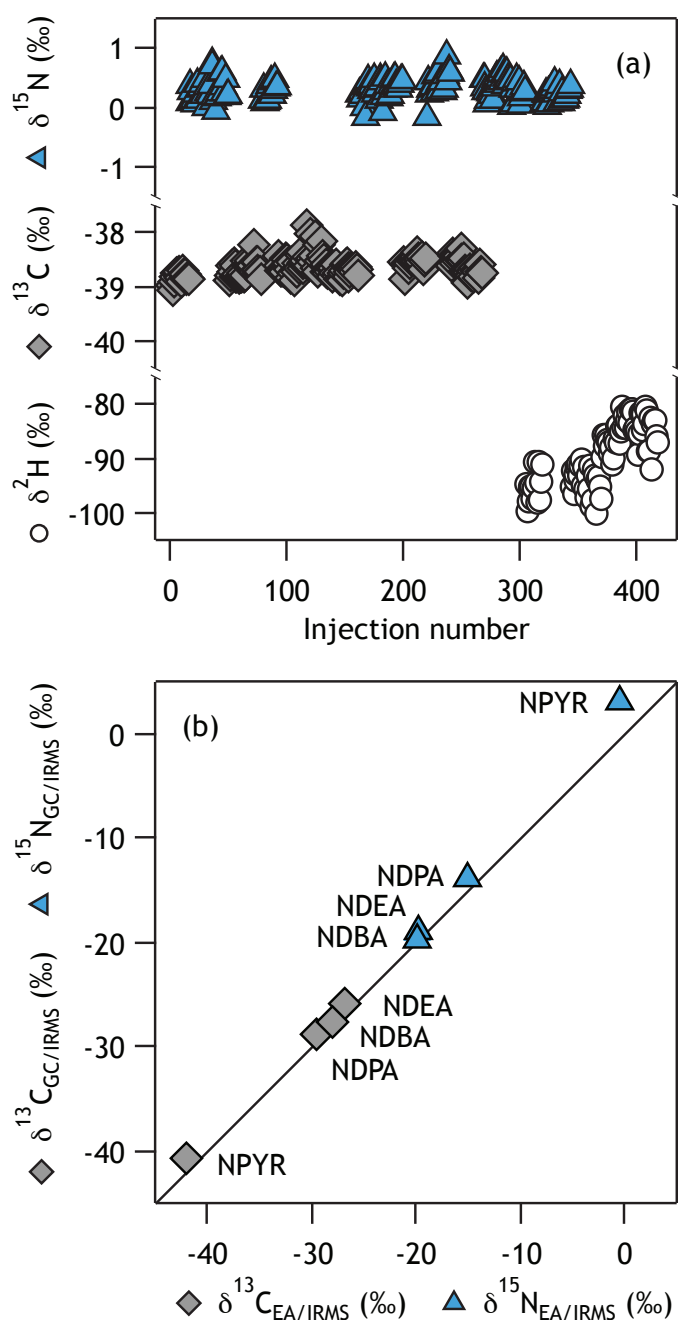


**Figure 2.1:** (a) Long-term reproducibility of 430 measurements of  $\delta^{13}\text{C}$ ,  $\delta^{15}\text{N}$ , and  $\delta^2\text{H}$  of *N*-nitrosodimethylamine (NDMA) by GC/IRMS over a total time period of 12 months. (b) Comparison of  $\delta^{13}\text{C}$  and  $\delta^{15}\text{N}$  values of *N*-nitrosodiethylamine (NDEA), *N*-nitrosodipropylamine (NDPA), *N*-nitrosodibutylamine (NDBA), and *N*-nitrosopyrrolidine (NPYR) measured by GC/IRMS vs. values obtained from analysis of the pure compound by EA/IRMS.

Finally, we determined method quantification limits (MQLs) for C isotope analysis of *N*-nitrosamines. MQLs represent the lowest analyte concentration with which  $\delta^{13}\text{C}$  can be determined accurately given the typical total uncertainty of C isotope ratio measurements of  $\pm 0.5\text{‰}$  (see Jochmann et al.<sup>141</sup> for procedural details). In Figures 2.2a and b, we show exemplarily the derivation of MQLs for NDMA and NDPA as well as the fact that their C isotope ratios can be determined reliably in a concentration range of 0.1 - 1 mM and 0.03 - 0.3 mM, respectively. Data for NDEA, NDBA, and NPYR can be found in Figure S2.4. The MQLs for all five *N*-nitrosamines are listed in Table 2.2 and range from 0.18 (for NDPA) to 0.60 nmol C (for NPYR) injected on column. As suggested by the high operational conversion efficiencies, MQLs of all *N*-nitrosamines are low. Even though comparisons across different procedures and instrumentations are difficult, our data show that MQLs for *N*-nitrosamines are substantially lower than typically reported values of 0.8 - 1 nmol C.<sup>81,111,125</sup>

### Nitrogen isotope analysis

Measurements of N isotope ratios of *N*-nitrosamines were carried out with similar precision ( $\leq \pm 0.3\text{‰}$ ,  $n = 167$ ) and reproducibility as those for C isotope ratios over one year (Figures 2.1a and S2.2).  $\delta^{15}\text{N}$  values varied more than those for  $\delta^{13}\text{C}$  and ranged from  $-19.7 \pm 0.1\text{‰}$  to  $+3.1 \pm 0.2\text{‰}$ . Figure 2.1b shows a comparison of  $\delta^{15}\text{N}$  values of NDEA, NDPA, NDBA, and NPYR determined by GC/IRMS with data from pure compound analysis by EA/IRMS. For NDEA and NDBA, deviations of N isotope ratio measurements by GC/IRMS were within typical uncertainties of  $\pm 1\text{‰}$  (Table 2.1).  $\delta^{15}\text{N}$  values of NDPA and NPYR, in contrast, showed a very reproducible off-set by  $+1.3 \pm 0.1\text{‰}$  and  $+3.6 \pm 0.5\text{‰}$  (Table 2.1). An elucidation of the origins of the offsets is beyond the scope of this work.

Operational  $\text{N}_2$ -conversion efficiencies to the analyte gas  $\text{N}_2$  were between 2.8 Vs/nmol N for NDMA and NPYR and 3.7 Vs/nmol N for NDPA (Figure S2.3). Our numbers for *N*-nitrosamines are again higher than  $\text{N}_2$ -conversion efficiencies for previous measurements of aromatic amines (0.8 - 1.7 Vs/nmol N) and benzotriazoles (1.7 - 2.2 Vs/nmol N).<sup>111</sup> This observation supports the above interpretation of high  $\text{CO}_2$ -conversion efficiencies.

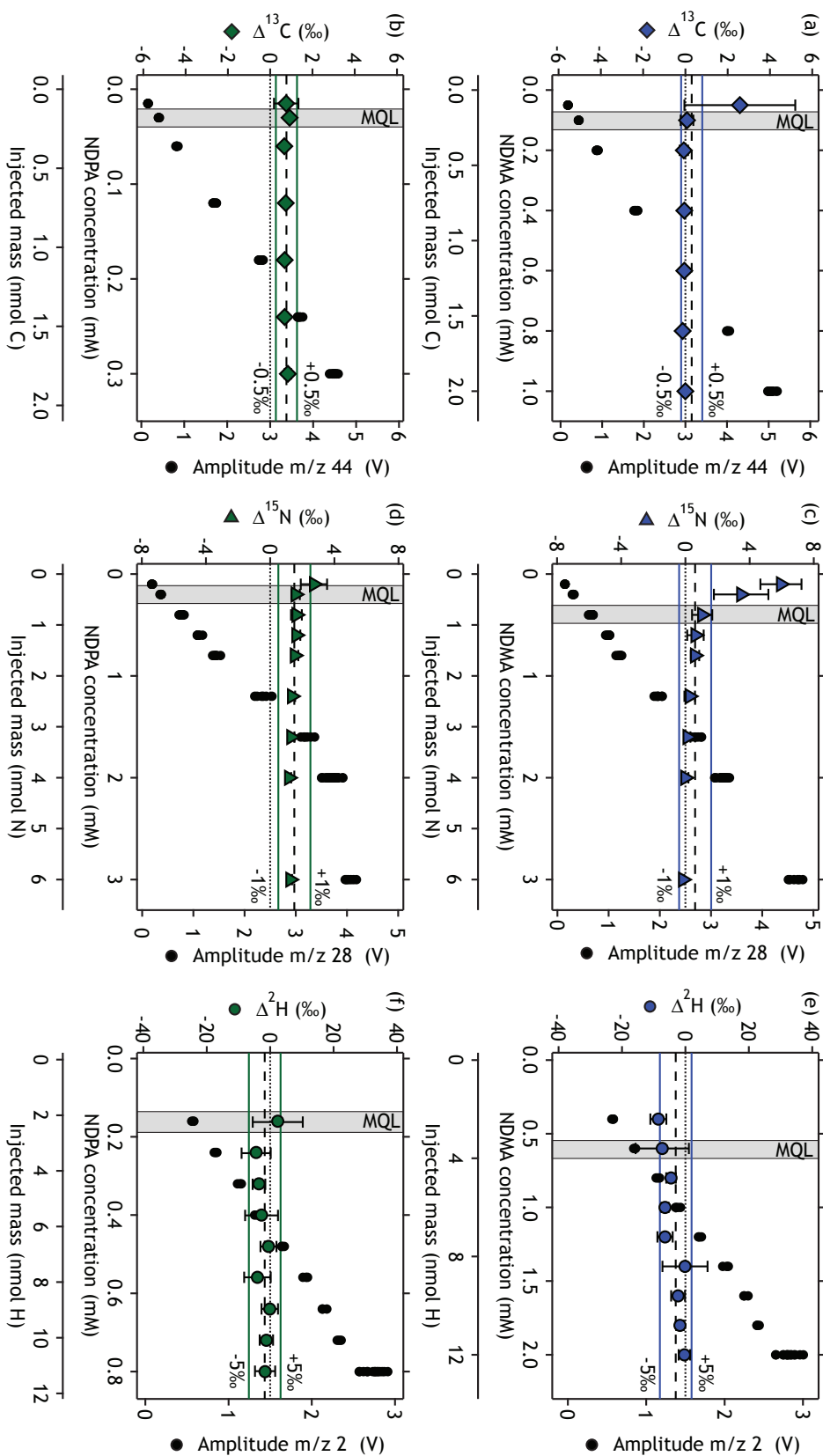


**Figure 2.2:** Accuracies of C, N, and H isotope signatures as function of (a, c, e) NDMA and (b, d, f) NDPA concentration. For NDPA, accuracies are expressed as deviations from isotopic reference signatures. Because of the absence of an isotopic reference standard for NDMA, accuracies are expressed as deviation from the mean isotope signature of a repeatedly measured NDMA at concentrations of 1 mM, 2 mM, and 1.6 mM for C, N, and H isotope analysis, respectively (see Table 2.1). MQLs were determined according to the moving mean procedure<sup>141</sup> with intervals of  $\pm 0.5\%$ ,  $\pm 1\%$ , and  $\pm 5\%$  for C, N, and H isotope analysis (colored lines), respectively. MQLs are indicated by gray bars and moving means by dashed lines.



**Table 2.1:** C, N, and H isotope signatures ( $\delta^{13}\text{C}$ ,  $\delta^{15}\text{N}$ , and  $\delta^2\text{H}$ ) of *N*-nitrosamines measured by GC/IRMS and their deviations from reference isotope signatures measured by EA/IRMS ( $\Delta^{13}\text{C}$ ,  $\Delta^2\text{H}$ ,  $\Delta^{15}\text{N}$ ). Deviations of isotope signatures measured after solid-phase extraction (SPE-GC/IRMS, method 2) and after ethyl acetate evaporation from 10 to 1 mL are reported for GC/IRMS measurements of *N*-nitrosamine in-house standards ( $\Delta_{\text{Std}}^{13}\text{C}$ ,  $\Delta_{\text{Std}}^{15}\text{N}$ , and  $\Delta_{\text{Std}}^2\text{H}$ ).

Compound	$\delta^{13}\text{C}$ (‰)		$\Delta^{13}\text{C}$ <sup>a,b</sup> (‰)		$\Delta_{\text{Std}}^{13}\text{C}$ <sup>c</sup> (‰)	
	EA/IRMS <sup>d</sup>	GC/IRMS <sup>b</sup>		after SPE <sup>e</sup>	after solvent evaporation <sup>e</sup>	
NDMA	<sup>-f</sup>	-38.6 ± 0.2	<sup>-f</sup>	0.2 ± 0.1	<0.1 ± 0.2	
NDEA	-26.9 ± 0.2	-25.8 ± 0.3	1.1 ± 0.4	-0.2 ± 0.1	<0.1 ± 0.3	
NDPA	-29.6 ± 0.1	-28.8 ± 0.2	0.8 ± 0.2	<0.1 ± 0.3	0.3 ± 0.1	
NDBA	-28.1 ± 0.1	-27.6 ± 0.2	0.5 ± 0.2	0.2 ± 0.4	0.4 ± 0.2	
NPYR	-42.1 ± 0.1	-40.6 ± 0.3	1.5 ± 0.3	0.2 ± 0.2	0.2 ± 0.2	
$\delta^{15}\text{N}$ (‰)						
	GC/IRMS <sup>e</sup>		$\Delta^{15}\text{N}$ <sup>a,g</sup> (‰)		$\Delta_{\text{Std}}^{15}\text{N}$ <sup>c</sup> (‰)	
	EA/IRMS <sup>d</sup>	GC/IRMS <sup>e</sup>		after SPE <sup>h</sup>	after solvent evaporation <sup>e</sup>	
NDMA	<sup>-f</sup>	0.3 ± 0.2	<sup>-f</sup>	0.7 ± 0.2	0.5 ± 0.3	
NDEA	-19.8 ± 0.1	-18.9 ± 0.3	0.9 ± 0.3	0.3 ± 0.1	0.3 ± 0.1	
NDPA	-15.1 ± 0.1	-13.8 ± 0.1	1.3 ± 0.1	0.1 ± 0.1	0.1 ± 0.1	
NDBA	-19.9 ± 1.2	-19.7 ± 0.1	0.2 ± 1.2	0.1 ± 0.1	0.1 ± 0.1	
NPYR	-0.5 ± 0.5	3.1 ± 0.2 <sup>i</sup>	3.6 ± 0.5 <sup>i</sup>	<0.1 ± 0.4	0.2 ± 0.3	
$\delta^2\text{H}$ (‰)						
	GC/IRMS <sup>j</sup>		$\Delta_{\text{Std}}^2\text{H}$ <sup>c</sup> (‰)			
				after SPE <sup>h</sup>	after solvent evaporation <sup>e</sup>	
NDMA	<sup>-f</sup>	-89.2 ± 5.8	<sup>-f</sup>	0.4 ± 2.8	0.4 ± 3.7	
NDEA	<sup>-f</sup>	-173.0 ± 6.4	<sup>-f</sup>	0.8 ± 2.9	1.7 ± 5.1	
NDPA	<sup>-f</sup>	-145.0 ± 4.8	<sup>-f</sup>	1.4 ± 3.1	0.7 ± 2.6	
NDBA	<sup>-f</sup>	-179.4 ± 5.6	<sup>-f</sup>	2.4 ± 2.4	0.4 ± 1.5	
NPYR	<sup>-f</sup>	-221.8 ± 4.2	<sup>-f</sup>	-0.5 ± 2.9	3.6 ± 2.8	

<sup>a</sup> Trueness is expressed as mean deviation of isotope signatures measured with GC/IRMS from reference isotope signatures determined by EA/IRMS. <sup>b</sup> n = 161 <sup>c</sup> Deviation from repeatedly measured *N*-nitrosamine in-house standards by GC/IRMS

<sup>d</sup> n = 5 <sup>e</sup> n = 9 <sup>f</sup> no EA-value <sup>g</sup> n = 167 <sup>h</sup> n = 18 <sup>i</sup> n = 166 <sup>j</sup> n = 89-90



The efficient conversion of *N*-nitrosamines is reflected in low MQLs for N isotope analysis. Figures 2.2c and d show the wide concentration range for which  $\delta^{15}\text{N}$  of NDMA (0.4-3 mM) and NDPA (0.2-3 mM) could be determined accurately. Based on an uncertainty interval of  $\pm 1\%$ , we derived MQLs for all five *N*-nitrosamines. MQLs amount to 0.40-0.80 nmol N injected on column (Table 2.2, Figure S2.4) and did not show any specific trend with the type of *N*-nitrosamine.

### Hydrogen isotope analysis

H isotope signatures of *N*-nitrosamines were determined over a time period of 2 months with precisions between  $\pm 4.2$  to  $\pm 6.4\%$  ( $n = 90$ , Table 2.1). This uncertainty is within the range of reported precisions for  $\delta^2\text{H}$  of  $\pm 5\%$ .<sup>81</sup>  $\delta^2\text{H}$  values of the *N*-nitrosamines were distinctly different between  $-222 \pm 4\%$  to  $-89 \pm 6\%$  (Table 2.1, Figures 2.1a and S2.2). The conversion to  $\text{H}_2$  was most efficient for NDEA (0.95 Vs/nmol H) and NDPA (0.94 Vs/nmol H), but the differences among the five *N*-nitrosamines were small (i.e., 0.8 Vs/nmol H for NDBA, NPYR, and NDMA, Figure S2.3). Figures 2.2e and f show the operational concentration ranges for accurate H isotope analysis of NDMA (0.6-2 mM) and NDPA (0.2-0.8 mM). MQLs determined for all *N*-nitrosamines with an uncertainty interval of  $\pm 5\%$  were between 2.2 nmol H (for NDPA) and 5.8 nmol H (for NPYR) injected on column (Table 2.2, Figure S2.4). Note that despite widespread application of  $\delta^2\text{H}$ -analysis of organic compounds by GC/IRMS,<sup>86</sup> only few MQLs for  $\delta^2\text{H}$  determination<sup>93,104</sup> and no  $\text{H}_2$ -conversion efficiencies have been reported so far.

**Table 2.2:** Method quantification limits (MQL) for C, N, and H isotope analysis of *N*-nitrosamines and corresponding amplitudes (Amp) determined according to the moving mean procedure<sup>141</sup> with intervals of  $\pm 0.5\%$ ,  $\pm 1\%$ , and  $\pm 5\%$ , respectively. MQLs are expressed as concentrations of the *N*-nitrosamine solutions and as corresponding masses of C, N, and H injected on column.

	$\delta^{13}\text{C}$			$\delta^{15}\text{N}$			$\delta^2\text{H}$		
	MQL		Amp 44	MQL		Amp 28	MQL		Amp 2
	(mM)	(nmol C)	(mV)	(mM)	(nmol N)	(mV)	(mM)	(nmol H)	(mV)
NDMA	0.10	0.20	440±10	0.40	0.80	670±30	0.60	3.6	850±10
NDEA	0.10	0.40	930±20	0.40	0.80	750±40	0.30	3.0	790±10
NDPA	0.03	0.18	400±10	0.20	0.40	370±10	0.16	2.2	570±10
NDBA	0.03	0.24	480±10	0.20	0.40	320±10	0.24	4.3	860±20
NPYR	0.12	0.60	790±20	0.20	0.40	270±10	0.72	5.8	1210±30

### 2.3.2 C, N, and H isotope analysis of *N*-nitrosamines after solid-phase extraction (SPE) from aqueous samples

Even though several SPE procedures for the analysis of *N*-nitrosamines with GC/- or LC/MS analysis exist, none of them addressed the consequences for stable isotope ratios of the analytes. We modified two existing SPE methods<sup>135,136</sup> described above and compared their performance for the enrichment of *N*-nitrosamines from 1 L of tap water and from buffered aqueous solutions. Method 1 is based on the use of activated carbon as sorbent, whereas method 2 relies on a combination of Oasis HLB with coconut charcoal. No difference was observed for extraction from tap water vs. buffered solution and the average recoveries are reported in Table S2.2. Both methods performed equally well for the extraction of NDEA, NDPA, and NDBA and recoveries ranged from  $77 \pm 3\%$  to  $83 \pm 6\%$  (method 1) and  $79 \pm 11\%$  to  $86 \pm 4\%$  (method 2, Table S2.2). With method 1, however, we obtained a NDMA recovery of only  $31 \pm 6\%$ . In contrast, NDMA recoveries with method 2 were within the range found for the other *N*-nitrosamines, that is  $88 \pm 3\%$ . Note that the SPE-procedure with NPYR was only conducted with method 2 and showed the same recovery as for NDMA (Table S2.2). Owing to the higher NDMA recovery, we evaluated SPE method 2 coupled to GC/IRMS analysis in terms of measurement accuracy.

The deviation of C, N, and H isotope signatures of the *N*-nitrosamines after solid-phase extraction with method 2 from GC/IRMS reference values are denoted as  $\Delta_{\text{Std}}^{13}\text{C}$ ,  $\Delta_{\text{Std}}^{15}\text{N}$ , and  $\Delta_{\text{Std}}^2\text{H}$  and are shown in Table 2.1. Neither the SPE procedure, nor evaporation of the final SPE eluates from 10 mL of ethyl acetate to 1 mL induced any significant isotope fractionation in one of the *N*-nitrosamines. All  $\Delta_{\text{Std}}^h\text{E}$  values were within total uncertainties of  $\pm 0.5\text{‰}$ ,  $\pm 1\text{‰}$ , and  $\pm 5\text{‰}$  for C, N, and H isotope analysis, respectively (Table 2.1). The SPE-GC/IRMS procedure based on SPE method 2 was therefore considered suitable for C, N, and H isotope analysis of *N*-nitrosamines in aqueous samples.

### 2.3.3 Tracking NDMA isotope signatures during water chloramination

Figure 2.3a shows the kinetics of NDMA formation during chloramination of ranitidine at pH 8 for 48 hours. Ranitidine disappearance followed pseudo-first order kinetics (Figure S2.5) due to a 17-fold excess of  $\text{NH}_2\text{Cl}$ . The corresponding second-order rate constant for the reaction of ranitidine with  $\text{NH}_2\text{Cl}$  was  $9.5 \pm 0.3 \text{ M}^{-1}\text{s}^{-1}$ . Compared

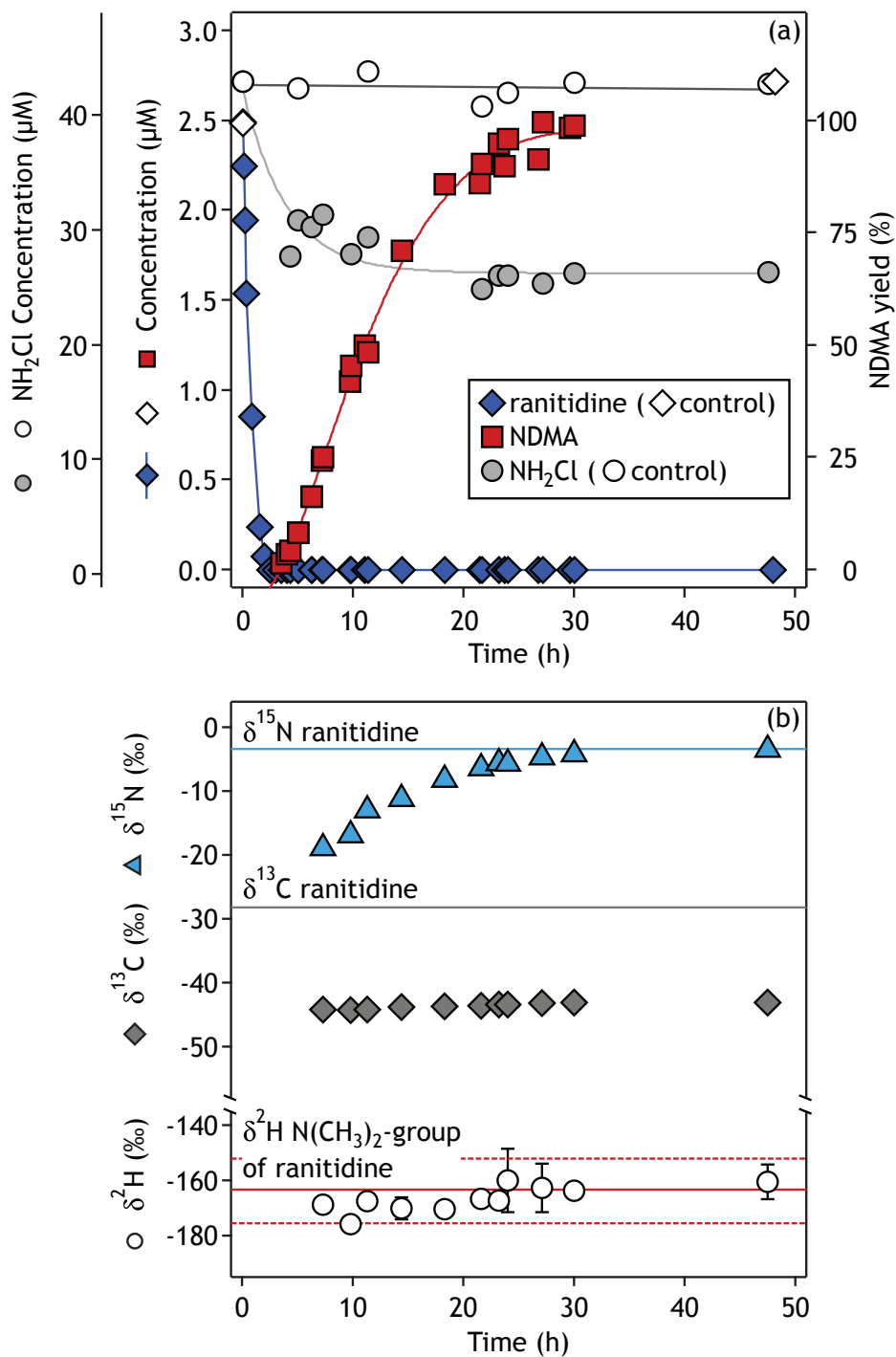


**Figure 2.3:** (a) NDMA formation from reaction of  $2.5 \mu\text{M}$  ranitidine with  $43 \mu\text{M}$   $\text{NH}_2\text{Cl}$  at pH 8.0 and (b) C, N, and H isotope signatures of NDMA (data points) measured by GC/IRMS. Standard deviations of all C and N isotope measurements were  $\leq 0.2\text{‰}$  and are not shown here. The blue and gray line represent the bulk average  $\delta^{13}\text{C}$  and  $\delta^{15}\text{N}$  values of ranitidine used in the chloramination experiment. The red line represents the  $\delta^2\text{H}$  value of H atoms in the  $\text{N}(\text{CH}_3)_2$ -moiety of ranitidine from NMR measurements.

to the measured initial ranitidine concentration ( $2.5\ \mu\text{M}$ ), the molar NDMA yield was  $97 \pm 4\%$ . Previously reported NDMA yields were based on *nominal* ranitidine concentrations and amounted to up to 80% for experiments conducted at the same pH but with  $\text{NH}_2\text{Cl}$  in 10'000-fold excess.<sup>76</sup>

Figure 2.3b illustrates the trends of C, N, and H isotope signatures in NDMA over the course of 48 hours.  $\delta^{15}\text{N}$  values increased, that is they became less negative as NDMA formed. In contrast,  $\delta^{13}\text{C}$  and  $\delta^2\text{H}$  values remained largely constant throughout the experiment. This observation implies that the C–H bonds in the  $\text{N}(\text{CH}_3)_2$ -group were not directly involved in the elementary reaction step leading to NDMA. The H isotope signature of  $-168 \pm 8\text{‰}$  represents the average  $\delta^2\text{H}$  value of the 6 H atoms in NDMA. This number is identical within error with the  $\delta^2\text{H}$  value of the H atoms in the  $\text{N}(\text{CH}_3)_2$ -group of ranitidine determined by quantitative deuterium NMR ( $-163 \pm 12\text{‰}$ ). Because NDMA was formed stoichiometrically from ranitidine, one can assume that every  $\text{N}(\text{CH}_3)_2$ -moiety of ranitidine was transformed to NDMA. The agreement of  $\delta^2\text{H}$  values for the  $\text{N}(\text{CH}_3)_2$ -group in NDMA and ranitidine therefore confirms the trueness of isotope ratio measurements by SPE-GC/IRMS.

The constant  $\delta^{13}\text{C}$  values of NDMA ( $-43.7 \pm 0.6\text{‰}$ , Figure 2.3b) also support the above hypothesis that the  $\text{N}(\text{CH}_3)_2$ -group in ranitidine remains intact during conversion to NDMA. Because of the stoichiometric yield of NDMA, this value also represents the  $\delta^{13}\text{C}$  value of the  $\text{N}(\text{CH}_3)_2$ -group in ranitidine. The difference between the  $\delta^{13}\text{C}$  value of the  $\text{N}(\text{CH}_3)_2$ -group and that of the entire ranitidine molecule ( $-28.2 \pm 0.3\text{‰}$ ) was  $-15.4\text{‰}$  and shows that  $^{12}\text{C}$  and  $^{13}\text{C}$  atoms are not equally distributed over all C atoms in ranitidine. In fact,  $^{12}\text{C}$  isotopes are located preferentially in the  $\text{N}(\text{CH}_3)_2$ -group, whereas  $^{13}\text{C}$  is more likely to be found in the other 11 C atoms with an average  $\delta^{13}\text{C}$  of  $-25.4\text{‰}$ . Such site-specific C and H isotope ratios are commonly used to detect food adulterations<sup>143,144</sup> but they have only rarely been used so far to track sources of organic contaminants.<sup>145,146</sup>

The enrichment of  $^{15}\text{N}$  in NDMA from  $-18.9 \pm 0.2\text{‰}$  to  $-3.5 \pm 0.04\text{‰}$  over time hints at the mechanism of its formation reaction, even though an elucidation of NDMA formation mechanisms is beyond the scope of this study. The trend shown in Figure 2.3b is due to a strong, normal N isotope fractionation. This behavior, which was observed in various (photo)chemical and biological contaminant transformation reactions,<sup>106,108,147–152</sup> is likely associated with the cleavage of a bond to N in the rate-limiting step. We can therefore speculate that important reaction steps that may be responsible for NDMA formation such as the addition of  $\text{NH}_2\text{Cl}$  to  $\text{N}(\text{CH}_3)_2$  and its oxidation to a N-nitroso

compound,<sup>58,79</sup> happen prior to the N-bond cleavage step or are not rate-limiting. Note that the final  $\delta^{15}\text{N}$  value of NDMA matches the one for the average of 4 N atoms of ranitidine (Figure 2.3b). In contrast to the  $\delta^{13}\text{C}$  values of NDMA, the agreement of  $\delta^{15}\text{N}$  values is merely coincidental, because N isotopes are presumably distributed unevenly in ranitidine and the final  $\delta^{15}\text{N}$  value also reflects a currently unknown contribution of  $\text{NH}_2\text{Cl}$ .

## 2.4 Conclusion

Analysis of C, N, and H isotope ratios of NDMA and other *N*-nitrosamines can be made accurately using standard procedures for SPE-GC/IRMS and the proposed analytical procedure is well-suited for laboratory studies on the different mechanisms of *N*-nitrosamine formation. Current knowledge suggests that pathways to NDMA differ depending on the disinfectant used as well as on the type of precursor molecule.<sup>50</sup> However, it is currently unknown whether C, N, or H isotope fractionation trends of NDMA could be used to distinguish alternative pathways, for example those involving hydrazine intermediates<sup>55,58</sup> from nitrosation reactions.<sup>56,60,80</sup> Future work also needs to address the question whether pathway-dependent isotope fractionation changes with NDMA-yield,  $\text{NH}_2\text{Cl}$  consumption, and  $\delta^{15}\text{N}$  value of  $\text{NH}_2\text{Cl}$ .

Finally, the concentrations of NDMA in this work are approximately 1000-fold above the recommended NDMA guidance values. Substantial amounts of water thus need to be processed to obtain *N*-nitrosamines in quantities that are large enough for accurate stable isotope analysis. Solid-phase extractions of up to 10 L have been used successfully for C and N isotope ratio measurements of pesticides in the  $\mu\text{g L}^{-1}$ -range.<sup>153</sup> Similar procedures need to be developed for NDMA to exploit the information obtained from CSIA for the mitigation of NDMA and other *N*-nitrosamines in water treatment facilities.

## Acknowledgement

This work was supported by the Swiss National Science Foundation (Project no. 200021-140545). We thank Stefano Bernasconi, Stuart Bishop, and Madalina Jaggi for elemental analyzer-IRMS measurements and Saskia Zimmermann-Steffens, Fabian Soltermann, and Jennifer Schollée for experimental support and valuable discussions.



# Supporting Information to Chapter 2

## S2.1 Chemicals

All chemicals in this study were used as received. *N*-nitrosodimethylamine (NDMA, 5000  $\mu\text{g}/\text{ml}$  in methanol, 99.9%), *N*-nitrosodiethylamine (NDEA, 99.9%), *N*-nitrosodipropylamine (NDPA, 99.9%), *N*-nitrosodibutylamine (NDBA), *N*-nitrosopyrrolidine (NPYR, 99%) and ranitidine hydrochloride were purchased from Sigma-Aldrich. Analyte stock and calibration solutions were made in ethyl acetate ( $\geq 99.7\%$ , Sigma-Aldrich). Other solvents used were methanol (99.99%, Fisher Scientific), pentane ( $\geq 99.0\%$ , Sigma-Aldrich) and dichloromethane (EMSURE for analysis, Merck). Aqueous solutions were prepared with deionized water (18.1  $\text{M}\Omega \cdot \text{cm}$ , Barnstead NANOpure Diamond Water Purification System). For  $\text{NH}_2\text{Cl}$  preparation, ammonium chloride ( $\geq 99.5\%$ , Fluka) and sodium hypochlorite (6-14%  $\text{HOCl}$ , Sigma-Aldrich) were used. 2,2'-azino-bis(3-ethylbenzothiazoline-6-sulfonic acid) diammonium salt (ABTS,  $\geq 98\%$ ), sodium nitrite ( $\geq 99\%$ ), potassium iodide ( $\geq 99\%$ ), and sodium thiosulfate ( $\text{Na}_2\text{S}_2\text{O}_3$ ,  $\geq 98\%$ ) were purchased from Sigma-Aldrich. The pH-value of the potassium phosphate buffer ( $\text{KH}_2\text{PO}_4$ , puriss,  $\geq 99.5\%$ , Sigma-Aldrich) was adjusted by addition of sodium hydroxide pellets ( $\text{NaOH}$ , puriss,  $\geq 99\%$ , Sigma Aldrich) or  $\text{NaOH}$  solution (Sigma-Aldrich).

For gas chromatographic analysis helium ( $\text{He}$ , 99.999%) was used as carrier gas. GC/IRMS analysis required  $\text{CO}_2$  (99.999%) and  $\text{N}_2$  (99.999%) as reference gases as well as  $\text{O}_2$  (99.9995%) from Carbagas (Rümlang, Switzerland).

**Table S2.1:** C, N, and H isotope reference standards purchased from A. Schimmelmann (Indiana University, USA).

Compounds	Formula	$\delta^{13}\text{C}$ (‰)	$\delta^{15}\text{N}$ (‰)	$\delta^2\text{H}$ (‰)
Iodomethane #1	$\text{CH}_3\text{I}$	$-54.59 \pm 0.02$		
N-methyl-piperidine	$\text{C}_6\text{H}_{13}\text{N}$	$-33.73 \pm 0.02$		
Acetic anhydride	$\text{C}_4\text{H}_6\text{O}_3$	$-20.98 \pm 0.03$		
Icosanoic acid methyl ester #Y	$\text{C}_{21}\text{H}_{42}\text{O}_2$	$-0.72 \pm 0.02$		
Nicotine #2	$\text{C}_{10}\text{H}_{14}\text{N}_2$	$+7.72 \pm 0.02$		
Nicotine #5	$\text{C}_{10}\text{H}_{14}\text{N}_2$		$-6.03 \pm 0.04$	
N-methyl-piperidine	$\text{C}_6\text{H}_{13}\text{N}$		$+0.34 \pm 0.13$	
Acetanilide #2	$\text{C}_8\text{H}_9\text{NO}$		$+19.56 \pm 0.03$	
Acetanilide #3	$\text{C}_8\text{H}_9\text{NO}$		$+40.57 \pm 0.06$	
Ethyl myristate #n14E	$\text{C}_{16}\text{H}_{32}\text{O}_2$			$-231.2 \pm 2.7$
Heptadecane #2	$\text{C}_{17}\text{H}_{36}$			$-117.9 \pm 2.3$
N,N-dimethylaniline	$\text{C}_8\text{H}_{11}\text{N}$			$-48.2 \pm 2.2$
Hexadecane #2	$\text{C}_{16}\text{H}_{34}$			$-9.1 \pm 1.4$
Icosanoic acid methyl ester #20M	$\text{C}_{21}\text{H}_{42}\text{O}_2$			$+505.5 \pm 1.7$



## S2.2 GC/IRMS chromatogram of *N*-nitrosamines

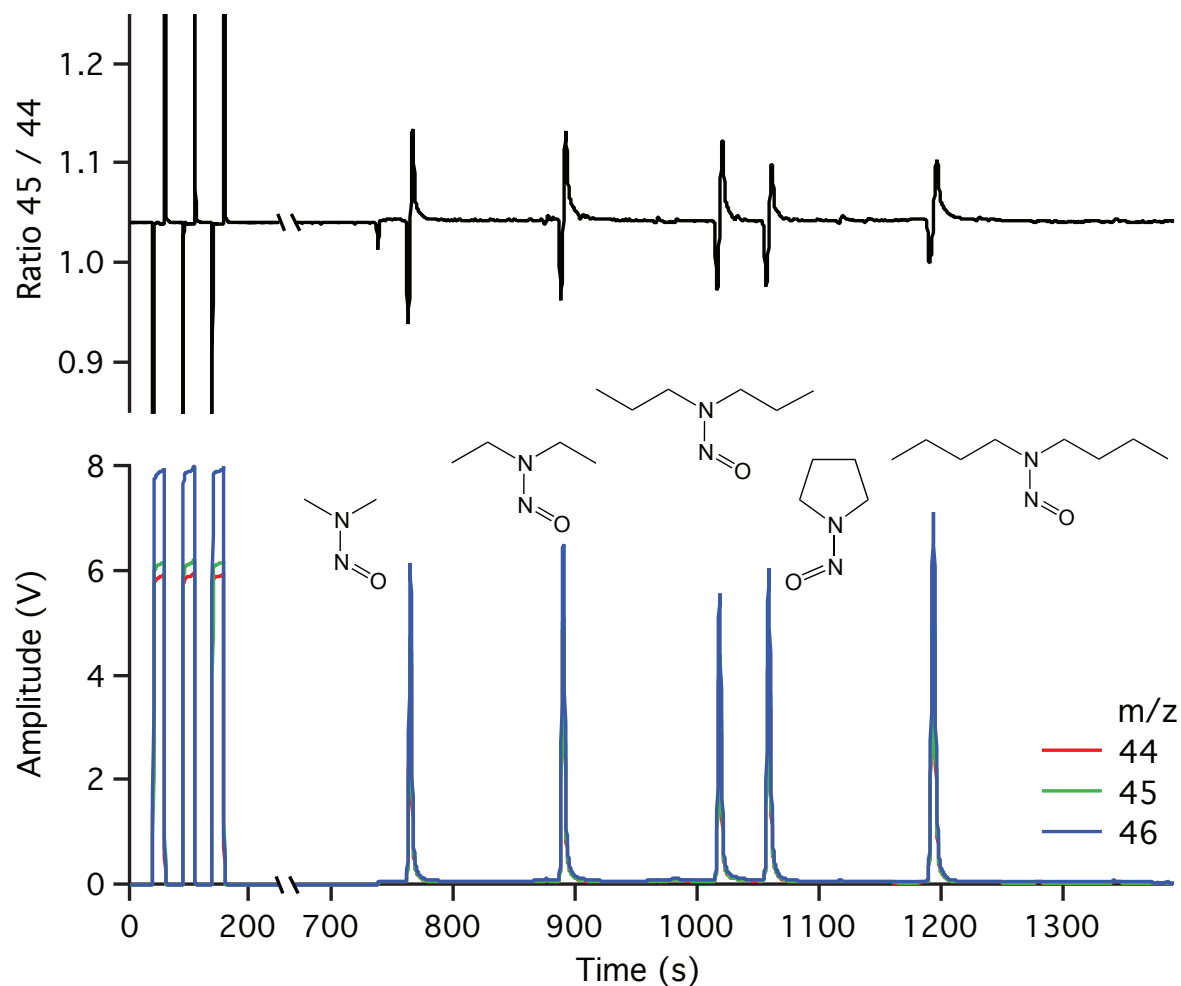


**Figure S2.1:** Chromatogram of C isotope analysis of 1 mM NDMA, 0.5 mM NDEA, 0.3 mM NDPA, 0.6 mM NPYR, and 0.3 mM NDBA as well as the S-shaped 45 / 44 ratio signal (isotope swing).

## S2.3 Reproducibility of C, N, and H isotope analysis of *N*-nitrosamines

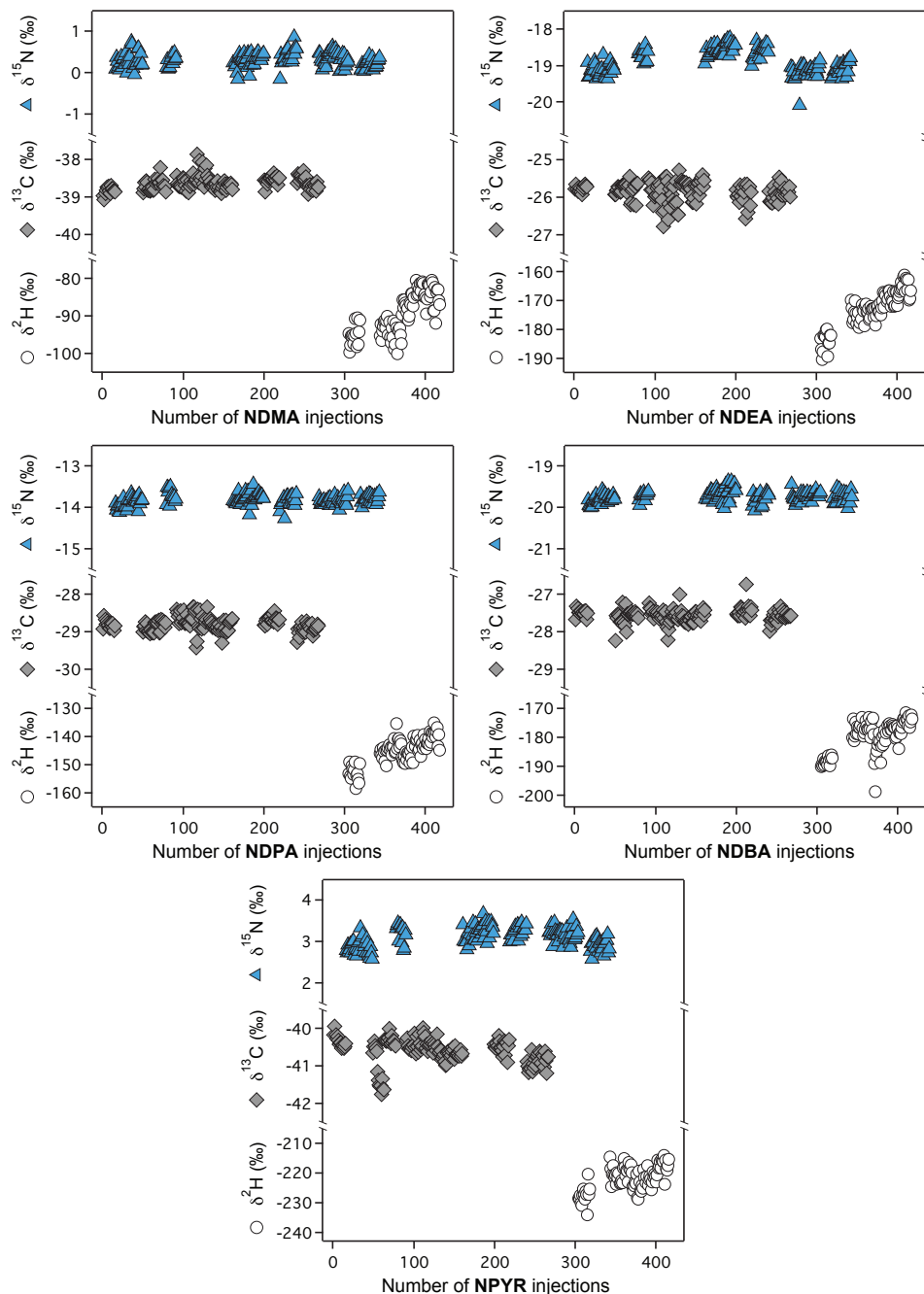


**Figure S2.2:** Reproducibility of  $\delta^{13}\text{C}$ ,  $\delta^{15}\text{N}$ , and  $\delta^2\text{H}$  measurements of NDMA, NDEA, NDPA, NDBA, and NPYR by GC/IRMS over a time period of 8 months for C, 12 months for N, and 2 months for H isotope analysis.

## S2.4 Conversion efficiency of *N*-nitrosamines to analyte gases for IRMS analysis

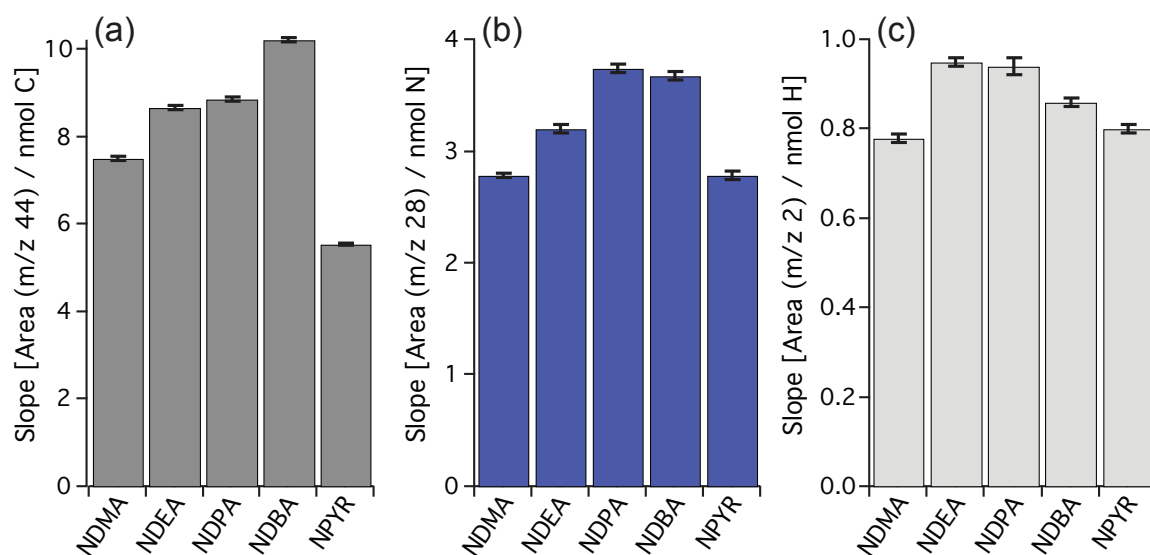


**Figure S2.3:** Operational conversion efficiencies of *N*-nitrosamines to a)  $\text{CO}_2$ , b)  $\text{N}_2$ , and c)  $\text{H}_2$  for C, N, and H isotope analysis, respectively. Conversion efficiency was defined as linear regression of peak areas in Vs at the respective m/z ratio vs. the nominal amount of injected mass of C, N, and H.

## S2.5 Method quantification limits for accurate isotope analysis of *N*-nitrosamines

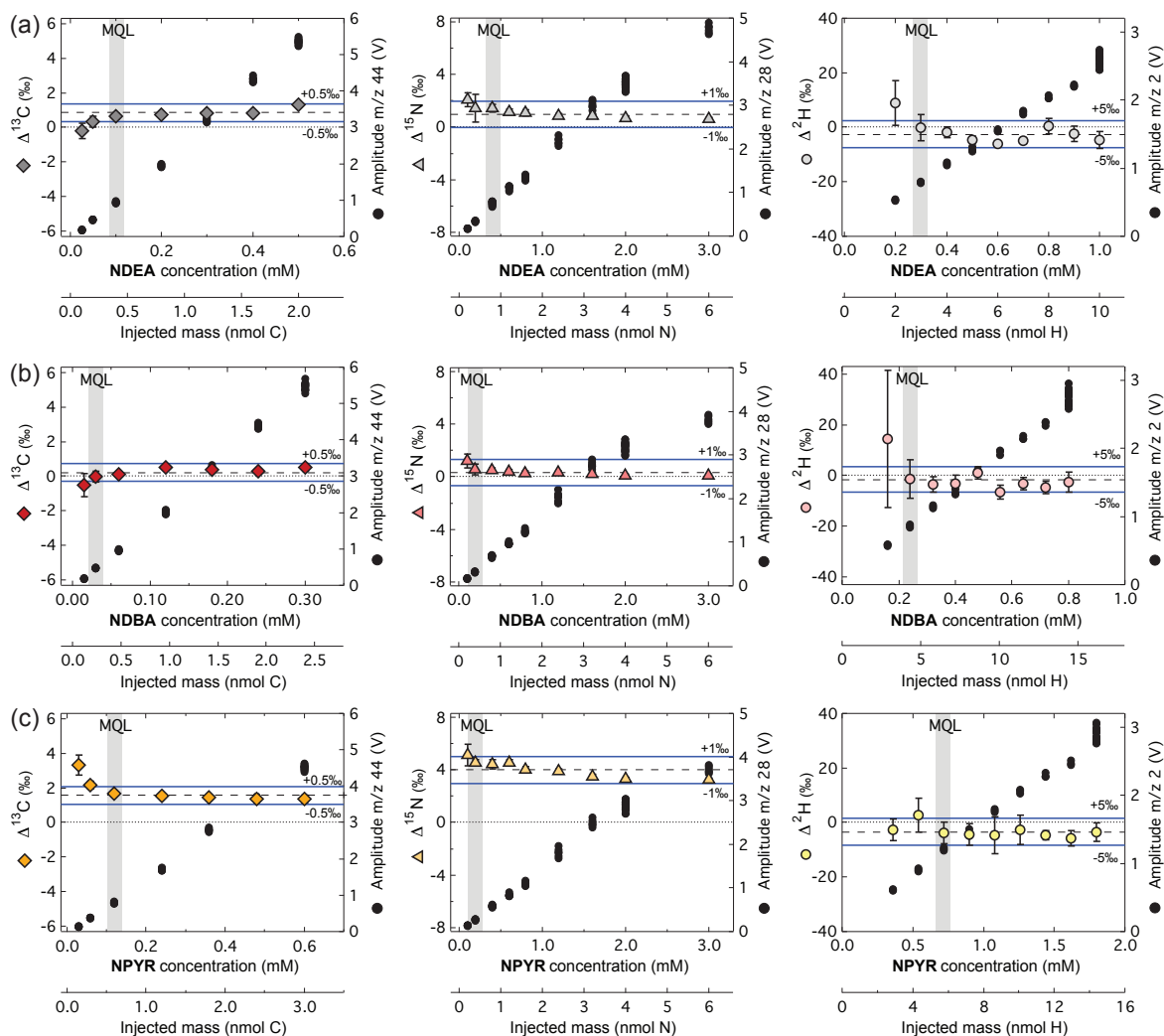


**Figure S2.4:** Accuracies of C, N, and H isotope signatures of a) NDEA, b) NDBA, and c) NPYR. Amplitudes increased linearly with increasing concentrations. MQLs were determined according to the moving mean procedure with intervals of  $\pm 0.5\text{‰}$ ,  $\pm 1\text{‰}$ , and  $\pm 5\text{‰}$  for C, N, and H isotope analysis (blue lines), respectively. MQLs are indicated by gray bars and moving means by dashed lines.

## S2.6 C, N, and H isotope analysis of *N*-nitrosamines after solid-phase extraction (SPE) from aqueous samples

**Table S2.2:** Solid-phase extraction (SPE) of *N*-nitrosamines from aqueous solution at pH 7 using Method 1 (activated carbon cartridges) and Method 2 (combination of Oasis HLB and coconut charcoal cartridges). Analyte recoveries are reported after the SPE procedure and after solvent (ethyl acetate) evaporation from 10 mL to 1 mL or to smaller volumes. Reported values are averaged recoveries from tap water and phosphate buffer.

	Recovery (%)				
	after SPE		after solvent evaporation to		
	Method 1 <sup>a</sup>	Method 2 <sup>b</sup>	1 mL	0.5 mL	0.1 mL
NDMA	31±6	88±3	83±4	71±4	51±1
NDEA	77±3	86±4	90±5	82±6	65±3
NDPA	78±4	81±10	92±7	87±6	70±0.4
NDBA	83±6	79±11	92±7	88±9	73±1
N PYR	- <sup>c</sup>	88±4	92±7	88±9	72±2

<sup>a</sup> n = 4    <sup>b</sup> n = 6    <sup>c</sup> NPYR not included in the analysis

## S2.7 NDMA formation during chloramination of ranitidine

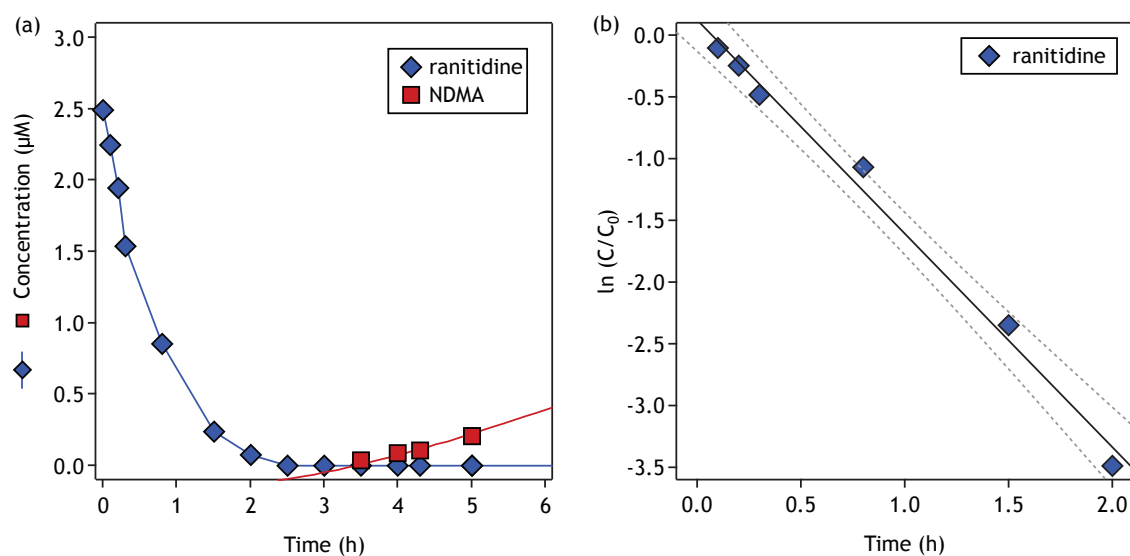
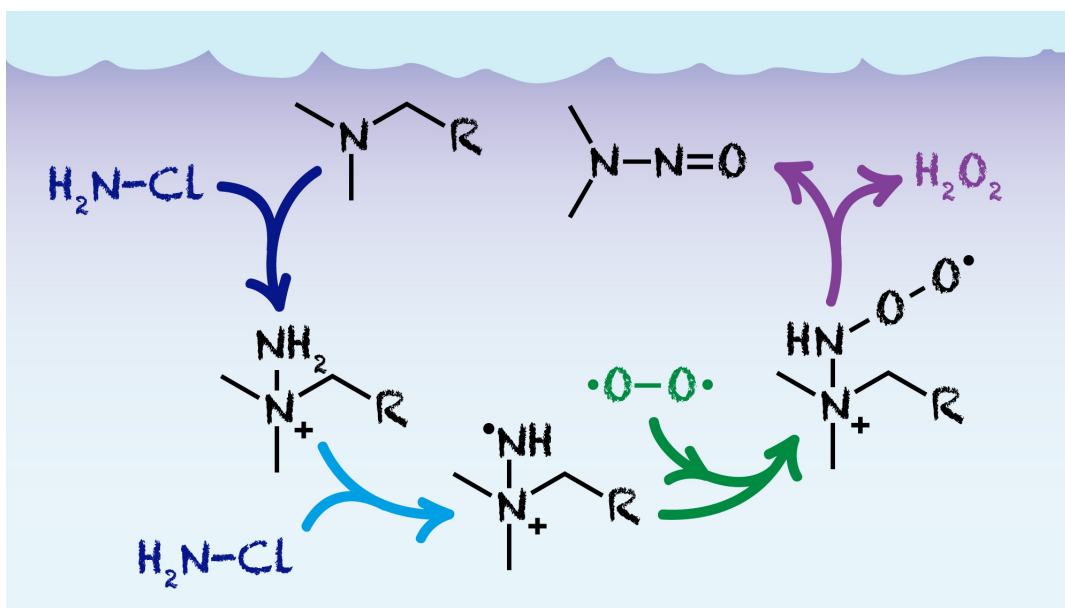


**Figure S2.5:** Panel (a): Close-up of initial ranitidine concentration trend and NDMA formation during chloramination of ranitidine. Panel (b): Disappearance of ranitidine during reaction with  $43\ \mu\text{M}$   $\text{NH}_2\text{Cl}$ . The solid line represents the linear regression with the slope corresponding to a pseudo-first order rate constant,  $k_{\text{obs}}$  of  $(4.08 \pm 0.11) \times 10^{-4}\ \text{s}^{-1}$ .

## Chapter 3

### Formation of *N*-Nitrosodimethylamine during Chloramination of Secondary and Tertiary Amines: Role of Molecular Oxygen and Radical Intermediates



Stephanie Spahr, Olaf A. Cirpka, Urs von Gunten, and Thomas B. Hofstetter. Submitted to *Environmental Science and Technology*

---

*Spahr, S. designed and performed all experiments, analyzed data, and wrote the manuscript. Cirpka, O. A. contributed to the discussion of the results. Von Gunten, U. and Hofstetter, T. B. supervised the project, contributed to the discussion of the results and revision of the manuscript.*

## Abstract

*N*-nitrosodimethylamine (NDMA) is a carcinogenic disinfection by-product from water chloramination. Despite the identification of numerous NDMA precursors, essential parts of the reaction mechanism such as the incorporation of molecular O<sub>2</sub> are poorly understood. In laboratory model systems for the chloramination of secondary and tertiary amines, we investigated the kinetics of precursor disappearance and NDMA formation, quantified the stoichiometries of monochloramine (NH<sub>2</sub>Cl) and aqueous O<sub>2</sub> consumption, derived <sup>18</sup>O-kinetic isotope effects (<sup>18</sup>O-KIE) for the reactions of aqueous O<sub>2</sub>, and studied the impact of radical scavengers on NDMA formation. While the molar NDMA yields from five *N,N*-dimethylamine-containing precursors varied between 1.4% and 90%, we observed the stoichiometric removal of one O<sub>2</sub> per *N,N*-dimethylamine group of the precursor indicating that the oxygenation of N atoms did not determine the molar NDMA yield. Small <sup>18</sup>O-KIEs between  $1.0026 \pm 0.0003$  and  $1.0092 \pm 0.0009$  found for all precursors as well as completely inhibited NDMA formation in the presence of radical scavengers (ABTS and trolox) imply that O<sub>2</sub> reacted with radical species. Our study suggests that aminyl radicals from the oxidation of organic amines by NH<sub>2</sub>Cl and *N*-peroxyl radicals from the reaction of aminyl radicals with aqueous O<sub>2</sub> are part of the NDMA formation mechanism.



### 3.1 Introduction

*N*-nitrosodimethylamine (NDMA) and other *N*-nitrosamines are potent carcinogens that can be formed as disinfection by-products (DBPs) during chlorination, chloramination, and ozonation of drinking water and wastewater.<sup>45,50,115,154,155</sup> Despite the identification of numerous NDMA precursor compounds and suggestions for NDMA mitigation under different treatment conditions,<sup>41,50,66,68,70,72,74,156–161</sup> many aspects of the reaction mechanisms leading to NDMA remain elusive. In fact, the chloramination of amine-containing organic compounds has been identified as a major source of *N*-nitrosamines.<sup>30,50,61</sup> Secondary amines such as dimethylamine (DMA) are reported as frequently occurring NDMA precursors with molar NDMA yields of up to 4%.<sup>55,58,123</sup> Similar yields (<6%) observed during chloramination of tertiary amines with *N,N*-dimethylamine functional groups were interpreted as evidence for their transformation to secondary amines prior to NDMA formation.<sup>30,55,72,73,75,123,124</sup> However, NDMA yields are substantially higher (>60%) if the tertiary *N,N*-dimethylamine moiety is bound via one methylene group to a (hetero)aromatic ring such as in the pharmaceutical ranitidine.<sup>67,72,76,123,162</sup> These high yields suggest that secondary amines are probably not central intermediates in reactions leading to NDMA. It remains unclear, however, whether differing NDMA yields from secondary and tertiary amines indeed reflect differing reaction mechanisms.

To date, there is only limited understanding of how NDMA is formed during the reaction of chloramine with tertiary amines. Based on the detection of cationic dimethylhydrazine intermediates during chloramination of ranitidine, Le Roux et al. proposed that  $\text{NH}_2\text{Cl}$  is attacked through nucleophilic substitution by the tertiary amine moiety of the precursor compound.<sup>79</sup> Moreover, the extent of NDMA formation depends on the molecular structure of the tertiary amine.<sup>67,80</sup> Heterolytic bond dissociation energies for the elementary reaction to NDMA suggest that leaving groups capable of forming stable carbocations (e.g., methylfuranes) are key for high yields of NDMA.<sup>67,80</sup> These studies provide important evidence for the initial chloramination reaction and possible factors influencing the formation of NDMA. However, information about the consumption of  $\text{NH}_2\text{Cl}$  and  $\text{O}_2$  in central reactions, such as the incorporation of aqueous  $\text{O}_2$  into the N–O bond of NDMA, is scarce and mainly circumstantial due to the challenges of characterizing transient reactive (oxygen) intermediates.

Regardless of the yield of NDMA formation during chloramination, reactions of aqueous  $\text{O}_2$  play an important role in the NDMA formation pathway. While chloramination experiments with  $^{18}\text{O}$ -labeled  $\text{H}_2\text{O}$  showed no incorporation of  $^{18}\text{O}$  into NDMA, the

amount of NDMA formed increased with increasing concentrations of aqueous  $O_2$ .<sup>58,76</sup> Although thermodynamically feasible, reactions of ground state triplet oxygen ( $^3O_2$ ) with even-electron species such as the known NDMA precursors are spin forbidden elementary reactions and thus too slow to lead to the oxygenation of organic amines or  $NH_2Cl$ .<sup>163–166</sup> As a consequence, molecular  $O_2$  can only react after activation to singlet oxygen ( $^1O_2$ ), through reduction to superoxide ( $O_2^{\bullet-}$ ), or in reactions with radical species.<sup>163,166–168</sup> Previous work suggests that the latter is the most likely option for NDMA formation during chloramination because neither the addition of  $\beta$ -carotene as  $^1O_2$  scavenger nor the addition of superoxide dismutase as  $O_2^{\bullet-}$  quencher had an effect on NDMA formation during chloramination of DMA.<sup>58</sup> In contrast, formation of NDMA through radical intermediates has been proposed for breakpoint chlorination of DMA<sup>169</sup> as well as for chloramination of quaternary amines.<sup>78</sup> But direct experimental evidence for radical reactions with aqueous  $O_2$  is still lacking.

The goal of this study was to elucidate the reactions of aqueous  $O_2$  and  $NH_2Cl$  with regard to contributions of radical intermediates to NDMA formation during chloramination. To this end, we performed laboratory experiments with five NDMA precursor compounds, namely, ranitidine, 5-(dimethylaminomethyl)furfuryl alcohol (DFUR), *N,N*-dimethylbenzylamine (DMBA), 2,4,6-tris(dimethylaminomethyl)phenol (TDMAP), and dimethylamine (DMA). Evidence for potential NDMA formation mechanisms was obtained from (i) the kinetics of precursor disappearance and NDMA formation, (ii) the quantification of aqueous  $O_2$  and  $NH_2Cl$  consumption, (iii) the analysis of oxygen isotope fractionation of aqueous  $O_2$ , and (iv) the study of the impact of various radical scavengers on NDMA formation. We used the analysis of oxygen isotope ratios ( $^{18}O/^{16}O$ ) of aqueous  $O_2$  for the first time in the context of DBP formation. This methodology is well established for studies on activation of oxygen in enzymes and by transition metal complexes<sup>170–173</sup> and reveals the mechanisms of  $O_2$  activation from the magnitude of  $^{18}O$ -kinetic isotope effects.

## 3.2 Experimental Section

### 3.2.1 Chemicals

A list of all chemicals including suppliers and purities is provided in the Supporting Information (SI). Monochloramine ( $\text{NH}_2\text{Cl}$ ) stock solutions (30 mM) were prepared daily by mixing hypochlorite and ammonium chloride at pH 9.5 (molar Cl:N ratio of 1:1.05) as described previously.<sup>137,138</sup>

### 3.2.2 Chloramination experiments

Chloramination experiments were carried out with five NDMA precursors as listed in the introduction section and in Table 3.1. Unless stated otherwise, reactors contained 10 mM phosphate buffer at pH 8.0 in amber glass bottles of volumes between 100 and 1000 mL. Organic amines were added from either methanolic, ethanolic, or aqueous stock solutions to reach initial concentrations of 15  $\mu\text{M}$  (see Figure S3.4). Reactions were initiated by addition of  $\text{NH}_2\text{Cl}$  in 15- to 18-fold excess corresponding to initial concentrations of 225-270  $\mu\text{M}$ . For concentration analysis and reaction product identification, 1 mL of aqueous sample was withdrawn at selected time points and the reaction was quenched by adding 5  $\mu\text{L}$  of a  $\text{Na}_2\text{S}_2\text{O}_3$  solution (100 g/L). Note that the use of  $\text{Na}_2\text{SO}_3$  is not recommended owing to its reactivity with DFUR (Figure S3.5).  $\text{NH}_2\text{Cl}$  concentrations were quantified by either membrane introduction mass spectrometry (MIMS) or colorimetric methods (see chemical analyses). For continuous monitoring of the concentration of aqueous  $\text{O}_2$ , we filled an aliquot of the reaction solution in 11 mL amber glass vials that were closed without headspace with butyl rubber stoppers and aluminum crimp caps, and immersed a needle-type fiber-optic oxygen microsensor into each vial. Two types of control experiments were set up identically to assess the stability of the organic amine in the absence of  $\text{NH}_2\text{Cl}$  and to quantify the self-decay rate constant of  $\text{NH}_2\text{Cl}$  in the absence of the organic amine. Molar NDMA yields were calculated by dividing the measured concentration of NDMA by the initial concentration and the number of *N,N*-dimethylamine groups of the precursor.

To assess the reactivity of  $\text{NH}_2\text{Cl}$  with the furfuryl alcohol moiety of DFUR, we quantified the concentration of  $\text{NH}_2\text{Cl}$  during the reaction of 3  $\mu\text{M}$  furfuryl alcohol with 45  $\mu\text{M}$   $\text{NH}_2\text{Cl}$  in 10 mM phosphate buffer at pH 8.0. To study the impact of radical scavengers on NDMA formation, we added either the hydroxyl radical scavenger *tert*-butanol (*t*-BuOH, 40 mM final concentration) or peroxy radical scavengers, namely 2,2'-azino-bis(3-ethylbenzothiazoline-6-sulfonic acid) (ABTS, 2 mM) or *rac*-6-

hydroxy-2,5,7,8-tetramethylchromane-2-carboxylic acid (trolox, 0.5 mM), to the reaction of DFUR ( $3\text{ }\mu\text{M}$  or  $15\text{ }\mu\text{M}$ ) with  $\text{NH}_2\text{Cl}$  ( $45\text{ }\mu\text{M}$  or  $225\text{ }\mu\text{M}$ ). Experiments with radical scavengers differed regarding to the sequence of reactant addition and  $\text{NH}_2\text{Cl}$  quantification method. *t*-BuOH was spiked to a phosphate buffered solution containing DFUR before the addition of  $\text{NH}_2\text{Cl}$ . In contrast, ABTS was added immediately after spiking the DFUR-containing buffer with  $\text{NH}_2\text{Cl}$ . Trolox was dissolved in phosphate buffer to which DFUR as well as  $\text{NH}_2\text{Cl}$  were added. We quantified the  $\text{NH}_2\text{Cl}$  concentration with the ABTS method and MIMS in the presence of *t*-BuOH and trolox, respectively. When ABTS was added as a radical scavenger, we observed the oxidation of ABTS which was used to quantify the amount of consumed  $\text{NH}_2\text{Cl}$  (Figure S3.21). Control experiments were set up to assess the reactivity of the organic amine or  $\text{NH}_2\text{Cl}$  with the radical scavengers.

To quantify the formation of  $\text{H}_2\text{O}_2$  during the reaction of DFUR ( $50\text{ }\mu\text{M}$ ) with  $\text{NH}_2\text{Cl}$  ( $750\text{ }\mu\text{M}$ ), we filled the reaction solution into 11 mL amber glass vials that were closed headspace-free and monitored the decrease of  $\text{O}_2$  concentration as described above. When the consumed  $\text{O}_2$  was stoichiometrically equal to the initial nominal concentration of DFUR, we added  $100\text{ }\mu\text{L}$  catalase from bovine liver ( $0.3\text{ g L}^{-1}$  final concentration). The observed increase in aqueous  $\text{O}_2$  concentration upon addition of catalase corresponds to half of the  $\text{H}_2\text{O}_2$  concentration. To assess the stability of  $\text{H}_2\text{O}_2$  during the NDMA formation reaction, we added  $50\text{ }\mu\text{M}$   $\text{H}_2\text{O}_2$  immediately after the reaction of DFUR ( $50\text{ }\mu\text{M}$ ) with  $\text{NH}_2\text{Cl}$  ( $750\text{ }\mu\text{M}$ ) was initiated and determined the recovery of  $\text{H}_2\text{O}_2$  by addition of catalase after 3.3 h. A more detailed description of experiments with catalase is provided in the SI (section S3.13).

### 3.2.3 Oxygen isotope fractionation experiments

The fractionation of stable O isotopes of aqueous  $\text{O}_2$  was studied in amber reactors containing a magnetic stir bar and 11 mL of a 3 mM  $\text{NH}_2\text{Cl}$  solution in 10 mM phosphate buffer (pH 8.0). The vessels were closed without headspace and an oxygen microsensor was introduced to measure continuously the concentration of aqueous  $\text{O}_2$ . 15 to  $200\text{ }\mu\text{M}$  of the organic amine (ranitidine, DFUR, DMBA, or TDMAP) was added to the reactor while stirring to initiate the reaction. Once the amount of consumed  $\text{O}_2$  equaled the initial nominal concentration of the added organic amine, the reaction was quenched by creating a  $\text{N}_2$  headspace following the procedure of Pati et al.<sup>174</sup> To this end, 3 mL of solution was replaced by  $\text{N}_2$  gas with a gas-tight glass syringe. Partitioning of  $\text{O}_2$  to the  $\text{N}_2$ -headspace was promoted through horizontal shaking for 30 min at 200 rpm while

keeping the vessels upside down. Control samples containing 3 mM  $\text{NH}_2\text{Cl}$  without organic amine or 200  $\mu\text{M}$  organic amine without  $\text{NH}_2\text{Cl}$  were prepared similarly. Owing to much slower reaction kinetics of DMA and  $\text{NH}_2\text{Cl}$ , we prepared twelve replicate samples containing 200  $\mu\text{M}$  DMA and 3 mM  $\text{NH}_2\text{Cl}$  as well as twelve control samples with 3 mM  $\text{NH}_2\text{Cl}$ . Two reactive batches and one control batch were processed at selected time points over a time period of 4 days. In experiments with DMBA, TDMA, and DMA, we additionally determined the concentration of NDMA immediately after sample quenching in the withdrawn reaction solution.

### 3.2.4 Chemical analyses

Concentrations of ranitidine, DFUR, and NDMA were quantified with reverse phase HPLC coupled to a UV-vis detector using previously described methods (see section S3.3 for details).<sup>162</sup> Transformation products formed during chloramination of ranitidine and DFUR were analyzed by liquid chromatography-high-resolution tandem mass spectrometry (LC-HR-MS/MS) using an adjusted analytical method described in Gulde et al.<sup>175</sup> (see section S3.4 for details).

#### Quantification of aqueous $\text{O}_2$

Concentrations of aqueous  $\text{O}_2$  were continuously measured with needle-type fiber-optic oxygen microsenors connected to a 4-channel transmitter (PreSens Precision Sensing GmbH, Germany). Four oxygen sensors were operated simultaneously after daily calibration with air-saturated and oxygen-free water.  $\text{O}_2$  concentrations were corrected for variations in temperature.

#### Quantification of $\text{NH}_2\text{Cl}$

Concentrations of  $\text{NH}_2\text{Cl}$  were determined spectrophotometrically using ABTS,<sup>139</sup> *N,N*-diethyl-*p*-phenylenediamine (DPD),<sup>176</sup> and indophenol<sup>177</sup> as well as by membrane introduction mass spectrometry (MIMS).<sup>178</sup> A Varian Cary 100 Bio UV-visible spectrophotometer was used for colorimetric assays which are described in the SI (section S3.5). MIMS analysis was performed using a MIMS 2000 (Microlab, Aarhus, Denmark) equipped with a multi-port valve to enable an automatic measurement of multiple samples. The membrane inlet temperature was set to 40°C and the sample flow rate was 4 mL min<sup>-1</sup>. Steady-state signals of  $m/z$  51 and  $m/z$  53 were reached after 2 minutes and measured for 6-8 minutes. The software used for analysis of MIMS signals is described

elsewhere.<sup>178</sup> We used  $\text{NH}_2\text{Cl}$  calibration rows from either 10 - 50  $\mu\text{M}$  or 50 - 300  $\mu\text{M}$ . Note that ranitidine, DFUR, NDMA, and trolox did not produce any interfering signals in the mass spectrometer. In NDMA formation experiments, we detected an interference at  $m/z$  51 that was presumably created from an unknown reaction intermediate (see FigureS3.2). In this case, quantification of  $\text{NH}_2\text{Cl}$  was performed at  $m/z$  53. All reported  $\text{NH}_2\text{Cl}$  concentrations were corrected by the self-decay of  $\text{NH}_2\text{Cl}$  observed in controls containing chloramine only. Note that the four methods used for determining  $\text{NH}_2\text{Cl}$  concentrations led to differing results when  $\text{NH}_2\text{Cl}$  was quantified during NDMA formation (FigureS3.3). The total turnover of  $\text{NH}_2\text{Cl}$  determined at the end of these experiments was, however, identical (section S3.5).

### 3.2.5 Stable oxygen isotope analysis

$^{18}\text{O}/^{16}\text{O}$  ratios of aqueous  $\text{O}_2$  were measured with gas chromatography isotope ratio mass spectrometry (GC/IRMS) following recently developed procedures of Pati et al.<sup>174</sup> Briefly, sample vials to which a 3 mL  $\text{N}_2$  headspace had been introduced were mounted on a CombiPAL autosampler (CTC Analytics) equipped with a 2.5 mL gas-tight headspace syringe. The syringe was flushed with  $\text{N}_2$  gas for 1 min before withdrawing 250  $\mu\text{L}$  of the headspace from the sample. The gaseous sample was injected into a split injector (5 mm ID quartz liner, 200°C) of a Trace GC (Thermo Fisher Scientific) that was equipped with a Rt-Molsieve 5Å PLOT column (Restek, 30 m x 32 mm ID, 30  $\mu\text{m}$  film thickness at 30°C) to separate  $\text{O}_2$  from  $\text{N}_2$ . Helium (99.999%) was used as carrier gas at 80 kPa and the split flow was 40 mL min<sup>-1</sup>.  $\text{O}_2$  pulses were introduced into a GC combustion III interface (Thermo Fisher Scientific) equipped with a Nafion membrane for removal of water and subsequently entered a Delta Plus XL IRMS (Thermo Fisher Scientific).

O isotope ratios are expressed in the delta notation as  $\delta^{18}\text{O}$  in permil (eq. 3.1) relative to Vienna Standard Mean Ocean Water (VSMOW). Sample sequences included standards generated from air-saturated phosphate buffer, which were measured after every 6 samples to ensure accuracy of  $\delta^{18}\text{O}$  measurements in a standard bracketing procedure. Blank samples containing oxygen-free water were analyzed in triplicates at the end of each sequence for blank corrections of diffusive  $\text{O}_2$  input during sample preparation and injection (see Pati et al.<sup>174</sup> for details).

$$\delta^{18}\text{O} = \frac{(^{18}\text{O}/^{16}\text{O})_{\text{sample}}}{(^{18}\text{O}/^{16}\text{O})_{\text{VSMOW}}} - 1 \quad (3.1)$$

We used Igor Pro software (WaveMetrics Inc., Lake Oswego OR, USA) to derive O isotope enrichment factors,  $\varepsilon_{\text{O}}$ , with a nonlinear least-square regression according to equation 3.2, where  $\delta^{18}\text{O}$  and  $\delta^{18}\text{O}_0$  are O isotope signatures determined in samples from oxygen isotope fractionation experiments and in standards, respectively.  $c/c_0$  is the fraction of remaining aqueous  $\text{O}_2$ .

$$\frac{\delta^{18}\text{O} + 1}{\delta^{18}\text{O}_0 + 1} = (c/c_0)^{\varepsilon_{\text{O}}} \quad (3.2)$$

Average  $^{18}\text{O}$ -kinetic isotope effects ( $^{18}\text{O}$ -KIE) of both O atoms were determined with equation 3.3.<sup>172,179</sup> Uncertainties of  $\varepsilon_{\text{O}}$  and  $^{18}\text{O}$ -KIEs are reported as 95% confidence intervals.

$$^{18}\text{O-KIE} = \frac{1}{1 + \varepsilon_{\text{O}}} \quad (3.3)$$

### 3.3 Results and Discussion

#### 3.3.1 Chloramination of amines: Kinetics, reaction products, and stoichiometry of $\text{NH}_2\text{Cl}$ and $\text{O}_2$ consumption

##### Chloramination of ranitidine

The reaction of ranitidine ( $14\ \mu\text{M}$ ) with  $\text{NH}_2\text{Cl}$  ( $270\ \mu\text{M}$ ) at pH 8.0 produced NDMA with a molar yield of 89.9% in agreement with previous observations.<sup>67,72,76,162</sup> Figure 3.1a shows the kinetics of the disappearance of ranitidine, dissolved  $\text{O}_2$ , and  $\text{NH}_2\text{Cl}$  as well as the formation of NDMA. Within one hour, ranitidine was depleted following pseudo-first order kinetics (Figure S3.8). The second-order rate constant for the reaction of ranitidine with  $\text{NH}_2\text{Cl}$  was  $6.1 \pm 0.3\ \text{M}^{-1}\text{s}^{-1}$  in agreement with a previous study.<sup>162</sup>

The formation of NDMA only started after 1.6 h (dashed vertical line in Figure 3.1a) when ranitidine had disappeared completely suggesting the presence of a critical intermediate. Indeed, NDMA formation was concomitant with the decline of a transient reaction product (yellow stars, Figure 3.1a) with  $m/z$   $[\text{M}+\text{H}^+] = 365.1049$  corresponding to the molecular formula  $\text{C}_{13}\text{H}_{21}\text{N}_4\text{O}_4\text{SCl}$ . We report this intermediate with arbitrary peak areas due to the lack of standard materials. The mass of  $\text{C}_{13}\text{H}_{21}\text{N}_4\text{O}_4\text{SCl}$  exceeds that of ranitidine ( $m/z$   $[\text{M}+\text{H}^+] = 315.1485$ ) by 50 Da, which corresponds to



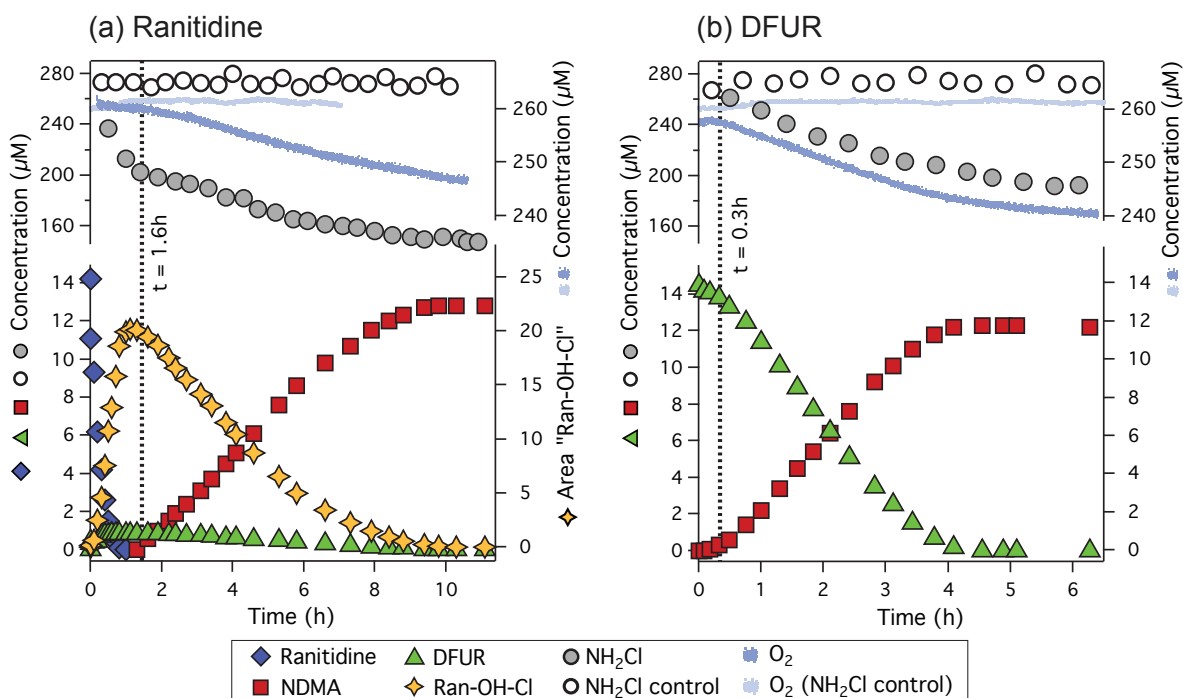


**Figure 3.1:** NDMA formation during the reaction of  $\text{NH}_2\text{Cl}$  ( $270\ \mu\text{M}$ ) with (a) ranitidine ( $15\ \mu\text{M}$ ) over 11 h and (b) DFUR ( $15\ \mu\text{M}$ ) over 6.5 h in 10 mM phosphate buffer at pH 8.0. Consumption of  $\text{NH}_2\text{Cl}$  and aqueous  $\text{O}_2$  is depicted as grey circles and light blue line, respectively. Note break in y-axes and scale change.

the presence of an additional hydroxyl group (+OH), an additional Cl atom (+Cl), and a loss of 2 hydrogen atoms ( $-2\text{H}$ ). The intermediate, which we refer to as Ran-OH-Cl, was identified in a previous study for the chloramination of ranitidine under similar experimental conditions.<sup>79</sup> MS/MS fragmentation patterns of Ran-OH-Cl suggest that the 2-(dimethylamino)methylfuran moiety remained intact during chloramination (Figure S3.15). Apparently, chlorination and hydroxylation of ranitidine occurred at the thioethyl-*N*-methyl-2-nitroethene-1,1-diamine moiety. Note that we measured only minor concentrations of 5-(dimethylaminomethyl)furfuryl alcohol (DFUR,  $m/z$   $[\text{M}+\text{H}^+] = 156.1021$ , Figure 3.1a), a known NDMA precursor.<sup>67</sup> Small amounts of DFUR as well as the coincidence of NDMA formation with the disappearance of Ran-OH-Cl suggest that the latter was the primary NDMA precursor during chloramination of ranitidine.

The concentration trends of  $\text{NH}_2\text{Cl}$  and  $\text{O}_2$  reveal that the transformation of ranitidine within the first 1.6 h involved  $\text{NH}_2\text{Cl}$  but not dissolved  $\text{O}_2$  because its concentration remained constant until ranitidine disappeared. In contrast, the disappearance of Ran-



OH-Cl and the concomitant formation of NDMA after 1.6 h were accompanied by a decline in  $\text{NH}_2\text{Cl}$  and  $\text{O}_2$  concentration (Figure 3.1a). The total amount of consumed  $\text{NH}_2\text{Cl}$  during chloramination of ranitidine amounted to  $124 \pm 2 \mu\text{M}$  corresponding to 8.7 times the initial ranitidine concentration (Table 3.1).  $\text{NH}_2\text{Cl}$  consumption rates were distinctly different before and after 1.6 h and enabled us to attribute the loss of  $\text{NH}_2\text{Cl}$  to the transformation of ranitidine vs. the formation of NDMA (Figure S3.9a). To compare the two kinetic regimes, we report operational pseudo-first order rate constants for the consumption of  $\text{NH}_2\text{Cl}$ . During the transformation of ranitidine,  $60.5 \mu\text{M}$   $\text{NH}_2\text{Cl}$  were consumed with a rate constant  $k_{\text{obs}, 1}^{\text{NH}_2\text{Cl}}$  of  $(7.2 \pm 0.5) \cdot 10^{-5} \text{ s}^{-1}$ . This share of  $\text{NH}_2\text{Cl}$  consumption equaled 4.3 times the initial ranitidine concentration. The overstoichiometric  $\text{NH}_2\text{Cl}$  consumption suggests that multiple sites of the thioethyl-*N*-methyl-2-nitroethene-1,1-diamine moiety (e.g., S and N atoms) were chlorinated as suggested previously by Le Roux et al.<sup>79</sup> During the formation of NDMA,  $63 \mu\text{M}$   $\text{NH}_2\text{Cl}$  were consumed corresponding to 4.4 times the initial ranitidine concentration (Table 3.1). The rate constant of  $\text{NH}_2\text{Cl}$  consumption ( $k_{\text{obs}, 2}^{\text{NH}_2\text{Cl}} = (1.1 \pm 0.04) \cdot 10^{-5} \text{ s}^{-1}$ ) was 7-fold smaller than the one observed during transformation of ranitidine implying differing reactions of  $\text{NH}_2\text{Cl}$  with ranitidine and reaction intermediates such as Ran-OH-Cl, respectively. The overstoichiometric  $\text{NH}_2\text{Cl}$  consumption during NDMA formation indicates that  $\text{NH}_2\text{Cl}$  might be involved in several reactions of the multi-step NDMA formation pathway. Experiments with differing ranitidine to  $\text{NH}_2\text{Cl}$  ratios underscore the importance of  $\text{NH}_2\text{Cl}$  because maximum NDMA yields from ranitidine were only reached in presence of  $\geq 15$ -fold excess of  $\text{NH}_2\text{Cl}$  (Figure S3.7).

In contrast to overstoichiometric  $\text{NH}_2\text{Cl}$  consumption, we observed a stoichiometric disappearance of dissolved  $\text{O}_2$  during the formation of NDMA. After 10 h, NDMA formation was complete and the amount of consumed  $\text{O}_2$  ( $14.3 \pm 0.3 \mu\text{M}$ ) matched the initial concentration of ranitidine ( $14.2 \pm 0.1 \mu\text{M}$ ) within analytical uncertainty. The stoichiometries of  $\text{O}_2$  and  $\text{NH}_2\text{Cl}$  consumption are compiled in Tables 3.1 and S3.1. To assess whether the molar reaction stoichiometry determined in the ranitidine experiment also applies for other amine-containing NDMA precursors, we chloraminated two tertiary amines, which are known to produce high molar NDMA yields, namely DFUR and *N,N*-dimethylbenzylamine (DMBA) as well as 2,4,6-tris-(dimethylaminomethyl)phenol (TDMAP) and dimethylamine (DMA), which are known to produce significantly lower molar NDMA yields.

### Chloramination of other tertiary amines with high molar NDMA yield

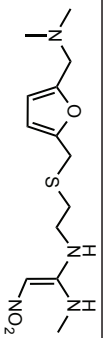
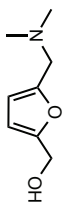
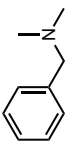
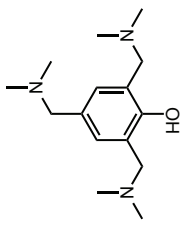
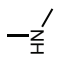
Chloramination of DFUR and DMBA under experimental conditions that were identical to experiments with ranitidine (pH 8.0, 270  $\mu\text{M}$   $\text{NH}_2\text{Cl}$ , Figure 3.1b and S3.10) led to high molar NDMA yields of 84.6% and 82.5%, respectively, in agreement with previously reported values.<sup>67,123</sup> DFUR and DMBA are structurally similar to ranitidine and are likely transformed to NDMA by the same reaction mechanism. This interpretation is supported by almost identical reaction stoichiometries (Table 3.1). The consumption of aqueous  $\text{O}_2$  was stoichiometric ( $15.2 \pm 0.3 \mu\text{M}$  vs.  $14.5 \mu\text{M}$  of initial DFUR concentration), while the consumption of  $\text{NH}_2\text{Cl}$  ( $68.2 \pm 2.9 \mu\text{M}$ ) exceeded the initial DFUR concentration by a factor of 4.7 (Table 3.1, data for DMBA see Table S3.2). To assess whether reactions of  $\text{NH}_2\text{Cl}$  with the heterocyclic ring of DFUR contributed to the overall  $\text{NH}_2\text{Cl}$  consumption, we conducted experiments with 3  $\mu\text{M}$  furfuryl alcohol and 45  $\mu\text{M}$   $\text{NH}_2\text{Cl}$  under otherwise identical experimental conditions (Figure S3.17). No significant decrease in the  $\text{NH}_2\text{Cl}$  concentration was observed within 30 h indicating that the initial reaction of  $\text{NH}_2\text{Cl}$  and DFUR happens exclusively at the *N,N*-dimethylamine group of DFUR.

While the molar NDMA yield and the reaction stoichiometries were almost identical for ranitidine, DFUR, and DMBA, the reaction kinetics differed significantly. Figures 3.1b and S3.10 show that NDMA formation during chloramination of DFUR and DMBA was completed within 4 h and 6 h, respectively, and was thus faster than NDMA formation from ranitidine (within 10 h). During chloramination of DFUR, we observed a short lag phase within the first 0.3 h of the reaction in which only 0.3  $\mu\text{M}$  of NDMA were formed but no measurable amounts of  $\text{O}_2$  and  $\text{NH}_2\text{Cl}$  disappeared. After 0.3 h, the reaction accelerated and the formation of NDMA coincided with the disappearance of DFUR,  $\text{O}_2$ , and  $\text{NH}_2\text{Cl}$  (Figure S3.8b).  $\text{NH}_2\text{Cl}$  was consumed with a pseudo-first order rate constant of  $(2.2 \pm 0.1) \cdot 10^{-5} \text{ s}^{-1}$ , which is twice the  $k_{\text{obs}, 2}^{\text{NH}_2\text{Cl}}$  observed during NDMA formation from ranitidine. Even after NDMA formation ceased (after 4 h), the consumption of  $\text{NH}_2\text{Cl}$  continued with a smaller  $k_{\text{obs}}^{\text{NH}_2\text{Cl}}$  of  $(7.7 \pm 0.7) \cdot 10^{-6} \text{ s}^{-1}$  (Figure S3.9b). This finding suggests that some additional minor reactions of  $\text{NH}_2\text{Cl}$  contributed to the observed overstoichiometric  $\text{NH}_2\text{Cl}$  consumption. A tentatively identified reaction product with molecular formula  $\text{C}_5\text{H}_5\text{ClO}_2$  ( $m/z$   $[\text{M}+\text{H}^+] = 133.0053$ ) indicates that  $\text{NH}_2\text{Cl}$  reacts with intermediates of the NDMA formation reaction leading to chlorinated furfuryl alcohol as final reaction product (for possible molecular structures see Figure S3.16).

**Chloramination of tertiary and secondary amines with low molar NDMA yield**

Molar NDMA yields from chloramination of TDMAP and DMA were normalized to the number of *N,N*-dimethylamine groups of the precursor molecule and amounted to 15.8% and 1.4%, respectively. Our data is in good agreement with previously reported NDMA yields of 18.4% for TDMAP<sup>123</sup> and 1.2 - 2.3% for DMA.<sup>67,123</sup> The kinetics of NDMA formation and concomitant  $\text{NH}_2\text{Cl}$  and  $\text{O}_2$  consumption are shown in Figure S3.11. Despite significantly smaller molar NDMA yields from TDMAP and DMA, the stoichiometries of  $\text{NH}_2\text{Cl}$  and  $\text{O}_2$  consumption were similar to the one for ranitidine, DFUR, and DMBA. The consumed amount of  $\text{O}_2$  corresponded with the initial concentration of *N,N*-dimethylamine groups, while the amount of reacted  $\text{NH}_2\text{Cl}$  exceeded the initial concentrations of *N,N*-dimethylamine groups by a factor of 3.9 and 2.2 for TDMAP and DMA, respectively (Tables 3.1 and S3.2). The overstoichiometric consumption of  $\text{NH}_2\text{Cl}$  in experiments with low-yield NDMA precursors indicates that unidentified reactions other than NDMA formation likely contribute to the disappearance of  $\text{NH}_2\text{Cl}$ . The stoichiometric  $\text{O}_2$  consumption in experiments with high- and low-yield NDMA precursors hints at the same mechanism of N-atom oxygenation of secondary and tertiary amines. However, reactions with dissolved  $\text{O}_2$  do not necessarily lead to the formation of NDMA and it is likely that other factors such as the molecular structure of the precursor molecule determine the molar NDMA yield. Note that chloramination of DMA was too slow to carry out reliable  $\text{O}_2$  concentration measurements over the entire experiment period ( $> 3$  days, Figure S3.11). The reported reaction stoichiometry of  $> 0.6$  in Table 3.1 indicates that a higher number should be expected based on an observed stoichiometric  $\text{O}_2$  consumption in experiments with higher initial concentrations of DMA ( $43\ \mu\text{M}$ ) and  $\text{NH}_2\text{Cl}$  ( $1000\ \mu\text{M}$ , Figure S3.12).

**Table 3.1:** NDMA formation from the reaction of ranitidine, 5-(dimethylaminomethyl)furfuryl alcohol (DFUR), *N,N*-dimethylbenzylamine (DMBA), 2,4,6-tris(dimethylaminomethyl)phenol (TDMAP), and dimethylamine (DMA) with  $\text{NH}_2\text{Cl}$  in 10 mM phosphate buffer at pH 8.0 in the presence and absence of *tert*-butanol (*t*-BuOH), ABTS, and trolox. Reported are molecular structure of the precursor, molar NDMA yields, reaction stoichiometries, and oxygen kinetic isotope effects ( $^{18}\text{O}$ -KIEs).

precursor	molecular structure	NDMA yield <sup>a</sup> (%)	molar reaction stoichiometry $\text{N}(\text{CH}_3)_2$ -group : $\text{O}_2$ <sup>b</sup> : $\text{NH}_2\text{Cl}$ <sup>b</sup>	$^{18}\text{O}$ -KIE (-)
<b>Ranitidine</b>  + <i>t</i> -BuOH (40 mM)		89.9 ± 0.1  87.8 ± 0.2	1.0 : 1.0 : 8.7 <sup>c</sup> (4.4 <sup>d</sup> )  n.m. <sup>e</sup> : n.m. : 6.6 <sup>c</sup>	1.0061 ± 0.0004
<b>DFUR</b>  + <i>t</i> -BuOH (40 mM) + ABTS (2 mM) + trolox (0.5 mM)		84.6 ± 0.4	1.0 : 1.1 : 4.7	1.0060 ± 0.0006
		80.6 ± 0.1 <0.7 <sup>f</sup> <0.7 <sup>f</sup>	n.m. <sup>e</sup> : n.m. : 4.0 <sup>c</sup> 0.9 : 0 : 16 0.1 : n.m. : 7.5	
<b>DMBA</b>		82.5 ± 0.2	1.0 : 1.1 : 4.7	1.0026 ± 0.0003
<b>TDMAP</b>		15.8 ± 0.01	1.0 : 1.0 : 3.9	1.0092 ± 0.0009
<b>DMA</b>		1.4 ± 0.1	1.0 : >0.6 <sup>g</sup> : 2.2	1.0077 ± 0.0012

<sup>a</sup> per  $\text{N}(\text{CH}_3)_2$ -group of the precursor      <sup>b</sup> ± 0.1 - 0.2      <sup>c</sup> total  $\text{NH}_2\text{Cl}$  consumption      <sup>d</sup>  $\text{NH}_2\text{Cl}$  consumption during NDMA formation  
<sup>e</sup> not measured      <sup>f</sup> <0.1  $\mu\text{M}$  NDMA      <sup>g</sup> determined after approx. 50% of the total reaction time

### 3.3.2 Oxygen isotope fractionation during the reaction of aqueous O<sub>2</sub>

To gain new insights into the reaction of O<sub>2</sub> during chloramination of secondary and tertiary amines, we conducted oxygen isotope analyses of aqueous O<sub>2</sub>. Figure 3.2a shows that the consumption of O<sub>2</sub> measured after completion of the chloramination of ranitidine was stoichiometric regardless of the initial ranitidine concentration. The same observation was made for all of the five studied organic amines (Figures S3.18, S3.19). In these experiments, we determined the <sup>18</sup>O/<sup>16</sup>O ratios of aqueous O<sub>2</sub> at natural abundance, which are reported as δ<sup>18</sup>O-values (eq. 3.1). As shown for ranitidine in Figure 3.2b, δ<sup>18</sup>O-values of aqueous O<sub>2</sub> increased with decreasing fraction of remaining aqueous O<sub>2</sub>. The observed O isotope fractionation shows that O<sub>2</sub> molecules containing <sup>16</sup>O reacted preferentially. The extent of O isotope fractionation was quantified with an <sup>18</sup>O-kinetic isotope effect (<sup>18</sup>O-KIE, eq. 3.3) of 1.0061 ± 0.0004, which reflects the ratio of reaction rate constants of light and heavy O isotopes (<sup>16</sup>k<sub>O<sub>2</sub></sub>/<sup>18</sup>k<sub>O<sub>2</sub></sub>). In the present case, <sup>16</sup>O<sub>2</sub> reacted approximately 0.6% faster than <sup>16</sup>O<sup>18</sup>O molecules. The reaction of aqueous O<sub>2</sub> during the chloramination of DFUR, DMBA, TDMPA, and DMA resulted in similar <sup>18</sup>O-KIE values between 1.0026 and 1.0092 (Table 3.1).

The <sup>18</sup>O-KIEs found in our experiments are small compared to the range of known values of up to 1.05 for the reduction of O<sub>2</sub> and the activation of O<sub>2</sub> by enzymes and transition metal complexes.<sup>170–173,180–183</sup> The magnitude of <sup>18</sup>O-KIEs is a proxy for the number of electrons transferred to O<sub>2</sub> as well as for the formation and cleavage of bonds to oxygen atoms in reactions up to and including the first irreversible reaction step.<sup>172,173</sup> Theoretical calculations show that one and two electron reductions of O<sub>2</sub> to O<sub>2</sub><sup>•−</sup> and O<sub>2</sub><sup>(−II)</sup> are accompanied by the largest <sup>18</sup>O isotope effects in the order of 1.03 and 1.05, respectively.<sup>170,171</sup> The small <sup>18</sup>O-KIE values below 1.01 measured here for chloramination reactions imply that the disappearance of aqueous O<sub>2</sub> was not associated with the formation of O<sub>2</sub><sup>•−</sup> and O<sub>2</sub><sup>(−II)</sup>. Indeed, none of the studied organic amines are powerful reductants that would enable the reduction of O<sub>2</sub>. Such an interpretation is in agreement with the previously reported lack of O<sub>2</sub><sup>•−</sup> detection after addition of superoxide dismutase to the chloramination of DMA.<sup>58</sup> Moreover, O<sub>2</sub><sup>•−</sup> and O<sub>2</sub><sup>(−II)</sup> could react with organic amine precursors, chloramine, or reaction intermediates thus causing an overstoichiometric consumption of O<sub>2</sub>.

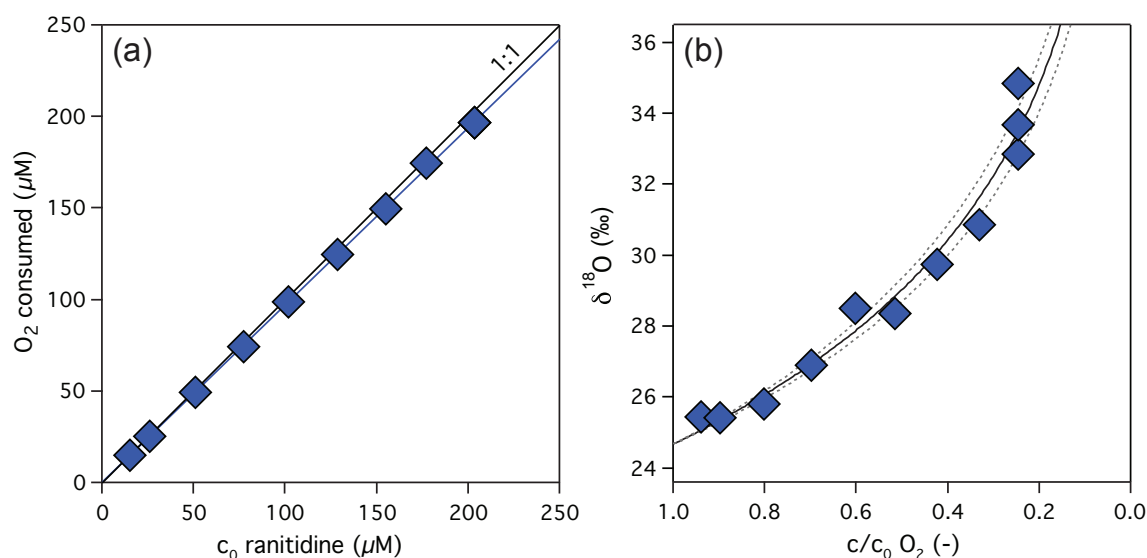


**Figure 3.2:** Reaction of ranitidine (15–200  $\mu M$ ) with  $NH_2Cl$  (3 mM) in 10 mM phosphate buffer at pH 8.0. (a) Consumption of aqueous  $O_2$  after completion of the chloramination reactions vs. initial concentration,  $c_0$ , of ranitidine. (b) Oxygen isotope fractionation shown as changes of  $\delta^{18}O$ -values in aqueous  $O_2$  vs. fraction of remaining  $O_2$  ( $c/c_0$ ). The solid line represents the nonlinear least-square regression with eq. 3.2 and dashed lines are 95% confidence intervals of the fit.

Much smaller  $^{18}O$  isotope effects between 1.01 and 1.03 are known for the reversible binding of  $O_2$  to transition-metal complexes (e.g., with  $Co^{II}$ ,  $Cu^{II}$ ) and the reductive activation of  $O_2$  at enzyme active site metal centers.<sup>172,179,180,182,183</sup> The smallest  $^{18}O$  isotope effects of 1.004–1.005 have been assigned to the reversible binding of  $O_2$  to oxygen transport proteins such as myoglobin.<sup>170</sup> These proteins have paramagnetic transition metals (e.g.,  $Fe^{II}$ ) in their active site, which allows binding of triplet state  $O_2$ . The  $^{18}O$ -KIE values associated with chloramination of amines (Table 3.1) are in the same range than observed for the  $O_2$  binding to odd electron chemical species but we exclude the presence of transition metals in our experiments. Small  $^{18}O$ -KIE values thus suggest that the NDMA formation mechanism involves the binding of  $O_2$  to not yet identified radical intermediates. Such elementary reactions could explain the stoichiometric disappearance of aqueous  $O_2$  but require the presence of organic radicals, with which ground state  $O_2$  can react in a spin allowed process. Because  $O_2$  neither reacts with any of the organic amines nor with  $NH_2Cl$  alone, we hypothesize that radical intermediates are formed after the initial reaction of the organic amine with chloramine.

### 3.3.3 Impact of radical scavengers on NDMA formation

The presence of radical intermediates was investigated by chloramination of ranitidine and DFUR in the presence of three radical scavengers, namely *tert*-butanol (*t*-BuOH), ABTS, and trolox. *t*-BuOH, which serves as a scavenger for hydroxyl radicals ( $\bullet\text{OH}$ ),<sup>184</sup> did not affect the formation of NDMA (Table 3.1). In agreement with previous studies,<sup>58,169</sup> we found almost identical molar NDMA yields from the reaction of ranitidine or DFUR (both 15  $\mu\text{M}$ ) with  $\text{NH}_2\text{Cl}$  (225  $\mu\text{M}$ ) in the presence and absence of 40 mM of *t*-BuOH. Addition of *t*-BuOH did also not influence the extent of chloramine consumption (see Tables 3.1 and S3.1, Figure S3.20). These observations suggest that hydroxyl radicals neither contributed to the formation of NDMA nor to the consumption of  $\text{NH}_2\text{Cl}$ .<sup>185</sup>

Chloramination experiments with ABTS or trolox strongly contrast those with *t*-BuOH in that NDMA formation from DFUR was completely suppressed. In the presence of 2 mM ABTS or 0.5 mM trolox, the reaction of DFUR with  $\text{NH}_2\text{Cl}$  did not lead to the formation of NDMA over a time period of 36 h and 4 days, respectively (Figures S3.21b and S3.24b). This finding contrasts the formation of >80% NDMA within 4–8 h without radical scavenger (Figures 3.1b and S3.24a). ABTS and trolox are both known to react with a wide range of reactive oxygen species including (alk)oxyl ( $\text{R-O}\bullet$ ), nitroxyl ( $\text{N-O}\bullet$ ), (aryl)peroxyl ( $\text{R-O-O}\bullet$ ), and nitryl ( $\text{N-O-O}\bullet$ ) radicals through a one electron or H atom transfer, respectively.<sup>186–194</sup> Control experiments containing radical scavengers and either DFUR or  $\text{NH}_2\text{Cl}$  showed that ABTS and trolox did not react with DFUR and that reactions with  $\text{NH}_2\text{Cl}$  were of minor relevance within the time frame of the reactions (Figures S3.21 and S3.23). Hence, ABTS and trolox reacted with reaction intermediates formed from the reaction of DFUR and  $\text{NH}_2\text{Cl}$ . The inhibition of NDMA formation in the presence of ABTS or trolox implies that reaction intermediates were radicals. Similar observations regarding lower NDMA yields in the presence of trolox were made by Schreiber and Mitch<sup>169</sup> using DMA as precursor under differing experimental conditions. Furthermore, in experiments with trolox, we did no longer observe an interference at  $m/z$  51 during MIMS measurements, which was indicative for a transient intermediate formed during chloramination of DFUR (Figure S3.25).

To gain additional insights into the impact of radical scavengers on the NDMA formation mechanism, we quantified the consumption of DFUR,  $\text{NH}_2\text{Cl}$ , and  $\text{O}_2$ . In the presence of ABTS or trolox, DFUR disappeared at an approximately 15-fold and 8-fold smaller rate, respectively, compared to experiments without radical scavenger (Tables 3.1



and S3.1, Figure S3.24). The significantly retarded DFUR transformation suggests that radical scavengers reduce radical intermediates concomitant with the regeneration of DFUR. Regenerated DFUR again reacts with  $\text{NH}_2\text{Cl}$  leading to a continuous consumption of  $\text{NH}_2\text{Cl}$  until the latter is completely consumed as shown in the experiment with ABTS (Figure S3.21). The amount of consumed  $\text{NH}_2\text{Cl}$  increased by a factor of 3.3 and 2.3 in the presence of ABTS and trolox, respectively (Table S3.1). Note that colorimetric methods for  $\text{NH}_2\text{Cl}$  quantification were impeded in the presence of ABTS. We observed, however, that ABTS was oxidized during the reaction of DFUR with  $\text{NH}_2\text{Cl}$ , which was applied in 16-fold excess (Figure S3.21). The amount of oxidized ABTS equaled the initial concentration of chloramine ( $225\text{ }\mu\text{M}$ ) after 23 h indicating complete  $\text{NH}_2\text{Cl}$  consumption (Table S3.1 and Figure S3.21). While aqueous  $\text{O}_2$  measurements were unsuccessful in the presence of trolox, the concentration of  $\text{O}_2$  remained constant in experiments with ABTS (Table 3.1, Figure S3.22). The constant  $\text{O}_2$  concentration may be due to the fact that radical intermediates reacted more rapidly with ABTS than with aqueous  $\text{O}_2$  and the former was present in excess (2 mM ABTS vs. 0.25 mM  $\text{O}_2$ ). An alternative explanation is that oxygen-centered peroxy radicals, formed from the reaction of radical intermediates with  $\text{O}_2$ , were reduced back completely to  $\text{O}_2$  by ABTS.

### 3.3.4 Potential NDMA formation mechanisms involving radical intermediates

Changes of  $^{18}\text{O}/^{16}\text{O}$  of aqueous  $\text{O}_2$  as well as inhibited NDMA formation in the presence of radical scavengers point at the presence of radical intermediates in the NDMA formation mechanism. This conclusion is also in agreement with the observed NDMA formation kinetics in Figure 3.1. After a short lag phase, NDMA was formed concomitant with the degradation of DFUR showing that only reaction steps at the very beginning of the reaction were rate-determining, while later reaction steps leading to NDMA occurred almost instantaneously in agreement with fast reactions involving radical species.

Figure 3.3 shows a potential mechanism for a precursor molecule with a *N,N*-dimethylamine-methylfurane structure (ranitidine, DFUR; compound **1** in Figure 3.3) but is thought to apply likewise for other tertiary amines studied here (DMBA, TDMAP). Previous studies showed that chloramination of tertiary amines is initiated by a nucleophilic substitution reaction to a dimethylhydrazine-type compound (**2**).<sup>79,80</sup> Our investigation provides experimental evidence for the reaction of  $\text{O}_2$  with transient intermediates that are likely of radical nature. The latter could be generated as aminyl



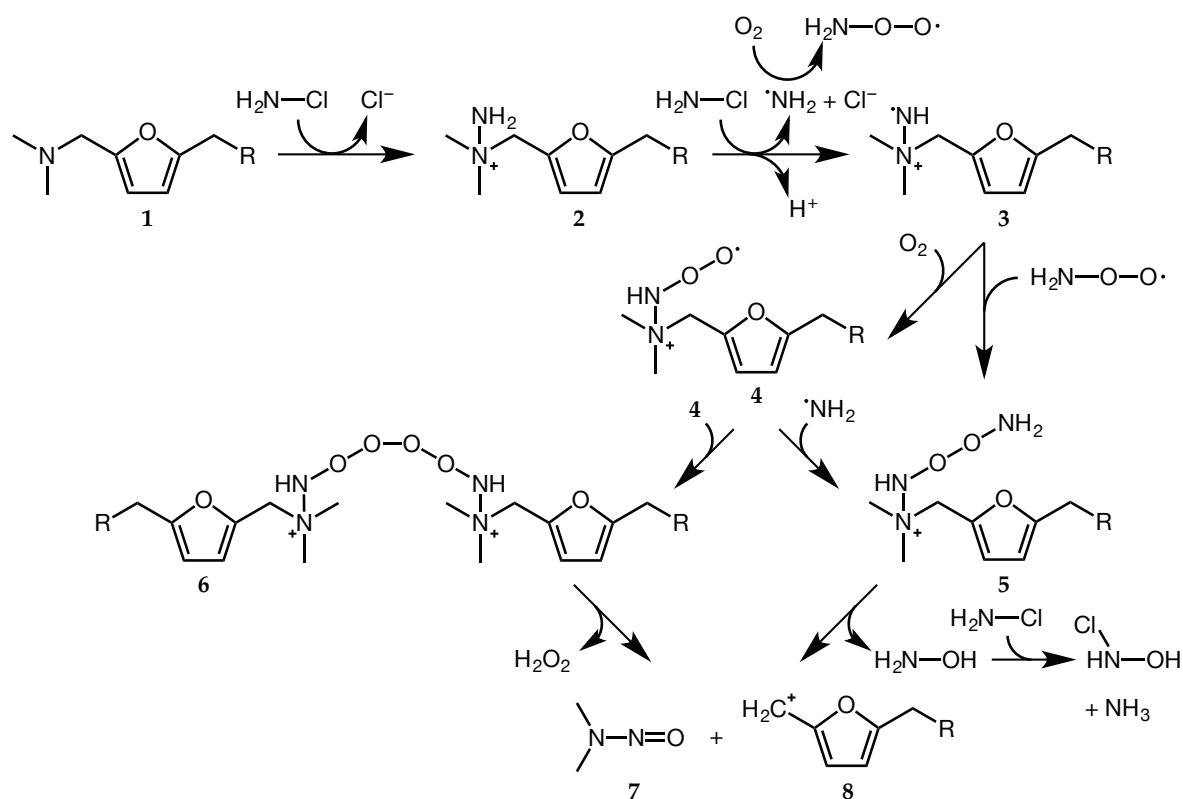


**Figure 3.3:** NDMA (7) formation from chloramination of *N,N*-dimethylamine-methylfuran moieties (1) through hypothetical intermediates: substituted hydrazine (2), aminyl radicals (3 and  $\bullet\text{NH}_2$ ), *N*-peroxyl radicals (4). Note that decomposition of the *N*-peroxyl coupling product (6) leads to formation of 2 equivalents of NDMA and methyl-furan carbocations (8) but only one is shown here.

radicals (3 and  $\text{H}_2\text{N}\bullet$ ) from the one-electron oxidation of 2 by  $\text{NH}_2\text{Cl}$ . Support for this assumption comes from observations that reactions of chloramines with  $\text{Fe}^{2+}$ , phenols, or tertiary amines (e.g., chlorpromazine, aminopyrine) lead to N-centered radicals at considerable rates.<sup>195–198</sup> The overstoichiometric consumption of  $\text{NH}_2\text{Cl}$  during the formation of NDMA (Table 3.1) indicates that  $\text{NH}_2\text{Cl}$  might play an important role not only for the initial nucleophilic substitution reaction, but also for the generation of radical intermediates.

Reactions of short-lived aminyl radicals are key to rationalize the stoichiometric consumption of  $\text{O}_2$  as well as  $^{18}\text{O}$ -KIEs. We hypothesize that aminyl radicals such as 3 exist as N-centered radicals and would not be prone to typical rearrangement to carbon centered peroxy radicals because the  $\text{HN}\bullet$  moiety is not bound to a C atom.<sup>199</sup> N-centered aminyl radicals can be oxygenated by molecular  $\text{O}_2$  to amino-peroxy radicals (4 and  $\text{H}_2\text{N}-\text{O}-\text{O}\bullet$ ) with rate constants of  $10^9 \text{ M}^{-1} \text{ s}^{-1}$ .<sup>200–202</sup> Such a reaction of triplet

O<sub>2</sub> is spin allowed, consistent with <sup>18</sup>O-KIEs < 1.01, and could thus be responsible for formation of the nitroso bond of NDMA.<sup>170,183</sup>

Figure 3.3 illustrates possible pathways leading from aminyl radical **3** to NDMA. The coupling of two *N*-peroxyl radicals **4** to compound **6** followed by the decay of **6** through the Bennett mechanism<sup>203,204</sup> seems a likely option. This pathway results in the formation of two equivalents of NDMA and methyl-furfuryl carbocations (**8**) and one equivalent of hydrogen peroxide (H<sub>2</sub>O<sub>2</sub>). In separate experiments, we indeed detected H<sub>2</sub>O<sub>2</sub> by adding catalase to reactors, in which 50 μM DFUR had been transformed to NDMA in the presence of 750 μM NH<sub>2</sub>Cl (Figure S3.26). Upon addition of catalase, which converts two molecules of H<sub>2</sub>O<sub>2</sub> to one molecule of O<sub>2</sub>, we measured 5.0 ± 1.6 μM of additional O<sub>2</sub>, which corresponds to a H<sub>2</sub>O<sub>2</sub> concentration of 7.0-13 μM at the *end* of the chloramination experiment (see section S3.13 for details). These numbers correspond to 28-52% of the theoretical maximum of 25 μM H<sub>2</sub>O<sub>2</sub> assuming a stoichiometric NDMA yield from 50 μM DFUR. Because H<sub>2</sub>O<sub>2</sub> was not stable when added at the beginning of a chloramination experiment (40% loss of H<sub>2</sub>O<sub>2</sub> within 3.3 h, Figure S3.26; e.g. through partial transformation by chloramine<sup>205</sup>), we conclude that the effective concentration of H<sub>2</sub>O<sub>2</sub> during NDMA formation must have been higher.

The proposed reaction pathway through species **1** → **2** → **3** → **4** → **6** → NDMA is plausible based on our experimental evidence but this interpretation strongly relies on selective coupling of amino-peroxyl radicals (**4**). We cannot rule out reactions of H<sub>2</sub>N• with aqueous O<sub>2</sub> what would lead to an overstoichiometric consumption of O<sub>2</sub>, except if H<sub>2</sub>N–O–O• transforms **3** to **5**, from which NDMA could be cleaved off. Moreover, *N*-peroxyl radicals (**4** and H<sub>2</sub>N–O–O•) could decompose by alternative routes (e.g., to nitric oxide) that do not lead to NDMA but inevitably consume aqueous O<sub>2</sub>.<sup>206</sup> If such reactions were to happen, however, one would not expect to observe the disappearance of one molecule of O<sub>2</sub> per *N,N*-dimethylamine group of the precursor compound (see Table 3.1). Based on the same reasoning, we consider it unlikely that nitrosating agents (e.g., nitric oxide), which would be readily oxidized by O<sub>2</sub>, were involved in the reactions leading to NDMA. Note that compounds like TDMAP and DMA may also react along the proposed pathways to *N*-peroxyl radicals because these precursors also exhibit (near) stoichiometric O<sub>2</sub> consumption. However, their much smaller yields of NDMA show the importance of the molecular structure of the NDMA precursor. While tertiary amines that possess an electron-rich aromatic moiety could stabilize *N*-peroxyl intermediates and lead to the formation of stable carbocationic leaving groups, these criteria might not be fulfilled in case of TDMAP and secondary amines such as DMA.<sup>67</sup>

Finally, the pathways shown in Figure 3.3 only account for the reaction of 2 to 3 equivalents of chloramine per tertiary amine while our data suggest a more than 4-fold excess of chloramine consumption (Table 3.1), which might be caused by side reactions leading to reaction products other than NDMA.

### 3.4 Implications for water treatment

The radical pathway for NDMA formation, as described above, was proposed based on evidence from experiments in laboratory-grade buffer solutions containing the organic precursors and  $\text{NH}_2\text{Cl}$ . During chloramination of source waters used for drinking water production, naturally occurring antioxidants containing e.g., phenolic moieties might effectively scavenge peroxy radicals<sup>207,208</sup> leading to a net decrease of NDMA formation. However, it has been shown previously that NDMA was also formed during chloramination of natural water samples which were spiked with ranitidine.<sup>71</sup> Compared to experiments in ultra-pure water, NDMA formation was slowed down in lake and river water, presumably due to interactions of unidentified natural organic matter (NOM) components with ranitidine. However, the molar NDMA yield from ranitidine was not affected by the water matrix indicating that reactive intermediates of the NDMA formation pathway were not scavenged by natural organic matter.<sup>71</sup> Indeed, it is known that the selective coupling of peroxy radicals to tetroxide species (similar to **4**  $\rightarrow$  **6**) occurs in natural water samples.<sup>209–211</sup> This selective peroxy radical coupling is even exploited for the determination of  $\bullet\text{OH}$  in raw waters using *t*-BuOH.<sup>209–211</sup> The NDMA formation mechanism proposed here is thus also likely to be operational during chloramination of amine-containing source waters used for drinking water production.

To mitigate *N*-nitrosamine formation during full-scale water treatment, utilities using chloramine might need to implement additional treatment steps that lead to an abatement of NDMA precursors using e.g., granular activated carbon or oxidative pre-treatment with ozone.<sup>159,212</sup> However, these approaches might not entirely prevent the formation of NDMA owing to varying source water qualities and the wide spectrum of precursor compounds and treatment conditions leading to NDMA.<sup>159</sup> New methods for the identification of relevant precursors and NDMA formation pathways in source waters are required to select optimal water treatment conditions and NDMA mitigation strategies.

## Acknowledgement

This study was supported by the Swiss National Science Foundation (Project no. 200021-140545). We thank Fabian Soltermann, Rebekka Gulde, Sarah Pati, and Jakov Bolotin for analytical support as well as Michèle Heeb and Kristopher McNeill for valuable discussions.

# Supporting Information to Chapter 3

## S3.1 Safety considerations

*N*-nitrosamines are mutagenic and probably carcinogenic to humans. Work in a well-ventilated fume hood and wear appropriate protective clothing, goggles, and gloves. Keep away from heat, sparks, and flame.

## S3.2 Chemicals

All chemicals in this study were used as received. *N*-nitrosodimethylamine (NDMA, 5000  $\mu\text{g}/\text{ml}$  in methanol, 99.9%), ranitidine hydrochloride, *N,N*-dimethylbenzylamine (DMBA, 99%), 2,4,6-tris(dimethylaminomethyl)phenol (TDMAP, 95%), dimethylamine (DMA, 40 wt.% in  $\text{H}_2\text{O}$ ), furfuryl alcohol (98%), *tert*-butanol (*t*-BuOH,  $\geq 99.7\%$ ), sodium citrate tribasic dihydrate ( $\geq 99\%$ ), 2,2'-azino-bis(3-ethylbenzothiazoline-6-sulfonic acid) diammonium salt (ABTS,  $\geq 98\%$ ), sodium nitrite ( $\text{NaNO}_2$ ,  $\geq 99\%$ ), potassium iodide (KI,  $\geq 99\%$ ), sodium thiosulfate ( $\text{Na}_2\text{S}_2\text{O}_3$ ,  $\geq 98\%$ ), sodium sulfite ( $\text{Na}_2\text{SO}_3$ ,  $\geq 98\%$ ), and catalase from bovine liver (2825 units/mg) were purchased from Sigma-Aldrich. 5-(Dimethylaminomethyl)furfuryl alcohol hydrochloride (DFUR, 96%) was obtained from ABCR and *rac*-6-hydroxy-2,5,7,8-tetramethylchromane-2-carboxylic acid (Trolox,  $> 98\%$ ), *N,N*-diethyl-*p*-phenylenediamine sulfate (DPD,  $\geq 99.0\%$ ), and phenol ( $\geq 99.5\%$ ) from Fluka. Sulfuric acid (98%, for analysis), formic acid (98-100%), sodium nitroprusside dihydrate, ethylenedinitrilotetraacetic acid disodium salt dihydrate (EDTA), and hydrogen peroxide ( $\text{H}_2\text{O}_2$ , 30%) were purchased from Merck.

Analyte stock and calibration solutions were made in methanol (99.99%, Fisher Scientific) or ethanol ( $\geq 99.5\%$ , Merck). Aqueous solutions were prepared with deionized water ( $18.1 \text{ M}\Omega \cdot \text{cm}$ , Barnstead NANOpure Diamond Water Purification System). For  $\text{NH}_2\text{Cl}$  preparation, ammonium chloride ( $\geq 99.5\%$ , Fluka) and sodium hypochlorite (6-14%  $\text{HOCl}$ , Sigma-Aldrich) were used. The pH-value of the potassium phosphate buffer ( $\text{KH}_2\text{PO}_4$ , puriss,  $\geq 99.5\%$ , Sigma-Aldrich) was adjusted by addition of sodium hydroxide pellets ( $\text{NaOH}$ , puriss,  $\geq 99\%$ , Sigma-Aldrich) or  $\text{NaOH}$  solution (Sigma-Aldrich). Ammonium carbonate and sodium hydrogen carbonate were purchased from Merck (EMSURE for analysis).  $\text{N}_2$  gas (99.999%) was used to prepare  $\text{O}_2$  free water and to create the  $\text{N}_2$  headspace necessary for isotope analysis of dissolved  $\text{O}_2$ .

### S3.3 Quantification of ranitidine, DFUR, and NDMA

Concentrations of ranitidine, DFUR, and NDMA  $\geq 0.1 \mu\text{M}$  were measured by reverse phase HPLC (Dionex UltiMate 3000) with UV-vis detection at wavelengths corresponding to the absorption maxima of the analytes (320 nm for ranitidine, 224 nm for DFUR, and 228 nm for NDMA). For quantification of ranitidine and DFUR, 40  $\mu\text{L}$  of aqueous sample were analyzed using a XBridge column (LC-18, 5 cm x 3 mm, 2.5  $\mu\text{m}$ , WATERS) equipped with a XBridge guard column (C18, 2.5  $\mu\text{m}$ , WATERS). The flow rate was  $0.5 \text{ mL min}^{-1}$  and eluent mixtures consisted of 65/35% and 75/25% phosphate buffer (1 mM, pH 11.5) / methanol for analysis of ranitidine and DFUR, respectively. For NDMA analysis, an aqueous sample volume of 50  $\mu\text{L}$  was analyzed using a Supelcosil LC-18 column (25 cm x 4.6 mm, 5  $\mu\text{m}$ , Supelco) with a LC-18 guard column. The eluent mixture consisted of 90% phosphate buffer (1 mM, pH 7.0) and 10% methanol at a flow rate of  $1 \text{ mL min}^{-1}$ .

### S3.4 Transformation product identification

Transformation products formed during chloramination of ranitidine and DFUR were analyzed by liquid chromatography-high-resolution tandem mass spectrometry (LC-HR-MS/MS). The analytical method described in Gulde et al.<sup>175</sup> was adjusted as follows: eluent mixtures consisted of either 75% ammonium carbonate buffer (1 mM, pH 8.9) and 25% methanol at a flow rate of  $400 \mu\text{L min}^{-1}$  using a XBridge column (LC-18, 5 cm x 3 mm, 2.5  $\mu\text{m}$ , WATERS) or 90%  $\text{H}_2\text{O}$  + 0.1% formic acid and 10% methanol at a flow rate of  $1 \text{ mL min}^{-1}$  using a Supelcosil LC-18 column (25 cm x 4.6 mm, 5  $\mu\text{m}$ , Supelco). Electrospray ionization (ESI) was used in positive and negative mode, and ion detection was performed with a QExactive (Thermo Fisher Scientific). Full-scan HR-MS data were acquired within a  $m/z$  range of 50 - 750 with a resolution of 70 000. Targeted HR-MS/MS spectra were recorded for pre-selected masses with a resolution of 17 500. Xcalibur (Thermo) was used for data analysis. We confirmed suspected transformation products with reference standards. Transformation products without matching reference standards were tentatively identified using exact mass, proposed molecular formula, occurrence of expected isotope peaks, and MS/MS spectra.

## S3.5 Quantification of $\text{NH}_2\text{Cl}$

The quantification of aqueous stock solutions of  $\text{HOCl}$  (65 mM) and  $\text{NH}_2\text{Cl}$  (30 mM) was conducted as described previously using a Varian Cary 100 Bio UV-visible spectrophotometer.<sup>137,138,162,213</sup> In reaction mixtures containing tertiary amines and NDMA, direct spectrophotometric analysis of  $\text{NH}_2\text{Cl}$ , which was quantified at  $\lambda = 245$  nm, was hindered because of interfering absorbance caused by the precursors, reaction intermediates, or products. We therefore used membrane introduction mass spectrometry and three different colorimetric methods as described below.

### S3.5.1 Membrane introduction mass spectrometry (MIMS)

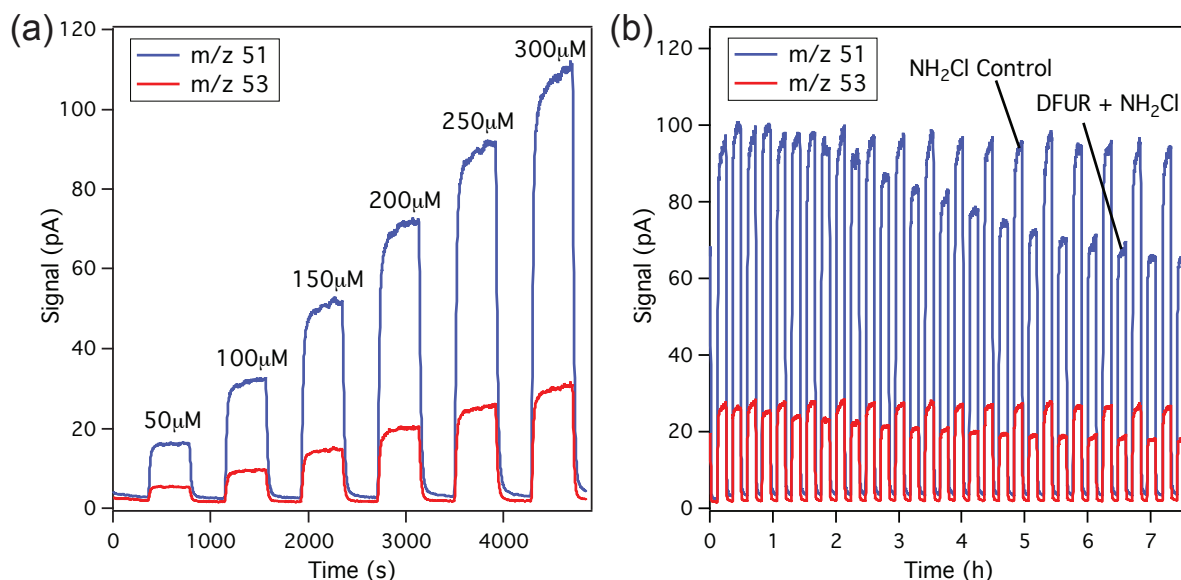


**Figure S3.1:** Analysis of monochloramine ( $\text{NH}_2\text{Cl}$ ) using membrane introduction mass spectrometry (MIMS). (a) Steady-state MS signals of a calibration series of  $\text{NH}_2\text{Cl}$  (50 - 300  $\mu\text{M}$ ) in 10 mM phosphate buffer at pH 8.0. The absolute MIMS signals depend on the settings of the amplifier, while the ratio of m/z 51 and m/z 53 remains constant. (b) MS signals from the analysis of  $\text{NH}_2\text{Cl}$  over 7.5 h in a control sample containing 250  $\mu\text{M}$   $\text{NH}_2\text{Cl}$  and in a reactive batch containing 15  $\mu\text{M}$  DFUR and 250  $\mu\text{M}$   $\text{NH}_2\text{Cl}$ . The control and the reactive sample were analyzed alternately by including a washing step (deionized water) in between to avoid carry-over.



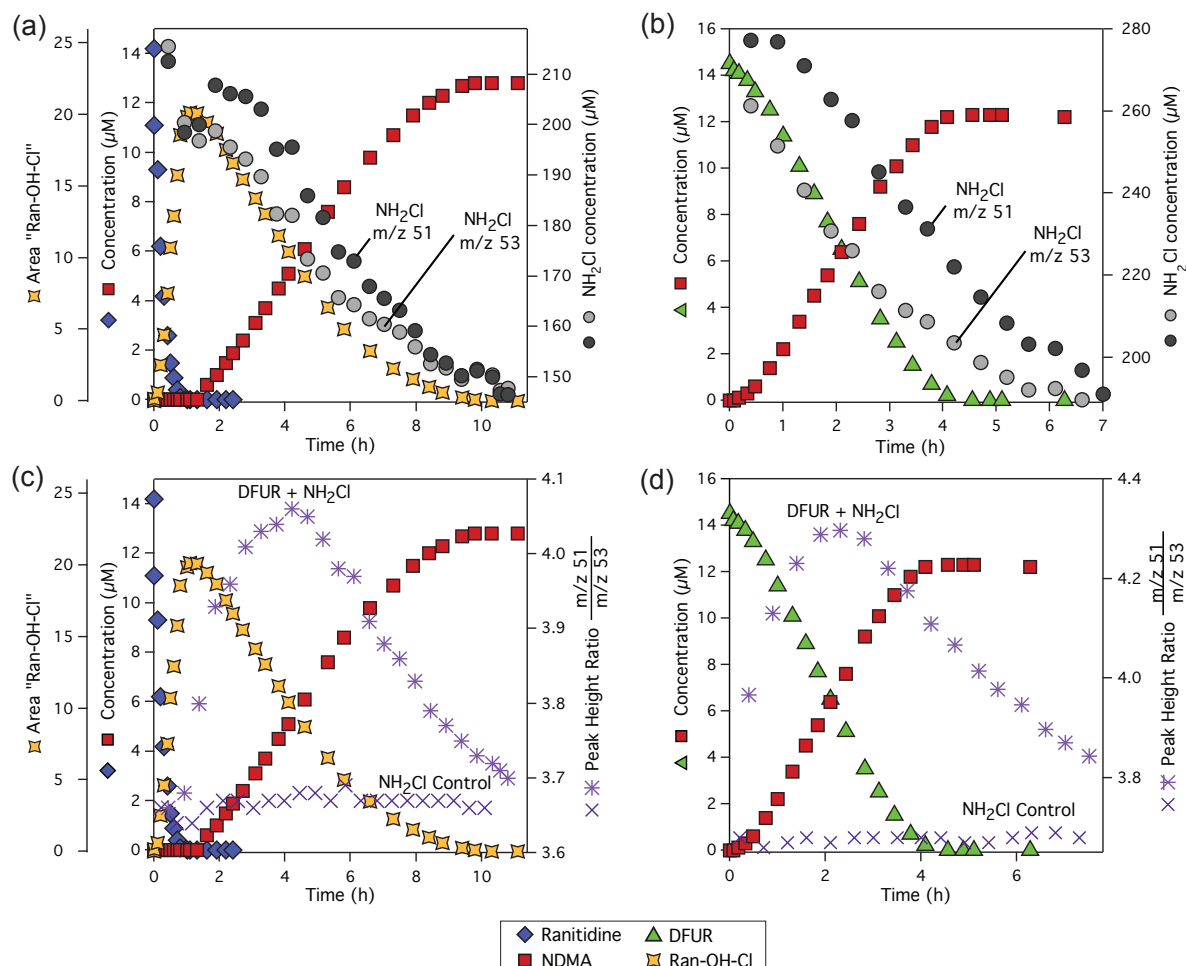


**Figure S3.2:**  $\text{NH}_2\text{Cl}$  consumption in NDMA formation experiments with (a, c) ranitidine and (b, d) DFUR.  $\text{NH}_2\text{Cl}$  concentrations were significantly different when evaluated with MIMS signals of m/z 51 and m/z 53. Using m/z 53, the decrease in  $\text{NH}_2\text{Cl}$  concentration corresponded well to the disappearance of Ran-OH-Cl (yellow stars in (a)) and DFUR (green triangles in (b)). Panels (c) and (d) show the ratios of peak heights of m/z 51 and m/z 53 over the time course of the chloramination reactions. The ratio remained constant in  $\text{NH}_2\text{Cl}$  controls containing 250  $\mu\text{M}$   $\text{NH}_2\text{Cl}$ , but significantly changed in reactive batches containing 15  $\mu\text{M}$  ranitidine or DFUR and 250  $\mu\text{M}$   $\text{NH}_2\text{Cl}$ . Owing to the peak shaped evolution of the peak height ratios, we hypothesize that an unidentified reaction intermediate produced a fragment with m/z 51 leading to the observed interference. All reported  $\text{NH}_2\text{Cl}$  concentrations quantified with MIMS were therefore evaluated using m/z 53.

### S3.5.2 Colorimetric methods

The **ABTS method** was conducted according to Pinkernell et al. (2000).<sup>139</sup> A 20 mL sample containing 1-10  $\mu\text{M}$   $\text{NH}_2\text{Cl}$  was placed in a 25 mL volumetric flask. 50  $\mu\text{L}$  of 0.1 M  $\text{NaNO}_2$  was added to quench  $\text{HOCl}$ . After 4 min, 1 mL of 1  $\text{g L}^{-1}$  ABTS, 3 mL of 0.5 M phosphate buffer (pH 6.1), and 150  $\mu\text{L}$  of 1 mM KI was added. The flask was filled with deionized water to 25 mL and mixed. After 10 min, the absorbance of  $\text{ABTS}^{\bullet+}$  was measured at 405 nm using a 1 cm quartz cuvette. A molar absorptivity of  $28500 \pm 950 \text{ M}^{-1} \text{ cm}^{-1}$  was used to calculate the concentration of  $\text{NH}_2\text{Cl}$ .

For the **DPD method**, we filled 1 mL of 0.5 M phosphate buffer, 1 mL of DPD reagent (0.15 g DPD + 0.8 mL 13.8 M  $\text{H}_2\text{SO}_4$  + 0.02 g EDTA), and 50  $\mu\text{L}$  of 14.5 mM KI into a 20 mL brown glass vial, added 10 mL of a  $\text{NH}_2\text{Cl}$  containing sample and mixed the solution. After 5 min, the absorbance of the stable radical cation ( $\text{DPD}^{\bullet+}$ , Wurster dye) was measured at 515 nm with a 1 cm quartz cuvette.<sup>176</sup> A calibration curve from 1 - 15  $\mu\text{M}$   $\text{NH}_2\text{Cl}$  was used for quantification.

The **indophenol method** was conducted according to Hach (2000).<sup>177</sup> A 20 mL sample was placed in a 25 mL volumetric flask with a magnetic stir bar. 0.5 g sodium citrate tribasic dihydrate was added and dissolved. 0.1 mL of nitroprusside reagent (0.5 g sodium nitroprusside dihydrate dissolved in 100 mL deionized water) and 1.2 mL phenol reagent (2.5 g  $\text{NaOH}$  + 10 g phenol in 100 mL deionized water) were added and mixed. By addition of a few droplets of 5 M  $\text{NaOH}$ , the pH of the solution was adjusted to  $12.1 \pm 0.1$ . The flask was filled to the 25 mL mark with deionized water and mixed. After 20 min, the absorbance of the formed indophenol was measured at 635 nm using a 1 cm quartz cuvette.<sup>177</sup> A calibration curve from 10-125  $\mu\text{M}$   $\text{NH}_2\text{Cl}$  was used for quantification.

All colorimetric assays were measured using a Varian Cary 100 Bio UV-visible spectrophotometer.

### S3.5.3 Comparison of different $\text{NH}_2\text{Cl}$ quantification methods

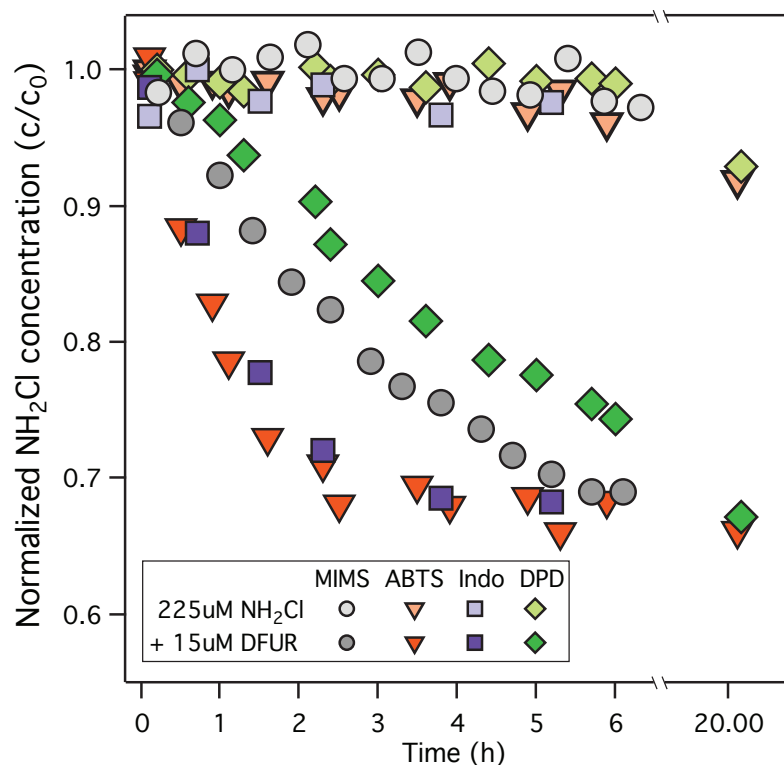


**Figure S3.3:** Concentrations of  $\text{NH}_2\text{Cl}$  monitored over 20 h in a control containing  $225\ \mu\text{M}$   $\text{NH}_2\text{Cl}$  (light colored symbols) and a reactive batch containing  $15\ \mu\text{M}$  DFUR and  $225\ \mu\text{M}$   $\text{NH}_2\text{Cl}$  (dark colored symbols).  $\text{NH}_2\text{Cl}$  was quantified using the MIMS signal  $m/z$  53 (grey circles) and three colorimetric methods based on the oxidation of ABTS (red triangles) and DPD (green diamonds) and the formation of an indophenolic compound (purple squares). All values were normalized to the initial  $\text{NH}_2\text{Cl}$  concentration measured with the respective method ( $c/c_0$ ).

We compared the analysis of  $\text{NH}_2\text{Cl}$  by mass spectrometry (MIMS) to three colorimetric methods that are based on (1) oxidation of ABTS,<sup>139</sup> (2) oxidation of DPD<sup>176</sup> using potassium iodide (KI) as catalyst, and (3) formation of a colored indophenolic compound via reaction of phenol with  $\text{NH}_2\text{Cl}$ .<sup>177</sup> While the ABTS as well as the DPD method determine the sum of reactive chloramine species ( $\text{NH}_2\text{Cl}$ ,  $\text{NHCl}_2$ , organochloramines) in a sample, the indophenol method is supposed to be selective for monochloramine.

MIMS as well as all three colorimetric methods performed equally well for the quantification of chloramine in control systems containing  $225\ \mu\text{M}$   $\text{NH}_2\text{Cl}$  in 10 mM phosphate buffer at pH 8.0 (Figure S3.3). In NDMA formation experiments with  $15\ \mu\text{M}$  DFUR and

225  $\mu\text{M}$   $\text{NH}_2\text{Cl}$ , we observed, however, significant differences in the performance of the selected methods. The chloramine concentrations determined with the ABTS method (red triangles in Figure S3.3) were within error identical to those obtained with the indophenol method (purple squares). Within the first 3 h of the reaction, the chloramine concentration dropped significantly by 30% and remained almost constant thereupon. In contrast, MIMS analysis (grey circles) showed a significantly slower and more steady decay of chloramine over 6 h. The kinetics of chloramine decay determined with the DPD method (green diamonds) resemble the results obtained with MIMS, but the chloramine concentration declined even slower. However, when NDMA formation was completed after 6 h, we obtained the same final chloramine concentration whether MIMS, ABTS, or the indophenol method were used. The total amount of consumed  $\text{NH}_2\text{Cl}$  after 6 h amounted to 34.1%, 33.8%, and 31.7% of the initial chloramine concentration for measurements with MIMS, ABTS, and indophenol, respectively. The DPD method seemed to underestimate the chloramine loss after 6 h (25.6%), but also showed a  $\text{NH}_2\text{Cl}$  consumption of 32.8% after 20 h (Figure S3.3).

In general, mass spectrometric measurements of chloramine seem to be more reliable than results obtained from indirect colorimetric methods because the response signal in MIMS analysis is directly produced by the analyte ( $\text{NH}_2\text{Cl}$ ). However, the produced ions  $m/z$  51 and  $m/z$  53 from  $\text{NH}_2\text{Cl}$  must be free from interferences because analysis with MIMS does not include any analyte separation step. As shown in Figure S3.2, we indeed observed an interference at  $m/z$  51 that might stem from an unknown reaction intermediate. Therefore, the signal  $m/z$  53 was used for  $\text{NH}_2\text{Cl}$  quantification, but we cannot exclude the possibility that this mass is biased as well.

An indirect quantification of chloramine with the ABTS and DPD method has the major disadvantage that ABTS and DPD are redox sensitive and readily undergo reactions with compounds other than chloramine. Substances known to create interferences include organic chloramines, nitrite, chromate, or oxidized manganese.<sup>177</sup> In NDMA formation experiments, we might produce reactive intermediates that could reduce the colored ABTS radicals back to ABTS what would lead to an overestimated  $\text{NH}_2\text{Cl}$  consumption. In contrast, the stable radical (Wurster dye) produced from oxidation of DPD does not seem to be reduced back. It rather seems that an intermediate species might oxidize DPD what leads to an underestimated  $\text{NH}_2\text{Cl}$  consumption. In both cases, reliable chloramine concentrations were obtained as soon as intermediate species were depleted at the end of the NDMA formation reaction. Unlike the ABTS and DPD method, the indophenol method is supposed to be specific for inorganic mono-

chloramine ( $\text{NH}_2\text{Cl}$ ) because the colored indophenolic compound can only form if there are two exchangeable hydrogens.<sup>177</sup> We can, however, not exclude that intermediate species reacted with either the catalyst (nitroprusside), phenol, or the indophenolic product what would cause an overestimation of the consumed  $\text{NH}_2\text{Cl}$ .

We here show that all of the used methods for chloramine quantification can be prone to interferences and it is difficult to identify which method provides the most reliable result in the studied reaction system. Caution is advised when applying any of the tested methods for  $\text{NH}_2\text{Cl}$  quantification in synthetic or natural samples in which reactive species could cause interferences. The here reported overstoichiometric  $\text{NH}_2\text{Cl}$  consumption at the end of the NDMA formation reaction is, however, valid and not caused by analytical errors because we found an identical  $\text{NH}_2\text{Cl}$  loss between 32% and 34% of the initial  $\text{NH}_2\text{Cl}$  concentration with the MIMS, ABTS, DPD, and indophenol method.

### S3.6 Aqueous vs. methanolic DFUR spike solution

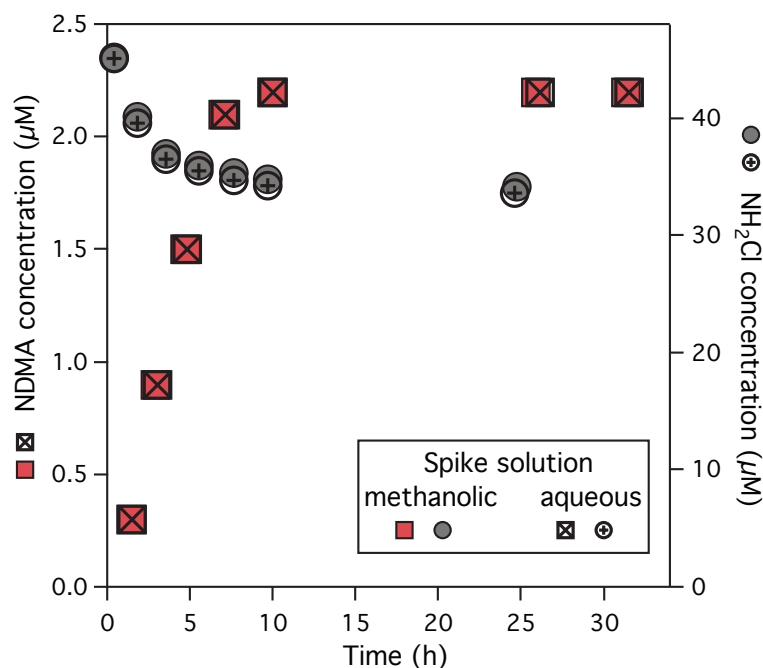


**Figure S3.4:** NDMA formation (squares) and  $\text{NH}_2\text{Cl}$  consumption (circles) during the reaction of DFUR ( $3\mu\text{M}$ ) with  $\text{NH}_2\text{Cl}$  ( $45\mu\text{M}$ ) in 10 mM phosphate buffer at pH 8.0. No difference in NDMA formation and  $\text{NH}_2\text{Cl}$  consumption was observed when DFUR was added as a methanolic or aqueous spike solution.

### S3.7 Reactivity of DFUR with chloramine quenchers: Sulfite vs. thiosulfate

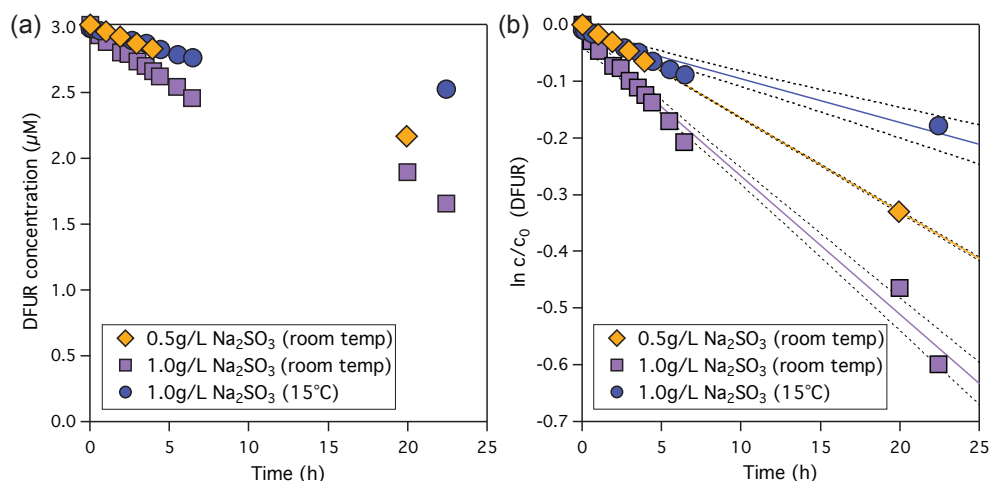


**Figure S3.5:** Reaction of 3 μM DFUR with 0.5 g L<sup>-1</sup> and 1 g L<sup>-1</sup> Na<sub>2</sub>SO<sub>3</sub> in 10 mM phosphate buffer at pH 8.0 at room temperature and 15°C. (a) Decline of the DFUR concentration over time and (b) determination of pseudo-first order rate constants ( $k_{obs}$ ) for DFUR degradation that is  $(4.59 \pm 0.05) \cdot 10^{-6} \text{ s}^{-1}$  for the reaction with 0.5 g L<sup>-1</sup> Na<sub>2</sub>SO<sub>3</sub>,  $(6.77 \pm 0.51) \cdot 10^{-6} \text{ s}^{-1}$  for 1 g L<sup>-1</sup> Na<sub>2</sub>SO<sub>3</sub> at room temperature, and  $(2.14 \pm 0.45) \cdot 10^{-6} \text{ s}^{-1}$  for 1 g L<sup>-1</sup> Na<sub>2</sub>SO<sub>3</sub> at 15°C.

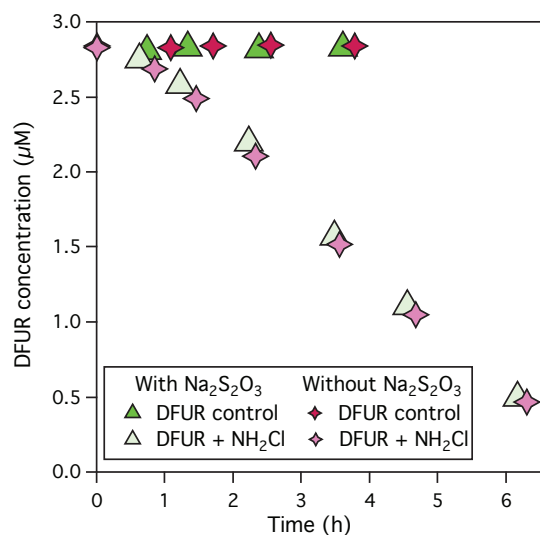


**Figure S3.6:** DFUR concentration in a control containing 3 μM DFUR and a reactive batch containing 3 μM DFUR and 45 μM NH<sub>2</sub>Cl in 10 mM phosphate buffer at pH 8.0 in the presence and absence of 0.5 g L<sup>-1</sup> Na<sub>2</sub>S<sub>2</sub>O<sub>3</sub> (green triangles and red stars, respectively). DFUR did not react with Na<sub>2</sub>S<sub>2</sub>O<sub>3</sub> over a time period of 4 h and the presence of Na<sub>2</sub>S<sub>2</sub>O<sub>3</sub> had no effect on the degradation of DFUR during chloramination.

### S3.8 Impact of the tertiary amine to chloramine ratio on NDMA formation

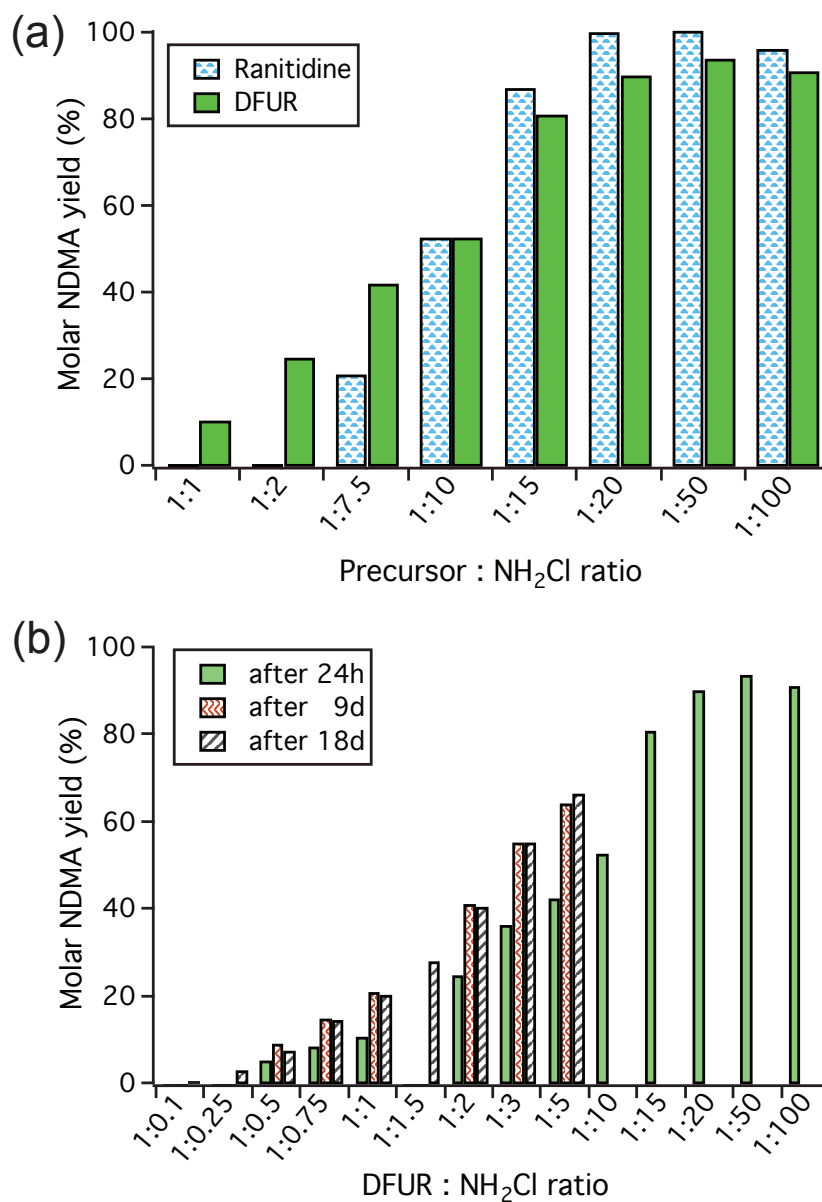


**Figure S3.7:** Impact of the ratio of tertiary amine to  $\text{NH}_2\text{Cl}$  on the molar NDMA yield in percent. Panel (a) shows molar NDMA yields formed after 24h from the chloramination of ranitidine (3  $\mu\text{M}$ ) or DFUR (3  $\mu\text{M}$ ) using precursor to  $\text{NH}_2\text{Cl}$  ratios from 1:1 to 1:100. Panel (b) shows the temporal evolution of molar NDMA yields obtained for different DFUR (3  $\mu\text{M}$ ) to  $\text{NH}_2\text{Cl}$  ratios of 1:0.1 to 1:100 after 24 hours, 6 days, and 18 days.

## S3.9 Chloramination of secondary and tertiary amines

### S3.9.1 Reaction kinetics and stoichiometry of $\text{NH}_2\text{Cl}$ and $\text{O}_2$ consumption

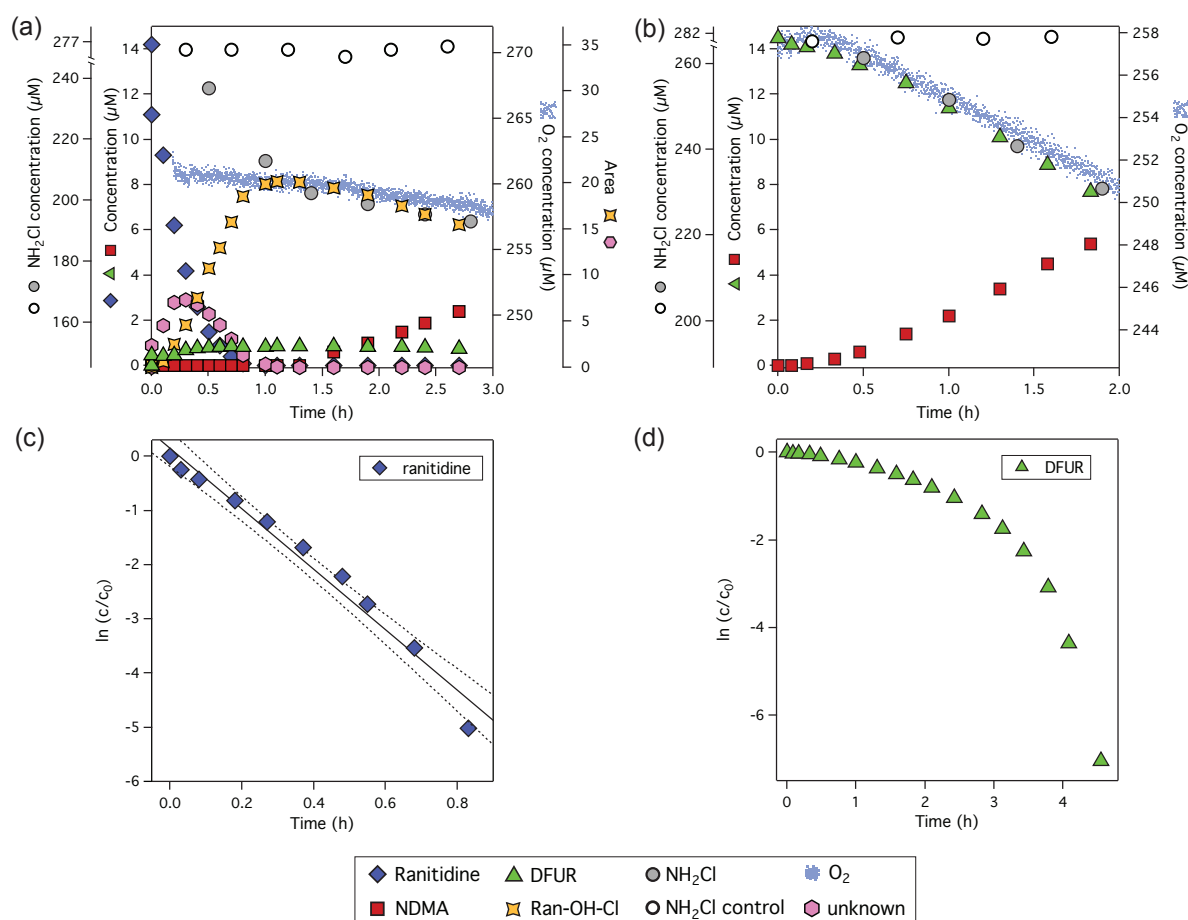


**Figure S3.8:** Initial kinetics of the reaction of  $\text{NH}_2\text{Cl}$  (270  $\mu\text{M}$ ) with (a) ranitidine (15  $\mu\text{M}$ ) and (b) DFUR (15  $\mu\text{M}$ ) in 10 mM phosphate buffer at pH 8.0. While ranitidine was transformed to Ran-OH-Cl, DFUR and other unknown transient intermediates prior to NDMA formation (panel a), the formation of NDMA was concomitant with the degradation of DFUR (panel b). Ranitidine was transformed with a pseudo-first order rate constant ( $k_{\text{obs}}$ ) of  $(1.55 \pm 0.08) \cdot 10^{-3} \text{ s}^{-1}$  obtained from linear regression shown in panel c. The transformation of DFUR increased non-linearly after a short lag phase of 0.3 h (panel d).



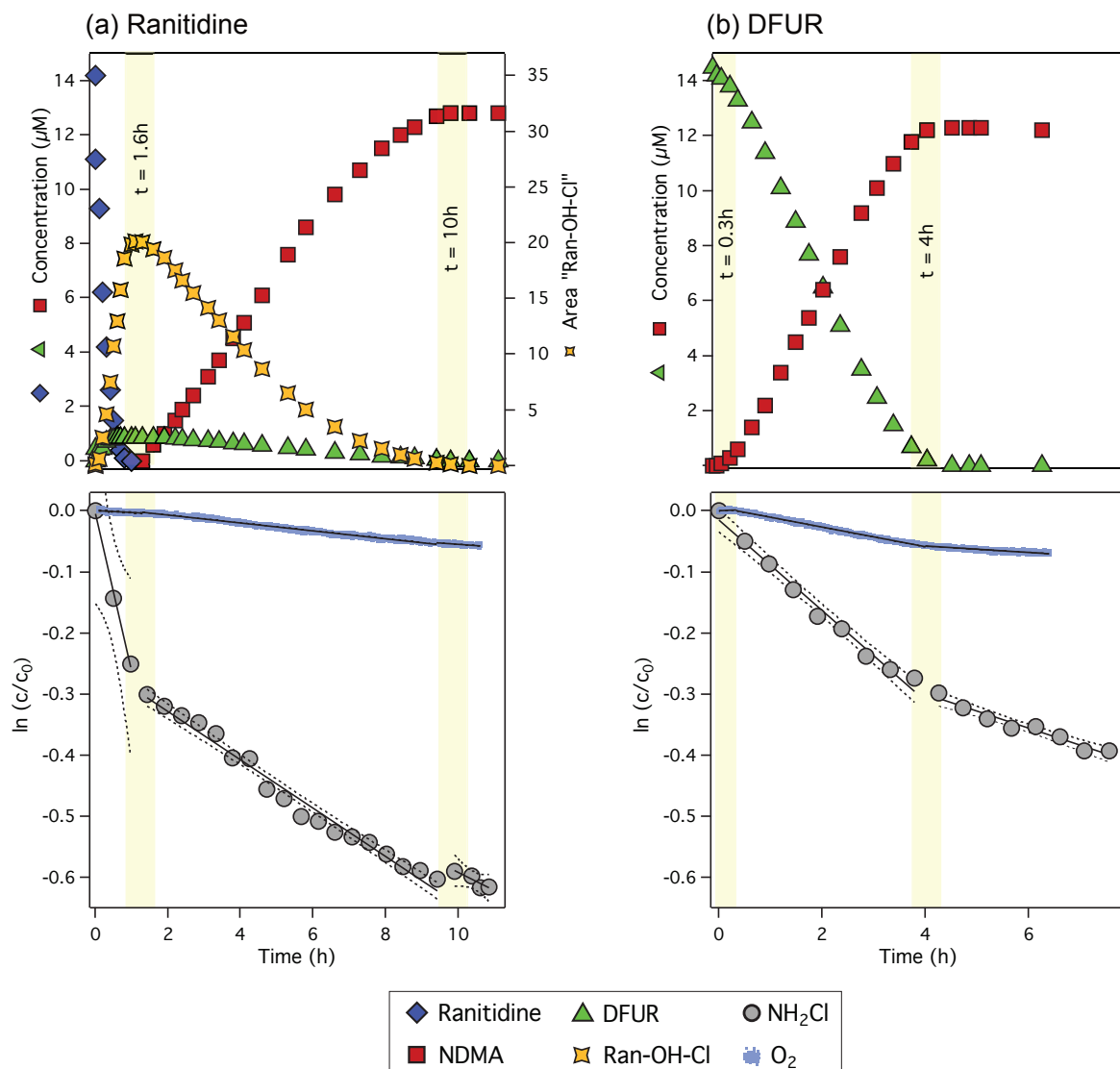


**Figure S3.9:** Three kinetic regimes were observed for the consumption of  $\text{NH}_2\text{Cl}$  and  $\text{O}_2$  during the reaction of (a) ranitidine ( $15\ \mu\text{M}$ ) and (b) DFUR ( $15\ \mu\text{M}$ ) with  $\text{NH}_2\text{Cl}$  ( $270\ \mu\text{M}$ ) in 10 mM phosphate buffer at pH 8.0. During ranitidine transformation,  $\text{NH}_2\text{Cl}$  disappeared with an operational pseudo-first order rate constant  $k_{\text{obs}, 1, \text{ran}}^{\text{NH}_2\text{Cl}} = (7.2 \pm 0.5) \cdot 10^{-5}\ \text{s}^{-1}$ . Afterwards, NDMA formation started and a smaller rate constant of  $k_{\text{obs}, 2, \text{ran}}^{\text{NH}_2\text{Cl}} = (1.1 \pm 0.04) \cdot 10^{-5}\ \text{s}^{-1}$  was observed. When NDMA formation was completed, we observed ongoing  $\text{NH}_2\text{Cl}$  consumption with  $k_{\text{obs}, 3, \text{ran}}^{\text{NH}_2\text{Cl}} = (8.6 \pm 2.7) \cdot 10^{-6}\ \text{s}^{-1}$ . The  $\text{O}_2$  concentration remained constant during ranitidine transformation and started to decrease after 1.6 h with a pseudo-first order rate constant  $k_{\text{obs}, \text{ran}}^{\text{O}_2}$  of  $(1.8 \pm 0.1) \cdot 10^{-6}\ \text{s}^{-1}$  (panel a). (b) During chloramination of DFUR, we observed a lag phase of 0.3 h. Afterwards,  $\text{NH}_2\text{Cl}$  was consumed with a pseudo-first order rate constant  $k_{\text{obs}, 1, \text{DFUR}}^{\text{NH}_2\text{Cl}} = (2.2 \pm 0.1) \cdot 10^{-5}\ \text{s}^{-1}$ . After NDMA formation was completed,  $\text{NH}_2\text{Cl}$  consumption continued with  $k_{\text{obs}, 2, \text{DFUR}}^{\text{NH}_2\text{Cl}} = (7.7 \pm 0.7) \cdot 10^{-6}\ \text{s}^{-1}$ .  $\text{O}_2$  decreased with  $k_{\text{obs}, \text{DFUR}}^{\text{O}_2} = (4.5 \pm 0.1) \cdot 10^{-6}\ \text{s}^{-1}$  during chloramination of DFUR. As soon as NDMA formation was completed,  $\text{O}_2$  consumption ceased.

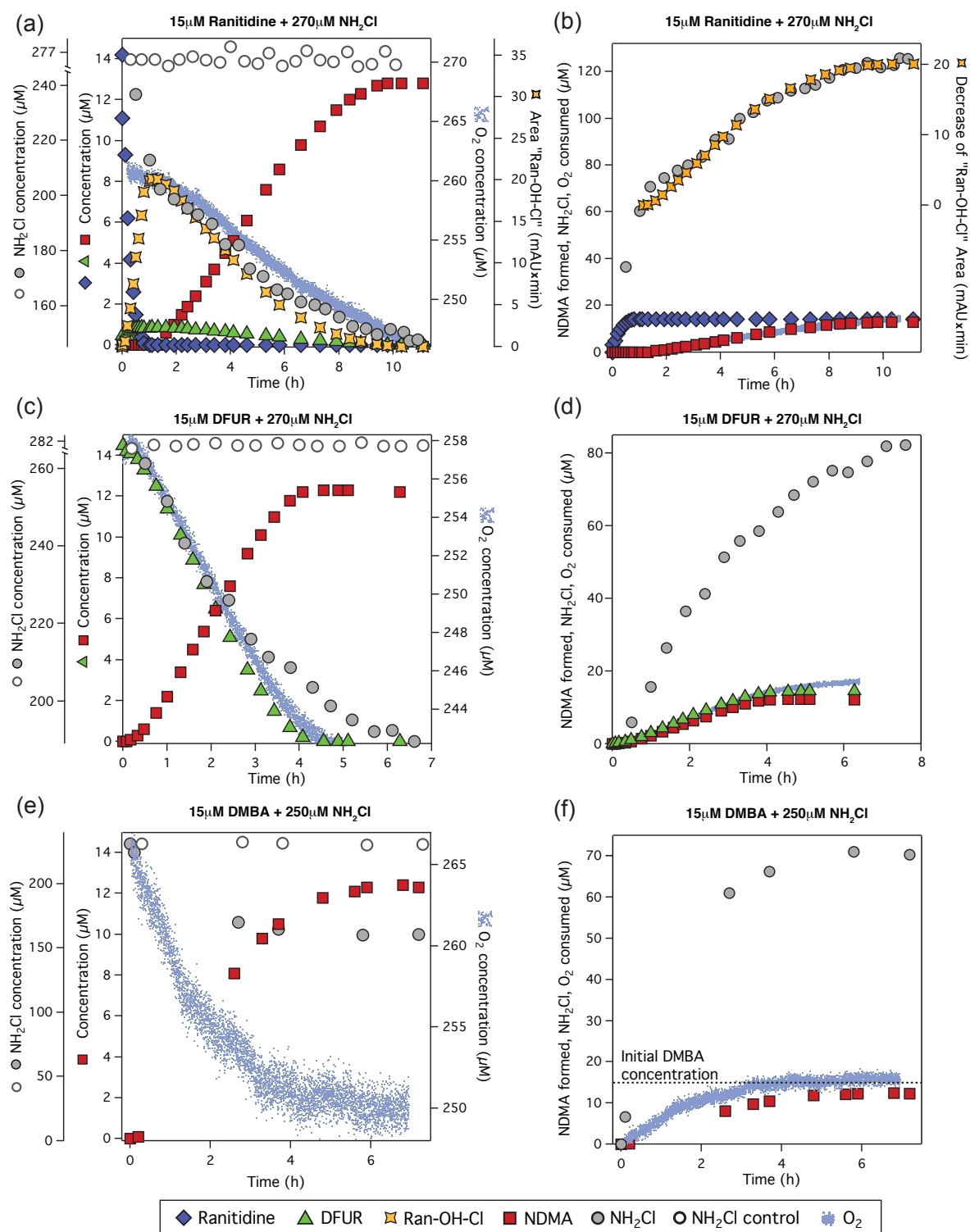


**Figure S3.10:** NDMA formation during chloramination of (a, b) ranitidine ( $15\ \mu\text{M}$ ), (c, d) DFUR ( $15\ \mu\text{M}$ ), and (e, f) DMBA ( $15\ \mu\text{M}$ ) in 10 mM phosphate buffer at pH 8.0. The right panels (a, c, e) show concentration profiles of the precursor,  $\text{NH}_2\text{Cl}$ ,  $\text{O}_2$ , and NDMA. The left panels (b, d, f) show NDMA formation as well as the amount of consumed precursor,  $\text{NH}_2\text{Cl}$ , and  $\text{O}_2$  on the same scale. Note that for ranitidine and DFUR we determined  $\text{NH}_2\text{Cl}$  with MIMS, while the ABTS method was used in the experiment with DMBA.

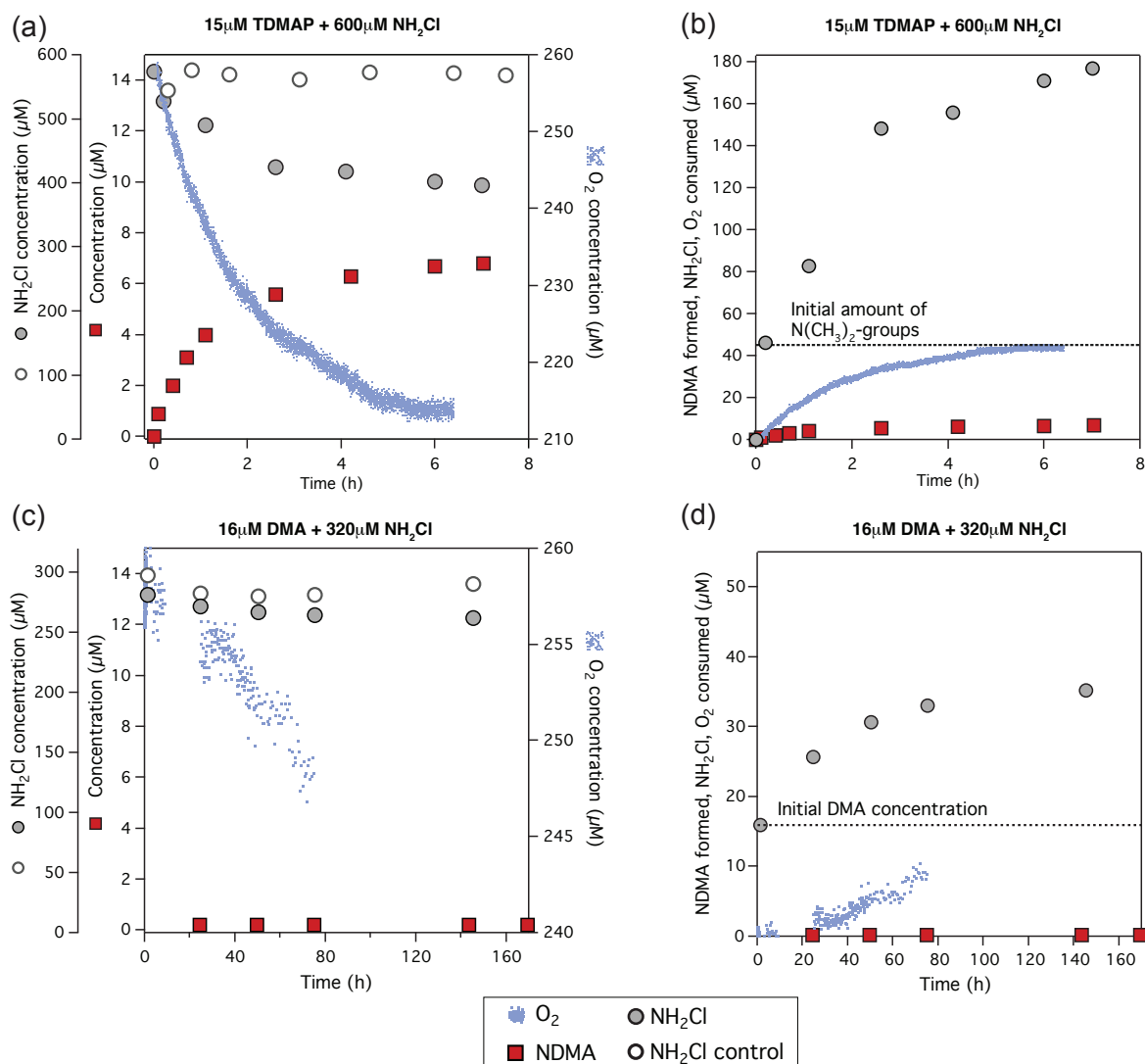


**Figure S3.11:** NDMA formation during chloramination of (a, b) TDMAP (15  $\mu\text{M}$  corresponding to 45  $\mu\text{M}$  *N,N*-dimethylamine groups) and (c, d) DMA (16  $\mu\text{M}$ ) in 10 mM phosphate buffer at pH 8.0. Note that we applied 600  $\mu\text{M}$   $\text{NH}_2\text{Cl}$  to 15  $\mu\text{M}$  TDMAP to reach a 13-fold excess of  $\text{NH}_2\text{Cl}$  compared to the initial concentration of *N,N*-dimethylamine groups. The right panels (a, c) show concentration profiles of  $\text{NH}_2\text{Cl}$ ,  $\text{O}_2$ , and NDMA. The left panels (b, d) show NDMA formation as well as the concentration of consumed  $\text{NH}_2\text{Cl}$  and  $\text{O}_2$  on the same scale. In experiments with TDMAP and DMA,  $\text{NH}_2\text{Cl}$  was quantified with the ABTS method.

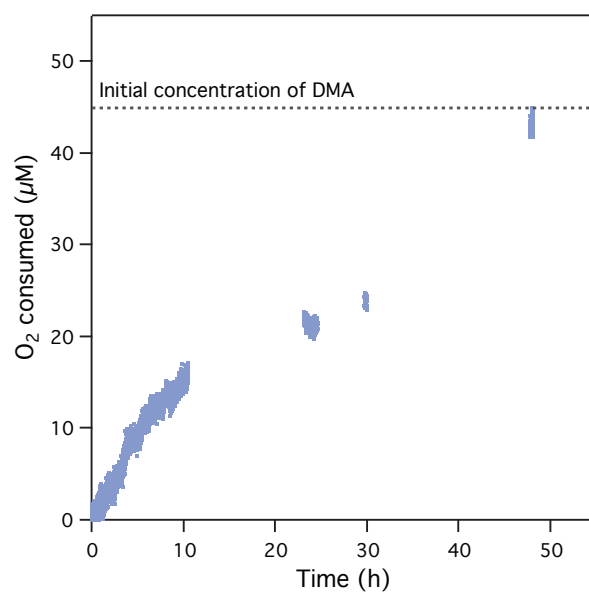


**Figure S3.12:** Concentration of consumed aqueous O<sub>2</sub> during the reaction of DMA (43 μM) with NH<sub>2</sub>Cl (1 mM) in 10 mM phosphate buffer at pH 8.0.

**Table S3.1:** NDMA formation during the reaction of  $\text{NH}_2\text{Cl}$  (45  $\mu\text{M}$  or 250  $\mu\text{M}$ ) with ranitidine (15  $\mu\text{M}$ ) or DFUR (3  $\mu\text{M}$  or 15  $\mu\text{M}$ ) in 10 mM phosphate buffer at pH 8.0 in the absence or presence of (i) *tert*-butanol (*t*-BuOH, 40 mM), (ii) ABTS (2 mM), or (iii) trolox (0.5 mM). Reported are the concentrations of consumed precursor,  $\text{O}_2$ , and  $\text{NH}_2\text{Cl}$  and formed NDMA in  $\mu\text{M}$  as well as reaction stoichiometries.

precursor	Consumption ( $\mu\text{M}$ )			Formation ( $\mu\text{M}$ )		molar reaction stoichiometry			
	$\text{N}(\text{CH}_3)_2\text{-group}$	$\text{O}_2$	$\text{NH}_2\text{Cl}$	NDMA	$\text{N}(\text{CH}_3)_2\text{-group}$	$\text{O}_2$	$\text{NH}_2\text{Cl}$	NDMA	
Ranitidine	14.2	14.3	123.5 (MIMS)	12.8	1.0	: 1.0	: 8.7	: 0.90	
Ranitidine	14.2	13.6	108.6 (ABTS)	13.2	1.0	: 1.0	: 7.6	: 0.93	
Ranitidine	15.0 <sup>a</sup>	n.m. <sup>b</sup>	97.0 (ABTS)	13.3	1.0	: n.m.	: 6.5	: 0.89	
Ranitidine + <i>t</i> -BuOH	15.0 <sup>a</sup>	n.m.	98.6 (ABTS)	13.2	1.0	: n.m.	: 6.6	: 0.88	
DFUR	14.5	15.2	68.2 (MIMS)	12.2	1.0	: 1.1	: 4.7	: 0.85	
DFUR	14.3	15.7	75.9 (ABTS)	12.9	1.0	: 1.1	: 5.3	: 0.90	
DFUR	15.0 <sup>a</sup>	n.m.	59.7 (ABTS)	12.5	1.0 <sup>a</sup>	: n.m.	: 4.0	: 0.84	
DFUR + <i>t</i> -BuOH	15.0 <sup>a</sup>	n.m.	59.9 (ABTS)	12.1	1.0 <sup>a</sup>	: n.m.	: 4.0	: 0.81	
DFUR	14.0	n.m.	n.m.	12.5	1.0	: n.m.	: n.m.	: 0.89	
DFUR + ABTS	12.5	0.0	223.3 (ABTS <sub>ox</sub> )	<0.1	0.9	: 0.0	: 15.9	: <0.7	
DFUR	2.8	n.m.	9.0 (MIMS)	2.4	1.0	: n.m.	: 3.2	: 0.85	
DFUR + trolox	0.34	n.m.	21.0 (MIMS)	<0.1	0.12	: n.m.	: 7.5	: <0.7	

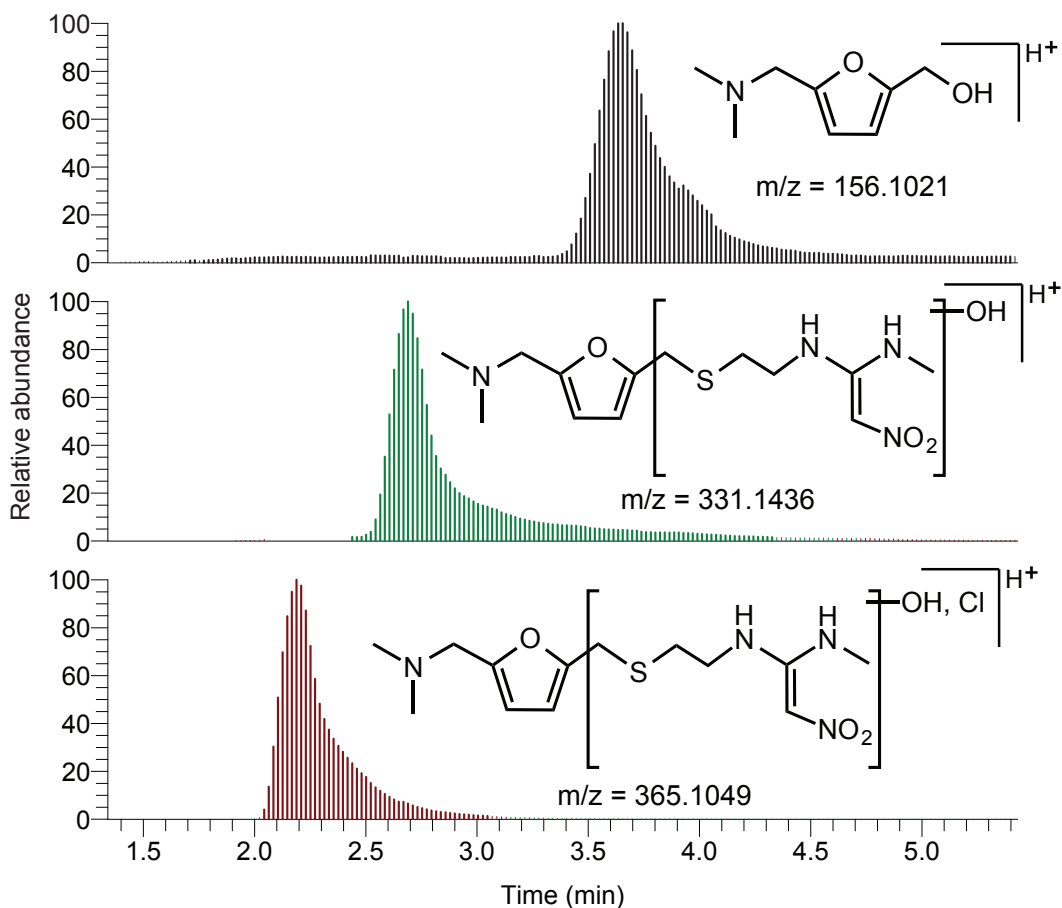
<sup>a</sup> nominal initial concentration      <sup>b</sup> not measured

**Table S3.2:** NDMA formation during the reaction of  $\text{NH}_2\text{Cl}$  ( $250\ \mu\text{M}$ ) with DMBA ( $15\ \mu\text{M}$ ),  $\text{NH}_2\text{Cl}$  ( $600\ \mu\text{M}$ ) with TDMAP ( $15\ \mu\text{M}$ ), and  $\text{NH}_2\text{Cl}$  ( $320\ \mu\text{M}$ ) with DMA ( $16\ \mu\text{M}$ ) in  $10\ \text{mM}$  phosphate buffer at pH 8.0. Reported are the concentrations of consumed precursor,  $\text{O}_2$ , and  $\text{NH}_2\text{Cl}$  and formed NDMA in  $\mu\text{M}$  as well as reaction stoichiometries.

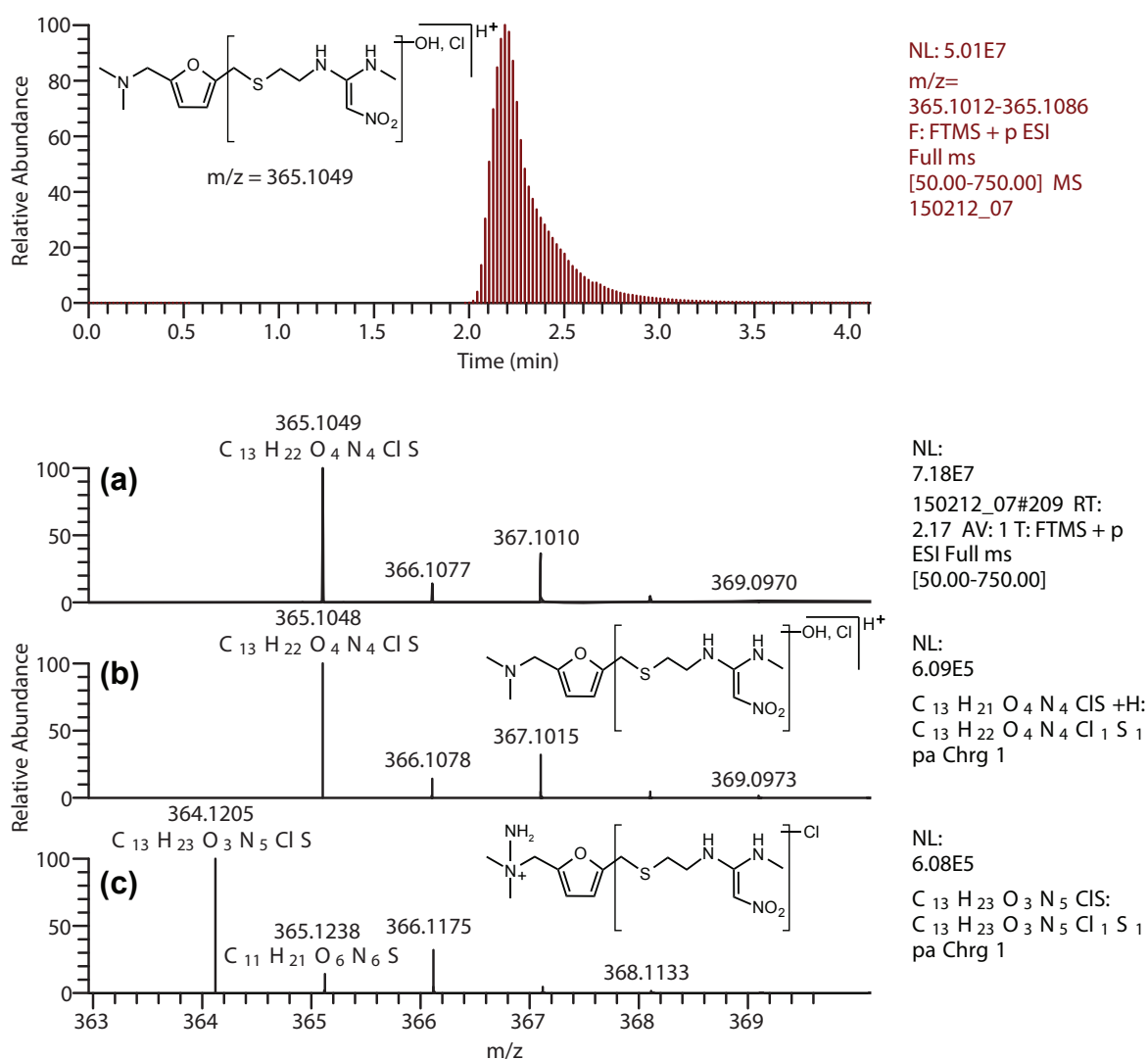
precursor	Consumption ( $\mu\text{M}$ )			Formation ( $\mu\text{M}$ )		molar reaction stoichiometry			
	$\text{N}(\text{CH}_3)_2\text{-group}$	$\text{O}_2$	$\text{NH}_2\text{Cl}$	NDMA		$\text{N}(\text{CH}_3)_2\text{-group}$	$\text{O}_2$	$\text{NH}_2\text{Cl}$	NDMA
DMBA	$15.0^{\text{a}}$	$15.8$	$70.6\ (\text{ABTS})$	$12.4$		$1.0^{\text{a}}$	$1.1$	$4.7$	$0.83$
TDMAP	$45.0^{\text{a}}$	$43.7$	$176.8\ (\text{ABTS})$	$7.1$		$1.0^{\text{a}}$	$1.0$	$3.9$	$0.16$
DMA	$16.0^{\text{a}}$	$9.0$	$35.4\ (\text{ABTS})$	$0.22$		$1.0^{\text{a}}$	$>0.6^{\text{b}}$	$2.2$	$0.014$
DMA	$43^{\text{a}}$	$43.3$	n.m.	$2.63$		$1.0^{\text{a}}$	$1.0$	n.m. <sup>c</sup>	$0.061$

<sup>a</sup> nominal initial concentration      <sup>b</sup> determined after approx. 50% of the total reaction time      <sup>c</sup> not measured

### S3.9.2 Transformation products

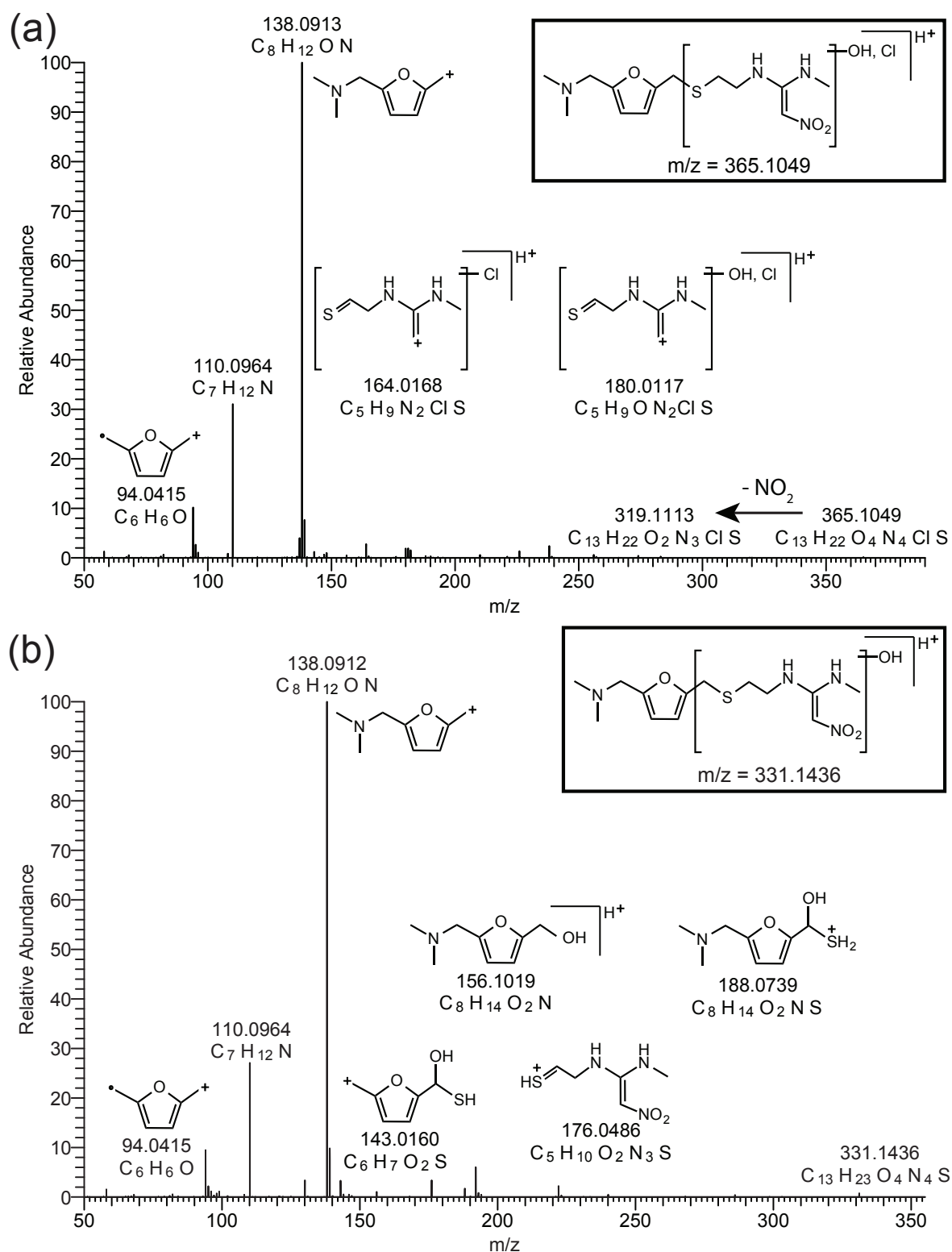


**Figure S3.13:** Retention time and exact mass of three transformation products found with LC-HR-MS/MS during the reaction of ranitidine ( $15\ \mu\text{M}$ ) with  $\text{NH}_2\text{Cl}$  ( $270\ \mu\text{M}$ ) in 10 mM phosphate buffer at pH 8.0. While the transformation product with  $m/z [\text{M}+\text{H}^+] = 156.1021$  was confirmed with a reference standard, transformation products with  $m/z [\text{M}+\text{H}^+] = 331.1436$  and  $m/z [\text{M}+\text{H}^+] = 365.1049$  were tentatively identified using exact mass, proposed molecular formula, occurrence of expected isotope peaks, and MS/MS spectra.

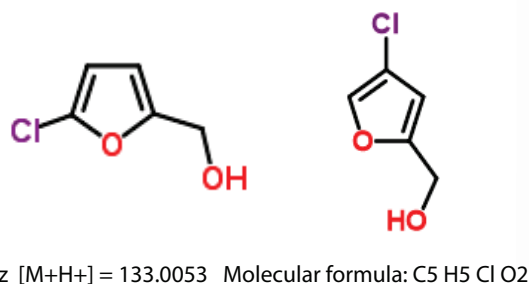


**Figure S3.14:** (a) LC-HR-MS/MS fragmentation pattern of a transformation product with  $m/z [M+H^+] = 365.1049$  and predicted fragmentation patterns of (b) hydroxylated, chlorinated ranitidine (Ran-OH-Cl) with molecular formula  $C_{13}H_{21}O_4N_4ClS$  and  $m/z [M+H^+] = 365.1048$  and (c) chlorinated dimethylhydrazine (Ran-NH<sub>2</sub>-Cl) with molecular formula  $C_{13}H_{23}O_3N_5ClS$  and  $m/z = 364.1205$ .



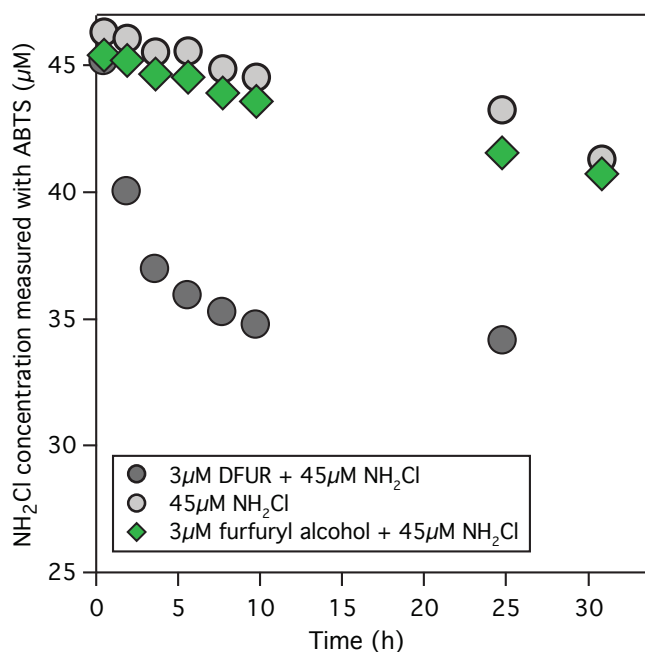


**Figure S3.15:** MS<sup>2</sup> spectra of molecular ion (a)  $m/z$   $[M+H]^+ = 365.1049$  corresponding to Ran-OH-Cl and (b)  $m/z$   $[M+H]^+ = 331.1436$  corresponding to Ran-OH in ESI positive mode.

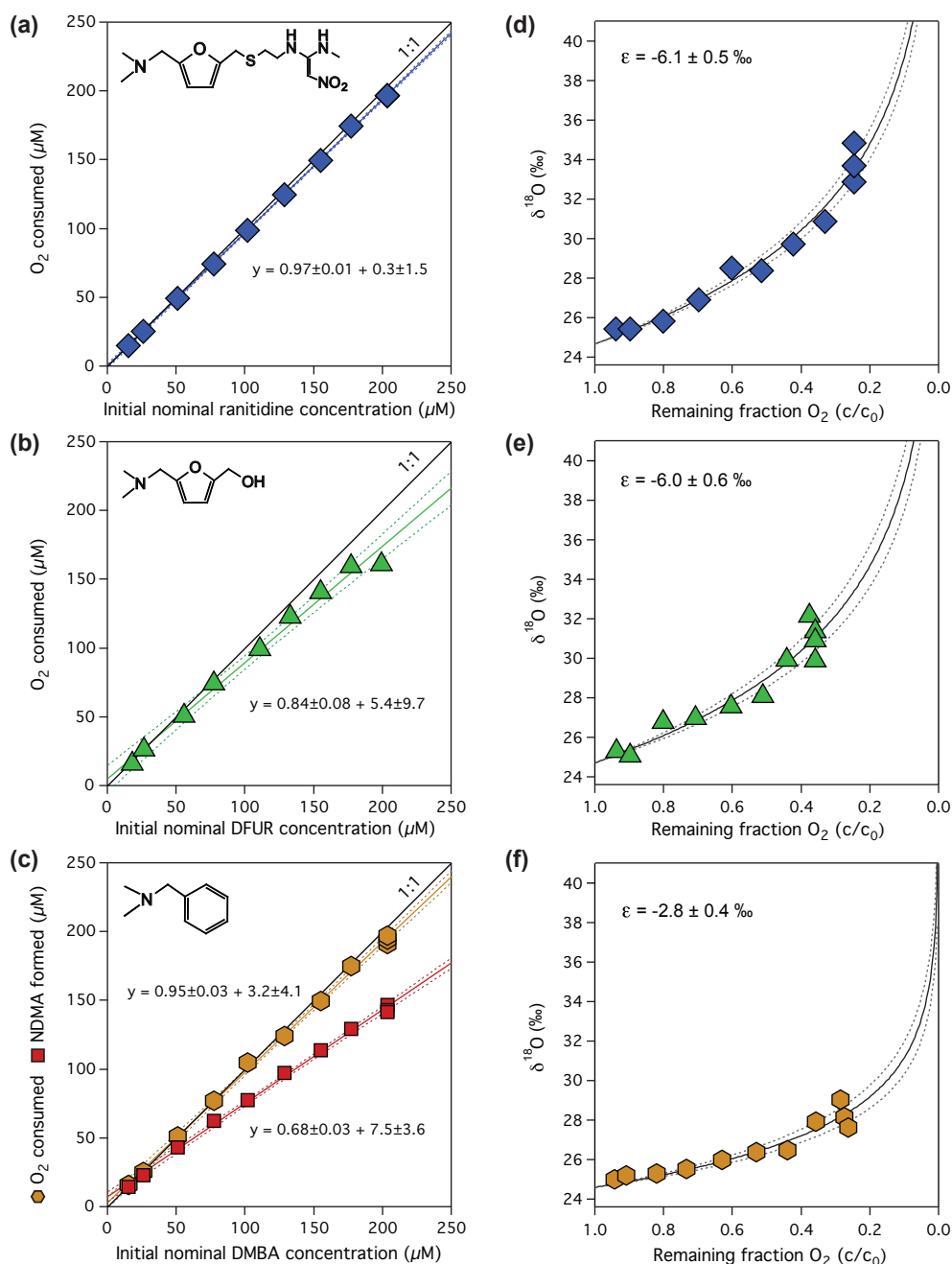


**Figure S3.16:** Potential transformation product with m/z [M+H<sup>+</sup>] = 133.0053 formed during chloramination of DFUR. Two suggested molecular structures corresponding to the formula C<sub>5</sub>H<sub>5</sub>ClO<sub>2</sub> using Chemspider.

### S3.10 Chloramination of furfuryl alcohol



**Figure S3.17:** NH<sub>2</sub>Cl concentration measured with the ABTS method over 30 h in three different batches containing (i) 3 μM DFUR and 45 μM NH<sub>2</sub>Cl, (ii) 45 μM NH<sub>2</sub>Cl, and (iii) 3 μM furfuryl alcohol and 45 μM NH<sub>2</sub>Cl in 10 mM phosphate buffer at pH 8.0. Note that NH<sub>2</sub>Cl concentrations were not corrected for the self-decay of chloramine observed in the NH<sub>2</sub>Cl control.

S3.11 Oxygen isotope analyses of aqueous O<sub>2</sub>

**Figure S3.18:** Consumption of aqueous O<sub>2</sub> during the reaction of  $\text{NH}_2\text{Cl}$  (3 mM) with (a) ranitidine, (b) DFUR, and (c) DMBA (all 15–200  $\mu\text{M}$ ) in 10 mM phosphate buffer at pH 8.0. Panels (d–f) show the corresponding  $\delta^{18}\text{O}$ -values of aqueous O<sub>2</sub> over the remaining fraction of O<sub>2</sub> ( $c/c_0$ ).  $\epsilon$ -values are oxygen isotope enrichment factors that were used to derive  $^{18}\text{O}$ -kinetic isotope effects. Note that we also measured the formation of NDMA in the experiment with DMBA. Dashed lines are 95% confidence intervals of the linear regression or nonlinear fit.

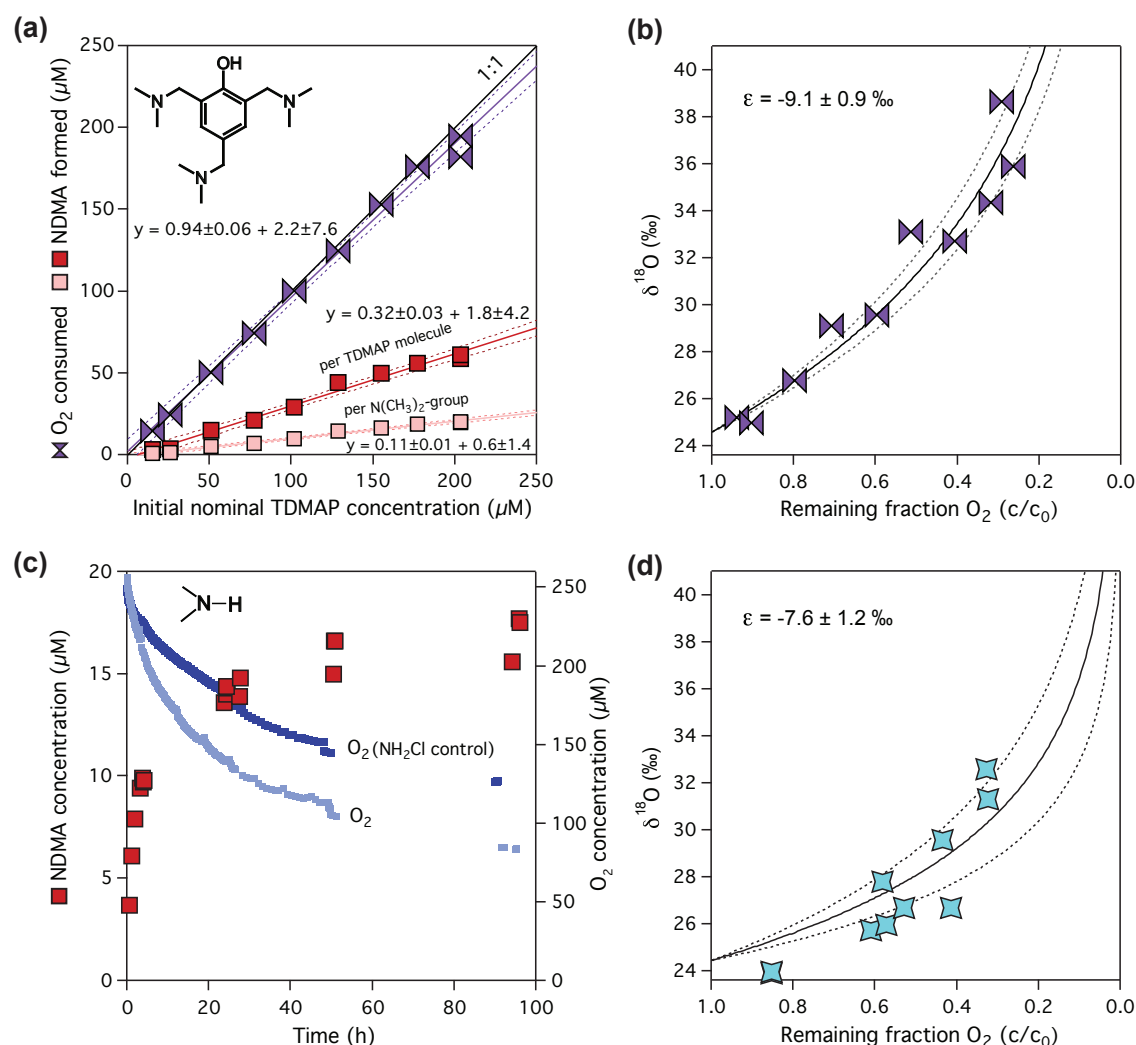


**Figure S3.19:** (a) Consumption of aqueous  $\text{O}_2$  during the reaction of TDMAP (15–200  $\mu\text{M}$ ) with  $\text{NH}_2\text{Cl}$  (3 mM) in 10 mM phosphate buffer at pH 8.0. Note that samples for O isotope analysis were quenched when the molar NDMA yield per *N,N*-dimethylamine group was 11% and thus slightly lower than the maximum NDMA yield of 16% (see Table S3.2). (b)  $\delta^{18}\text{O}$ -values of aqueous  $\text{O}_2$  over the remaining fraction of  $\text{O}_2$  ( $c/c_0$ ) during chloramination of TDMAP. (c) NDMA formation and  $\text{O}_2$  consumption over time in a reactive batch containing 200  $\mu\text{M}$  DMA and 3 mM  $\text{NH}_2\text{Cl}$  in 10 mM phosphate buffer at pH 8.0.  $\text{O}_2$  consumption was also quantified in a control containing 3 mM  $\text{NH}_2\text{Cl}$  without DMA. (d)  $\delta^{18}\text{O}$ -values of aqueous  $\text{O}_2$  over the remaining fraction of  $\text{O}_2$  ( $c/c_0$ ) during the reaction of DMA (200  $\mu\text{M}$ ) with  $\text{NH}_2\text{Cl}$  (3 mM).  $\varepsilon$ -values are oxygen isotope enrichment factors that were used to derive  $^{18}\text{O}$ -kinetic isotope effects. Dashed lines are 95% confidence intervals of the linear regression in panel (a) or the nonlinear fit in panels (b) and (d).

## S3.12 Experiments with radical scavengers

### S3.12.1 *tert*-Butanol

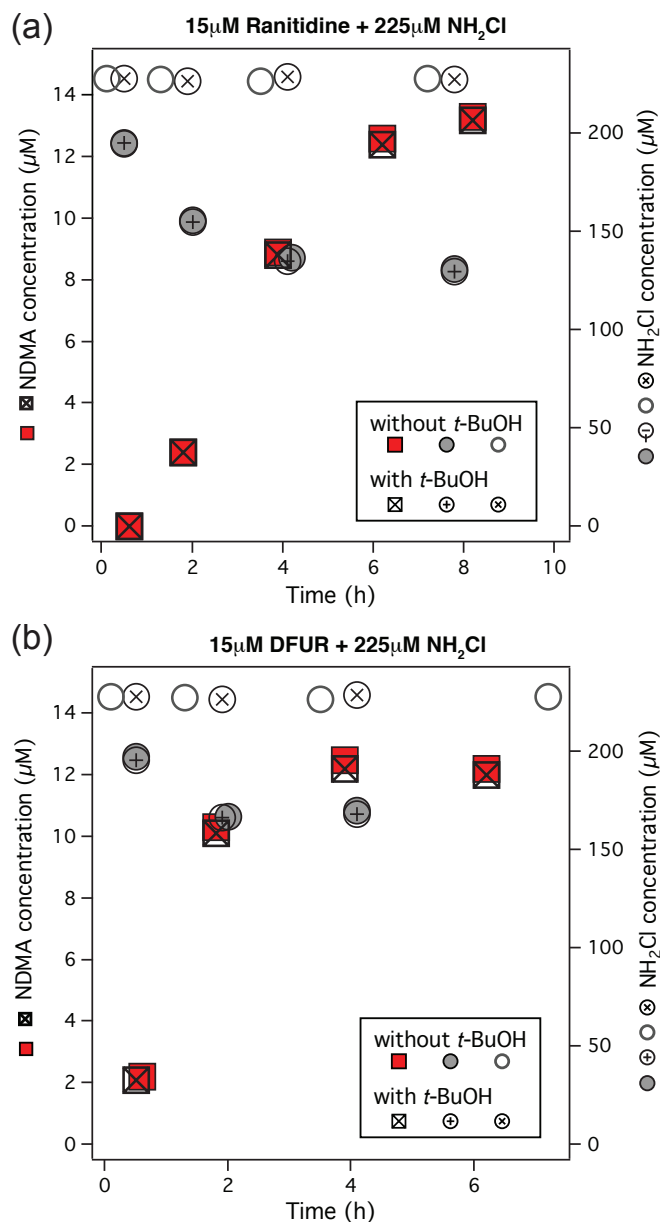


**Figure S3.20:** The presence of *tert*-butanol (40 mM) had no impact on NDMA formation and NH<sub>2</sub>Cl consumption during the reaction of (a) ranitidine (15  $\mu$ M) and (b) DFUR (15  $\mu$ M) with NH<sub>2</sub>Cl (225  $\mu$ M) in 10 mM phosphate buffer at pH 8.0. For reaction stoichiometries see Table S3.1.

## S3.12.2 ABTS

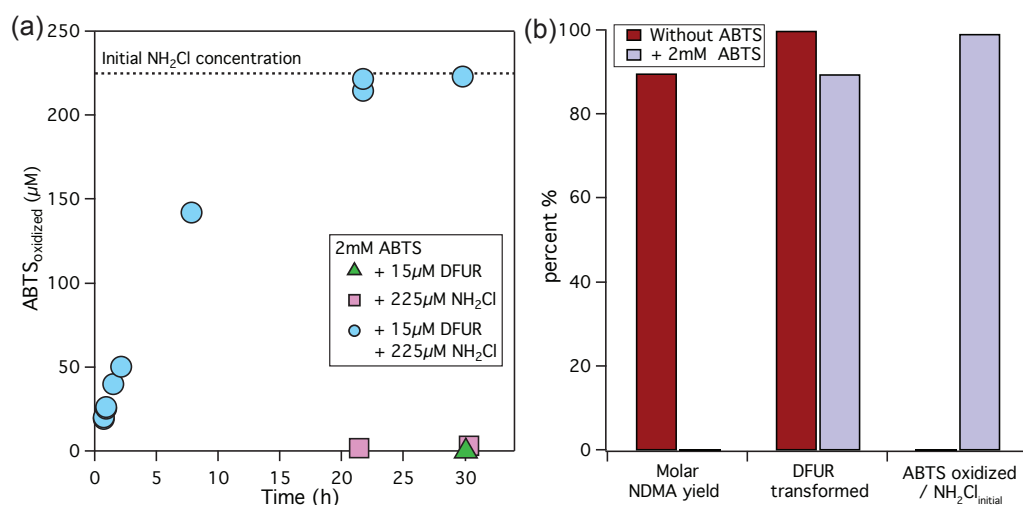


**Figure S3.21:** Reaction of DFUR (15  $\mu\text{M}$ ) with  $\text{NH}_2\text{Cl}$  (225  $\mu\text{M}$ ) in the presence and absence of ABTS (2 mM) in 10 mM phosphate buffer at pH 8.0. Panel (a) shows the concentration of oxidized ABTS over time in the presence of (i) 15  $\mu\text{M}$  DFUR (triangle), (ii) 225  $\mu\text{M}$   $\text{NH}_2\text{Cl}$  (squares), and (iii) 15  $\mu\text{M}$  DFUR and 225  $\mu\text{M}$   $\text{NH}_2\text{Cl}$  (circles). Panel (b) shows molar NDMA yields and the transformation of DFUR in percent as well as the percentage of oxidized ABTS per  $\text{NH}_2\text{Cl}$ .

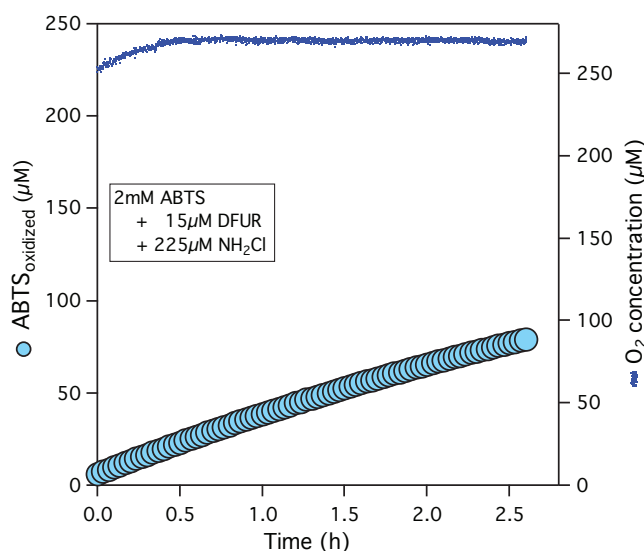


**Figure S3.22:** Concentration of oxidized ABTS and aqueous  $\text{O}_2$  during the reaction of DFUR (15  $\mu\text{M}$ ) with  $\text{NH}_2\text{Cl}$  (225  $\mu\text{M}$ ) in the presence of ABTS (2 mM) in 10 mM phosphate buffer at pH 8.0.

## S3.12.3 Trolox

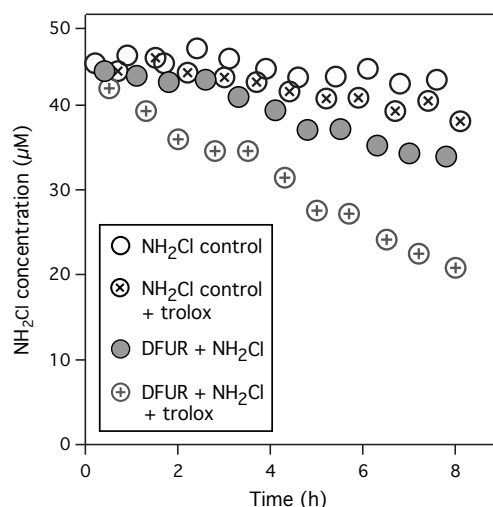


**Figure S3.23:** Effect of the antioxidant trolox on the consumption of  $\text{NH}_2\text{Cl}$  over 8 h (i) in controls containing  $\text{NH}_2\text{Cl}$  ( $45 \mu\text{M}$ ) in the absence or presence of trolox ( $0.5 \text{ mM}$ ) and (ii) in reactive batches containing DFUR ( $3 \mu\text{M}$ ) and  $\text{NH}_2\text{Cl}$  ( $45 \mu\text{M}$ ) in the absence or presence of trolox ( $0.5 \text{ mM}$ ) in  $10 \text{ mM}$  phosphate buffer at pH 8.0.  $\text{NH}_2\text{Cl}$  concentrations were measured with MIMS and evaluated with  $m/z$  53.

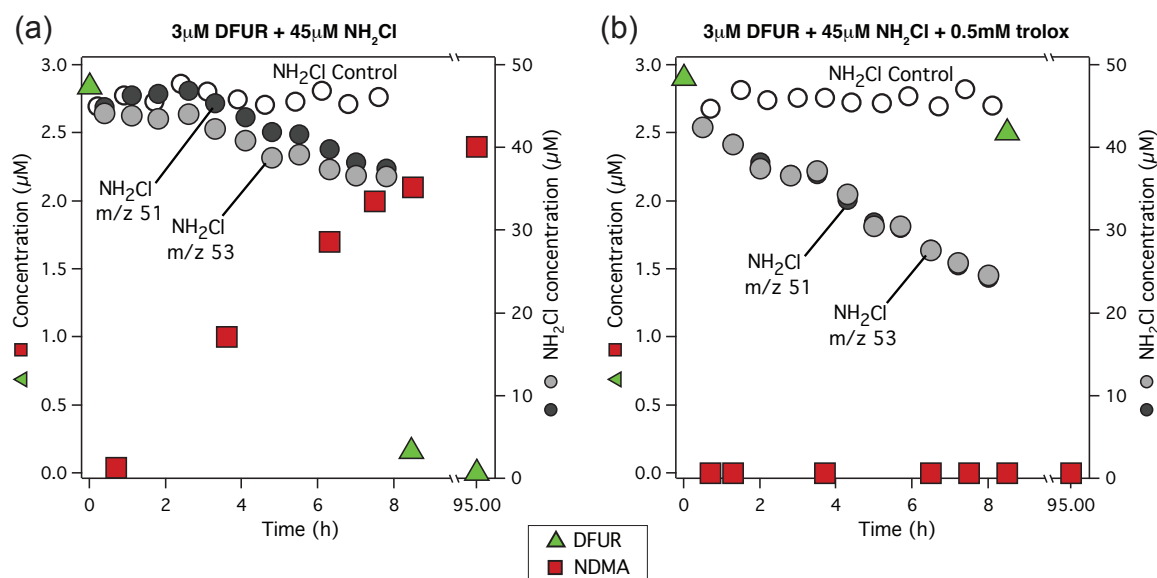


**Figure S3.24:** Effect of the antioxidant trolox on NDMA formation over 95 h. Reaction of DFUR ( $3 \mu\text{M}$ ) with  $\text{NH}_2\text{Cl}$  ( $45 \mu\text{M}$ ) in  $10 \text{ mM}$  phosphate buffer at pH 8.0 (a) in the absence of trolox and (b) in the presence of trolox ( $0.5 \text{ mM}$ ).  $\text{NH}_2\text{Cl}$  concentrations were measured with MIMS and evaluated with ions  $m/z$  51 and  $m/z$  53.

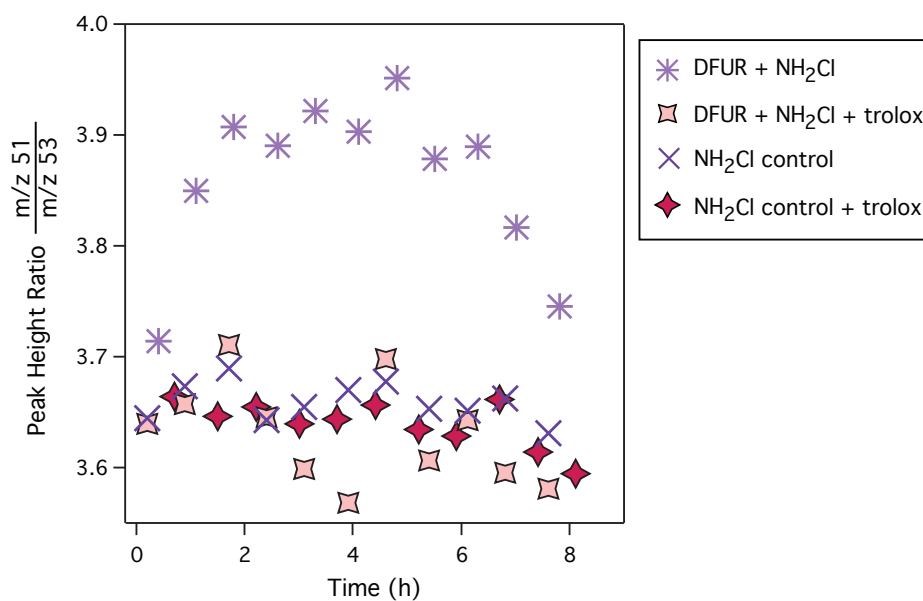


**Figure S3.25:** Ratios of peak heights of NH<sub>2</sub>Cl ions m/z 51 and m/z 53 measured with MIMS (i) in controls containing NH<sub>2</sub>Cl (45  $\mu$ M) in the absence or presence of trolox (0.5 mM) and (ii) in reactive batches containing DFUR (3  $\mu$ M) and NH<sub>2</sub>Cl (45  $\mu$ M) in the absence or presence of trolox (0.5 mM). The ratio of m/z 51 and m/z 53 remained constant in the control samples. We observed an interference on m/z 51 during chloramination of DFUR that was absent in the presence of the radical scavenger trolox.



### S3.13 Quantification of $\text{H}_2\text{O}_2$ through transformation to $\text{O}_2$ by catalase

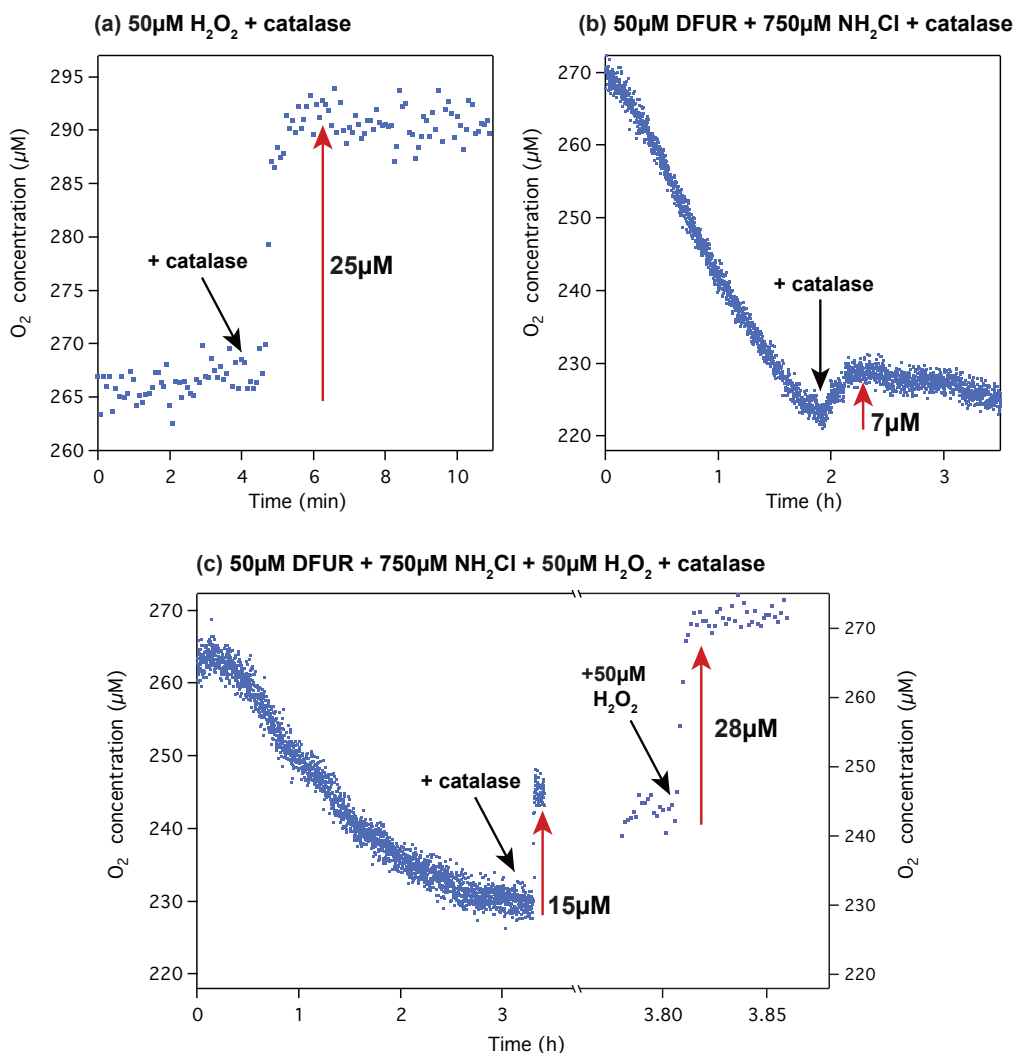


**Figure S3.26:** (a) Increase in  $\text{O}_2$  concentration after addition of catalase at 4 min to 50  $\mu\text{M}$   $\text{H}_2\text{O}_2$  (nominal concentration) in 10 mM phosphate buffer at pH 8.0. (b)  $\text{O}_2$  consumption over time in assays containing 50  $\mu\text{M}$  DFUR and 750  $\mu\text{M}$   $\text{NH}_2\text{Cl}$  in 10 mM phosphate buffer at pH 8.0. Catalase was added after 1.9 h when the amount of consumed  $\text{O}_2$  equaled the initial concentration of DFUR what indicated the completion of the NDMA formation reaction. We observed an increase of  $7 \pm 1.6 \mu\text{M}$  in the  $\text{O}_2$  concentration, whereupon 2  $\mu\text{M}$   $\text{O}_2$  might have been introduced through the addition of aqueous, oxic catalase solution. (c) Recovery of  $\text{H}_2\text{O}_2$  during chloramination of DFUR. 50  $\mu\text{M}$   $\text{H}_2\text{O}_2$  were added immediately after mixing 50  $\mu\text{M}$  DFUR with 750  $\mu\text{M}$   $\text{NH}_2\text{Cl}$ . Catalase was added after 3.3 h and the  $\text{O}_2$  concentration increased by 15  $\mu\text{M}$ . To assess the activity of catalase in the reaction solution, we spiked another 50  $\mu\text{M}$   $\text{H}_2\text{O}_2$  after 3.8 h to the catalase containing assay and observed an increase of 28  $\mu\text{M}$   $\text{O}_2$ .

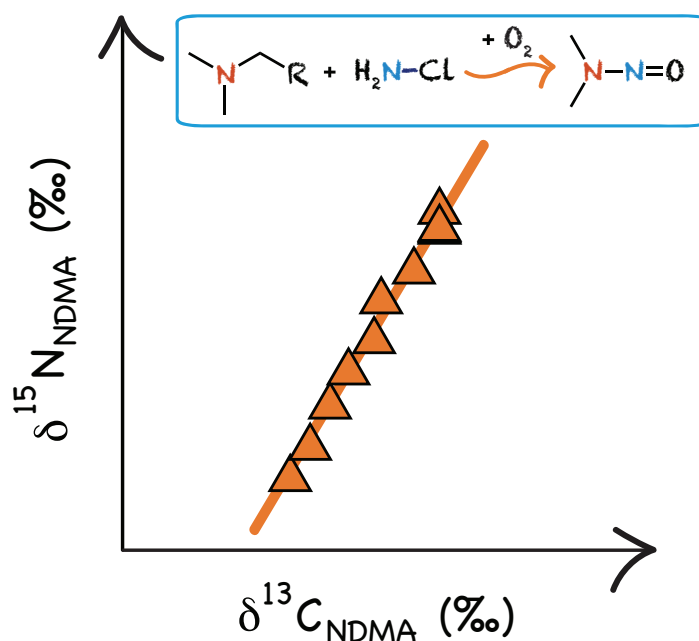
When we added catalase to  $50\text{ }\mu\text{M}$   $\text{H}_2\text{O}_2$  in  $10\text{ mM}$  phosphate buffer at  $\text{pH } 8.0$ , the concentration of  $\text{O}_2$  increased by  $25 \pm 3\text{ }\mu\text{M}$  (Figure S3.26a). As catalase converts two  $\text{H}_2\text{O}_2$  molecules to one  $\text{O}_2$  molecule, this value is in agreement with the theoretically expected formation of  $\text{O}_2$ .

We quantified the  $\text{H}_2\text{O}_2$  concentration that was present after completion of the chloramination reaction of DFUR in  $10\text{ mM}$  phosphate buffer at  $\text{pH } 8.0$ . Therefore, we monitored the consumption of  $\text{O}_2$  during the reaction of DFUR ( $50\text{ }\mu\text{M}$ ) with  $\text{NH}_2\text{Cl}$  ( $750\text{ }\mu\text{M}$ ) and added catalase as soon as the consumed  $\text{O}_2$  equaled the initial concentration of DFUR ( $50\text{ }\mu\text{M}$ ). Upon addition of catalase, the  $\text{O}_2$  concentration increased by  $7 \pm 1.6\text{ }\mu\text{M}$  (Figure S3.26b). As we spiked catalase as aqueous, oxic solution, we introduced at most  $2\text{ }\mu\text{M}$   $\text{O}_2$ . Thus, an increase of at least  $5 \pm 1.6\text{ }\mu\text{M}$   $\text{O}_2$  was caused by the presence of  $\text{H}_2\text{O}_2$ . Assuming the Bennett mechanism, chloramination of  $50\text{ }\mu\text{M}$  DFUR would lead to  $25\text{ }\mu\text{M}$   $\text{H}_2\text{O}_2$ . The quantified amount of  $7\text{ - }13\text{ }\mu\text{M}$   $\text{H}_2\text{O}_2$  thus accounts for approximately 28-52% of the theoretically formed  $\text{H}_2\text{O}_2$ .

The stability of  $\text{H}_2\text{O}_2$  in the reactive solution containing DFUR and  $\text{NH}_2\text{Cl}$  was assessed. To this end,  $50\text{ }\mu\text{M}$   $\text{H}_2\text{O}_2$  were added immediately after spiking  $750\text{ }\mu\text{M}$   $\text{NH}_2\text{Cl}$  to  $10\text{ mM}$  phosphate buffer ( $\text{pH } 8.0$ ) that contained  $50\text{ }\mu\text{M}$  DFUR. When the chloramination reaction was completed (indicated through stoichiometric  $\text{O}_2$  consumption after 3.3 h), we added catalase and observed an increase of  $14.9 \pm 2.4\text{ }\mu\text{M}$  in the  $\text{O}_2$  concentration corresponding to approximately  $30\text{ }\mu\text{M}$   $\text{H}_2\text{O}_2$  (Figure S3.26c). Thus, only 60% of the initially added  $\text{H}_2\text{O}_2$  could be recovered indicating that  $\text{H}_2\text{O}_2$  is not stable during chloramination of DFUR. As it is known that  $\text{NH}_2\text{Cl}$  inhibits peroxidase activity,<sup>214</sup> we tested the activity of catalase through addition of another  $50\text{ }\mu\text{M}$   $\text{H}_2\text{O}_2$  to the same reaction vessel (after 3.8 h, Figure S3.26c). Indeed, the  $\text{O}_2$  concentration increased by  $28 \pm 3\text{ }\mu\text{M}$  demonstrating that catalase was fully active.

## Chapter 4

### Stable Isotope Fractionation Trends in *N*-Nitrosodimethylamine as Proxy for Its Formation Pathway During Chloramination of Tertiary Amines



Stephanie Spahr, Urs von Gunten, and Thomas B. Hofstetter. In preparation for submission to *Environmental Science and Technology*

---

*Spahr, S. conducted all experiments, data analyses, and wrote the manuscript. Von Gunten, U. and Hofstetter, T. B. supervised the project, contributed to the discussion of the results and revision of the manuscript.*

## Abstract

To assess the formation of *N*-nitrosodimethylamine (NDMA) during drinking water disinfection and evaluate mitigation strategies, new tools are needed that systematically relate the formation of NDMA to the presence of relevant precursor compounds. In this study, we explore whether changes in the stable isotope ratios of NDMA can be used as proxy for NDMA precursor moieties and formation pathways. Using compound-specific isotope analysis (CSIA), we investigated  $^{13}\text{C}/^{12}\text{C}$ ,  $^2\text{H}/^1\text{H}$ , and  $^{15}\text{N}/^{14}\text{N}$  ratios of NDMA during chloramination of four tertiary amines that produce high yields of NDMA, namely ranitidine, 5-(dimethylaminomethyl)furfuryl alcohol, *N,N*-dimethylthiophene-2-methylamine and *N,N*-dimethylbenzylamine. While minor changes in C and H isotope ratios of NDMA revealed that the  $\text{N}(\text{CH}_3)_2$  group of NDMA originates from the tertiary amine, N isotope ratios of NDMA showed that  $\text{NH}_2\text{Cl}$  is the source of the N atom of the nitroso moiety. NDMA was enriched in  $^{15}\text{N}$  during its formation due to a complex sequence of reactions at N atoms and combined kinetic isotope effects. Correlated C and N isotope signatures of NDMA ( $\delta^{15}\text{N}$  versus  $\delta^{13}\text{C}$ ) revealed trends, which were characteristic for the NDMA formation pathway during chloramination of the selected tertiary amines. These isotope fractionation trends were robust under various treatment conditions and independent of the molar NDMA yield indicating the potential diagnostic power of CSIA to identify this important class of NDMA precursors during drinking water chloramination.

## 4.1 Introduction

*N*-nitrosamines are drinking water disinfection by-products (DBPs) of public and regulatory concern because of their mutagenicity and potential carcinogenicity.<sup>10,37</sup> *N*-nitrosodimethylamine (NDMA) is a frequently detected DBP in finished drinking waters and often exceeds guidance values of 9-100 ng/L.<sup>31,37,115,215</sup> NDMA is produced unintentionally when disinfectants such as chlorine, chloramine, or ozone react with organic compounds present in raw waters such as naturally occurring substances (e.g., natural organic matter),<sup>41,64,66,76,119</sup> or anthropogenic micropollutants (e.g., pharmaceuticals or pesticides).<sup>54,72,156</sup> Also chemicals used for water purification (e.g., polymeric coagulants) can lead to NDMA formation.<sup>69,70</sup> The different molecular structures and physico-chemical properties of NDMA precursors suggest that reaction mechanisms leading to NDMA differ among the various disinfection scenarios.<sup>28,30</sup> However, detailed knowledge about NDMA formation pathways remains scarce so that the systematic prediction and prevention of NDMA formation during water treatment is currently hampered. New tools are needed to relate the formation of NDMA to its precursors and to propose adequate mitigation strategies.

Previous studies demonstrated that changes in the stable isotope composition of DBPs at natural abundance can be used as probes for reactive precursor materials and DBP formation pathways.<sup>113,127,128</sup> Compound-specific isotope analysis (CSIA) was applied to monitor the change of  $^{13}\text{C}/^{12}\text{C}$  ratios in chloroform produced upon chlorination of lake water.<sup>113</sup> Chloroform was depleted in  $^{13}\text{C}$  due to an inverse kinetic isotope effect (KIE) that was indicative of the chlorination of phenolic moieties in NOM.<sup>113</sup> In contrast, chloroform was enriched in  $^{13}\text{C}$  due to a normal KIE when produced from other NOM moieties such as resorcinol.<sup>113</sup> KIEs are characteristic proxies for reaction mechanisms, because they reflect how chemical bonds of a molecule are broken or formed.<sup>82,83,216</sup> To date, CSIA is frequently applied to identify degradation pathways of contaminants in the environment.<sup>83,93,103,108</sup> In contrast, only very few studies have focused on applying CSIA to study formation pathways and precursors of potentially harmful reaction products such as DBPs.<sup>94,113,127</sup> We recently proposed an analytical procedure for C, H, and N isotope analysis of *N*-nitrosamines<sup>162</sup> but it remains unknown if changes in stable isotope ratios of NDMA (so called isotope fractionation) can provide information on NDMA precursors and formation pathways in a similar way as shown for chloroform.

One major route to NDMA is chloramination of amine-containing waters. Secondary amines (e.g. dimethylamine) and most tertiary amines produce low molar NDMA yields

of a few percent ( $<6\%$ ).<sup>58,61,76</sup> In contrast, tertiary amines with a *N,N*-dimethylamine ( $\text{N}(\text{CH}_3)_2$ ) moiety bound via a methylene group to a (hetero)aromatic ring (e.g., ranitidine) produce very high molar NDMA yields ( $>60\%$ ).<sup>67,72,76,162</sup> Our recent study suggests that radicals likely play an important role in this NDMA formation mechanism.<sup>217</sup> The initial reaction step of the tertiary amine with  $\text{NH}_2\text{Cl}$  is a nucleophilic substitution leading to the formation of a *N,N*-dimethylhydrazine-type intermediate (compound **2** in Figure 4.1).<sup>79,80</sup> Upon reaction with  $\text{NH}_2\text{Cl}$ , the latter is likely oxidized to a N-centered aminyl radical (compound **3**) that reacts with aqueous  $\text{O}_2$  to a *N*-peroxyl species (compound **4**) and subsequently to NDMA.<sup>217</sup> While methyl groups of the  $\text{N}(\text{CH}_3)_2$  moiety of the tertiary amine are not involved in any of the reaction steps, several bonds to nitrogen are broken and formed during NDMA formation. We hypothesize that constant C and H isotope ratios can be used as fingerprint for *N*-methyl groups that are transferred from the tertiary amine precursor to NDMA. In contrast, reactions involving nitrogen atoms might result in N isotope fractionation in NDMA that could reveal the pathway of its formation and the disinfectant and precursor involved.

The objective of this investigation was to evaluate whether changes in C, H, or N isotope ratios of NDMA can be used as proxy for NDMA precursor moieties and formation pathways. To this end, we conducted chloramination experiments with four tertiary amines, namely ranitidine, 5-(dimethylaminomethyl)furfuryl alcohol (DFUR), *N,N*-dimethylthiophene-2-methylamine (DMTA), and *N,N*-dimethylbenzylamine (DMBA, see Figure 4.1), and investigated C, H, and N isotope fractionation in NDMA during its formation. (i) Sources of C, H, and N atoms in NDMA were inferred by quantifying initial and site-specific isotope signatures of selected precursors as well as by conducting experiments with  $^{15}\text{N}$ -enriched monochloramine. (ii) Isotope-sensitive reaction steps of the NDMA formation pathway were identified from C and N isotope fractionation trends in selected tertiary amines and NDMA. (iii) We assessed whether isotope fractionation trends in NDMA are characteristic for its formation during chloramination of the selected tertiary amines and could be used as proxy for the NDMA formation pathway. Finally, our results enabled us to evaluate the diagnostic power of CSIA to identify this important class of NDMA precursors during drinking water chloramination.

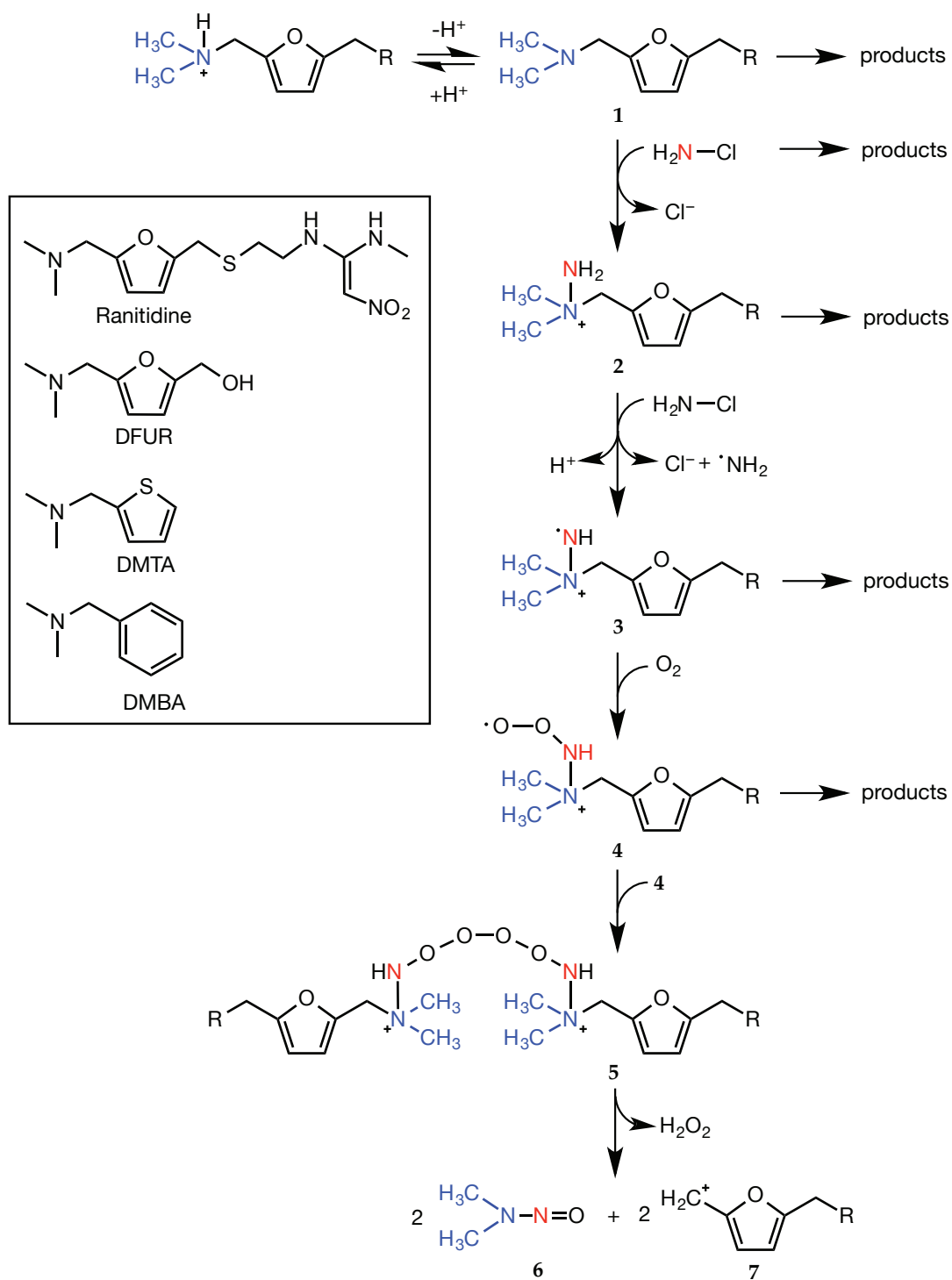


**Figure 4.1:** Previously proposed NDMA formation pathway during chloramination of selected tertiary amines, namely ranitidine, DFUR, DMTA, and DMBA.<sup>217</sup> Reactive intermediate species include a substituted dimethylhydrazine (**2**), an aminyl radical (**3**), and an *N*-peroxyl radical (**4**). Decomposition of the *N*-peroxyl coupling product (**5**) leads to formation of two equivalents of NDMA (**6**) and carbocations (**7**). In case of <100% molar NDMA yield, the precursors or reactive intermediates **2–4** react to unidentified products.

## 4.2 Experimental Section

### 4.2.1 Chemicals

A list of all chemicals including suppliers and purities is provided in the Supporting Information (SI).

### 4.2.2 NDMA formation experiments

Monochloramine ( $\text{NH}_2\text{Cl}$ ) stock solutions (30 mM) were prepared daily as described previously<sup>137,138</sup> by mixing hypochlorite ( $\text{HOCl}$ ) with either ammonium chloride ( $\text{NH}_4\text{Cl}$ ) or  $^{15}\text{N}$ -enriched ammonium sulfate ( $(\text{NH}_4)_2\text{SO}_4$ )<sup>218</sup> at pH 9.5 with a molar  $\text{Cl}:\text{N}$  ratio of 1:1.05.

Chloramination experiments were carried out in 14 amber glass bottles containing 1 L of 10 mM phosphate buffer (pH 8.0). Each reactor was spiked with 100  $\mu\text{L}$  of a methanolic stock solution to obtain initial concentrations of 3  $\mu\text{M}$  ranitidine or DFUR and 40  $\mu\text{M}$  DMTA or DMBA. The formation of NDMA was initiated through addition of  $\text{NH}_2\text{Cl}$  in 15-fold excess corresponding to concentrations of 45  $\mu\text{M}$  or 600  $\mu\text{M}$   $\text{NH}_2\text{Cl}$ , respectively. At predefined time points, one flask of 1 L was sacrificed. We measured the pH of the reaction solution, quantified the  $\text{NH}_2\text{Cl}$  concentration, and quenched the chloramine reaction by addition of 0.5 g  $\text{Na}_2\text{S}_2\text{O}_3$  to the reactor. To quantify the concentrations of NDMA, ranitidine, and DFUR, 1 mL of the solution was filled into 1.5 mL amber autosampler glass vials. For DMTA and DMBA analyses, 40 mL of the solution was transferred to 50 mL amber glass vials and the pH of the 10 mM phosphate buffer was adjusted to 11.3 through addition of 5 M  $\text{NaOH}$ . All samples were stored in the dark at 4°C until concentration analyses and further processing for isotope analyses. Two control experiments were set up to (i) quantify the stability of the organic amine precursor in the absence of  $\text{NH}_2\text{Cl}$  and (ii) determine the self-decay rate of  $\text{NH}_2\text{Cl}$  in the absence of organic amine. If not stated otherwise, reported  $\text{NH}_2\text{Cl}$  concentrations were corrected by the self-decay of  $\text{NH}_2\text{Cl}$ .

We investigated the impact of the buffer concentration and type on the chloramination kinetics and NDMA formation. To this end, experiments with DFUR (3  $\mu\text{M}$ ) and  $\text{NH}_2\text{Cl}$  (45  $\mu\text{M}$ ) were conducted in 1, 5, 10, and 50 mM phosphate buffer (pH 8.0) as well as in 10 mM arsenate, 10 mM carbonate, and 10 mM borate buffer (all pH 8.0). In addition, we examined the impact of the solution pH on NDMA formation kinetics and isotope fractionation of NDMA. For this purpose, the reaction of ranitidine or DFUR (3  $\mu\text{M}$ ) with  $\text{NH}_2\text{Cl}$  (45  $\mu\text{M}$ ) was monitored at pH 7.0 in 10 mM phosphate buffer.



### 4.2.3 Chemical analyses

The concentration of aqueous  $\text{NH}_2\text{Cl}$  stock solutions (30 mM) was quantified as described previously using a Varian Cary 100 Bio UV-visible spectrophotometer.<sup>137,138,162,213</sup> In reaction mixtures containing tertiary amines, reactive intermediates, and NDMA,  $\text{NH}_2\text{Cl}$  was quantified with a colorimetric method using 2,2'-azino-bis(3-ethylbenzothiazoline-6-sulfonic acid) diammonium salt (ABTS).<sup>139,162</sup> Concentrations of NDMA, ranitidine, and DFUR were determined down to 0.1  $\mu\text{M}$  by reverse phase HPLC with UV detection (Dionex UltiMate 3000) as described previously.<sup>162,217</sup>

Concentration measurements of DMTA and DMBA were carried out by solid-phase microextraction (SPME) coupled to GC/MS analysis (Thermo TRACE GC Ultra and Thermo TRACE DSQ II). 2 mL amber autosampler glass vials, which contained 0.3 g NaCl, were filled with 1.3 mL of sample (in 10 mM phosphate buffer, pH 11.3) and were shaken on a Vortex mixer to reach a final ionic strength of 4 M. Using a CTC CombiPAL autosampler, a polydimethylsiloxane/divinylbenzene (PDMS/DVB, 65  $\mu\text{m}$ , Supelco) coated SPME fibre (conditioned daily for 30 min at 250°C) was immersed directly into the samples and the analytes were allowed to adsorb for 45 min at 40°C.<sup>130</sup> In the split/splitless injector of the GC, analytes were thermally desorbed for 3 min at 270°C. The GC was equipped with 1 m DPTMDS (methyl/phenyl) deactivated fused-silica guard column (0.53 mm i.d., BGB) and a 30 m  $\times$  0.25 mm ZB-5ms column (0.25  $\mu\text{m}$ , Zebron, Phenomenex). Helium carrier gas was used at a constant pressure of 130 kPa. The temperature program was 1 min at 50°C, 10°C/min to 250°C, and 5 min at 250°C. DMTA and DMBA concentrations were quantified with an external calibration of 0.1 - 1.5  $\mu\text{M}$ .

### 4.2.4 Stable isotope analyses

Stable C, H, and N isotope ratios of NDMA were measured using gas chromatography isotope ratio mass spectrometry (GC/IRMS) coupled to solid-phase extraction (SPE) as reported recently.<sup>162</sup> C and N isotope analysis of DMTA and DMBA in aqueous samples was conducted with SPME-GC/IRMS. The SPME procedure, GC setup and temperature program was identical to that for GC/MS analysis, but a 30 m  $\times$  0.32 mm ZB-5ms column (1  $\mu\text{m}$ , Zebron, Phenomenex) was used. For all C and N isotope measurements, a self-made Ni/Ni/Pt reactor was operated at 1000°C as described previously.<sup>162</sup> Method quantification limits (MQLs) of the SPME-GC/IRMS measurements of DMTA and DMBA were determined according to the moving mean procedure of Jochmann

et al.<sup>141</sup> The linear range in which accurate C and N isotope analysis of DMTA and DMBA could be performed was 0.3-0.6  $\mu\text{M}$  and 2.5-16  $\mu\text{M}$ , respectively (DMTA data are shown in Figure S4.1). To determine the equilibrium isotope effect associated with the deprotonation of DMTA, we investigated the pH-dependent isotope fractionation of DMTA by SPME-GC/IRMS at pH 8.4, 8.7, 9.4, 10.4, and 11.3 in 10 mM phosphate buffer at ionic strength of 4 M using DMTA concentrations of 66  $\mu\text{M}$ , 12  $\mu\text{M}$  (pH 8.7 and 9.4), 6.6  $\mu\text{M}$ , and 5  $\mu\text{M}$ , respectively.<sup>130</sup>

Isotope ratios are reported in the delta-notation as  $\delta^{13}\text{C}$ ,  $\delta^2\text{H}$ , and  $\delta^{15}\text{N}$  (so called isotope signatures) relative to Vienna PeeDee Belemnite, Vienna standard mean ocean water, and air, respectively.<sup>125,162</sup> All isotope signatures are reported in permil (‰) as arithmetic mean of triplicate measurements ( $\pm\sigma$ ). We used a series of isotopic standard materials purchased from Indiana University<sup>219,220</sup> (full list see Spahr et al.<sup>162</sup>) as well as repeated measurements of in-house standards in standard bracketing procedures to ensure the accuracy of the measured isotope ratios. In-house standards of ranitidine, DFUR, DMTA, and  $\text{NH}_4\text{Cl}$  were obtained through C and N isotope ratio measurements with an elemental analyzer IRMS (data shown in Table S4.1). The isotopic analysis of  $\text{NH}_2\text{Cl}$  was impeded owing to its thermal instability and self-decay to ammonia. Instead, we used N isotope reference values of  $\text{NH}_4\text{Cl}$  or  $(\text{NH}_4)_2\text{SO}_4$ , from which  $\text{NH}_2\text{Cl}$  was produced, as a proxy for the initial  $\delta^{15}\text{N}$  values of  $\text{NH}_2\text{Cl}$ . This assumption was made based on high molar  $\text{NH}_2\text{Cl}$  yields (>94%) from the reaction of  $\text{HOCl}$  with  $\text{NH}_4\text{Cl}$  or  $(\text{NH}_4)_2\text{SO}_4$ .

### 4.2.5 Data evaluation

To study isotope fractionation in the tertiary amine precursors, we conducted chloramination experiments with two model compounds, namely DMTA and DMBA. Bulk isotope enrichment factors,  $\varepsilon_{\text{E}}^{\text{bulk}}$ , were derived from linear regression of  $\delta^{13}\text{C}$  and  $\delta^{15}\text{N}$  values versus fractional amount of remaining precursor ( $c/c_0$ ) according to eq. 4.1 (see Figure S4.3).<sup>83</sup>

$$\ln \left( \frac{\delta^h\text{E} + 1}{\delta^h\text{E}_0 + 1} \right) = \varepsilon_{\text{E}}^{\text{bulk}} \cdot \ln \left( \frac{c}{c_0} \right) \quad (4.1)$$

where  $\delta^h\text{E}_0$  and  $\delta^h\text{E}$  are isotope ratios of an element E in the precursor at the beginning and during the reaction, respectively. Apparent kinetic isotope effects,  $\text{AKIE}_{\text{E}}$ , were calculated according to eq. 4.2 considering the total number of atoms of an element E ( $n$ ), the number of atoms in reactive positions ( $x$ ), and the number of atoms in intramolecular competition ( $z$ ). While the  $\text{AKIE}_{\text{C}}$  is reported as an average kinetic iso-

tope effect for all C atoms in DMTA ( $n = x = 7$ ,  $z = 1$ ) and DMBA ( $n = x = 9$ ,  $z = 1$ ),  $\text{AKIE}_\text{N}$  is position-specific as both precursors only contain one N atom ( $n = x = z = 1$ ). Uncertainties of  $\varepsilon_\text{E}^\text{bulk}$  and  $\text{AKIE}_\text{E}$  are reported as 95% confidence interval.

$$\text{AKIE}_\text{E} = \frac{1}{1 + (n/x) \cdot z \cdot \varepsilon_\text{E}^\text{bulk}} \quad (4.2)$$

The overall observable  $\text{AKIE}_\text{N}$  in DMTA or DMBA during chloramination at pH 8.0 originates from an isotope-sensitive deprotonation step (eq. 4.3) which is associated with an  $^{15}\text{N}$ -equilibrium isotope effect,  $\text{EIE}_\text{N}^{\text{BH}^+ - \text{B}}$ , and the subsequent reaction of the neutral tertiary amine to a product (eq. 4.4) which is accompanied by an apparent kinetic isotope effect,  $\text{AKIE}_\text{N}^\text{B}$ . These EIEs and AKIEs were derived according to a previously established procedure of Skarpeli-Liati et al.<sup>130</sup>



where  $k_i$  and  $k_{-i}$  are rate constants of forward and backward reaction steps. The observable  $\text{AKIE}_\text{N}$  is the weighted average of the protonated ( $f_{\text{BH}^+}$ ) and deprotonated fraction ( $1 - f_{\text{BH}^+}$ ) of the tertiary amines and their respective isotope effects as shown in eq. S4.1.<sup>221</sup> The  $\text{AKIE}_\text{N}^\text{B}$  that originates from the reaction of the deprotonated species is given by eq. 4.5.  $f_{\text{BH}^+}$  at pH 8.0 was determined with eq. 4.6 using a  $\text{pK}_a$  of  $9.75 \pm 0.3$  for DMTA (derived from SPME-GC/IRMS measurements) and a  $\text{pK}_a$  of 9.0 for DMBA.<sup>222</sup>

$$\text{AKIE}_\text{N}^\text{B} = \frac{\text{AKIE}_\text{N}}{(f_{\text{BH}^+} \cdot \text{EIE}_\text{N}^{\text{BH}^+ - \text{B}}) + 1 - f_{\text{BH}^+}} \quad (4.5)$$

$$f_{\text{BH}^+} = (1 + 10^{\text{pH} - \text{pK}_a})^{-1} \quad (4.6)$$

The deprotonation  $\text{EIE}_\text{N}^{\text{BH}^+ - \text{B}}$  was calculated with eq. 4.7, where the equilibrium isotope enrichment factor,  $\varepsilon_\text{N}^{\text{BH}^+ - \text{B}}$ , was derived from the slope of the regression line of  $\delta^{15}\text{N}$  versus  $f_{\text{BH}^+}$  (see eq. 4.8 and Figure S4.4).<sup>130</sup>

$$\text{EIE}_\text{N}^{\text{BH}^+ - \text{B}} = \frac{1}{1 + \varepsilon_\text{N}^{\text{BH}^+ - \text{B}}} \quad (4.7)$$

$$\delta^{15}\text{N} = \varepsilon_\text{N}^{\text{BH}^+ - \text{B}} \cdot f_{\text{BH}^+} + \delta^{15}\text{N}_\text{ref} \quad (4.8)$$

## 4.3 Results and Discussion

### 4.3.1 Observable C, H, and N isotope fractionation trends in NDMA

We used 5-(dimethylaminomethyl)furfuryl alcohol (DFUR) as model compound for tertiary amines with high molar NDMA yield during chloramination and studied the NDMA formation kinetics as well as C, H, and N isotope ratios of NDMA. Figure 4.2a shows the formation of NDMA during the reaction of DFUR ( $3\text{ }\mu\text{M}$ ) with  $\text{NH}_2\text{Cl}$  ( $45\text{ }\mu\text{M}$ ) in 10 mM phosphate buffer at pH 8.0. The reaction was completed within 10 h with a molar NDMA yield of  $65 \pm 2\%$ . This value is approximately 10–20% lower than previously reported values.<sup>67,123,217</sup> We observed a lag-phase of approximately one hour, in which only  $0.2\text{ }\mu\text{M}$  DFUR was transformed to  $0.1\text{ }\mu\text{M}$  NDMA. After 1 h, DFUR disappeared at a faster rate in agreement with previous observations.<sup>217</sup> The formation of NDMA was concomitant with the disappearance of DFUR. This finding implies that reactive intermediates such as the *N,N*-dimethylhydrazine species (compound **2** in Figure 4.1) and possible radical intermediates (compounds **3** and **4**) are short-lived and transformed to NDMA and other unidentified products more rapidly than the initial transformation of DFUR to compound **2**. It is thus likely that only one rate-determining step governs the transformation from DFUR to NDMA, which might be the reaction of  $\text{NH}_2\text{Cl}$  with the tertiary amine precursor to compound **2**. The total consumption of  $\text{NH}_2\text{Cl}$  amounted to  $12.0\text{ }\mu\text{M}$  and thus exceeded the initial concentration of DFUR by a factor of 4.1 in agreement with previous findings.<sup>217</sup> No lag-phase was observed for the disappearance of  $\text{NH}_2\text{Cl}$  (Figure 4.2a) indicating that side reactions, which did not lead to NDMA, likely contributed to the over-stoichiometric consumption of  $\text{NH}_2\text{Cl}$ .

Figure 4.2b shows C, H, and N isotope signatures of NDMA during its formation.  $\delta^{15}\text{N}$  values of NDMA (depicted as upward directed triangles) increased within 10 h from  $-24.8\text{‰}$  to  $-8.7\text{‰}$ . This N isotope fractionation is caused by primary kinetic isotope effects that occur when chemical bonds to N are broken or formed in rate-determining reaction steps.<sup>83,106</sup> In contrast,  $\delta^{13}\text{C}$  and  $\delta^2\text{H}$  values of NDMA showed only small changes from  $-36.8\text{‰}$  to  $-34.3\text{‰}$  and  $-133.5\text{‰}$  to  $-110.7\text{‰}$ , respectively. The increase of  $\delta^2\text{H}$  values by  $+22.8 \pm 5\text{‰}$  is small compared to typical large H isotope fractionations amounting to several 100‰ for the chemical oxidation of  $\text{CH}_3$ -groups.<sup>103,223</sup> Thus, small changes in  $\delta^{13}\text{C}$  and  $\delta^2\text{H}$  values of NDMA are presumably due to secondary kinetic isotope effects that arise when C and H atoms are not directly involved in chemical reactions.

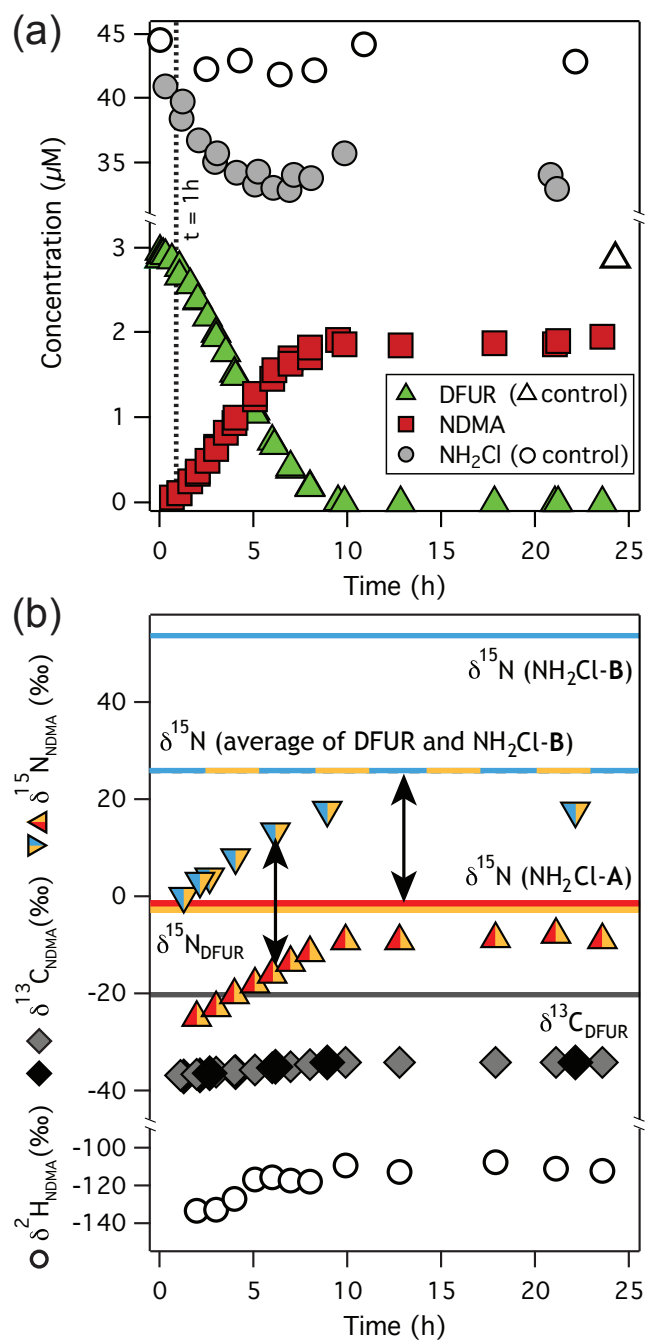


**Figure 4.2:** NDMA formation from the reaction of DFUR ( $3\ \mu\text{M}$ ) with  $\text{NH}_2\text{Cl}$  ( $45\ \mu\text{M}$ ) in 10 mM phosphate buffer (pH 8.0). Panel (a) shows DFUR degradation,  $\text{NH}_2\text{Cl}$  consumption, and NDMA formation over time. Symbols in panel (b) illustrate  $\delta^{15}\text{N}$ ,  $\delta^{13}\text{C}$ , and  $\delta^2\text{H}$  values of NDMA. Grey and yellow solid lines represent the initial  $\delta^{13}\text{C}$  and  $\delta^{15}\text{N}$  value of DFUR, respectively. The red and blue lines depict the initial  $\delta^{15}\text{N}$  values of two different  $\text{NH}_2\text{Cl}$  batches with which separate NDMA formation experiments were conducted leading to NDMA with different  $\delta^{15}\text{N}$  signatures (red-yellow vs. blue-yellow triangles). The blue-yellow line represents the average of the initial  $\delta^{15}\text{N}$  values of DFUR and  $\text{NH}_2\text{Cl-B}$ . Standard deviations of triplicate  $\delta^{15}\text{N}$ ,  $\delta^{13}\text{C}$ , and  $\delta^2\text{H}$  measurements were  $<0.2\text{‰}$ ,  $<0.4\text{‰}$ , and  $<5.0\text{‰}$ , respectively, and smaller than the depicted symbols.

### 4.3.2 Isotope ratios of NDMA reveal the origin of C, H, and N atoms in NDMA

#### Origin of the *N,N*-dimethylamine moiety in NDMA

C and H isotope signatures of NDMA enabled us to confirm that the *N,N*-dimethylamine ( $\text{N}(\text{CH}_3)_2$ ) moiety of NDMA originated from the tertiary amine precursor.<sup>162</sup> Minor changes in  $\delta^{13}\text{C}$  and  $\delta^2\text{H}$  values (Figure 4.2b) imply that reaction steps leading to NDMA did not involve the cleavage or formation of bonds to C or H atoms as illustrated in Figure 4.1. Indeed, we have shown previously that the  $\delta^2\text{H}$  values of NDMA corresponded well with the  $\delta^2\text{H}$  value of the  $\text{N}(\text{CH}_3)_2$  group of the tertiary amine precursor determined with quantitative deuterium nuclear magnetic resonance spectroscopy.<sup>162</sup> Based on  $\delta^2\text{H}$  measurements, it is reasonable to assume that  $\delta^{13}\text{C}$  values of NDMA also correspond with those of the  $\text{N}(\text{CH}_3)_2$  group of the tertiary amine. However,  $\delta^{13}\text{C}$  values of NDMA were 14.5‰ more negative than the average  $\delta^{13}\text{C}$  value of the 8 C atoms in DFUR (−19.8‰, grey line in Figure 4.2b) what indicates that  $^{12}\text{C}$  and  $^{13}\text{C}$  atoms are unevenly distributed in DFUR.  $^{12}\text{C}$  atoms were preferentially found in the  $\text{N}(\text{CH}_3)_2$  group, whereas  $^{13}\text{C}$  atoms were located in the other 6 C atoms with an average  $\delta^{13}\text{C}$  value of −14.9‰.

#### Origin of N atoms in NDMA

N isotope signatures of NDMA reflect the average isotope ratios of both N atoms of NDMA and can be used to reveal the sources of nitrogen. The N atom of the  $\text{N}(\text{CH}_3)_2$  group stems from the tertiary amine precursor (as demonstrated above), while the N atom of the nitroso group derives from  $\text{NH}_2\text{Cl}$ . For reasons of isotopic mass balance, the final  $\delta^{15}\text{N}$  value of NDMA should match the average value of the initial N isotope signatures of DFUR ( $\delta^{15}\text{N}_{\text{DFUR}} = -2.2\text{‰}$ , yellow line in Figure 4.2b) and monochloramine ( $\delta^{15}\text{N}_{\text{NH}_2\text{Cl-A}} = -1.4\text{‰}$ , red line) if all N atoms were transferred quantitatively from the precursors to NDMA (100% molar NDMA yield). However, in the present case, only 65% of DFUR was transformed to NDMA so that 35% of the N atoms ended up in unidentified products. Moreover, less than 5% of the N atoms of  $\text{NH}_2\text{Cl}$  were incorporated into NDMA (final concentration of 1.9  $\mu\text{M}$ ) because  $\text{NH}_2\text{Cl}$  was present in excess (initial concentration of 45  $\mu\text{M}$ ). Owing to the incomplete conversion of both precursors to NDMA, the final  $\delta^{15}\text{N}$  value of NDMA (upward directed triangles in Figure 4.2b) was 6.9‰ more negative than the average N isotope signature of both precursors.

Because the direct comparison of the final N isotope signature of NDMA with the initial one of its precursors cannot reveal the sources of N atoms in NDMA, we conducted a second independent NDMA formation experiment with the same DFUR of known isotopic composition, but with a different batch of monochloramine ( $\text{NH}_2\text{Cl-B}$ ). The latter had a  $\delta^{15}\text{N}_{\text{NH}_2\text{Cl-B}}$  value of +53.7‰ (blue line in Figure 4.2b) and was thus enriched in  $^{15}\text{N}$  by +55.1‰ compared to  $\text{NH}_2\text{Cl-A}$ . We observed the same extent of N isotope fractionation regardless of whether  $\text{NH}_2\text{Cl-A}$  or  $\text{NH}_2\text{Cl-B}$  reacted with DFUR ( $\delta^{15}\text{N}$  values changed by +16.1‰ versus +17.6‰ after completion of the reaction, respectively). Compared to the experiment with  $\text{NH}_2\text{Cl-A}$ ,  $\delta^{15}\text{N}$  values of NDMA were shifted towards more positive values with  $\text{NH}_2\text{Cl-B}$  (downward directed triangles in Figure 4.2b). The shift in N isotope values amounted to  $+26.9 \pm 2.2\text{‰}$  (indicated as black arrow in Figure 4.2b) and corresponds, within analytical uncertainty, to 50% of the difference between the two applied  $\text{NH}_2\text{Cl}$  batches, that is 27.6‰. This result confirms that one N atom in NDMA originates from  $\text{NH}_2\text{Cl}$  and one N atom stems from the tertiary amine precursor, in agreement with a previous study that applied  $^{15}\text{N}$  isotope labeled  $\text{NH}_2\text{Cl}$  to dimethylamine and measured the mass spectra of NDMA.<sup>61</sup>  $\delta^{13}\text{C}$  values of NDMA produced with  $\text{NH}_2\text{Cl-A}$  and  $\text{NH}_2\text{Cl-B}$  (grey and black diamonds, respectively, in Figure 4.2b) were identical, in agreement with the fact that both C atoms of the  $\text{N}(\text{CH}_3)_2$  group of NDMA originate from DFUR.

### 4.3.3 Isotope fractionation trends in tertiary amines and NDMA reflect the multistep NDMA formation pathway

As illustrated in Figure 4.1, NDMA formation is a multistep process in which N atoms play a key role. Deprotonation of tertiary amines occurs prior to the initial reaction with  $\text{NH}_2\text{Cl}$  leading to a hydrazine-type intermediate (compound **2** in Figure 4.1).<sup>79</sup> Subsequently, the  $\text{NH}_2$ -group of **2** is oxidized to a N-centered radical **3** that reacts with  $\text{O}_2$ .<sup>217</sup> The final release of NDMA from compound **5** requires the formation of a nitroso moiety as well as the cleavage of a C-N bond to the methylene group of the tertiary amine. As molar NDMA yields were smaller than 100%, tertiary amines or intermediate species also react to products other than NDMA. Every elementary reaction step depicted in Figure 4.1 might be associated with an isotope effect and could cause isotope fractionation in the precursors (tertiary amine and  $\text{NH}_2\text{Cl}$ ) as well as in NDMA. In the following, we evaluate which of these reactions contribute to the observable isotope fractionation in the tertiary amine precursor and in NDMA.



## C and N isotope fractionation in tertiary amines during chloramination

We studied C and N isotope fractionation in two tertiary amine model compounds, namely *N,N*-dimethylthiophene-2-methylamine (DMTA) and *N,N*-dimethylbenzylamine (DMBA) during chloramination. DMTA and DMBA are structurally similar to DFUR, known to produce high NDMA yields,<sup>67</sup> and are - in contrast to DFUR - amenable to isotope analysis by GC/IRMS. Figure 4.3a shows NDMA formation during the reaction of DMTA (40  $\mu$ M) with  $\text{NH}_2\text{Cl}$  (600  $\mu$ M) in 10 mM phosphate buffer at pH 8.0. Similar to the experiment with DFUR, NDMA formation was concurrent with the transformation of DMTA and consumption of  $\text{NH}_2\text{Cl}$ . After 4 h, a total amount of  $288 \pm 6 \mu\text{M}$   $\text{NH}_2\text{Cl}$  was consumed and a molar NDMA yield of  $75.4 \pm 0.1\%$  was observed in agreement with previously published data.<sup>67</sup> Chloramination of DMTA was accompanied by C and N isotope fractionation in the remaining tertiary amine (Figure 4.3b).  $\delta^{13}\text{C}$  as well as  $\delta^{15}\text{N}$  values of DMTA changed towards more positive values over time demonstrating that precursor molecules containing  $^{12}\text{C}$  and  $^{14}\text{N}$  reacted preferentially. While  $\delta^{13}\text{C}$  values increased by  $+8.6\text{‰}$  (from  $-35.6\text{‰}$  to  $-27.0\text{‰}$ ), a significantly stronger increase of  $+52.9\text{‰}$  was observed in  $\delta^{15}\text{N}$  values (from  $-4.5\text{‰}$  to  $+48.4\text{‰}$ ).

Generally, isotope fractionation in a reactant reflects all reaction steps up to and including the first irreversible one.<sup>83</sup> In multistep processes, observable isotope fractionation is, thus, a combination of several isotope effects and dominated by isotope-sensitive reaction steps with the highest activation energy.<sup>83</sup> While rate-determining steps of the NDMA formation reaction cannot be identified a priori, the data in Figures 4.2a and 4.3a provide information about the overall NDMA formation kinetics. As the transformation of the tertiary amine and formation of NDMA occur simultaneously without formation of long-lived intermediates, we conclude that only one rate-determining step governs the reaction. This step might be either the formation of the first reaction intermediate (compound **2** in Figure 4.1) or the formation of the N-centered radical (**3**) because reactions  $\mathbf{3} \rightarrow \mathbf{4} \rightarrow \mathbf{5}$  are expected to be significantly faster and irreversible due to the radical nature of the intermediates.

It is thus likely that reactions  $\mathbf{1} \rightarrow \mathbf{2}$  or  $\mathbf{1} \rightleftharpoons \mathbf{2} \rightarrow \mathbf{3}$  in Figure 4.1 cause N isotope fractionation in DMTA. However, the observed changes in N isotope ratios of DMTA, shown in Figure 4.3b, are not only caused by the transformation reaction of DMTA but also by its deprotonation. Recent studies showed that deprotonation of *N,N*-dimethylaniline and substituted anilines is associated with a  $^{15}\text{N}$  equilibrium isotope effect (EIE) of 1.014 - 1.0203.<sup>130,224,225</sup> We determined an EIE for deprotonation of DMTA, which was in the same range ( $\text{EIE}_{\text{N}}^{\text{BH}^+ - \text{B}} = 1.0103 \pm 0.0004$ , Table S4.2). Given that approximately



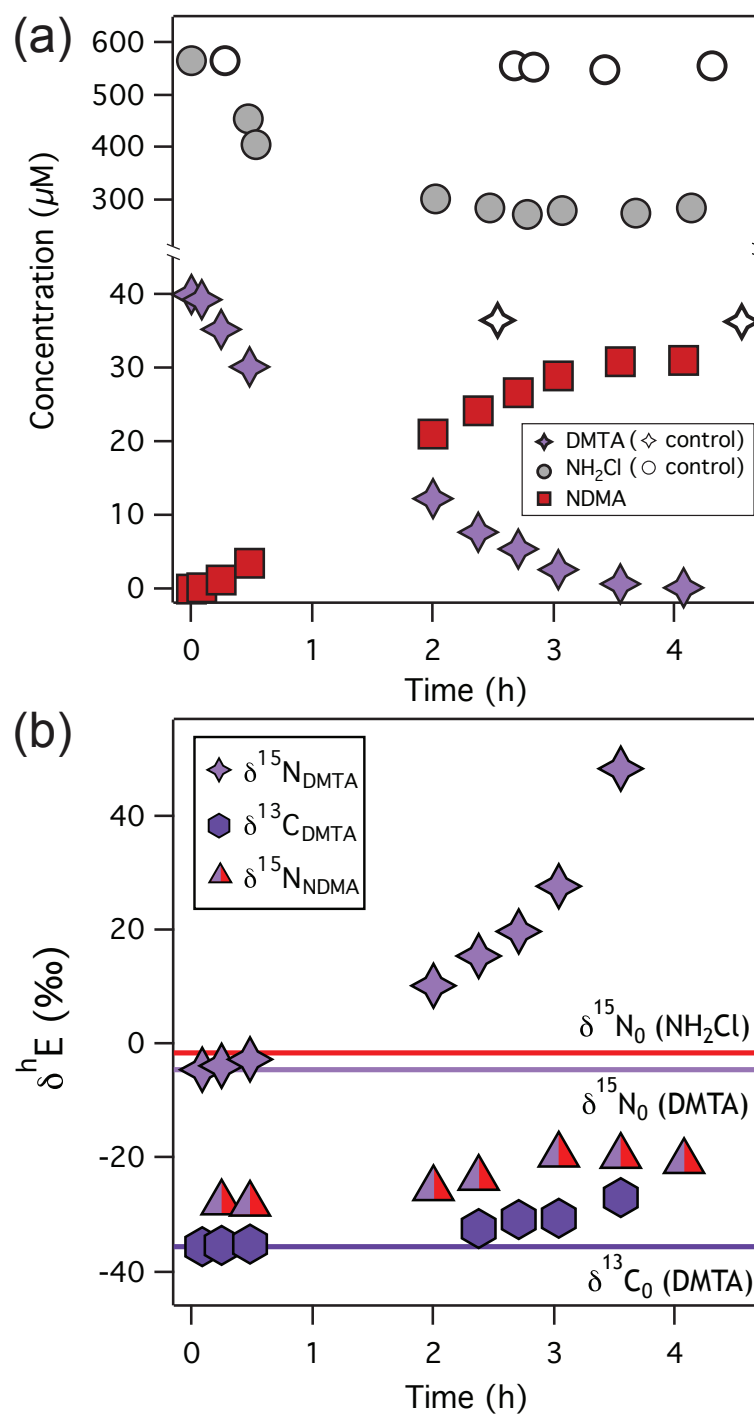


**Figure 4.3:** NDMA formation from the reaction of DMTA ( $40\ \mu\text{M}$ ) with  $\text{NH}_2\text{Cl}$  ( $600\ \mu\text{M}$ ) in 10 mM phosphate buffer at pH 8.0. Panel (a) shows DMTA degradation,  $\text{NH}_2\text{Cl}$  consumption, and NDMA formation over time. Symbols in panel (b) demonstrate  $\delta^{13}\text{C}$  and  $\delta^{15}\text{N}$  values of DMTA as well as  $\delta^{15}\text{N}$  values of the formed NDMA during chloramination. Solid lines represent the initial  $\delta^{13}\text{C}$  and  $\delta^{15}\text{N}$  values of DMTA and  $\text{NH}_2\text{Cl}$ . Standard deviations of triplicate  $\delta^{13}\text{C}$  and  $\delta^{15}\text{N}$  measurements of DMTA and NDMA were  $<0.2\text{‰}$  and  $<0.8\text{‰}$ , respectively, and smaller than the depicted symbols.

98% of the DMTA molecules are protonated at pH 8.0, the observed N isotope fractionation in DMTA was mainly caused by its deprotonation. Compared to the apparent N kinetic isotope effect,  $AKIE_N$ , of  $1.0127 \pm 0.0007$ , which was derived from the measured  $\delta^{15}N$  values of DMTA (Figure 4.3b), the  $AKIE_N^B$  associated with the reaction of deprotonated DMTA was small ( $1.0025 \pm 0.0011$ , Table S4.2). Assuming that the first reaction step (**1**  $\rightarrow$  **2** in Figure 4.1) is irreversible, this small, normal  $AKIE_N^B$  reflects the initial nucleophilic substitution reaction of the tertiary amine with  $NH_2Cl$ . In fact, nitrogen nucleophile isotope effects are expected to be small and normal.<sup>226</sup> Molar NDMA yields from DMTA were  $<100\%$  indicating that DMTA might form products other than compound **2** in isotope-sensitive side reactions (Figure 4.1). The  $AKIE_N^B$  would then reflect combined contributions of two or more KIEs. However, we assume that NDMA yields  $<100\%$  are rather caused by side reactions involving radical intermediates such as compounds **3** and **4** in Figure 4.1. DMTA is thus likely transformed stoichiometrically to compound **2** so that the  $AKIE_N^B$  reflects the nucleophilic substitution reaction.

The results obtained from chloramination of DMBA were almost identical to those with DMTA, despite a lower molar NDMA yield of  $58 \pm 0.6\%$  (see Figure S4.2 and Table S4.2). Using a  $pK_a$  value of 9.0 for DMBA<sup>222</sup> and the  $EIE_N^{BH^+-B}$  obtained for DMTA, the  $AKIE_N^B$  associated with the reactive transformation of DMBA was  $1.0056 \pm 0.0007$  and only slightly larger than the one for DMTA. This observation confirms our assumption that no isotope-sensitive side reactions are involved in the transformation of the tertiary amines and the  $AKIE_N^B$  reflects the initial nucleophilic substitution reaction leading to compound **2** in Figure 4.1.

In contrast to strong N isotope fractionation trends, changes in C isotope ratios of DMTA and DMBA were small (Figure 4.3b and S4.2b). We did not determine  $EIE_C$  for the deprotonation of DMTA, but assume small values of  $\leq 1.001$  as found for the deprotonation of substituted anilines.<sup>130</sup> Small changes in C isotope ratios of DMTA are in agreement with the observation that the methylthiophene-moiety of DMTA did not react with  $NH_2Cl$  (Figure S4.9). Consequently, the reaction of DMTA with  $NH_2Cl$  occurs exclusively at the  $N(CH_3)_2$  group of DMTA and only involves the N atom of this moiety. Small changes in  $\delta^{13}C$  values of DMTA and DMBA are thus due to secondary isotope effects (secondary  $AKIE_C$  of  $1.0021 \pm 0.0003$  and  $1.0014 \pm 0.0001$ , respectively) that arise because both methyl groups as well as the methylene group of the tertiary amines are in direct proximity to the reactive site.

### N isotope fractionation in NDMA during chloramination of tertiary amines

The normal N isotope fractionation trends in the tertiary amine precursors show that  $^{14}\text{N}$  atoms of DMTA and DMBA reacted preferentially with  $\text{NH}_2\text{Cl}$ . Indeed, NDMA was enriched in  $^{14}\text{N}$  at the beginning of the reaction (Figure 4.3b). Subsequently,  $\delta^{15}\text{N}$  values of NDMA increased over time (from  $-28.2\text{‰}$  to  $-19.8\text{‰}$ ) because an increasing share of  $^{15}\text{N}$  reacted. The N isotope fractionation trend observed in the tertiary amine precursors is thus consistent with the one observed in NDMA.

In general, isotope fractionation in NDMA can be caused by all reaction steps of the NDMA formation pathway (Figure 4.1). As described above, the nucleophilic substitution reaction (**1**  $\rightarrow$  **2**) is likely associated with a measurable nitrogen KIE because a N-N bond is formed.<sup>226</sup> In contrast, the formation of aminyl radicals (**2**  $\rightarrow$  **3**) is expected to be of minor relevance for the overall N isotope fractionation in NDMA because KIEs reported for N-atom oxidation of aromatic *N*-alkylamines are small.<sup>148,221</sup> The formation of peroxy radicals (**3**  $\rightarrow$  **4**) might be isotope sensitive as well but its contribution to the N isotope fractionation in NDMA is likely minor because radical reactions with  $\text{O}_2$  are expected to be faster than other reaction steps in the NDMA formation reaction.<sup>200</sup> The coupling of two peroxy radicals to a tetroxide species (**4**  $\rightarrow$  **5**) will not be reflected in the N isotope ratios of NDMA because only oxygen atoms are directly involved in the reaction. In contrast, the final release of NDMA (**5**  $\rightarrow$  **6**), which requires the formation of the N=O moiety as well as the cleavage of a C-N bond, likely contributed to the observable N isotope fractionation in NDMA.<sup>227</sup> In addition,  $\text{NH}_2\text{Cl}$  and radical intermediates could react in parallel side reactions to unidentified products other than NDMA, which might lead to isotope discrimination (Figure 4.1). Consequently, a combination of reactions and their KIEs causes the observed trend of increasing  $\delta^{15}\text{N}$  values of NDMA (Figures 4.2b and 4.3b), which is likely to be characteristic for NDMA formation from chloramination of tertiary amines.

#### 4.3.4 Isotope fractionation trends in NDMA as proxy for its formation pathway and precursors

Even though reaction steps that cause observable changes in N isotope ratios of NDMA cannot be identified unequivocally, we hypothesize that stable isotope fractionation trends in NDMA are characteristic for the NDMA formation pathway. Linear correlations of measured isotope signatures of two elements of a compound (e.g.,  $\delta^{15}\text{N}$  versus  $\delta^{13}\text{C}$ ) have been used frequently to distinguish and identify transformation path-

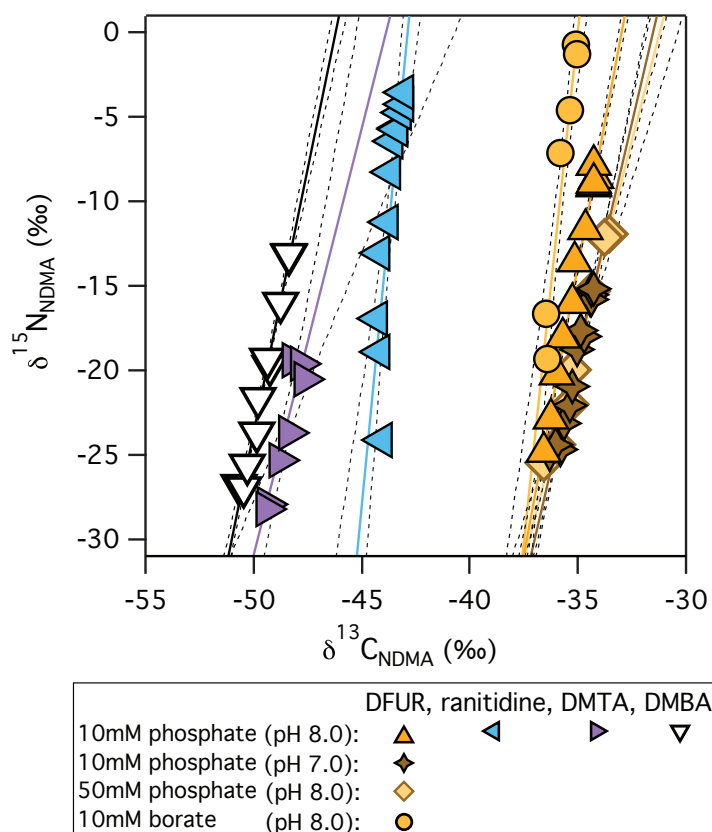


**Figure 4.4:**  $\delta^{15}\text{N}$  versus  $\delta^{13}\text{C}$  values of NDMA for the chloramination of four different tertiary amines namely DFUR ( $3\mu\text{M}$ ), ranitidine ( $3\mu\text{M}$ ), DMTA ( $40\mu\text{M}$ ), and DMBA ( $40\mu\text{M}$ ) in 10 mM phosphate buffer at pH 8.0. Chloramination experiments with DFUR were also conducted in 10 mM phosphate buffer (pH 7.0), 50 mM phosphate buffer (pH 8.0), and 10 mM borate buffer (pH 8.0). Solid lines represent linear regressions and dashed lines are the corresponding 95% confidence intervals. Standard deviations of triplicate  $\delta^{13}\text{C}$  and  $\delta^{15}\text{N}$  measurements of NDMA were  $<0.4\text{‰}$  and  $<0.6\text{‰}$ , respectively, and smaller than the depicted symbols.

ways of organic contaminants because dual isotope slopes are a strong indicator for the reaction mechanism.<sup>83,93,106,152</sup> Similarly, dual isotope slopes could serve as proxy for NDMA formation mechanisms and precursors. To test this hypothesis, we determined  $\delta^{13}\text{C}$  and  $\delta^{15}\text{N}$  values of NDMA during its formation from four tertiary amines, namely ranitidine, DFUR, DMTA, and DMBA, in independent chloramination experiments. Owing to the structural similarity of these precursors, NDMA formation is expected to proceed via the same reaction mechanism as proposed in Figure 4.1. C and N isotope fractionation patterns in NDMA should therefore be alike.

Figure 4.4 shows  $\delta^{15}\text{N}$  versus  $\delta^{13}\text{C}$  values of NDMA during its formation from chloramination of the selected tertiary amines. The initial  $\delta^{15}\text{N}$  values of NDMA were similar

(between  $-24.1\text{‰}$  and  $-28.2\text{‰}$ ) what is likely due to similar initial  $\delta^{15}\text{N}$  values of the precursors (between  $-2.2\text{‰}$  and  $-4.5\text{‰}$ , Table S4.1). In contrast, initial  $\delta^{13}\text{C}$  values of NDMA differed between  $-36.8\text{‰}$  and  $-50.7\text{‰}$  due to distinctly different initial  $\delta^{13}\text{C}$  values of the precursors (between  $-19.8\text{‰}$  and  $-35.5\text{‰}$ , Table S4.1). However, we observed for all precursors that changes in  $\delta^{13}\text{C}$  values of NDMA were minor, while  $\delta^{15}\text{N}$  values of NDMA significantly increased by  $+8.4\text{‰}$  to  $+20.6\text{‰}$  during its formation (Figures 4.4 and S4.5, Table S4.3). Correlation of  $\delta^{13}\text{C}$  and  $\delta^{15}\text{N}$  values of NDMA revealed characteristic trends that could, indeed, serve as proxy for the NDMA formation pathway during chloramination of the selected tertiary amines (Figure 4.4).  $\delta^{15}\text{N}_{\text{NDMA}} / \delta^{13}\text{C}_{\text{NDMA}}$ -slopes were  $6.9 \pm 0.5$ ,  $5.1 \pm 2.1$ , and  $6.3 \pm 0.6$  for chloramination of DFUR, DMTA, and DMBA, respectively, in 10 mM phosphate buffer at pH 8.0 (Table 4.1). These slopes were very similar and independent of the molar NDMA yield which was  $65 \pm 2\%$ ,  $75 \pm 0.1\%$ , and  $58 \pm 1\%$  for DFUR, DMTA, and DMBA, respectively, in agreement with previously reported values (Table 4.1, Figure S4.5).<sup>67</sup> For chloramination of ranitidine under the same reaction conditions, we observed a high molar NDMA yield of  $97 \pm 4\%$ <sup>162</sup> and a bigger  $\delta^{15}\text{N}_{\text{NDMA}} / \delta^{13}\text{C}_{\text{NDMA}}$ -slope of  $13.3 \pm 5.0$ . As our study reports the first correlated  $\delta^{13}\text{C}$  and  $\delta^{15}\text{N}$  values of NDMA, reference values for chloramination of amines do not yet exist. Therefore, it is difficult to assess whether differences in  $\delta^{15}\text{N}_{\text{NDMA}} / \delta^{13}\text{C}_{\text{NDMA}}$ -slopes are significant and indicative of changes in the reaction mechanism.

**Table 4.1:** Molar NDMA yield in percent as well as dual isotope slopes  $\delta^{15}\text{N}_{\text{NDMA}} / \delta^{13}\text{C}_{\text{NDMA}}$  for the reaction of DFUR ( $3\text{ }\mu\text{M}$ ), ranitidine ( $3\text{ }\mu\text{M}$ ), DMTA ( $40\text{ }\mu\text{M}$ ), and DMBA ( $40\text{ }\mu\text{M}$ ) with  $\text{NH}_2\text{Cl}$  ( $45\text{ }\mu\text{M}$  or  $600\text{ }\mu\text{M}$ , respectively) in 10 mM phosphate buffer at pH 8.0. Chloramination experiments with DFUR were conducted using differing buffer types and concentrations, and pH values.

Precursor	buffer		pH	molar NDMA yield (%)	$\delta^{15}\text{N}_{\text{NDMA}} / \delta^{13}\text{C}_{\text{NDMA}}$ (-)
	conc ( $\mu\text{M}$ )	type			
DFUR	10mM	phosphate	8.0	$65 \pm 2$	$6.9 \pm 0.5$
	10mM	phosphate	7.0	$66 \pm 1$	$5.5 \pm 0.6$
	50mM	phosphate	8.0	$68 \pm 1$	$5.0 \pm 0.9$
	10mM	borate	8.0	$88 \pm 1$	$12.3 \pm 3.5$
ranitidine	10mM	phosphate	8.0	$97 \pm 4$	$13.3 \pm 5.0$
DMTA	10mM	phosphate	8.0	$75 \pm 0.1$	$5.1 \pm 2.1$
DMBA	10mM	phosphate	8.0	$58 \pm 1$	$6.3 \pm 0.6$

Because all four selected tertiary amines likely produce NDMA via the same reaction pathway (Figure 4.1), we hypothesize that the here observed isotope fractionation trends and  $\delta^{15}\text{N}_{\text{NDMA}} / \delta^{13}\text{C}_{\text{NDMA}}$ -slopes in the range of 5.1 - 13.3 are characteristic for chloramination of the selected class of tertiary amines. Future studies need to evaluate whether chloramination of other tertiary amine-containing precursors also leads to C and N isotope fractionation trends similar to the ones observed in this study.

$\delta^{15}\text{N}_{\text{NDMA}} / \delta^{13}\text{C}_{\text{NDMA}}$ -slopes could serve as proxy for the NDMA formation pathway during chloramination of the here studied tertiary amines and might help to identify this important class of precursors in source waters used for drinking water production. However, such an application of CSIA requires that isotope fractionation trends in NDMA are a robust measure for NDMA formation from specific precursors. It has been shown previously that water matrix components, presumably natural organic matter, can slow down the formation of NDMA during chloramination of ranitidine without affecting the molar NDMA yield.<sup>71</sup> To test whether reaction conditions that change NDMA conversion rates affect N isotope fractionation trends in NDMA, we chloraminated the model precursor DFUR under various experimental conditions using differing buffer types and concentrations as well as differing pH values (Table 4.1). As shown in Figure S4.6, NDMA formation from DFUR was accelerated with increasing phosphate buffer concentration (from 1 mM - 50 mM, pH 8.0) indicating that the rate-determining reaction step is catalyzed in the presence of phosphate. However, the  $\delta^{15}\text{N}_{\text{NDMA}} / \delta^{13}\text{C}_{\text{NDMA}}$ -slope determined in the experiment with 50 mM phosphate buffer ( $5.0 \pm 0.9$ , Table 4.1) was similar to the value observed in 10 mM phosphate buffer ( $6.9 \pm 0.5$ ). Also decreasing the pH value of a 10 mM phosphate buffer from 8.0 to 7.0 did not have a significant effect on the  $\delta^{15}\text{N}_{\text{NDMA}} / \delta^{13}\text{C}_{\text{NDMA}}$ -slope ( $5.5 \pm 0.6$ ), even though NDMA formation was decelerated at pH 7.0 (Figures S4.11, S4.12, and S4.13). Likewise, the use of 10 mM borate and carbonate buffer instead of 10 mM phosphate or arsenate buffer significantly slowed down DFUR degradation and NDMA formation (Figure S4.7). The  $\delta^{15}\text{N}_{\text{NDMA}} / \delta^{13}\text{C}_{\text{NDMA}}$ -slope obtained in an experiment with borate buffer was  $12.3 \pm 0.5$  and, thus, bigger than other slopes obtained for chloramination of DFUR (Table 4.1). However, this value was similar to the one obtained during chloramination of ranitidine. These robust isotope fractionation trends indicate that NDMA formation during chloramination of DFUR proceeded via the same reaction mechanism even though the reaction conditions and NDMA formation kinetics varied.

## 4.4 Implications for CSIA as a tool to identify NDMA precursors

Our study provides first evidence that isotope fractionation trends in NDMA reflect its formation pathway. The slope of the linear correlation of  $\delta^{13}\text{C}$  and  $\delta^{15}\text{N}$  values of NDMA can serve as proxy for NDMA formation during chloramination of the studied class of tertiary amines, even under varying reaction conditions. Future studies need to investigate whether the observed range of  $\delta^{15}\text{N}_{\text{NDMA}} / \delta^{13}\text{C}_{\text{NDMA}}$ -slopes (from 5.0-13.3) is characteristic for chloramination of a broader range of tertiary amine-containing NDMA precursors. Moreover, the potential variability of C and N isotope fractionation trends in NDMA needs to be investigated, e.g., during chloramination of tertiary amines in the presence of natural organic matter. Current knowledge suggests that NDMA formation mechanisms differ depending on the precursor and disinfectant.<sup>30</sup> However, it is currently unknown if and to what extent differing NDMA formation pathways are reflected in isotope fractionation trends in NDMA and if these trends can be used to distinguish different pathways. Future studies need to systematically investigate whether differing NDMA formation pathways cause unique isotope fractionation trends. Compiling a repository of  $\delta^{15}\text{N}_{\text{NDMA}} / \delta^{13}\text{C}_{\text{NDMA}}$ -slopes for NDMA formation from differing precursors and disinfectants will be crucial to distinguish and identify relevant NDMA precursors in source waters used for drinking water production.

## Acknowledgement

This work was supported by the Swiss National Science Foundation (Project no. 200021-140545). We thank Jakov Bolotin for analytical support, Christine Egli for help with laboratory experiments, and Sarah Pati and Olaf A. Cirpka for valuable discussions.





# Supporting Information to Chapter 4

## S4.1 Safety considerations

*N*-nitrosamines are mutagenic and probably carcinogenic to humans. Wear appropriate protective clothing, goggles, and gloves and work in a well-ventilated chemical fume hood. Keep away from heat, sparks, and flames.

## S4.2 Chemicals

All chemicals were used without further purification. 5-(dimethylaminomethyl)furfuryl alcohol hydrochloride (DFUR, 96%) and *N,N*-dimethylthiophene-2-methylamine (DMTA) were purchased from ABCR and Santa Cruz Biotechnology, respectively. Ranitidine hydrochloride, *N,N*-dimethylbenzylamine (DMBA, 99%), *N*-nitrosodimethylamine (NDMA, 5000  $\mu\text{g}/\text{ml}$  in methanol, 99.9%), 2-thiophenemethanol (98%), 2,2'-azino-bis(3-ethylbenzothiazoline-6-sulfonic acid) diammonium salt (ABTS,  $\geq 98\%$ ), potassium iodide ( $\geq 99\%$ ), sodium nitrite ( $\text{NaNO}_2$ , 99%), sodium thiosulfate ( $\text{Na}_2\text{S}_2\text{O}_3$ ,  $\geq 98\%$ ), and potassium phosphate monobasic ( $\text{KH}_2\text{PO}_4$ , puriss,  $\geq 99.5\%$ ) were purchased from Sigma Aldrich. Sodium carbonate ( $\text{Na}_2\text{CO}_3$ ) and sodium bicarbonate ( $\text{NaHCO}_3$ ) were obtained from Merck. Boric acid ( $> 98\%$ ) and di-sodium hydrogen arsenate heptahydrate ( $\text{Na}_2\text{HAsO}_4$ , ACS  $> 98.5\%$ ) were from Fluka. For  $\text{NH}_2\text{Cl}$  preparation, we used sodium hypochlorite (6-14%  $\text{HOCl}$ , Sigma-Aldrich) and ammonium chloride ( $\text{NH}_4\text{Cl}$ , 99.5%, Fluka) or  $^{15}\text{N}$ -enriched ammonium sulfate ( $(\text{NH}_4)_2\text{SO}_4$ , USGS26) that was purchased from the International Atomic Energy Agency (IAEA).<sup>218</sup>

Analyte stock solutions were made in ethyl acetate (99.7%, Chromasolv for HPLC, Sigma Aldrich), or methanol (99.99%, Fisher Scientific). These solvents were also used for solid phase extraction (SPE) in addition to pentane (99.0%, Sigma-Aldrich). Aqueous solutions were prepared with deionised water (18.1  $\text{M}\Omega \cdot \text{cm}$ , Barnstead NANOpure Diamond Water Purification System). The pH value of buffered solutions was adjusted with sodium hydroxide pellets ( $\text{NaOH}$ , puriss,  $\geq 99\%$ , Sigma-Aldrich) or aqueous  $\text{NaOH}$  solution (Sigma-Aldrich). For SPME-GC/MS and SPME-GC/IRMS analyses the ionic strength of the samples was raised with sodium chloride ( $\text{NaCl}$ , 99.5%, Merck). Helium ( $\text{He}$ , 99.999%) was used as carrier gas for GC/MS and GC/IRMS analysis. Reference gases for GC/IRMS measurements were  $\text{CO}_2$  (99.999%),  $\text{N}_2$  (99.999%),  $\text{H}_2$  (99.999%) and  $\text{O}_2$  (99.999%) from Carbagas (Rümlang, Switzerland).

## S4.3 Stable isotope analysis

### S4.3.1 Reference isotope signatures

**Table S4.1:** C and N isotope signatures of in-house standards measured with elemental analyzer isotope ratio mass spectrometry (EA/IRMS).

Compound	$\delta^{15}\text{N}$	$\delta^{13}\text{C}$
ranitidine	$-3.36 \pm 0.11$	$-28.24 \pm 0.03$
DFUR	$-2.22 \pm 0.39$	$-19.76 \pm 0.03$
DMTA	$-4.52 \pm 0.08$	$-35.54 \pm 0.03$
$\text{NH}_4\text{Cl}$	$-1.44 \pm 0.03^{\text{a}}$	-
$(\text{NH}_4)_2\text{SO}_4^{\text{b}}$	$+53.7 \pm 0.4^{\text{a}}$	-

<sup>a</sup> Reported as proxy for the initial  $\delta^{15}\text{N}$  value of  $\text{NH}_2\text{Cl}$  generated from the reaction of  $\text{HOCl}$  with  $\text{NH}_4\text{Cl}$  or  $(\text{NH}_4)_2\text{SO}_4$

<sup>b</sup> Standard reference material USG26 obtained from IAEA <sup>218</sup>

### S4.3.2 Method quantification limits (MQLs) for C and N isotope analysis of DMTA

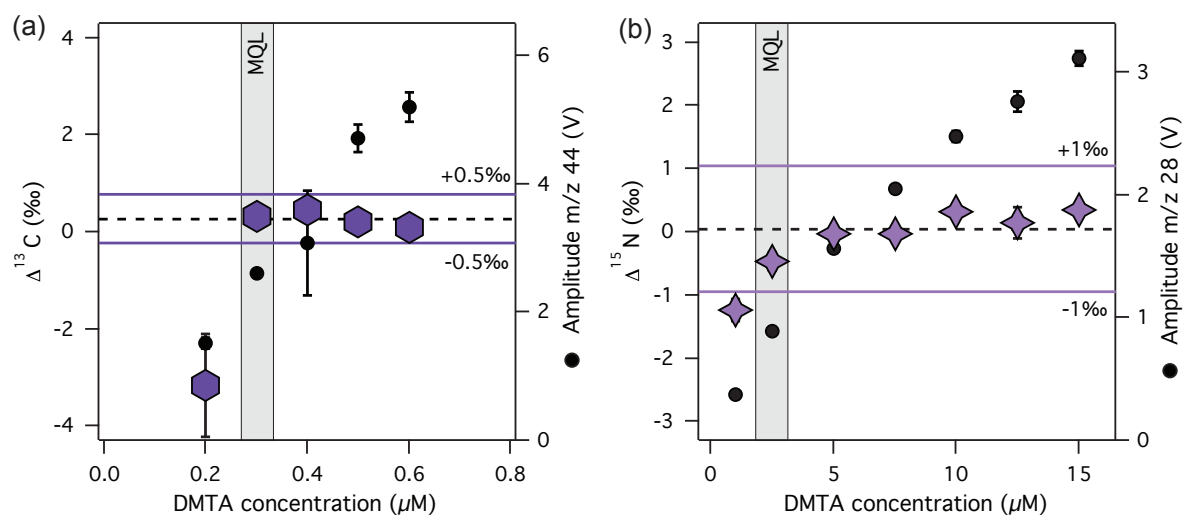


**Figure S4.1:** Accuracies of (a) C and (b) N isotope signatures of DMTA as function of the DMTA concentration. Amplitudes increased with increasing DMTA concentrations. MQLs were determined according to the moving mean procedure of Jochmann et al.<sup>141</sup> with intervals of  $\pm 0.5\text{‰}$  and  $\pm 1\text{‰}$  for C and N isotope analysis, respectively (purple lines). MQLs are indicated as grey bars and moving means by dashed lines.

## S4.4 Isotope fractionation in tertiary amines during chloramination

### S4.4.1 Isotope fractionation in DMTA and DMBA

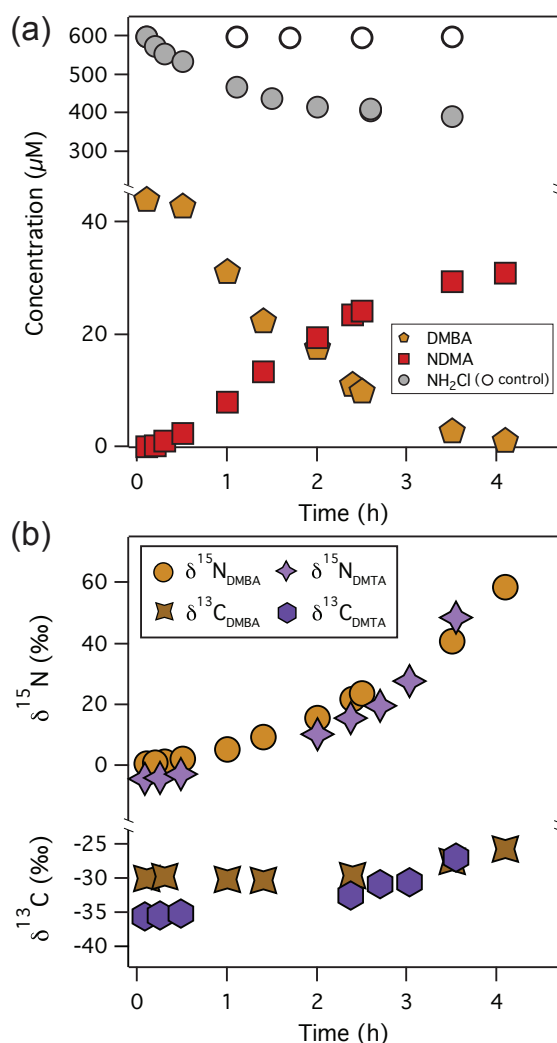


**Figure S4.2:** NDMA formation from the reaction of DMBA ( $40\ \mu\text{M}$ ) with  $\text{NH}_2\text{Cl}$  ( $600\ \mu\text{M}$ ) in 10 mM phosphate buffer at pH 8.0. Panel (a) shows DMBA degradation,  $\text{NH}_2\text{Cl}$  consumption, and NDMA formation over time. Panel (b) illustrates  $\delta^{13}\text{C}$  and  $\delta^{15}\text{N}$  values of DMBA (brown symbols) and DMTA (purple symbols) over time. Standard deviations of triplicate  $\delta^{13}\text{C}$  and  $\delta^{15}\text{N}$  measurements of DMTA and DMBA were  $<0.4\text{‰}$  and  $<0.8\text{‰}$ , respectively, and smaller than the depicted symbols.

### S4.4.2 Bulk isotope enrichment factors

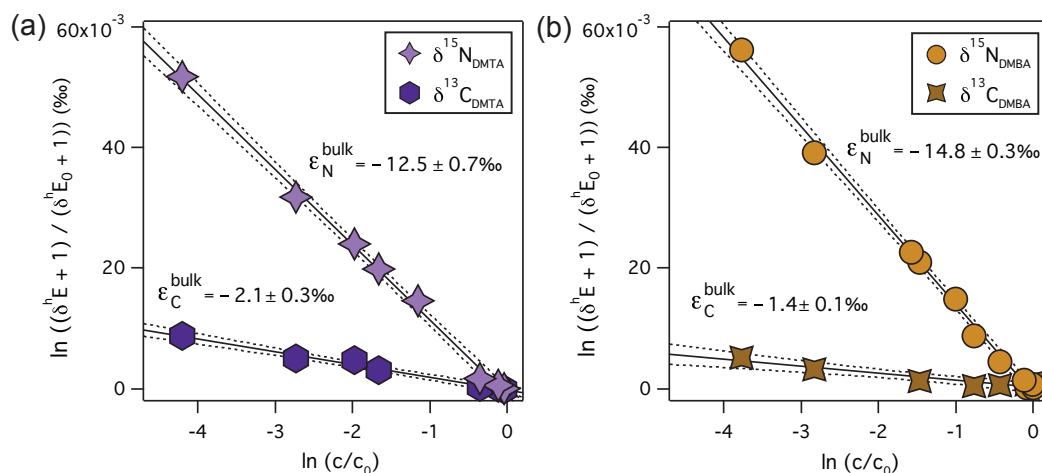


**Figure S4.3:** Linearized C and N isotope fractionation of (a) DMTA and (b) DMBA used to derive C and N bulk isotope enrichment factors,  $\epsilon_C^{\text{bulk}}$  and  $\epsilon_N^{\text{bulk}}$ , respectively.

### S4.4.3 $^{15}\text{N}$ equilibrium isotope effect associated with the deprotonation of DMTA

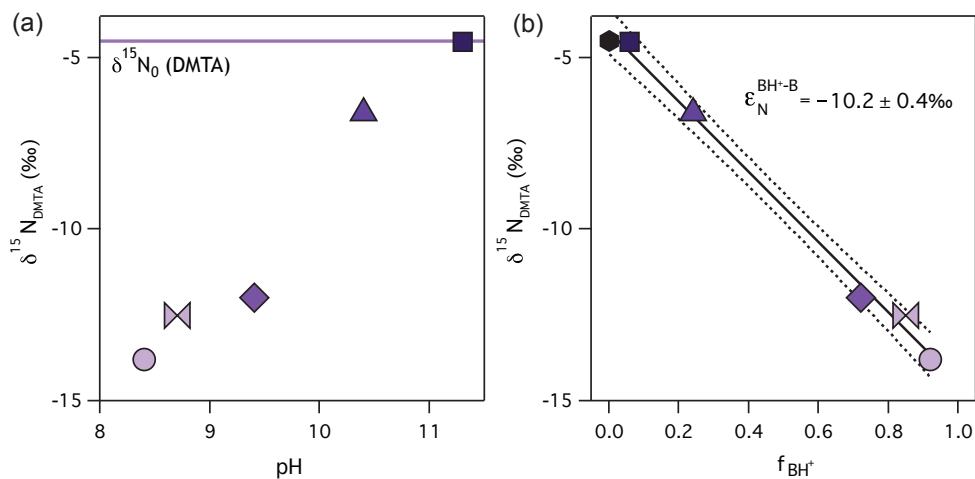


**Figure S4.4:** N isotope signatures ( $\delta^{15}\text{N}_{\text{DMTA}}$ ) measured with SPME-GC/IRMS in the neutral fraction of DMTA (a) versus pH of the aqueous DMTA samples (from 8.4-11.3) in 10 mM phosphate buffer and (b) versus the fraction of protonated DMTA species ( $f_{\text{BH}^+}$ ). The concentration of protonated DMTA in a sample was calculated using peak areas of the GC/IRMS measurements. The slope of the regression line corresponds to the enrichment factor for the deprotonation of DMTA ( $\epsilon_N^{\text{BH}^+-\text{B}}$ ). The standard deviation of triplicate  $\delta^{15}\text{N}_{\text{DMTA}}$  measurements was  $<0.8\text{‰}$  and smaller than the depicted symbols.

#### S4.4.4 Isotope enrichment factors and kinetic isotope effects associated with the reaction of DMTA and DMBA

**Table S4.2:** Carbon and nitrogen bulk isotope enrichment factors,  $\varepsilon_C^{\text{bulk}}$  and  $\varepsilon_N^{\text{bulk}}$ , and apparent kinetic isotope effects,  $\text{AKIE}_C$  and  $\text{AKIE}_N$ , for the chloramination of DMTA and DMBA.  $\text{EIE}_N^{\text{BH}^+-\text{B}}$  is the equilibrium isotope effect associated with deprotonation of DMTA.  $\text{AKIE}_N^{\text{B}}$  is the apparent kinetic isotope effect associated with the reaction of deprotonated DMTA and DMBA.

Compound	$\varepsilon_C^{\text{bulk}}$ (‰)	$\varepsilon_N^{\text{bulk}}$ (‰)	$\text{AKIE}_C$ (-)	$\text{AKIE}_N$ (-)	$\text{EIE}_N^{\text{BH}^+-\text{B}}$ (-)	$\text{AKIE}_N^{\text{B}}$ (-)
DMTA	$-2.1 \pm 0.3$	$-12.5 \pm 0.7$	$1.0021 \pm 0.0003$	$1.0127 \pm 0.0007$	$1.0103 \pm 0.0004$	$1.0025 \pm 0.0011$
DMBA	$-1.4 \pm 0.1$	$-14.8 \pm 0.3$	$1.0014 \pm 0.0001$	$1.0150 \pm 0.0003$	<sup>a</sup>	$1.0056 \pm 0.0007^{\text{b}}$

<sup>a</sup> not determined    <sup>b</sup> calculated with the  $\text{EIE}_N^{\text{BH}^+-\text{B}}$  of DMTA

The observable  $\text{AKIE}_N$  is the weighted average of the protonated ( $f_{\text{BH}^+}$ ) and deprotonated fraction ( $1-f_{\text{BH}^+}$ ) and their respective isotope effects as shown in eq. S4.1.<sup>130</sup>

$$\text{AKIE}_N = f_{\text{BH}^+} \cdot \text{EIE}_N^{\text{BH}^+-\text{B}} \cdot \text{AKIE}_N^{\text{B}} + (1 - f_{\text{BH}^+}) \cdot \text{AKIE}_N^{\text{B}} \quad (\text{S4.1})$$

#### S4.5 C, H, and N isotope ratios of NDMA during chloramination of four tertiary amines

**Table S4.3:** N isotope signatures of NDMA,  $\delta^{15}\text{N}_{\text{NDMA}}^{\text{ini}}$  and  $\delta^{15}\text{N}_{\text{NDMA}}^{\text{end}}$  in permil, determined at the beginning and the end of the reaction of ranitidine ( $3\mu\text{M}$ ), DFUR ( $3\mu\text{M}$ ), DMTA ( $40\mu\text{M}$ ), and DMBA ( $40\mu\text{M}$ ) with  $\text{NH}_2\text{Cl}$  which was added in 15-fold excess ( $45\mu\text{M}$  or  $600\mu\text{M}$ ), respectively. The molar NDMA yield corresponding to the  $\delta^{15}\text{N}_{\text{NDMA}}$  values is specified in percent.

Precursor	$\delta^{15}\text{N}_{\text{NDMA}}^{\text{ini}}$ (‰)	NDMA yield (%)	$\delta^{15}\text{N}_{\text{NDMA}}^{\text{end}}$ (‰)	NDMA yield (%)	$\Delta^{15}\text{N}_{\text{NDMA}}$ (‰)
ranitidine	-24.1	9	-3.5	97	+20.6
DFUR	-24.8	12	-8.7	65	+16.1
DMTA	-28.2	8	-19.8	75	+8.4
DMBA	-26.9	5	-13.2	58	+13.7

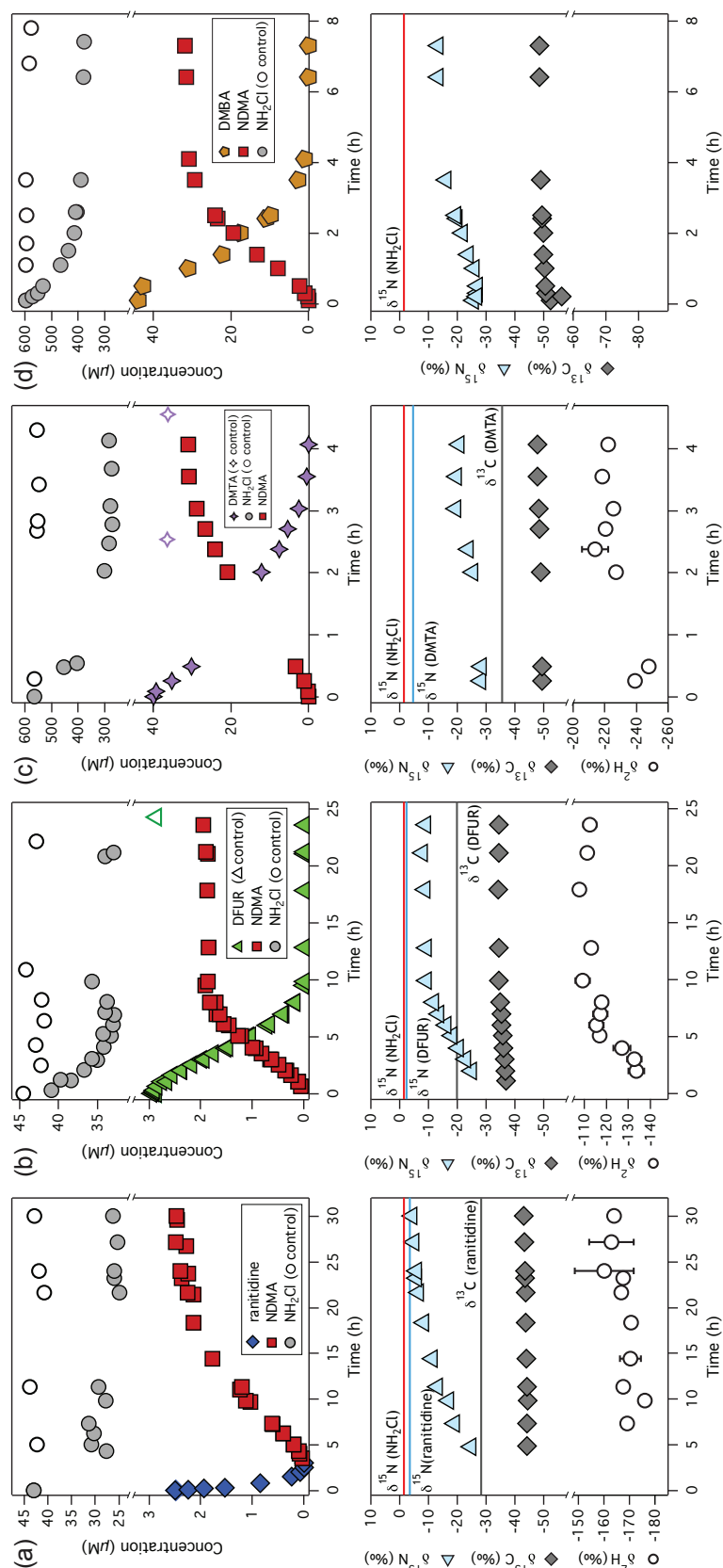


**Figure S4.5:** NDMA formation and corresponding C, H, and N isotope signatures of (a) ranitidine (3  $\mu\text{M}$ ), (b) DFUR (3  $\mu\text{M}$ ), (c) DMTA (40  $\mu\text{M}$ ), and (d) DMBA (40  $\mu\text{M}$ ) with  $\text{NH}_2\text{Cl}$  which was added in 15-fold excess (corresponding to concentrations of 45  $\mu\text{M}$  and 600  $\mu\text{M}$   $\text{NH}_2\text{Cl}$ ). Upper panels show the degradation of the tertiary amine precursor as well as the disappearance of  $\text{NH}_2\text{Cl}$  and formation of NDMA. Lower panels show  $\delta^{13}\text{C}$ ,  $\delta^2\text{H}$ , and  $\delta^{15}\text{N}$  values of NDMA over time. Solid lines represent initial  $\delta^{13}\text{C}$  and  $\delta^{15}\text{N}$  values of the tertiary amine precursors and  $\text{NH}_2\text{Cl}$ . Note that we used the reference isotope signature of  $\text{NH}_4\text{Cl}$  (Table S4.1) as proxy for the initial  $\delta^{15}\text{N}$  value of  $\text{NH}_2\text{Cl}$ . The initial C and N isotope signatures of NDMA were not determined. Standard deviations of triplicate  $\delta^{13}\text{C}$ ,  $\delta^2\text{H}$ , and  $\delta^{15}\text{N}$  measurements of NDMA were  $<0.4\%$ ,  $<11.5\%$ , and  $<0.5\%$ , respectively, and mostly smaller than the depicted symbols.

## S4.6 Impact of buffer concentration and type on NDMA formation kinetics and N isotope fractionation

### S4.6.1 Phosphate buffer concentration

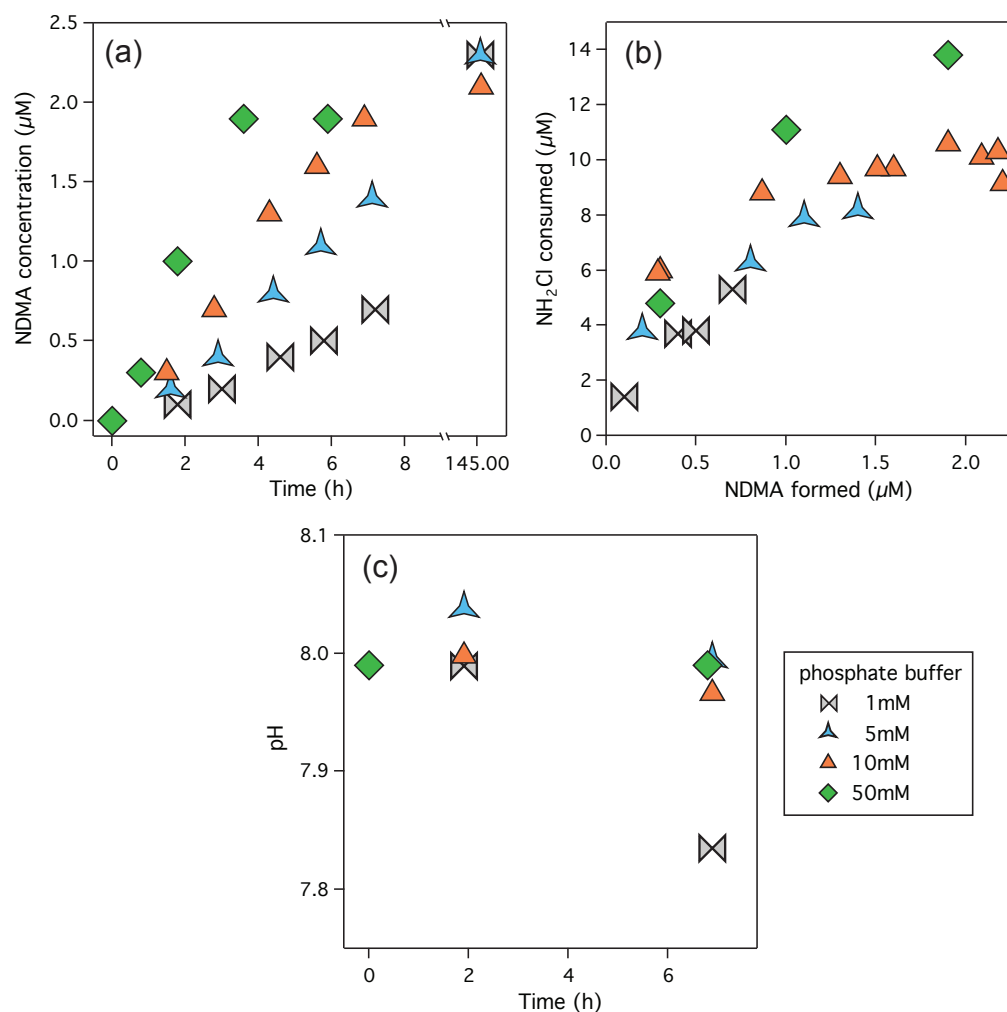


**Figure S4.6:** Reaction of DFUR (3  $\mu\text{M}$ ) with  $\text{NH}_2\text{Cl}$  (45  $\mu\text{M}$ ) in 1 mM, 5 mM, 10 mM, and 50 mM phosphate buffer at pH 8.0. Panel (a) shows NDMA formation over time, panel (b) depicts the concentration of consumed  $\text{NH}_2\text{Cl}$  versus formed NDMA concentration, and panel (c) shows the pH value during the chloramination reaction. The formation of NDMA was significantly accelerated with increasing phosphate buffer concentration, but the final NDMA yield was independent of the buffer concentration. Note that during the NDMA formation reaction, the pH value remained stable for all phosphate concentrations except that the pH significantly dropped when 1 mM phosphate buffer was used.



## S4.6.2 Buffer type

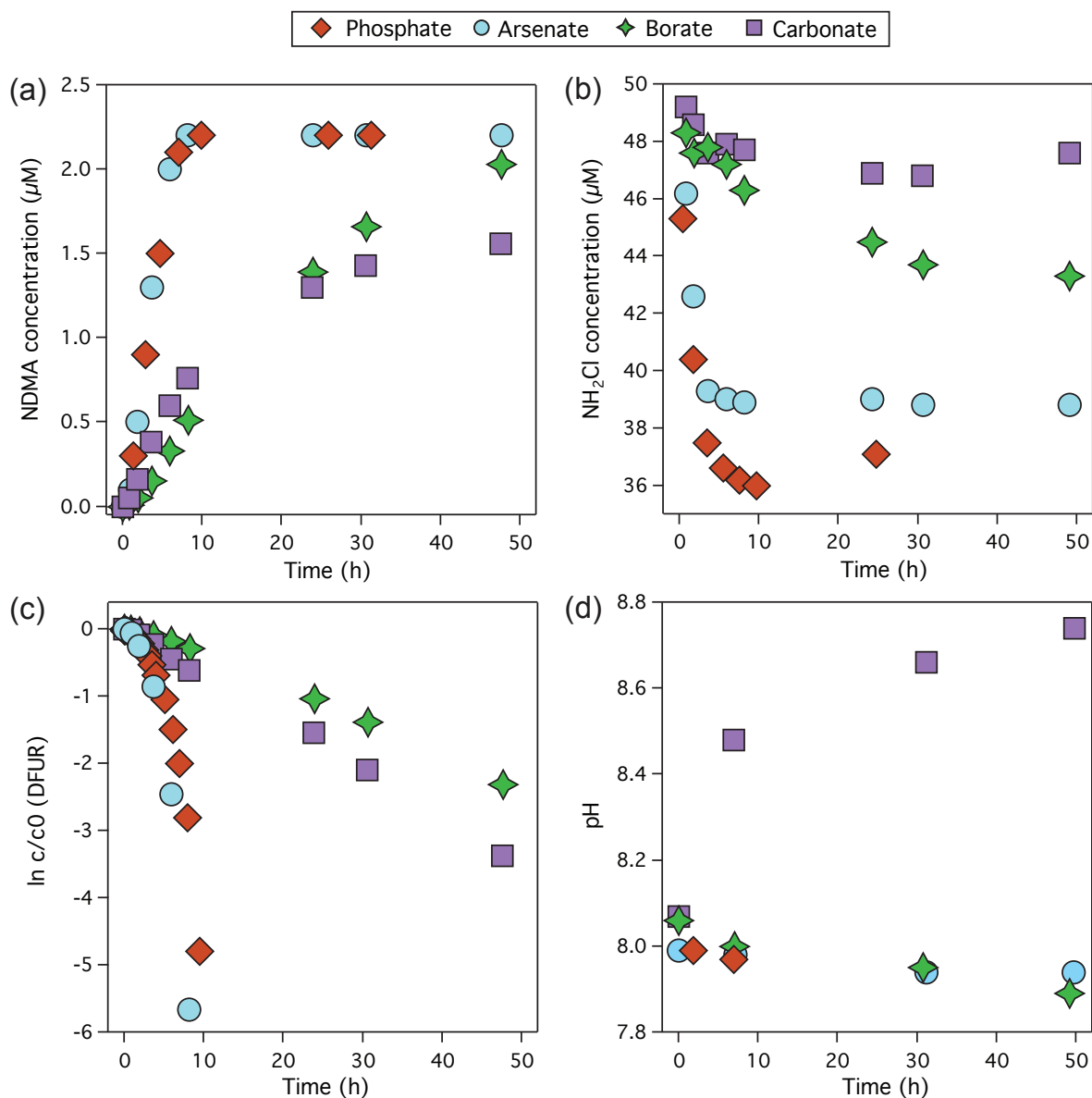


**Figure S4.7:** Reaction of DFUR (3  $\mu\text{M}$ ) with  $\text{NH}_2\text{Cl}$  (45  $\mu\text{M}$ ) in 10 mM phosphate, 10 mM arsenate, 10 mM borate, and 10 mM carbonate buffer at pH 8.0. Panel (a) shows the formation of NDMA, panel (b) the consumption of  $\text{NH}_2\text{Cl}$ , panel (c) the degradation of DFUR, and panel (d) the pH value over the time course of the reaction. Experiments in phosphate and arsenate buffer showed similar results in terms of NDMA formation, DFUR degradation, and  $\text{NH}_2\text{Cl}$  consumption. In contrast, results from experiments in borate buffer resembled those in carbonate buffer. The pH value of the carbonate buffer significantly increased during the chloramination reaction, while the pH remained widely stable when phosphate, arsenate, or borate were used.

### S4.6.3 Impact of buffer concentration and buffer type on N isotope fractionation in NDMA

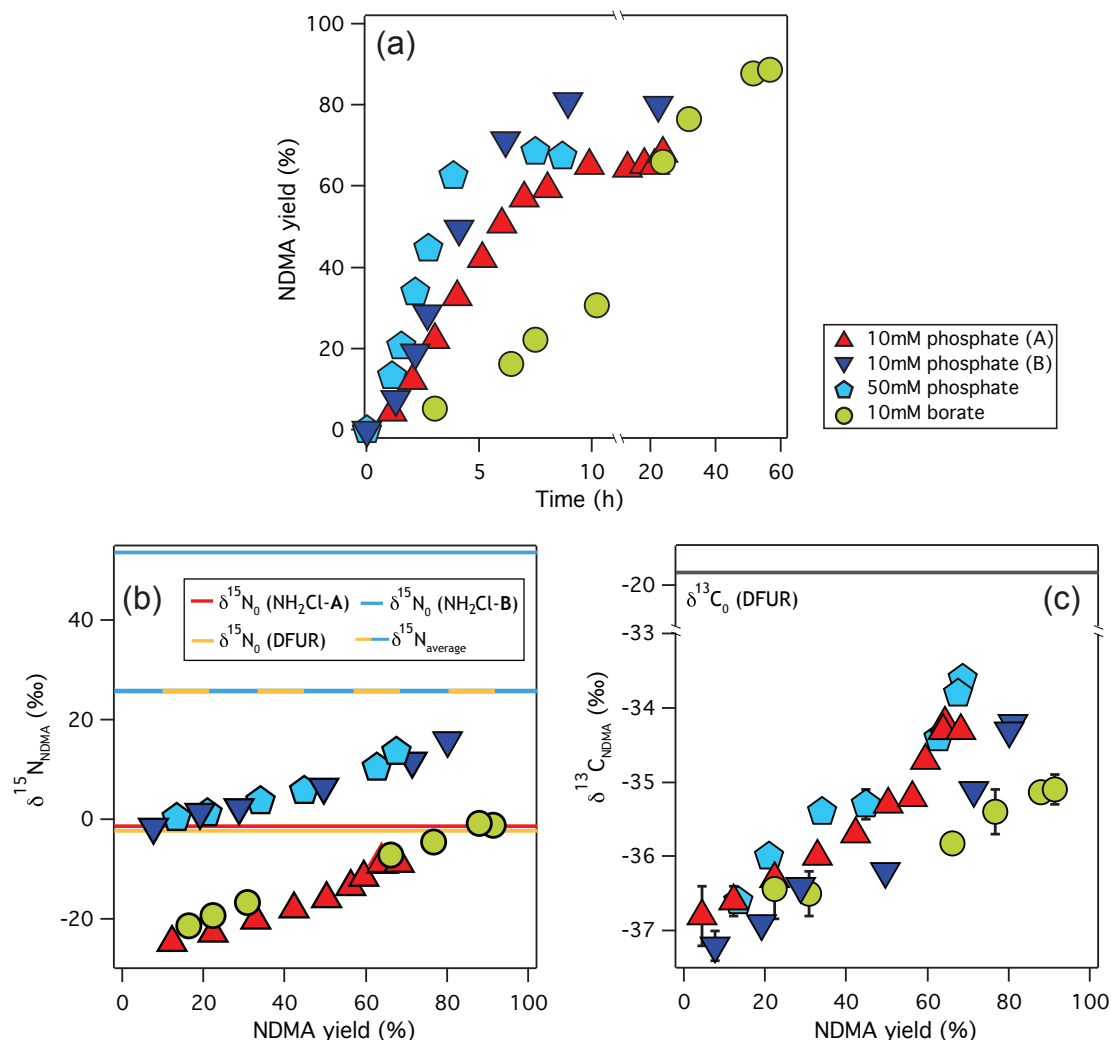


**Figure S4.8:** Panel (a) shows the NDMA yield in percent formed during the reaction of DFUR ( $3\ \mu\text{M}$ ) and  $\text{NH}_2\text{Cl}$  ( $45\ \mu\text{M}$ ) in 10 mM and 50 mM phosphate buffer and in 10 mM borate buffer at pH 8.0. Panels (b) and (c) show the corresponding  $\delta^{15}\text{N}$  and  $\delta^{13}\text{C}$  values of NDMA, respectively, versus the molar NDMA yield. Solid lines represent the initial isotope signatures of DFUR and  $\text{NH}_2\text{Cl}$ . Note that experiments in 10 mM phosphate buffer were conducted with  $\text{NH}_2\text{Cl-A}$  or  $\text{NH}_2\text{Cl-B}$  that had distinctly different initial  $\delta^{15}\text{N}$  values (red vs. blue line in panel b). The experiment in 10 mM borate buffer was only conducted with  $\text{NH}_2\text{Cl-A}$ , the one in 50 mM phosphate buffer only with  $\text{NH}_2\text{Cl-B}$  what explains the shift in absolute  $\delta^{15}\text{N}$  values of NDMA. The initial N isotope signature of  $\text{NH}_2\text{Cl}$  did not affect trends in N isotope signatures and  $\delta^{13}\text{C}$  values of NDMA.

## S4.7 Chloramination of 2-thiophenemethanol

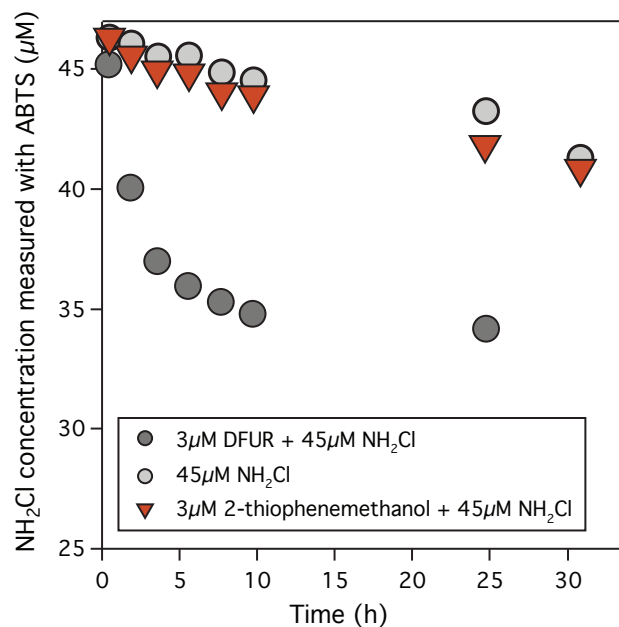


**Figure S4.9:**  $\text{NH}_2\text{Cl}$  concentration measured with the ABTS method over 30 h in three different batches containing (i)  $3\mu\text{M}$  DFUR and  $45\mu\text{M}$   $\text{NH}_2\text{Cl}$ , (ii)  $45\mu\text{M}$   $\text{NH}_2\text{Cl}$ , and (iii)  $3\mu\text{M}$  2-thiophenemethanol and  $45\mu\text{M}$   $\text{NH}_2\text{Cl}$  in 10 mM phosphate buffer at pH 8.0. Note that  $\text{NH}_2\text{Cl}$  concentrations were not corrected by the self-decay of chloramine observed in the  $\text{NH}_2\text{Cl}$  control.

## S4.8 pH-dependence of NDMA formation

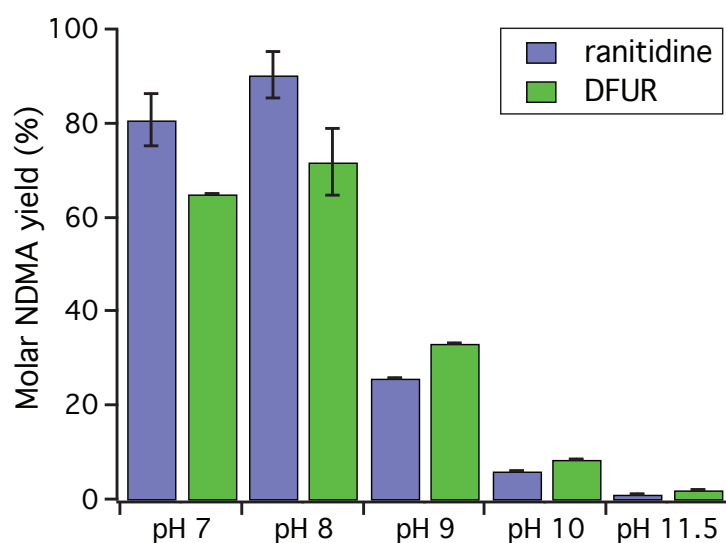


**Figure S4.10:** Influence of pH on the molar NDMA yield after 6 days from the reaction of ranitidine ( $3\ \mu\text{M}$ , blue) or DFUR ( $3\ \mu\text{M}$ , green) with  $\text{NH}_2\text{Cl}$  ( $45\ \mu\text{M}$ ). Experiments at pH 7, 8, and 11.5 were conducted in 10 mM phosphate buffer, while 10 mM carbonate buffer was used for experiments at pH 9 and 10.

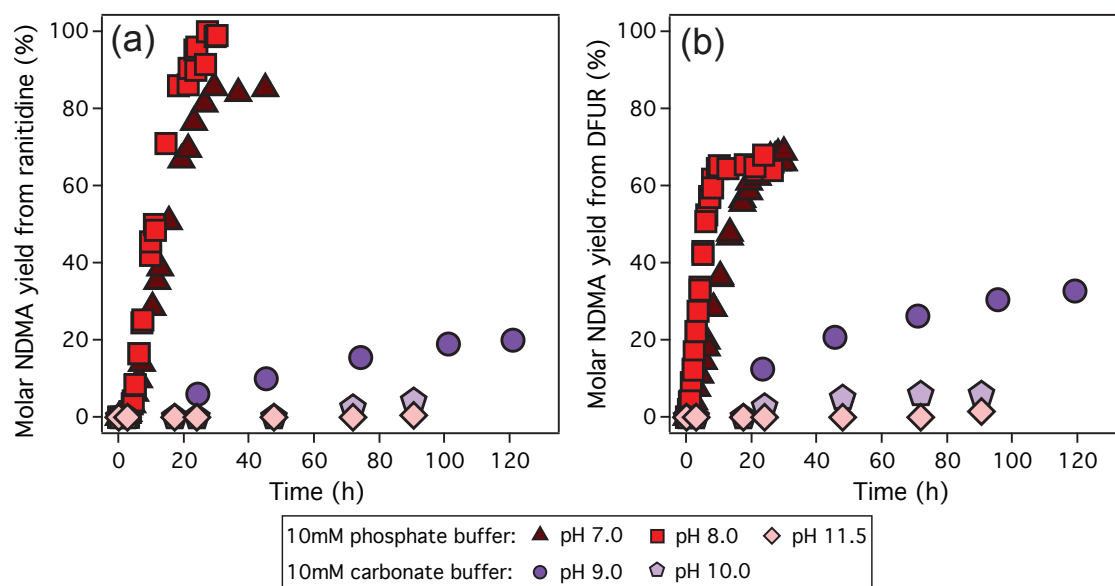


**Figure S4.11:** Influence of pH on the NDMA formation kinetics during chloramination ( $45\ \mu\text{M}$   $\text{NH}_2\text{Cl}$ ) of (a) ranitidine ( $3\ \mu\text{M}$ ) and (b) DFUR ( $3\ \mu\text{M}$ ). Experiments at pH 7, 8, and 11.5 were conducted in 10mM phosphate buffer, experiments at pH 9 and 10 in 10 mM carbonate buffer.

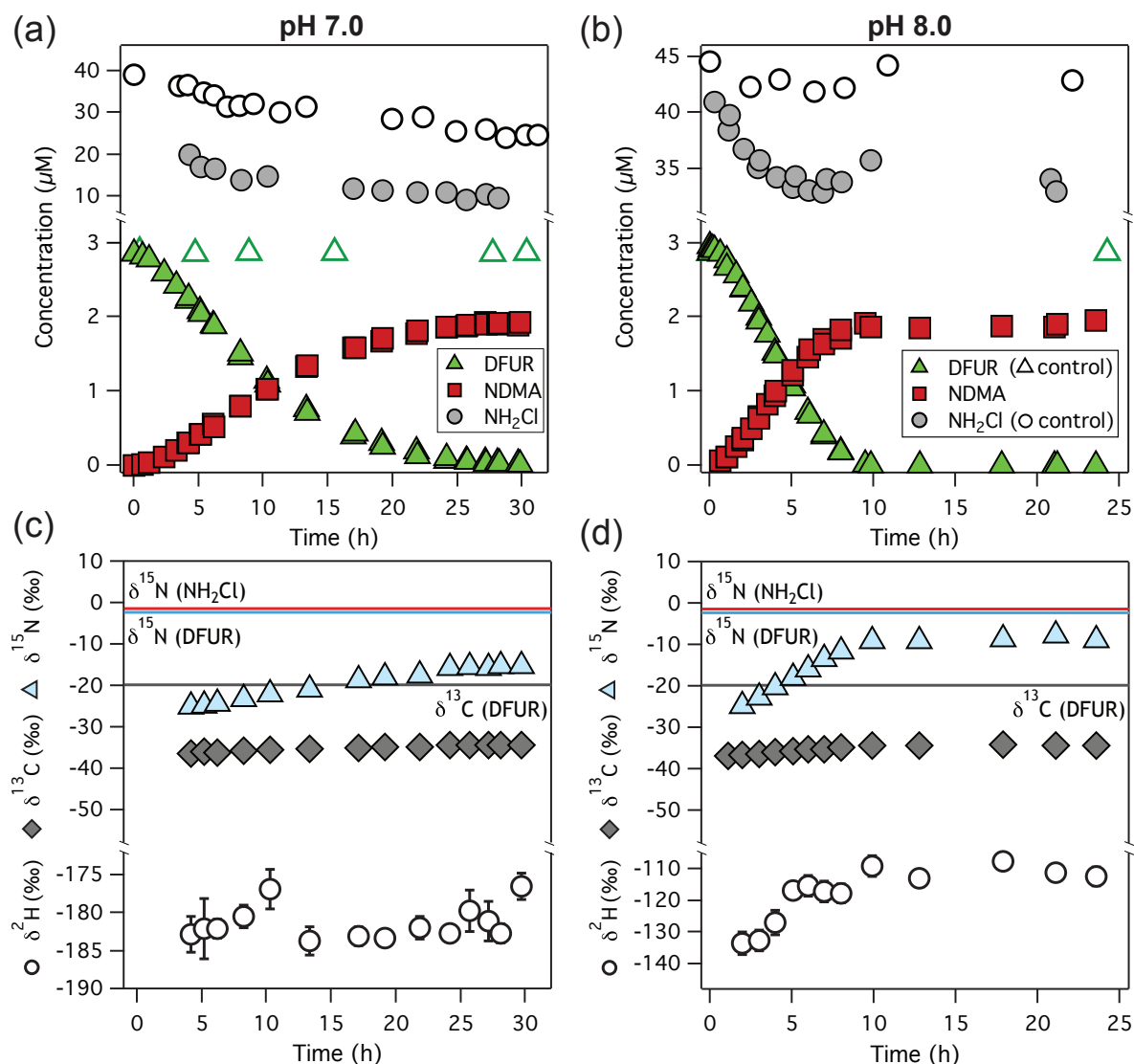


**Figure S4.12:** NDMA formation and corresponding C, H, and N isotope signatures of NDMA during the reaction of DFUR (3 μM) with NH<sub>2</sub>Cl (45 μM) at pH 7.0 and pH 8.0 in 10 mM phosphate buffer. Upper panels (a) and (b) show the kinetics of DFUR and NH<sub>2</sub>Cl degradation as well as NDMA formation at pH 7.0 and 8.0, respectively. Lower panels (c) and (d) show the corresponding δ<sup>13</sup>C, δ<sup>2</sup>H, and δ<sup>15</sup>N values of NDMA over time. Solid lines represent the initial C and N isotope signatures of the precursor compounds DFUR and NH<sub>2</sub>Cl. Note that we report the reference isotope signature of NH<sub>4</sub>Cl (Table S4.1) as proxy for the initial δ<sup>15</sup>N value of NH<sub>2</sub>Cl. Standard deviations of triplicate δ<sup>13</sup>C, δ<sup>2</sup>H, and δ<sup>15</sup>N measurements of NDMA were <0.4‰, <4.0‰, and <0.3‰, respectively, and mostly smaller than the depicted symbols.

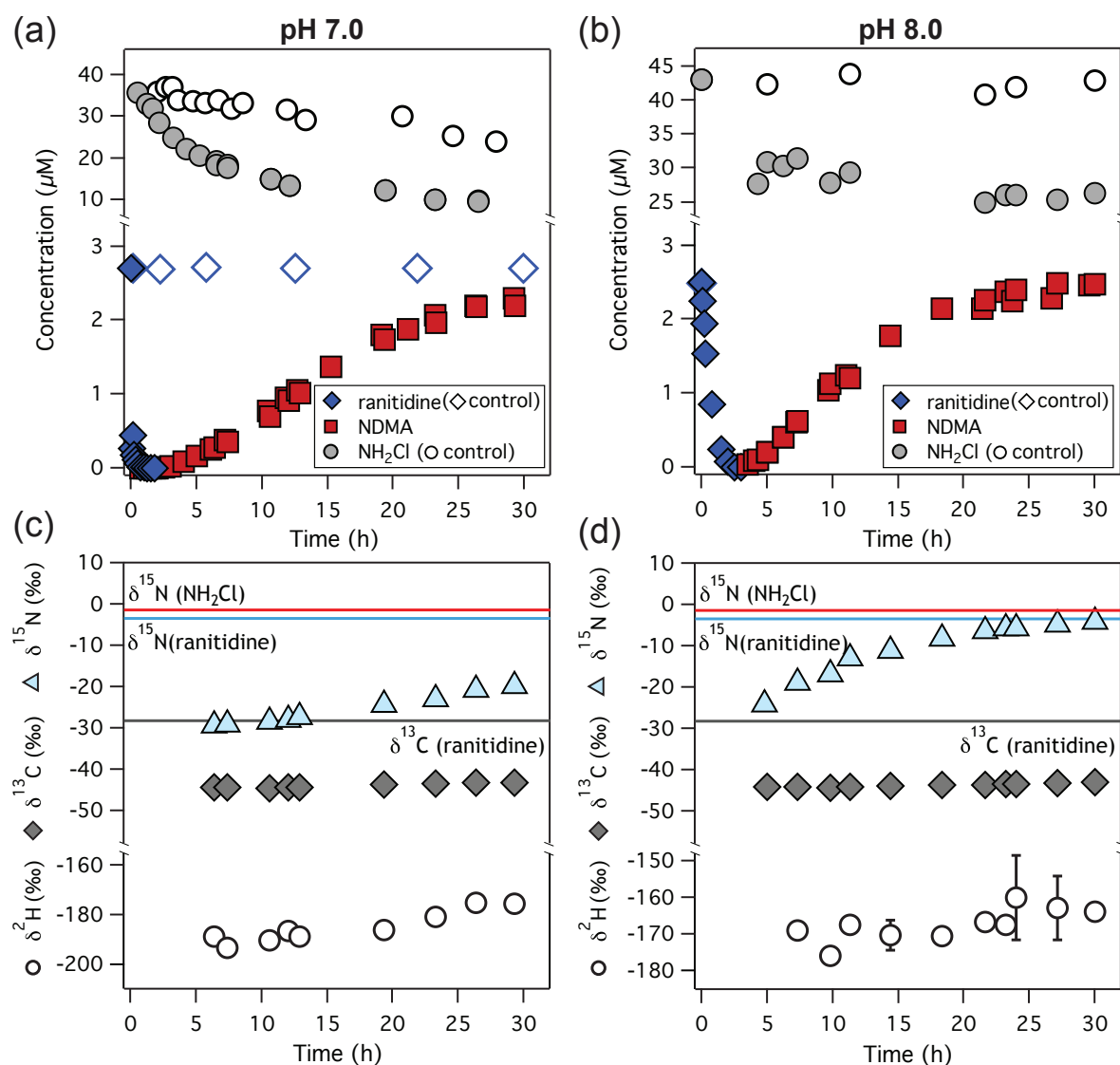


**Figure S4.13:** NDMA formation and corresponding C, H, and N isotope signatures of NDMA during the reaction of ranitidine ( $3\ \mu\text{M}$ ) with  $\text{NH}_2\text{Cl}$  ( $45\ \mu\text{M}$ ) at pH 7.0 and pH 8.0 in 10 mM phosphate buffer. Upper panels (a) and (b) show the kinetics of ranitidine and  $\text{NH}_2\text{Cl}$  degradation as well as NDMA formation at pH 7.0 and 8.0, respectively. Lower panels (c) and (d) show the corresponding  $\delta^{13}\text{C}$ ,  $\delta^2\text{H}$ , and  $\delta^{15}\text{N}$  values of NDMA over time. Solid lines represent the initial C and N isotope signatures of the precursor compounds ranitidine and  $\text{NH}_2\text{Cl}$ . Note that we report the reference isotope signature of  $\text{NH}_4\text{Cl}$  (Table S4.1) as proxy for the initial  $\delta^{15}\text{N}$  value of  $\text{NH}_2\text{Cl}$ . Standard deviations of triplicate  $\delta^{13}\text{C}$ ,  $\delta^2\text{H}$ , and  $\delta^{15}\text{N}$  measurements of NDMA were  $<0.3\text{‰}$ ,  $<11.5\text{‰}$ , and  $<0.5\text{‰}$ , respectively, and mostly smaller than the depicted symbols.

## S4.9 N isotope signatures versus NDMA yield

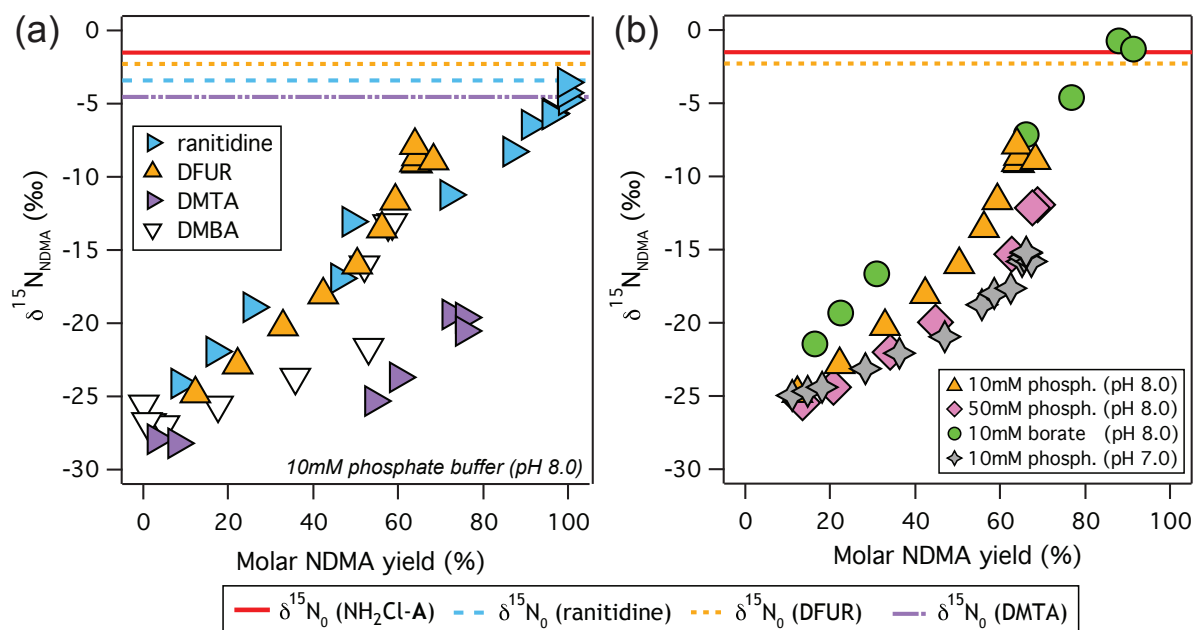


**Figure S4.14:**  $\delta^{15}\text{N}$  values of NDMA versus molar NDMA yield. Experiments were conducted (a) with different precursor compounds, namely ranitidine ( $3\ \mu\text{M}$ ), DFUR ( $3\ \mu\text{M}$ ), DMTA ( $40\ \mu\text{M}$ ), and DMBA ( $40\ \mu\text{M}$ ) with  $\text{NH}_2\text{Cl}$  which was added in 15-fold excess ( $45\ \mu\text{M}$  and  $600\ \mu\text{M}$ , respectively) in 10 mM phosphate buffer at pH 8.0 and (b) with DFUR ( $3\ \mu\text{M}$ ) and  $\text{NH}_2\text{Cl}$  ( $45\ \mu\text{M}$ ) using either 10 mM or 50 mM phosphate buffer at pH 8.0, 10 mM borate buffer at pH 8.0, or 10 mM phosphate buffer at pH 7.0. Solid lines represent initial  $\delta^{15}\text{N}$  values of the precursor compounds and  $\text{NH}_2\text{Cl}$ . Standard deviations of triplicate  $\delta^{15}\text{N}$  measurements were  $<0.6\text{‰}$  and smaller than the depicted symbols.





## Chapter 5

### Conclusions and Outlook

## 5.1 CSIA for investigating NDMA formation pathways

The findings presented in this study demonstrate that CSIA is a viable approach to (i) gain new insights into NDMA formation mechanisms and (ii) obtain proxies for NDMA formation pathways and reactive precursor moieties in form of stable isotope fractionation trends. In laboratory model systems, NDMA formation was studied during chloramination of secondary and tertiary amines, which have been previously identified as important NDMA precursor compounds.<sup>30</sup>

The presented results suggest that NDMA is formed in a complex multi-step process in which the reaction of dissolved  $O_2$  with radical intermediates plays an important role. C, H, and N isotope signatures of NDMA enabled a source apportionment of elements of NDMA, which revealed that the  $N(CH_3)_2$  group of NDMA stemmed from the organic amine while the N atom of the  $N=O$  moiety originated from chloramine. This finding is in agreement with the proposed nucleophilic substitution reaction of the deprotonated organic amine with chloramine as first reaction step. New insights into subsequent reaction steps involving dissolved  $O_2$  were obtained from oxygen isotope analysis of aqueous  $O_2$ , which was applied for the first time in the context of a DBP formation study. Changes in  $^{18}O/^{16}O$  ratios of  $O_2$  were indicative of a reaction of  $O_2$  with radicals, which was confirmed in experiments with radical scavengers. While the chemical structure and properties of radical intermediates remain to be identified, the presented results hint at NDMA formation via a *N*-peroxyl radical coupling mechanism. As shown previously by Shen and Andrews, water matrix components can significantly slow down NDMA formation during chloramination of the studied tertiary amines while only having a minor effect on the molar NDMA yield.<sup>124</sup> Future studies need to investigate the interactions of water matrix components such as natural organic matter with tertiary amines or reactive (radical) intermediates during chloramination.

The presented study further provides first evidence that isotope fractionation trends in NDMA reflect its formation pathway. N isotope ratios of NDMA changed towards more positive values during its formation from chloramination of four tertiary amines with similar molecular structure and high molar NDMA yields (>60%). While the reaction steps that caused this observed N isotope fractionation in NDMA could not be identified unequivocally due to the complex NDMA formation mechanism, linear trends in  $\delta^{15}N$  versus  $\delta^{13}C$  values of NDMA were characteristic for NDMA formation during chloramination of the selected tertiary amines (Figure 5.1).  $\delta^{15}N_{NDMA} / \delta^{13}C_{NDMA}$ -slopes

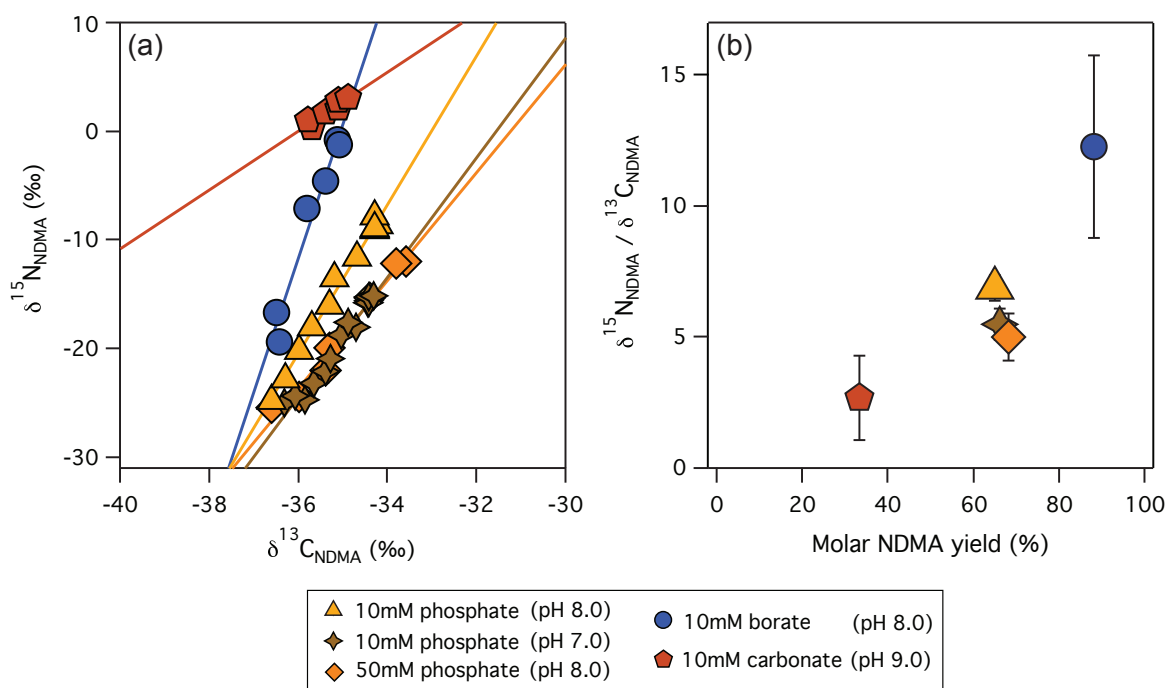


**Figure 5.1:** (a)  $\delta^{15}\text{N}$  versus  $\delta^{13}\text{C}$  values of NDMA formed during the reaction of DFUR ( $3\ \mu\text{M}$ ) with  $\text{NH}_2\text{Cl}$  ( $45\ \mu\text{M}$ ) under the specified reaction conditions. Solid lines represent linear regressions. (b)  $\delta^{15}\text{N}_{\text{NDMA}} / \delta^{13}\text{C}_{\text{NDMA}}$ -slopes versus the molar NDMA yield from DFUR. Experiments were conducted in 10 mM phosphate buffer (pH 7.0 and 8.0), 50 mM phosphate buffer (pH 8.0), 10 mM borate buffer (pH 8.0), and 10 mM carbonate buffer (pH 9.0).

did not show significant changes when chloramination conditions were varied and might thus serve as proxy for NDMA formation from this important class of precursors. This dissertation paves the way for future studies that need to address the question of whether isotope fractionation trends in NDMA are (i) robust under (varying) conditions encountered in water treatment, (ii) specific fingerprints for NDMA precursor compounds, and (iii) instrumental in identifying NDMA precursors in natural waters.

## 5.2 Potential variability of isotope fractionation trends in NDMA

As highlighted in Chapter 4, isotope fractionation trends in NDMA were robust even under differing experimental conditions. Figure 5.1 shows that  $\delta^{15}\text{N}_{\text{NDMA}} / \delta^{13}\text{C}_{\text{NDMA}}$ -slopes were in the same range (between  $5.0 \pm 0.9$  and  $6.9 \pm 0.5$ ) when NDMA was formed during chloramination of DFUR in 10 mM vs. 50 mM phosphate buffer and at pH

7.0 vs. 8.0. This observation demonstrates that NDMA was formed via the same reaction mechanism even though reaction kinetics varied. However, the additional data presented in Figure 5.1 are a first indication that observable isotope fractionation trends can vary depending on the chloramination conditions. In 10 mM borate buffer at pH 8.0, DFUR was very efficiently converted to NDMA (88% molar NDMA yield) and a bigger  $\delta^{15}\text{N}_{\text{NDMA}} / \delta^{13}\text{C}_{\text{NDMA}}$ -slope of  $12.3 \pm 3.5$  was obtained. This value is, however, still in the same range than the slope observed during chloramination of ranitidine ( $13.3 \pm 5.0$ ). In contrast, a significantly smaller slope of  $2.7 \pm 1.6$  was found in 10 mM carbonate buffer at pH 9.0, where only 33% of the initial DFUR concentration was converted to NDMA. These data suggest a correlation between  $\delta^{15}\text{N}_{\text{NDMA}} / \delta^{13}\text{C}_{\text{NDMA}}$ -slopes and the molar NDMA yield (Figure 5.1b). This finding indicates that competing reactions leading to products other than NDMA were likely isotope-sensitive and thus influenced the isotopic composition of NDMA. Such isotope-sensitive side reactions can also explain changes in the initial N isotope signature of NDMA as depicted in Figure 5.1a. While NDMA formed in phosphate and borate buffer was depleted in  $^{15}\text{N}$  at the beginning of the reaction ( $\delta^{15}\text{N}_{\text{ini}} \approx -20$  to  $-25\text{‰}$ ), NDMA was approximately  $+20\text{‰}$  more enriched in  $^{15}\text{N}$  when formed in 10 mM carbonate buffer at pH 9.0 ( $\delta^{15}\text{N}_{\text{ini}} = 0.3\text{‰}$ ). This observation suggests that unidentified reaction products, which were potentially formed from the reaction of carbonate with radical intermediates, were enriched in  $^{14}\text{N}$  leading to  $^{15}\text{N}$ -enriched NDMA. While these preliminary data are a first indication for the potential variability of isotope fractionation trends, further research is needed to systematically study (i) the extent to which  $\delta^{15}\text{N}_{\text{NDMA}} / \delta^{13}\text{C}_{\text{NDMA}}$ -slopes vary during chloramination of selected model precursors, (ii) the factors influencing the variability of N isotope fractionation trends (e.g., pH, buffer catalysis, competing parallel reactions), and (iii) the potential of using  $\delta^{15}\text{N}_{\text{NDMA}} / \delta^{13}\text{C}_{\text{NDMA}}$ -slopes as proxy for NDMA formation from specific precursors under varying conditions encountered in water treatment.

### 5.3 Isotope fractionation trends as fingerprints for NDMA formation pathways and precursors

Based on the current knowledge, NDMA formation pathways can be distinctly different depending on the chemical disinfectant used and the NDMA precursor compounds present in source waters.<sup>30</sup> Even though most NDMA formation pathways have not yet been fully explored, it is likely that differing reaction mechanisms are associated with

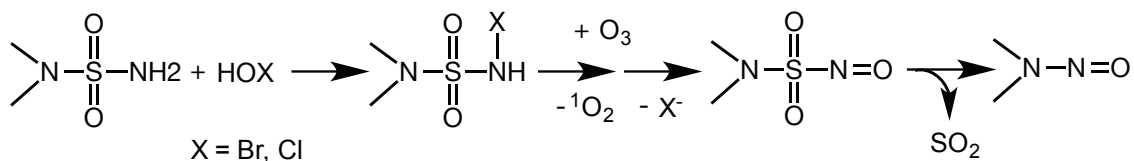


**Figure 5.2:** Simplified reaction mechanism for the hypohalous acid (HOX) assisted formation of NDMA during ozonation of  $N,N$ -dimethylsulfamide (DMS).<sup>54</sup>

different kinetic isotope effects, because different chemical bonds are broken or formed. Changes in the isotopic composition of NDMA might thus reflect differing NDMA formation pathways and could be used as fingerprints for NDMA precursor compounds or functional groups therein.

The data presented in Chapter 4 demonstrate that trends in correlated  $\delta^{15}N$  and  $\delta^{13}C$  values of NDMA are indeed characteristic for chloramination of the selected class of tertiary amines. To investigate whether differing NDMA formation pathways cause unique fingerprints in the form of isotope fractionation trends, the presented SPE-GC/IRMS method (Chapter 2) should be applied to systematically study C, H, and N isotope ratios of NDMA formed from various precursor materials and disinfection / oxidation conditions in laboratory model systems. In particular, ozonation of  $N,N$ -dimethylsulfamide (DMS), which is a transformation product of the fungicide tolylfluanide, will be interesting to investigate. Similar to the tertiary amines selected in the presented study, DMS is efficiently converted to NDMA with molar NDMA yields up to >50%.<sup>41,54</sup> However, the NDMA formation pathway from DMS is distinctly different from the one proposed for tertiary amines in that no hydrazine-like intermediates are formed (Figure 5.2). Instead, DMS is transformed in a hypohalous acid assisted ozonation reaction to a nitrosodimethylsulfamide which undergoes an intramolecular rearrangement to form NDMA and  $SO_2$ .<sup>54</sup> Similar to NDMA formation from the studied tertiary amines, fractionation is expected to be strongest in N isotopes, because N atoms are directly involved in the formation of the N-N bond and the nitroso-moiety of NDMA. However, owing to different chemical reactions leading to NDMA formation, N isotope ratios in NDMA formed during ozonation of DMS might change in a distinctly different manner compared to chloramination of tertiary amines.

Future studies should also focus on chloramination of differing amine-containing NDMA precursors including dimethylamine, micropollutants containing tertiary-amine functional groups and quaternary amine-based water treatment polymers.<sup>72,78</sup> Trends in  $\delta^{15}N$  versus  $\delta^{13}C$  values of NDMA obtained in these reactions could reveal (i) whether

NDMA is formed via the same reaction mechanism including, for example, dimethylamine as a common intermediate and (ii) whether differing amine-containing precursors in natural waters can be distinguished based on characteristic isotope fractionation trends. The results presented in Chapter 3 indicate that NDMA formation from secondary and tertiary amines proceeds via the same reaction mechanism especially concerning the reaction of dissolved oxygen with reactive intermediates. However, molar NDMA yields from the selected precursors varied between 1.4% and 90%. It remains to be studied whether isotope fractionation trends in NDMA formed from secondary and tertiary amines with low molar NDMA yield match those observed from the studied tertiary amines with high molar NDMA yield (Figure 5.1). In this case, isotope fractionation trends would confirm a common reaction pathway and can serve as proxy for the class of amine-containing precursors. It could then be evaluated whether such a common fingerprint of amine-containing precursors differs from the fingerprint of e.g., organic matter-derived NDMA precursors. Such differing isotopic fingerprints would be an important prerequisite to distinguish and identify different classes of precursors in natural waters.

## 5.4 Roadmap for the application of CSIA to identify NDMA precursors in natural waters

To enable the identification of NDMA precursor compounds in real water samples, a repository of isotope fractionation trends needs to be compiled from systematic studies of NDMA formation from various precursors and disinfection / oxidation scenarios in laboratory model systems. In a next step, source waters used for drinking water production should be spiked with selected NDMA precursors prior to disinfection to investigate whether water matrix components affect isotope fractionation trends in NDMA pertinent to specific NDMA formation pathways. For example, groundwater or lake water samples could be spiked with ranitidine prior to the addition of pre-formed chloramine. Trends in correlated  $\delta^{15}\text{N}$  and  $\delta^{13}\text{C}$  values of NDMA can then be compared to those identified in laboratory experiments (Chapter 4) to assess the effects of natural organic matter or other water matrix components on the NDMA formation mechanism and the resulting isotope fractionation in NDMA. Finally, CSIA can be applied to identify relevant NDMA precursors in natural waters. The comparison of C and N isotope fractionation trends in NDMA formed during disinfection of source water samples with those obtained in laboratory model systems might provide a reaction-related characterization

of functional groups responsible for NDMA formation in the source waters. Following this precursor identification, appropriate precursor abatement strategies such as pre-oxidation with ozone or adsorption on activated carbon can be implemented to mitigate NDMA formation.<sup>68,159,212</sup>

However, one major challenge that needs to be overcome towards the application of CSIA in drinking water is the selective enrichment of NDMA to concentrations of  $\geq 45 \text{ mg L}^{-1}$  required for accurate stable isotope analysis. As described in Chapter 2, the newly developed GC/IRMS method is coupled to solid-phase extraction, which enables a 1000-fold enrichment of NDMA.<sup>162</sup> Accurate C, H, and N isotope analysis thus works for aqueous samples containing  $\geq 45 \mu\text{g L}^{-1}$  NDMA which is approximately 1000-fold above typical NDMA drinking water guideline values. Substantial amounts of drinking water would have to be processed, which is only feasible by the development of automated SPE-procedures. To selectively enrich NDMA from natural water matrices, molecularly imprinted polymers (MIP) might be used in addition to the proposed SPE procedure. MIPs have been recently developed for NDMA and other *N*-nitrosamines, but have not yet been employed as sample clean-up method coupled to GC/IRMS analysis.<sup>228,229</sup> In the future, CSIA could also be applied to a broader range of potentially harmful DBPs. Here, the focus should be set on investigating formation pathways and precursors of unregulated and highly genotoxic iodinated DBPs such as iodoacetic acid or iodoacetamide.<sup>10,230,231</sup>





# Bibliography

- [1] Cutler, D., Miller, G., The role of public health improvements in health advances: The twentieth-century United States, *Demography*, **2005**, 42, 1–22.
- [2] Crittenden, J. C., Trussell, R. R., Hand, D. W., Howe, K. J., Tchobanoglous, G., *MWHs Water Treatment: Principles and Design, Third Edition*, John Wiley & Sons Inc., **2012**.
- [3] Xie, Y., *Disinfection By-Products in Drinking Water: Formation, Analysis, and Control*, Lewis Publishers, CRC Press, Taylor & Francis Group, **2004**.
- [4] Richardson, S. D., Postigo, C., Drinking water disinfection by-products, in *Emerging Organic Contaminants and Human Health*, Barceló, D., ed., Springer Berlin Heidelberg, **2012**, 93–137.
- [5] Sedlak, D. L., von Gunten, U., The chlorine dilemma, *Science*, **2011**, 331, 42–43.
- [6] Krasner, S. W., The formation and control of emerging disinfection by-products of health concern, *Phil. Trans. R. Soc. A*, **2009**, 367, 4077–4095.
- [7] Rook, J. J., Haloforms in drinking water, *J. Am. Water Works Ass.*, **1976**, 68, 168–172.
- [8] Rook, J. J., Formation of haloforms during chlorination of natural waters, *J. Water Treat. Exam.*, **1974**, 23, 234–243.
- [9] Nieuwenhuijsen, M. J., Toledano, M. B., Eaton, N. E., Fawell, J., Elliott, P., Chlorination disinfection byproducts in water and their association with adverse reproductive outcomes: A review, *Occup. Environ. Med.*, **2000**, 57, 73–85.
- [10] Richardson, S. D., Plewa, M. J., Wagner, E. D., Schoeny, R., DeMarini, D. M., Occurrence, genotoxicity, and carcinogenicity of regulated and emerging disinfection by-products in drinking water: A review and roadmap for research, *Mutat. Res.*, **2007**, 636, 178–242.
- [11] Villanueva, C. M., Cantor, K. P., Grimalt, J. O., Malats, N., Silverman, D., Tardon, A., Garcia-Closas, R., Serra, C., Carrato, A., Castaño Vinyals, G., Marcos, R., Rothman, N., Real, F. X., Dosemeci, M., Kogevinas, M., Bladder cancer and exposure to water disinfection by-products through ingestion, bathing, showering, and swimming in pools, *Am. J. Epidemiol.*, **2007**, 165, 148–156.

- [12] Karanfil, T., Krasner, W., Stuart, Westerhoff, P., Xie, Y., Recent advances in disinfection by-product formation, occurrence, control, health effects, and regulations, in *Disinfection By-Products in Drinking Water*, Karanfil, T., Krasner, S. W., Westerhoff, P., Xie, Y., eds., chap. 1, American Chemical Society: Washington, DC, **2008**, 2–19.
- [13] Roberson, A., J., The evolution of disinfection by-products regulations: Past, present, and future, in *Disinfection By-Products in Drinking Water*, Karanfil, T., Krasner, S. W., Westerhoff, P., Xie, Y., eds., chap. 2, American Chemical Society: Washington, DC, **2008**, 22–35.
- [14] Camel, V., Bermond, A., The use of ozone and associated oxidation processes in drinking water treatment, *Water Res.*, **1998**, 32, 3208–3222.
- [15] von Gunten, U., Ozonation of drinking water: Part I. Oxidation kinetics and product formation, *Water Res.*, **2003**, 37, 1443–1467.
- [16] Mestankova, H., Parker, A. M., Bramaz, N., Canonica, S., Schirmer, K., von Gunten, U., Linden, K. G., Transformation of Contaminant Candidate List (CCL3) compounds during ozonation and advanced oxidation processes in drinking water: Assessment of biological effects, *Water Res.*, **2016**, 93, 110–120.
- [17] Hua, G., Reckhow, D. A., Comparison of disinfection byproduct formation from chlorine and alternative disinfectants, *Water Res.*, **2007**, 41, 1667–1678.
- [18] von Gunten, U., Ozonation of drinking water: Part II. Disinfection and by-product formation in presence of bromide, iodide or chlorine, *Water Res.*, **2003**, 37, 1469–1487.
- [19] Richardson, S. D., Thruston, A. D., Caughran, T. V., Chen, P. H., Collette, T. W., Schenck, K. M., Lykins, B. W., Rav-Acha, C., Glezer, V., Identification of new drinking water disinfection by-products from ozone, chlorine dioxide, chloramine, and chlorine, in *Environmental Challenges*, Belkin, S., ed., Springer Netherlands, **2000**, 95–102.
- [20] Pan, Y., Li, W., An, H., Cui, H., Wang, Y., Formation and occurrence of new polar iodinated disinfection byproducts in drinking water, *Chemosphere*, **2016**, 144, 2312–2320.
- [21] Pan, Y., Li, W., Li, A., Zhou, Q., Shi, P., Wang, Y., A new group of disinfection byproducts in drinking water: Trihalo-hydroxy-cyclopentene-diones, *Environ. Sci. Technol.*, **2016**, 50, 7344–7352.
- [22] Richardson, S. D., Postigo, C., Discovery of new emerging DBPs by high-resolution mass spectrometry, in *Applications of Time-of-Flight and Orbitrap Mass Spectrometry in Environmental, Food, Doping, and Forensic Analysis*, Pérez, S., Eichhorn, P., Barceló, D., eds., vol. 71, Elsevier, **2016**, 335–356.

- 
- [23] Plewa, M. J., Wagner, E. D., Richardson, S. D., Thruston Jr., A. D., Woo, Y.-T., McKague, A. B., Chemical and biological characterization of newly discovered iodoacid drinking water disinfection byproducts, *Environ. Sci. Technol.*, **2004**, 38, 4713–4722.
- [24] Muellner, M. G., Wagner, E. D., McCalla, K., Richardson, S. D., Woo, Y.-T., Plewa, M. J., Haloacetonitriles vs. regulated haloacetic acids: Are nitrogen-containing DBPs more toxic?, *Environ. Sci. Technol.*, **2007**, 41, 645–651.
- [25] Plewa, M. J., Wagner, E. D., Muellner, M. G., Hsu, K.-M., Richardson, S. D., Comparative mammalian cell toxicity of N-DBPs and C-DBPs, in *Disinfection By-Products in Drinking Water*, Karanfil, T., Krasner, S. W., Westerhoff, P., Xie, Y., eds., chap. 3, American Chemical Society: Washington, DC, **2008**, 36–50.
- [26] Stalter, D., O'Malley, E., von Gunten, U., Escher, B. I., Fingerprinting the reactive toxicity pathways of 50 drinking water disinfection by-products, *Water Res.*, **2016**, 91, 19–30.
- [27] Yang, X., Fan, C., Shang, C., Zhao, Q., Nitrogenous disinfection byproducts formation and nitrogen origin exploration during chloramination of nitrogenous organic compounds, *Water Res.*, **2010**, 44, 2691–2702.
- [28] Bond, T., Templeton, M. R., Graham, N., Precursors of nitrogenous disinfection by-products in drinking water - A critical review and analysis, *J. Hazard. Mater.*, **2012**, 235-236, 1–16.
- [29] Zeng, T., Plewa, M. J., Mitch, W. A., *N*-nitrosamines and halogenated disinfection byproducts in U.S. full advanced treatment trains for potable reuse, *Water Res.*, **2016**, 101, 176–186.
- [30] Shah, A. D., Mitch, W. A., Halonitroalkanes, halonitriles, haloamides, and *N*-nitrosamines: A critical review of nitrogenous disinfection byproduct formation pathways, *Environ. Sci. Technol.*, **2012**, 46, 119–131.
- [31] Charrois, J. W. A., Boyd, J. M., Froese, K. L., Hrudey, S. E., Occurrence of *N*-nitrosamines in Alberta public drinking-water distribution systems, *J. Environ. Eng. Sci.*, **2007**, 6, 103–114.
- [32] Sacher, F., Schmidt, C., Lee, C., von Gunten, U., *Strategies for Minimizing Nitrosamine Formation During Disinfection*, AWWA Research Foundation, Denver, CO, **2008**.
- [33] United States Environmental Protection Agency (U.S. EPA). Occurrence Data for the Unregulated Contaminant Monitoring Rule - UCMR 2 (2008-2010), <https://www.epa.gov/dwucmr/occurrence-data-unregulated-contaminant-monitoring-rule> (accessed June 28, 2016).

- [34] Leavey-Roback, S. L., Sugar, C. A., Krasner, S. W., Suffet, I. H. M., NDMA formation during drinking water treatment: A multivariate analysis of factors influencing formation, *Water Res.*, **2016**, 95, 300–309.
- [35] Wagner, E. D., Hsu, K.-M., Lagunas, A., Mitch, W. A., Plewa, M. J., Comparative genotoxicity of nitrosamine drinking water disinfection byproducts in salmonella and mammalian cells, *Mutat. Res.*, **2012**, 741, 109–115.
- [36] World Health Organization (WHO), International Agency for Research On Cancer. IARC Monographs on the Evaluation of Carcinogenic Risks to Humans. Volume 1 Some Inorganic Substances, Chlorinated Hydrocarbons, Aromatic Amines, *N*-Nitroso Compounds and Natural Products., <http://monographs.iarc.fr/ENG/Monographs/vol1-42/mono1.pdf> (accessed June 28, 2016).
- [37] United States Environmental Protection Agency (U.S. EPA). Office of Research and Development (ORD), National Center for Environmental Assessment. Integrated Risk Information System (IRIS). Technical Fact Sheet *N*-Nitrosodimethylamine, [www.epa.gov/fedfac/technical-fact-sheet-n-nitrosodimethylamine-ndma](http://www.epa.gov/fedfac/technical-fact-sheet-n-nitrosodimethylamine-ndma) (accessed June 28, 2016).
- [38] Jobb, D., Hunsinger, R., Meresz, O., Taguchi, V., Removal of *N*-nitrosodimethylamine from the Oshweken (six nations) water supply. Final report, *Ontario Ministry of Environment and Energy*, **1994**.
- [39] Schäfer, A. I., Mitch, W., Walewijk, S., Munoz, A., Teuten, E., Reinhard, M., Micropollutants in water recycling: A case study of *N*-nitrosodimethylamine (NDMA) exposure from water versus food, in *Sustainable Water for the Future: Water Recycling versus Desalination*, Escobar, I. C., Schäfer, A. I., eds., vol. 2, Elsevier, **2010**, 203–228.
- [40] Najm, I., Trussell, R. R., NDMA formation in water and wastewater, *J. Am. Water Works Ass.*, **2001**, 2, 92–99.
- [41] Schmidt, C. K., Brauch, H.-J., *N,N*-Dimethylsulfamide as precursor for *N*-nitrosodimethylamine (NDMA) formation upon ozonation and its fate during drinking water treatment, *Environ. Sci. Technol.*, **2008**, 42, 6340–6346.
- [42] Spiegelhalder, B., Preussmann, R., Contamination of toiletries and cosmetic products with volatile and nonvolatile *N*-nitroso carcinogens, *J. Cancer Res. Clin. Oncol.*, **1984**, 108, 160–163.
- [43] Mitch, W. A., Sharp, J. O., Trussell, R. R., Valentine, R. L., Alvarez-Cohen, L., Sedlak, D. L., *N*-nitrosodimethylamine (NDMA) as a drinking water contaminant: A review, *Environ. Eng. Sci.*, **2003**, 20, 389–404.
- [44] Mitch, W. A., Sedlak, D. L., Formation of *N*-nitrosodimethylamine (NDMA) from dimethylamine during chlorination, *Environ. Sci. Technol.*, **2002**, 36, 588–595.

- 
- [45] Andrzejewski, P., Kasprzyk-Hordern, B., Nawrocki, J., *N*-nitrosodimethylamine (NDMA) formation during ozonation of dimethylamine-containing waters, *Water Res.*, **2008**, 42, 863–870.
- [46] Zhao, Y. Y., Boyd, J. M., Woodbeck, M., Andrews, R., Hrudey, S., Li, X.-F., Analysis of *N*-nitrosamines formed in various source waters treated with eleven disinfection processes, in *Disinfection By-Products in Drinking Water*, Karanfil, T., Krasner, S. W., Westerhoff, P., Xie, Y., eds., chap. 20, American Chemical Society: Washington, DC, **2008**, 289–303.
- [47] Planas, C., Palacios, O., Ventura, F., Rivera, J., Caixach, J., Analysis of nitrosamines in water by automated SPE and isotope dilution GC/HRMS. Occurrence in the different steps of a drinking water treatment plant, and in chlorinated samples from a reservoir and a sewage treatment plant effluent., *Talanta*, **2008**, 76, 906–913.
- [48] Australian Government. National Health and Medical Research Council. Australian Drinking Water Guidelines 6, 2011, <https://www.nhmrc.gov.au/guidelines-publications/eh52>.
- [49] World Health Organization (WHO). *N*-Nitrosodimethylamine in Drinking-water. Background Document for Development of WHO Guidelines for Drinking-water Quality, [http://www.who.int/water\\_sanitation\\_health/dwq/chemicals/ndma/en/](http://www.who.int/water_sanitation_health/dwq/chemicals/ndma/en/) (accessed June 28, 2016).
- [50] Krasner, S. W., Mitch, W. A., McCurry, D. L., Hanigan, D., Westerhoff, P., Formation, precursors, control, and occurrence of nitrosamines in drinking water: A review, *Water Res.*, **2013**, 47, 4433–4450.
- [51] Plumlee, M. H., López-Mesas, M., Heidlberger, A., Ishida, K. P., Reinhard, M., *N*-nitrosodimethylamine (NDMA) removal by reverse osmosis and UV treatment and analysis via LC/MSMS, *Water Res.*, **2008**, 42, 347–355.
- [52] Lee, C., Choi, W., Yoon, J., UV photolytic mechanism of *N*-nitrosodimethylamine in water: Roles of dissolved oxygen and solution pH, *Environ. Sci. Technol.*, **2005**, 39, 9702–9709.
- [53] Gan, W., Bond, T., Yang, X., Westerhoff, P., Role of chlorine dioxide in *N*-nitrosodimethylamine formation from oxidation of model amines, *Environ. Sci. Technol.*, **2015**, 49, 11429–11437.
- [54] von Gunten, U., Salhi, E., Schmidt, C. K., Arnold, W. A., Kinetics and mechanisms of *N*-nitrosodimethylamine formation upon ozonation of *N,N*-dimethylsulfamide-containing waters: Bromide catalysis, *Environ. Sci. Technol.*, **2010**, 44, 5762–5768.

- [55] Mitch, W. A., Sedlak, D. L., Characterization and fate of *N*-nitrosodimethylamine precursors in municipal wastewater treatment plants, *Environ. Sci. Technol.*, **2004**, 38, 1445–1454.
- [56] Choi, J., Valentine, R. L., *N*-nitrosodimethylamine formation by free-chlorine-enhanced nitrosation of dimethylamine, *Environ. Sci. Technol.*, **2003**, 37, 4871–4876.
- [57] Yang, L., Chen, Z., Shen, J., Xu, Z., Liang, H., Tian, J., Ben, Y., Zhai, X., Shi, W., Li, G., Reinvestigation of the nitrosamine-formation mechanism during ozonation, *Environ. Sci. Technol.*, **2009**, 43, 5481–5487.
- [58] Schreiber, I. M., Mitch, W. A., Nitrosamine formation pathway revisited: The importance of chloramine speciation and dissolved oxygen, *Environ. Sci. Technol.*, **2006**, 40, 6007–6014.
- [59] Choi, J., Duirk, S. E., Valentine, R. L., Mechanistic studies of *N*-nitrosodimethylamine (NDMA) formation in chlorinated drinking water, *J. Environ. Monit.*, **2002**, 4, 249–252.
- [60] Andrzejewski, P., Nawrocki, J., *N*-nitrosodimethylamine formation during treatment with strong oxidants of dimethylamine containing water, *Water Sci. Technol.*, **2007**, 56, 125–131.
- [61] Choi, J., Valentine, R. L., Formation of *N*-nitrosodimethylamine (NDMA) from reaction of monochloramine: A new disinfection by-product, *Water Res.*, **2002**, 36, 817–824.
- [62] Gerecke, A. C., Sedlak, D. L., Precursors of *N*-nitrosodimethylamine in natural waters, *Environ. Sci. Technol.*, **2003**, 37, 1331–1336.
- [63] Dotson, A., Westerhoff, P., Krasner, S. W., Nitrogen enriched dissolved organic matter (DOM) isolates and their affinity to form emerging disinfection by-products, *Water Sci. Technol.*, **2009**, 60, 135–143.
- [64] Kristiana, I., Tan, J., Joll, C. A., Heitz, A., von Gunten, U., Charrois, J. W., Formation of *N*-nitrosamines from chlorination and chloramination of molecular weight fractions of natural organic matter, *Water Res.*, **2013**, 47, 535–546.
- [65] Fang, J., Yang, X., Ma, J., Shang, C., Zhao, Q., Characterization of algal organic matter and formation of DBPs from chlor(am)ination, *Water Res.*, **2010**, 44, 5897–5906.
- [66] Wert, E. C., Rosario-Ortiz, F. L., Intracellular organic matter from cyanobacteria as a precursor for carbonaceous and nitrogenous disinfection byproducts, *Environ. Sci. Technol.*, **2013**, 47, 6332–6340.



- 
- [67] Selbes, M., Kim, D., Ates, N., Karanfil, T., The roles of tertiary amine structure, background organic matter and chloramine species on NDMA formation, *Water Res.*, **2013**, 47, 945–953.
- [68] Lee, C., Schmidt, C., Yoon, J., von Gunten, U., Oxidation of *N*-nitrosodimethylamine (NDMA) precursors with ozone and chlorine dioxide: Kinetics and effect on NDMA formation potential, *Environ. Sci. Technol.*, **2007**, 41, 2056–2063.
- [69] Padhye, L., Luzinova, Y., Cho, M., Mizaikoff, B., Kim, J. H., Huang, C. H., Poly-DADMAC and dimethylamine as precursors of *N*-nitrosodimethylamine during ozonation: Reaction kinetics and mechanisms, *Environ. Sci. Technol.*, **2011**, 45, 4353–4359.
- [70] Park, S.-H., Wei, S., Mizaikoff, B., Taylor, A. E., Favero, C., Huang, C.-H., Degradation of amine-based water treatment polymers during chloramination as *N*-nitrosodimethylamine (NDMA) precursors, *Environ. Sci. Technol.*, **2009**, 43, 1360–1366.
- [71] Shen, R., Andrews, S. A., NDMA formation kinetics from three pharmaceuticals in four water matrices, *Water Res.*, **2011**, 45, 5687–5694.
- [72] Shen, R., Andrews, S. A., Demonstration of 20 pharmaceuticals and personal care products (PPCPs) as nitrosamine precursors during chloramine disinfection, *Water Res.*, **2011**, 45, 944–952.
- [73] Padhye, L. P., Kim, J.-H., Huang, C.-H., Oxidation of dithiocarbamates to yield *N*-nitrosamines by water disinfection oxidants, *Water Res.*, **2013**, 47, 725–736.
- [74] Xu, B., Qin, C., Hu, C.-Y., Lin, Y.-L., Xia, S.-J., Xu, Q., Mwakagenda, S. A., Bi, X., Gao, N.-Y., Degradation kinetics and *N*-nitrosodimethylamine formation during monochloramination of chlortoluron, *Sci. Total Environ.*, **2012**, 417–418, 241–247.
- [75] Mitch, W. A., Schreiber, I. M., Degradation of tertiary alkylamines during chlorination/chloramination: Implications for formation of aldehydes, nitriles, halo-nitroalkanes, and nitrosamines, *Environ. Sci. Technol.*, **2008**, 42, 4811–4817.
- [76] Le Roux, J., Gallard, H., Croué, J.-P., Chloramination of nitrogenous contaminants (pharmaceuticals and pesticides): NDMA and halogenated DBPs formation, *Water Res.*, **2011**, 45, 3164–3174.
- [77] Shen, R., Andrews, S. A., Formation of NDMA from ranitidine and sumatriptan: The role of pH, *Water Res.*, **2013**, 47, 802–810.
- [78] Kemper, J. M., Walse, S. S., Mitch, W. A., Quaternary amines as nitrosamine precursors: A role for consumer products?, *Environ. Sci. Technol.*, **2010**, 44, 1224–1231.

- [79] Le Roux, J., Gallard, H., Croué, J.-P., Papot, S., Deborde, M., NDMA formation by chloramination of ranitidine: Kinetics and mechanisms, *Environ. Sci. Technol.*, **2012**, 46, 11095–11103.
- [80] Liu, Y. D., Selbes, M., Zeng, C., Zhong, R., Karanfil, T., Formation mechanism of NDMA from ranitidine, trimethylamine, and other tertiary amines during chloramination: A computational study, *Environ. Sci. Technol.*, **2014**, 48, 8653–8663.
- [81] Schmidt, T. C., Zwank, L., Elsner, M., Berg, M., Meckenstock, R. U., Haderlein, S. B., Compound-specific stable isotope analysis of organic contaminants in natural environments: A critical review of the state of the art, prospects, and future challenges, *Anal. Bioanal. Chem.*, **2004**, 378, 283–300.
- [82] Hofstetter, T. B., Schwarzenbach, R. P., Bernasconi, S. M., Assessing transformation processes of organic compounds using stable isotope fractionation, *Environ. Sci. Technol.*, **2008**, 42, 7737–7743.
- [83] Elsner, M., Stable isotope fractionation to investigate natural transformation mechanisms of organic contaminants: Principles, prospects and limitations, *J. Environ. Monit.*, **2010**, 12, 2005–2031.
- [84] Hofstetter, T. B., Berg, M., Assessing transformation processes of organic contaminants by compound-specific stable isotope analyses, *TrAC-Trends Anal. Chem.*, **2011**, 30, 618–627.
- [85] Schmidt, T. C., Jochmann, M. A., Origin and fate of organic compounds in water: Characterization by compound-specific stable isotope analysis, *Annu. Rev. Anal. Chem.*, **2012**, 5, 133–155.
- [86] Jochmann, M. A., Schmidt, T. C., *Compound-specific Stable Isotope Analysis*, The Royal Society of Chemistry, Cambridge, UK, **2012**.
- [87] Sessions, A. L., Isotope-ratio detection for gas chromatography, *J. Sep. Sci.*, **2006**, 29, 1946–1961.
- [88] Philp, R. P., The emergence of stable isotopes in environmental and forensic geochemistry studies: A review, *Environ. Chem. Lett.*, **2007**, 5, 57–66.
- [89] Höhener, P., Aelion, C. M., Fundamentals of environmental isotopes and their use in biodegradation, in *Environmental Isotopes in Biodegradation and Bioremediation*, Aelion, M. C., Höhener, P., Hunkeler, D., Aravena, R., eds., CRC Press, **2010**, 3–22.
- [90] Slater, G. F., Stable isotope forensics-When isotopes work, *Environ. Forensics*, **2003**, 4, 13–23.
- [91] Elsner, M., Zwank, L., Hunkeler, D., Schwarzenbach, R. P., A new concept linking observable stable isotope fractionation to transformation pathways of organic pollutants, *Environ. Sci. Technol.*, **2005**, 39, 6896–6916.



- 
- [92] Pati, S. G., Kohler, H.-P. E., Pabis, A., Paneth, P., Parales, R. E., Hofstetter, T. B., Substrate and enzyme specificity of the kinetic isotope effects associated with the dioxygenation of nitroaromatic contaminants, *Environ. Sci. Technol.*, **2016**, 50, 6708–6716.
- [93] Wijker, R. S., Bolotin, J., Nishino, S. F., Spain, J. C., Hofstetter, T. B., Using compound-specific isotope analysis to assess biodegradation of nitroaromatic explosives in the subsurface, *Environ. Sci. Technol.*, **2013**, 47, 6872–6883.
- [94] Elsner, M., Chartrand, M., Vanstone, N., Couloume, G. L., Sherwood Lollar, B., Identifying abiotic chlorinated ethene degradation: Characteristic isotope patterns in reaction products with nanoscale zero-valent iron, *Environ. Sci. Technol.*, **2008**, 42, 5963–5970.
- [95] Beneteau, K., Aravena, R., Frape, S., Isotopic characterization of chlorinated solvents - Laboratory and field results, *Org. Geochem.*, **1999**, 30, 739–753.
- [96] Sherwood Lollar, B., Slater, G. F., Sleep, B., Witt, M., Klecka, G. M., Harkness, M., Spivack, J., Stable carbon isotope evidence for intrinsic bioremediation of tetrachloroethene and trichloroethene at Area 6, Dover Air Force Base, *Environ. Sci. Technol.*, **2001**, 35, 261–269.
- [97] Blessing, M., Schmidt, T. C., Dinkel, R., Haderlein, S. B., Delineation of multiple chlorinated ethene sources in an industrialized area - A forensic field study using compound-specific isotope analysis, *Environ. Sci. Technol.*, **2009**, 43, 2701–2707.
- [98] Hunkeler, D., Andersen, N., Aravena, R., Bernasconi, S. M., Butler, B. J., Hydrogen and carbon isotope fractionation during aerobic biodegradation of benzenes, *Environ. Sci. Technol.*, **2001**, 35, 3462–3467.
- [99] Mancini, S. A., Devine, C. E., Elsner, M., Nandi, M. E., Ulrich, A. C., Edwards, E. A., Sherwood Lollar, B., Isotopic evidence suggests different initial reaction mechanisms for anaerobic benzene biodegradation, *Environ. Sci. Technol.*, **2008**, 42, 8290–8296.
- [100] Morasch, B., Richnow, H. H., Schink, B., Meckenstock, R. U., Stable hydrogen and carbon isotope fractionation during microbial toluene degradation: Mechanistic and environmental aspects, *Appl. Environ. Microbiol.*, **2001**, 67, 4842–4849.
- [101] Ahad, J. M. E., Sherwood Lollar, B., Edwards, E. A., Slater, G. F., Sleep, B. E., Carbon isotope fractionation during anaerobic biodegradation of toluene: Implications for intrinsic bioremediation, *Environ. Sci. Technol.*, **2000**, 34, 892–896.
- [102] McKelvie, J. R., Lindstrom, J. E., Beller, H. R., Richmond, S. A., Sherwood Lollar, B., Analysis of anaerobic BTX biodegradation in a subarctic aquifer using isotopes and benzylsuccinates, *J. Contam. Hydrol.*, **2005**, 81, 167–186.

- [103] Elsner, M., McKelvie, J., Lacrampe-Couloume, G., Sherwood Lollar, B., Insight into methyl *tert*-butyl ether (MTBE) stable isotope fractionation from abiotic reference experiments, *Environ. Sci. Technol.*, **2007**, 41, 5693–5700.
- [104] Kujawinski, D. M., Stephan, M., Jochmann, M. A., Krajenke, K., Haas, J., Schmidt, T. C., Stable carbon and hydrogen isotope analysis of methyl *tert*-butyl ether and *tert*-amyl methyl ether by purge and trap-gas chromatography-isotope ratio mass spectrometry: Method evaluation and application, *J. Environ. Monit.*, **2010**, 12, 347–354.
- [105] Berg, M., Bolotin, J., Hofstetter, T. B., Compound-specific nitrogen and carbon isotope analysis of nitroaromatic compounds in aqueous samples using solid-phase microextraction coupled to GC/IRMS, *Anal. Chem.*, **2007**, 79, 2386–2393.
- [106] Pati, S. G., Shin, K., Skarpeli-Liati, M., Bolotin, J., Eustis, S. N., Spain, J. C., Hofstetter, T. B., Carbon and nitrogen isotope effects associated with the dioxygenation of aniline and diphenylamine, *Environ. Sci. Technol.*, **2012**, 46, 11844–11853.
- [107] Kujawinski, D. M., Zhang, L., Schmidt, T. C., Jochmann, M. A., When other separation techniques fail: Compound-specific carbon isotope ratio analysis of sulfonamide containing pharmaceuticals by high-temperature-liquid chromatography-isotope ratio mass spectrometry, *Anal. Chem.*, **2012**, 84, 7656–7663.
- [108] Maier, M. P., De Corte, S., Nitsche, S., Spaett, T., Boon, N., Elsner, M., C & N isotope analysis of diclofenac to distinguish oxidative and reductive transformation and to track commercial products, *Environ. Sci. Technol.*, **2014**, 48, 2312–2320.
- [109] Kujawinski, D. M., Wolbert, J. B., Zhang, L., Jochmann, M. A., Widory, D., Baran, N., Schmidt, T. C., Carbon isotope ratio measurements of glyphosate and AMPA by liquid chromatography coupled to isotope ratio mass spectrometry, *Anal. Bioanal. Chem.*, **2013**, 405, 2869–2878.
- [110] Maier, M. P., Qiu, S., Elsner, M., Enantioselective stable isotope analysis (ESIA) of polar herbicides, *Anal. Bioanal. Chem.*, **2013**, 405, 2825–2831.
- [111] Spahr, S., Huntscha, S., Bolotin, J., Maier, M. P., Elsner, M., Hollender, J., Hofstetter, T. B., Compound-specific isotope analysis of benzotriazole and its derivatives, *Anal. Bioanal. Chem.*, **2013**, 405, 2843–2856.
- [112] Huntscha, S., Hofstetter, T. B., Schymanski, E. L., Spahr, S., Hollender, J., Bio-transformation of benzotriazoles: Insights from transformation product identification and compound-specific isotope analysis, *Environ. Sci. Technol.*, **2014**, 48, 4435–4443.
- [113] Arnold, W. A., Bolotin, J., von Gunten, U., Hofstetter, T. B., Evaluation of functional groups responsible for chloroform formation during water chlorination

- using compound specific isotope analysis, *Environ. Sci. Technol.*, **2008**, 42, 7778–7785.
- [114] Dai, N., Mitch, W. A., Relative importance of *N*-nitrosodimethylamine compared to total *N*-nitrosamines in drinking waters, *Environ. Sci. Technol.*, **2013**, 47, 3648–3656.
- [115] Russell, C. G., Blute, N. K., Via, S., Wu, X., Chowdhury, Z., Nationwide assessment of nitrosamine occurrence and trends, *J. Am. Water Works Ass.*, **2012**, 104, 205–217.
- [116] California Department of Public Health. Drinking Water Notification Levels and Response Levels: An Overview, <http://www.cdph.ca.gov/certlic/drinkingwater/documents/notificationlevels/\notificationlevels.pdf> (accessed June 28, 2016).
- [117] Health Canada. Guidelines for Canadian Drinking Water Quality: Guideline Technical Document *N*-Nitrosodimethylamine (NDMA), [www.hc-sc.gc.ca/ewh-semt/pubs/water-eau/ndma/index-eng.php](http://www.hc-sc.gc.ca/ewh-semt/pubs/water-eau/ndma/index-eng.php) (accessed June 28, 2016).
- [118] Sharma, V. K., Kinetics and mechanism of formation and destruction of *N*-nitrosodimethylamine in water - A review, *Sep. Purif. Technol.*, **2012**, 88, 1–10.
- [119] Chen, Z., Valentine, R. L., Formation of *N*-nitrosodimethylamine (NDMA) from humic substances in natural water., *Environ. Sci. Technol.*, **2007**, 41, 6059–6065.
- [120] Chen, W.-H., Young, T. M., NDMA formation during chlorination and chloramination of aqueous diuron solutions, *Environ. Sci. Technol.*, **2008**, 42, 1072–1077.
- [121] Dai, N., Mitch, W. A., Influence of amine structural characteristics on *N*-nitrosamine formation potential relevant to postcombustion CO<sub>2</sub> capture systems, *Environ. Sci. Technol.*, **2013**, 47, 13175–13183.
- [122] Goldman, M. J., Fine, N. A., Rochelle, G. T., Kinetics of *N*-nitrosopiperazine formation from nitrite and piperazine in CO<sub>2</sub> capture, *Environ. Sci. Technol.*, **2013**, 47, 3528–3534.
- [123] Le Roux, J., Gallard, H., Croué, J.-P., Formation of NDMA and halogenated DBPs by chloramination of tertiary amines: The influence of bromide ion, *Environ. Sci. Technol.*, **2012**, 46, 1581–1589.
- [124] Shen, R., Andrews, S. A., NDMA formation from amine-based pharmaceuticals - Impact from prechlorination and water matrix, *Water Res.*, **2013**, 47, 2446–2457.
- [125] Elsner, M., Jochmann, M. A., Hofstetter, T. B., Hunkeler, D., Bernstein, A., Schmidt, T. C., Schimmelpfennig, A., Current challenges in compound-specific stable isotope analysis of environmental organic contaminants, *Anal. Bioanal. Chem.*, **2012**, 403, 2471–2491.

- [126] Hunkeler, D., Laier, T., Breider, F., Jacobsen, O. S., Demonstrating a natural origin of chloroform in groundwater using stable carbon isotopes, *Environ. Sci. Technol.*, **2012**, 46, 6096–6101.
- [127] Breider, F., Albers, C. N., Hunkeler, D., Assessing the role of trichloroacetyl-containing compounds in the natural formation of chloroform using stable carbon isotopes analysis, *Chemosphere*, **2013**, 90, 441–448.
- [128] Breider, F., Hunkeler, D., Mechanistic insights into the formation of chloroform from natural organic matter using stable carbon isotope analysis, *Geochim. Cosmochim. Acta*, **2014**, 125, 85–95.
- [129] Breider, F., Hunkeler, D., Investigating chloroperoxidase-catalyzed formation of chloroform from humic substances using stable chlorine isotope analysis, *Environ. Sci. Technol.*, **2014**, 48, 1592–1600.
- [130] Skarpeli-Liati, M., Arnold, W. A., Turgeon, A., Cramer, C. J., Hofstetter, T. B., pH-Dependent equilibrium isotope fractionation associated with compound-specific nitrogen and carbon isotope analysis by SPME-GC/IRMS, *Anal. Chem.*, **2011**, 83, 1641–1648.
- [131] Penning, H., Elsner, M., Intramolecular carbon and nitrogen isotope analysis by quantitative dry fragmentation of the phenylurea herbicide isoproturon in a combined injector/capillary reactor prior to GC separation, *Anal. Chem.*, **2007**, 79, 8399–8405.
- [132] Meyer, A. H., Penning, H., Lowag, H., Elsner, M., Precise and accurate compound specific carbon and nitrogen isotope analysis of atrazine: Critical role of combustion oven conditions, *Environ. Sci. Technol.*, **2008**, 42, 7757–7763.
- [133] Batt, A. L., Kostich, M. S., Lazorchak, J. M., Analysis of ecologically relevant pharmaceuticals in wastewater and surface water using selective solid-phase extraction and UPLC-MS/MS, *Anal. Chem.*, **2008**, 80, 5021–5030.
- [134] Petrie, B., Barden, R., Kasprzyk-Hordern, B., A review on emerging contaminants in wastewaters and the environment: Current knowledge, understudied areas and recommendations for future monitoring, *Water Res.*, **2015**, 72, 3–27.
- [135] Yoon, S., Nakada, N., Tanaka, H., A new method for quantifying *N*-nitrosamines in wastewater samples by gas chromatography-triple quadrupole mass spectrometry, *Talanta*, **2012**, 97, 256–261.
- [136] Krauss, M., Hollender, J., Analysis of nitrosamines in wastewater: Exploring the trace level quantification capabilities of a hybrid linear ion trap/orbitrap mass spectrometer, *Anal. Chem.*, **2008**, 80, 834–842.

- 
- [137] Soltermann, F., Lee, M., Canonica, S., von Gunten, U., Enhanced *N*-nitrosamine formation in pool water by UV irradiation of chlorinated secondary amines in the presence of monochloramine, *Water Res.*, **2013**, 47, 79–90.
- [138] Valentine, R. L., Brandt, K. I., Jafvert, C. T., A spectrophotometric study of the formation of an unidentified monochloramine decomposition product, *Water Res.*, **1986**, 20, 1067–1074.
- [139] Pinkernell, U., Nowack, B., Gallard, H., von Gunten, U., Methods for the photometric determination of reactive bromine and chlorine species with ABTS, *Water Res.*, **2000**, 34, 4343–4350.
- [140] Coplen, T. B., Guidelines and recommended terms for expression of stable-isotope-ratio and gas-ratio measurement results, *Rapid Commun. Mass Spectrom.*, **2011**, 25, 2538–2560.
- [141] Jochmann, M. A., Blessing, M., Haderlein, S. B., Schmidt, T. C., A new approach to determine method detection limits for compound-specific isotope analysis of volatile organic compounds, *Rapid Commun. Mass Spectrom.*, **2006**, 20, 3639–3648.
- [142] Sherwood Lollar, B., Hirschorn, S. K., Chartrand, M. M. G., Lacrampe-Couloume, G., An approach for assessing total instrumental uncertainty in compound-specific carbon isotope analysis: Implications for environmental remediation studies, *Anal. Chem.*, **2007**, 79, 3469–3475.
- [143] Ogrinc, N., Košir, I., Spangenberg, J., Kidrič, J., The application of NMR and MS methods for detection of adulteration of wine, fruit juices, and olive oil. A review, *Anal. Bioanal. Chem.*, **2003**, 376, 424–430.
- [144] Greule, M., Tumino, L. D., Kronewald, T., Hener, U., Schleucher, J., Mosandl, A., Keppler, F., Improved rapid authentication of vanillin using  $\delta^{13}\text{C}$  and  $\delta^2\text{H}$  values, *Eur. Food Res. Technol.*, **2010**, 231, 933–941.
- [145] Vetter, W., Armbruster, W., Betson, T. R., Schleucher, J., Kapp, T., Lehnert, K., Baseline isotopic data of polyhalogenated compounds, *Anal. Chim. Acta*, **2006**, 577, 250–256.
- [146] McKelvie, J. R., Elsner, M., Simpson, A. J., Sherwood Lollar, B., Simpson, M. J., Quantitative site-specific  $^2\text{H}$  NMR investigation of MTBE: Potential for assessing contaminant sources and fate, *Environ. Sci. Technol.*, **2010**, 44, 1062–1068.
- [147] Hartenbach, A., Hofstetter, T. B., Aeschbacher, M., Sander, M., Kim, D., Strathmann, T. J., Arnold, W. A., Cramer, C. J., Schwarzenbach, R. P., Variability of nitrogen isotope fractionation during the reduction of nitroaromatic compounds with dissolved reductants, *Environ. Sci. Technol.*, **2008**, 42, 8352–8359.

- [148] Skarpeli-Liati, M., Pati, S. G., Bolotin, J., Eustis, S. N., Hofstetter, T. B., Carbon, hydrogen, and nitrogen isotope fractionation associated with oxidative transformation of substituted aromatic *N*-alkyl amines, *Environ. Sci. Technol.*, **2012**, 46, 7189–7198.
- [149] Tobler, N. B., Hofstetter, T. B., Schwarzenbach, R. P., Assessing iron-mediated oxidation of toluene and reduction of nitroaromatic contaminants in anoxic environments using compound-specific isotope analysis, *Environ. Sci. Technol.*, **2007**, 41, 7773–7780.
- [150] Hartenbach, A. E., Hofstetter, T. B., Tentscher, P. R., Canonica, S., Berg, M., Schwarzenbach, R. P., Carbon, hydrogen, and nitrogen isotope fractionation during light-induced transformations of atrazine, *Environ. Sci. Technol.*, **2008**, 42, 7751–7756.
- [151] Meyer, A. H., Elsner, M.,  $^{13}\text{C}/^{12}\text{C}$  and  $^{15}\text{N}/^{14}\text{N}$  isotope analysis to characterize degradation of atrazine: Evidence from parent and daughter compound values, *Environ. Sci. Technol.*, **2013**, 47, 6884–6891.
- [152] Reinicke, S., Simonsen, A., Sørensen, S. R., Aamand, J., Elsner, M., C and N isotope fractionation during biodegradation of the pesticide metabolite 2,6-dichlorobenzamide (BAM): Potential for environmental assessments, *Environ. Sci. Technol.*, **2012**, 46, 1447–1454.
- [153] Schreglmann, K., Hoeche, M., Steinbeiss, S., Reinicke, S., Elsner, M., Carbon and nitrogen isotope analysis of atrazine and desethylatrazine at sub-microgram per liter concentrations in groundwater, *Anal. Bioanal. Chem.*, **2013**, 405, 2857–2867.
- [154] Mitch, W. A., Sedlak, D. L., Factors controlling nitrosamine formation during wastewater chlorination, *Water Sci. Technol.*, **2002**, 2, 191–198.
- [155] Zimmermann, S. G., Wittenwiler, M., Hollender, J., Krauss, M., Ort, C., Siegrist, H., von Gunten, U., Kinetic assessment and modeling of an ozonation step for full-scale municipal wastewater treatment: Micropollutant oxidation, by-product formation and disinfection, *Water Res.*, **2011**, 45, 605–617.
- [156] Oya, M., Kosaka, K., Asami, M., Kunikane, S., Formation of *N*-nitrosodimethylamine (NDMA) by ozonation of dyes and related compounds, *Chemosphere*, **2008**, 73, 1724–1730.
- [157] Chen, Z., Valentine, R. L., The influence of the pre-oxidation of natural organic matter on the formation of *N*-nitrosodimethylamine (NDMA), *Environ. Sci. Technol.*, **2008**, 42, 5062–5067.
- [158] Selbes, M., Kim, D., Karanfil, T., The effect of pre-oxidation on NDMA formation and the influence of pH, *Water Res.*, **2014**, 66, 169–179.



- [159] McCurry, D. L., Krasner, S. W., von Gunten, U., Mitch, W. A., Determinants of disinfectant pretreatment efficacy for nitrosamine control in chloraminated drinking water, *Water Res.*, **2015**, 84, 161–170.
- [160] Shah, A. D., Krasner, S. W., Lee, C. F. T., von Gunten, U., Mitch, W. A., Trade-offs in disinfection byproduct formation associated with precursor preoxidation for control of *N*-nitrosodimethylamine formation, *Environ. Sci. Technol.*, **2012**, 46, 4809–4818.
- [161] Krasner, S. W., Lee, C. F. T., Mitch, W. A., von Gunten, U., *Development of a Bench-Scale Test to Predict the Formation of Nitrosamines*, Water Research Foundation, Denver, **2012**.
- [162] Spahr, S., Bolotin, J., Schleucher, J., Ehlers, I., von Gunten, U., Hofstetter, T. B., Compound-specific carbon, nitrogen, and hydrogen isotope analysis of *N*-nitrosodimethylamine in aqueous solutions, *Anal. Chem.*, **2015**, 87, 2916–2924.
- [163] Taube, H., Mechanisms of oxidation with oxygen, *J. Gen. Physiol.*, **1965**, 49, 29–50.
- [164] Valentine, J. S., Foote, C. S., Greenberg, A., Liebman, J. F., *Active Oxygen in Biochemistry*, SEARCH Series, Volume 3, Springer Netherlands, **1995**.
- [165] Foote, C. S., Valentine, J. S., Greenberg, A., Liebman, J. F., *Active Oxygen in Chemistry*, SEARCH Series, Volume 2, Springer Netherlands, **1995**.
- [166] Kearns, D. R., Physical and chemical properties of singlet molecular oxygen, *Chem. Rev.*, **1971**, 71, 395–427.
- [167] Valentine, J. S., Dioxygen reactions, in *Bioinorganic Chemistry*, Bertini, I., Gray, H. B., Lippard, S. J., Valentine, J. S., eds., University Science Books, Mill Valley, California, **1994**, 253–314.
- [168] Armstrong, D. A., Huie, R. E., Koppenol, W. H., Lyman, S. V., Merényi, G., Neta, P., Ruscic, B., Stanbury, D. M., Steenken, S., Wardman, P., Standard electrode potentials involving radicals in aqueous solution: Inorganic radicals (IUPAC Technical Report), *Pure Appl. Chem.*, **2015**, 87, 1139–1150.
- [169] Schreiber, I. M., Mitch, W. A., Enhanced nitrogenous disinfection byproduct formation near the breakpoint: Implications for nitrification control, *Environ. Sci. Technol.*, **2007**, 41, 7039–7046.
- [170] Tian, G., Klinman, J. P., Discrimination between  $^{16}\text{O}$  and  $^{18}\text{O}$  in oxygen binding to the reversible oxygen carriers hemoglobin, myoglobin, hemerythrin, and hemocyanin: A new probe for oxygen binding and reductive activation by proteins, *J. Am. Chem. Soc.*, **1993**, 115, 8891–8897.

- [171] Roth, J. P., Klinman, J. P., Oxygen-18 isotope effects as a probe of enzymatic activation of molecular oxygen, in *Isotope Effects in Chemistry and Biology*, Kohen, A., Limbach, H.-H., eds., New York: CRC Press / Taylor & Francis, **2006**, 645–669.
- [172] Ashley, D. C., Brinkley, D. W., Roth, J. P., Oxygen isotope effects as structural and mechanistic probes in inorganic oxidation chemistry, *Inorg. Chem.*, **2010**, 49, 3661–3675.
- [173] Roth, J. P., Oxygen isotope effects as probes of electron transfer mechanisms and structures of activated O<sub>2</sub>, *Acc. Chem. Res.*, **2009**, 42, 399–408.
- [174] Pati, S. G., Bolotin, J., Brennwald, M. S., Kohler, H.-P. E., Werner, R. A., Hofstetter, T. B., Measurement of oxygen isotope ratios (<sup>18</sup>O/<sup>16</sup>O) of aqueous O<sub>2</sub> in small samples by gas chromatography isotope ratio mass spectrometry (GC/IRMS), *Rapid Commun. Mass Spectrom.*, **2016**, 30, 684–690.
- [175] Gulde, R., Meier, U., Schymanski, E. L., Kohler, H.-P. E., Helbling, D. E., Derrer, S., Rentsch, D., Fenner, K., Systematic exploration of biotransformation reactions of amine-containing micropollutants in activated sludge, *Environ. Sci. Technol.*, **2016**, 50, 2908–2920.
- [176] Eaton, A. D., Clesceri, L. S., Rice, E. W., Greenberg, A. E., *Standard Methods for the Examination of Water and Wastewater*, 21 ed., American Public Health Association, American Water Works Association, and Water Environment Federation, **2005**.
- [177] Harp, D. L., Specific determination of inorganic monochloramine in chlorinated wastewaters, *Water Environ. Res.*, **2000**, 72, 706–713.
- [178] Soltermann, F., Widler, T., Canonica, S., von Gunten, U., Comparison of a novel extraction-based colorimetric (ABTS) method with membrane introduction mass spectrometry (MIMS): Trichloramine dynamics in pool waters, *Water Res.*, **2014**, 58, 258–268.
- [179] Francisco, W. A., Tian, G., Fitzpatrick, P. F., Klinman, J. P., Oxygen-18 kinetic isotope effect studies of the tyrosine hydroxylase reaction: Evidence of rate limiting oxygen activation, *J. Am. Chem. Soc.*, **1998**, 120, 4057–4062.
- [180] Lanci, M. P., Roth, J. P., Oxygen isotope effects upon reversible O<sub>2</sub>-binding reactions: Characterizing mononuclear superoxide and peroxide structures, *J. Am. Chem. Soc.*, **2006**, 128, 16006–16007.
- [181] Roth, J. P., Advances in studying bioinorganic reaction mechanisms: Isotopic probes of activated oxygen intermediates in metalloenzymes, *Curr. Opin. Chem. Biol.*, **2007**, 11, 142–150.



- [182] Stahl, S. S., Francisco, W. A., Merckx, M., Klinman, J. P., Lippard, S. J., Oxygen kinetic isotope effects in soluble methane monooxygenase, *J. Biol. Chem.*, **2001**, 276, 4549–4553.
- [183] Mirica, L. M., McCusker, K. P., Munos, J. W., Liu, H., Klinman, J. P.,  $^{18}\text{O}$  kinetic isotope effects in non-heme iron enzymes: Probing the nature of Fe/O<sub>2</sub> intermediates, *J. Am. Chem. Soc.*, **2008**, 130, 8122–8123.
- [184] Elovitz, M. S., von Gunten, U., Hydroxyl radical/ozone ratios during ozonation processes. I. The R<sub>ct</sub> concept, *Ozone-Sci. Eng.*, **1999**, 21, 239–260.
- [185] Poskrebyshev, G. A., Huie, R. E., Neta, P., Radiolytic reactions of monochloramine in aqueous solutions, *J. Phys. Chem. A*, **2003**, 107, 7423–7428.
- [186] Bartosz, G., Janaszewska, A., Ertel, D., Bartosz, M., Simple determination of peroxy radical-trapping capacity, *Biochem. Mol. Biol. Int.*, **1998**, 46, 519–528.
- [187] Goldstein, S., Czapski, G., Kinetics of nitric-oxide autoxidation in aqueous solution in the absence and presence of various reductants. The nature of the oxidizing intermediates, *J. Am. Chem. Soc.*, **1995**, 117, 12078–12084.
- [188] Neta, P., Huie, R. E., Ross, A. B., Rate constants for reactions of peroxy radicals in fluid solutions, *J. Phys. Chem. Ref. Data*, **1990**, 19, 413–513.
- [189] Elia, P., Azoulay, A., Zeiri, Y., On the efficiency of water soluble antioxidants, *Ultrason. Sonochem.*, **2012**, 19, 314–324.
- [190] Priyadarsini, K. I., Kapoor, S., Naik, D. B., One- and two-electron oxidation reactions of trolox by peroxynitrite, *Chem. Res. Toxicol.*, **2001**, 14, 567–571.
- [191] Alberto, M. E., Russo, N., Grand, A., Galano, A., A physicochemical examination of the free radical scavenging activity of Trolox: Mechanism, kinetics and influence of the environment, *Phys. Chem. Chem. Phys.*, **2013**, 15, 4642–4650.
- [192] Bisby, R. H., Morgan, C. G., Hamblett, I., Gorman, A. A., Quenching of singlet oxygen by Trolox C, ascorbate, and amino acids: Effects of pH and temperature, *J. Phys. Chem. A*, **1999**, 103, 7454–7459.
- [193] Pattison, D. I., Davies, M. J., Asmus, K.-D., Absolute rate constants for the formation of nitrogen-centred radicals from chloramines/amides and their reactions with antioxidants, *J. Chem. Soc., Perkin Trans. 2*, **2002**, 1461–1467.
- [194] Aliaga, C., Lissi, E., Augusto, O., Linares, E., Kinetics and mechanism of the reaction of a nitroxide radical (Tempol) with a phenolic antioxidant, *Free Radical Res.*, **2003**, 37, 225–230.
- [195] Vikesland, P. J., Valentine, R. L., Modeling the kinetics of ferrous iron oxidation by monochloramine, *Environ. Sci. Technol.*, **2002**, 36, 662–668.

- [196] Vikesland, P. J., Valentine, R. L., Reaction pathways involved in the reduction of monochloramine by ferrous iron, *Environ. Sci. Technol.*, **2000**, 34, 83–90.
- [197] Heasley, V. L., Fisher, A. M., Herman, E. E., Jacobsen, F. E., Miller, E. W., Ramirez, A. M., Royer, N. R., Whisenand, J. M., Zoetewey, D. L., Shellhamer, D. F., Investigations of the reactions of monochloramine and dichloramine with selected phenols: Examination of humic acid models and water contaminants, *Environ. Sci. Technol.*, **2004**, 38, 5022–5029.
- [198] Kalyanaraman, B., Sohnle, P. G., Generation of free radical intermediates from foreign compounds by neutrophil-derived oxidants., *J. Clin. Invest.*, **1985**, 75, 1618–1622.
- [199] Hawkins, C. L., Davies, J. M., Reaction of HOCl with amino acids and peptides: EPR evidence for rapid rearrangement and fragmentation reactions of nitrogen-centred radicals, *J. Chem. Soc., Perkin Trans. 2*, **1998**, 1937–1946.
- [200] Clarke, K., Edge, R., Johnson, V., Land, E. J., Navaratnam, S., Truscott, T. G., Direct observation of  $\bullet\text{NH}_2$  reactions with oxygen, amino acids, and melanins, *J. Phys. Chem. A*, **2008**, 112, 1234–1237.
- [201] Crowley, J. N., Sodeau, J. R., Reaction between the amidogen radical,  $\bullet\text{NH}_2$ , and molecular-oxygen in low-temperature matrices, *J. Phys. Chem.*, **1989**, 93, 4785–4790.
- [202] Fautitano, A., Buttafava, A., Martinotti, F., Bortolus, P., First electron spin resonance identification of a nitrogen peroxy radical as intermediate in the photo-oxidation of 2,2,6,6-tetramethylpiperidine derivatives, *J. Phys. Chem.*, **1984**, 88, 1187–1190.
- [203] Bennett, J. E., Summers, R., Product studies of mutual termination reactions of *sec*-alkylperoxy radicals: Evidence for non-cyclic termination, *Can. J. Chem.*, **1974**, 52, 1377–1379.
- [204] Russell, G. A., Deuterium-isotope effects in the autoxidation of aralkyl hydrocarbons: Mechanism of the interaction of peroxy radicals, *J. Am. Chem. Soc.*, **1957**, 79, 3871–3877.
- [205] McKay, G., Sjelín, B., Chagnon, M., Ishida, K. P., Mezyk, S. P., Kinetic study of the reactions between chloramine disinfectants and hydrogen peroxide: Temperature dependence and reaction mechanism, *Chemosphere*, **2013**, 92, 1417–1422.
- [206] Li, J., Blatchley III, E. R., UV photodegradation of inorganic chloramines, *Environ. Sci. Technol.*, **2009**, 43, 60–65.
- [207] Chimi, H., Cillard, J., Cillard, P., Rahmani, M., Peroxyl and hydroxyl radical scavenging activity of some natural phenolic antioxidants, *J. Am. Oil Chem. Soc.*, **1991**, 68, 307–312.

- [208] Nimse, S. B., Pal, D., Free radicals, natural antioxidants, and their reaction mechanisms, *RSC Adv.*, **2015**, 5, 27986–28006.
- [209] Nöthe, T., Fahlenkamp, H., von Sonntag, C., Ozonation of wastewater: Rate of ozone consumption and hydroxyl radical yield, *Environ. Sci. Technol.*, **2009**, 43, 5990–5995.
- [210] Flyunt, R., Leitzke, A., Mark, G., Mvula, E., Reisz, E., Schick, R., von Sonntag, C., Determination of  $\bullet\text{OH}$ ,  $\text{O}_2^{\bullet-}$ , and hydroperoxide yields in ozone reactions in aqueous solution, *J. Phys. Chem. B*, **2003**, 107, 7242–7253.
- [211] Lee, Y., Gerrity, D., Lee, M., Bogeat, A. E., Salhi, E., Gamage, S., Trenholm, R. A., Wert, E. C., Snyder, S. A., von Gunten, U., Prediction of micropollutant elimination during ozonation of municipal wastewater effluents: Use of kinetic and water specific information, *Environ. Sci. Technol.*, **2013**, 47, 5872–5881.
- [212] Hanigan, D., Zhang, J., Herckes, P., Krasner, S. W., Chen, C., Westerhoff, P., Adsorption of *N*-nitrosodimethylamine precursors by powdered and granular activated carbon, *Environ. Sci. Technol.*, **2012**, 46, 12630–12639.
- [213] Soulard, M., Bloc, F., Hatterer, A., Diagrams of existence of chloramines and bromamines in aqueous solution, *J. Chem. Soc. Dalton*, **1981**, 2300–2310.
- [214] Buck, S., Stein, K., Schwedt, G., Use of a peroxidase reactor in flow injection analysis for the determination of chloramine and the inhibition kinetics, *Anal. Chim. Acta*, **1999**, 390, 141–146.
- [215] Woods, G. C., Dickenson, E. R. V., Evaluation of final UCMR2 database: Nationwide trend in NDMA, *J. Am. Water Works Ass.*, **2015**, 107, E58–E68.
- [216] Hunkeler, D., Elsner, M., Principles and mechanisms of isotope fractionation, in *Environmental Isotopes in Biodegradation and Bioremediation*, Aelion, M. C., Höhener, P., Hunkeler, D., Aravena, R., eds., CRC Press, **2010**, 23–42.
- [217] Spahr, S., Cirpka, O. A., von Gunten, U., Hofstetter, T. B., Formation of *N*-nitrosodimethylamine during chloramination of secondary and tertiary amines: Role of molecular oxygen and radical intermediates, **2016**, submitted to *Environ. Sci. Technol.*
- [218] Böhlke, J. K., Gwinn, C. J., Coplen, T. B., New reference materials for nitrogen-isotope-ratio measurements, *Geostandard Newslett.*, **1993**, 17, 159–164.
- [219] Schimmelmann, A., Albertino, A., Sauer, P. E., Qi, H., Molinie, R., Mesnard, F., Nicotine, acetanilide and urea multi-level  $^2\text{H}$ -,  $^{13}\text{C}$ - and  $^{15}\text{N}$ -abundance reference materials for continuous-flow isotope ratio mass spectrometry, *Rapid Commun. Mass Spectrom.*, **2009**, 23, 3513–3521.

- [220] Schimmelmann, A., Lewan, M. D., Wintsch, R. P., D/H isotope ratios of kerogen, bitumen, oil, and water in hydrous pyrolysis of source rocks containing kerogen types I, II, IIS, and III, *Geochim. Cosmochim. Acta*, **1999**, 63, 3751–3766.
- [221] Skarpeli-Liati, M., Jiskra, M., Turgeon, A., Garr, A. N., Arnold, W. A., Cramer, C. J., Schwarzenbach, R. P., Hofstetter, T. B., Using nitrogen isotope fractionation to assess the oxidation of substituted anilines by manganese oxide, *Environ. Sci. Technol.*, **2011**, 45, 5596–5604.
- [222] Rosenblatt, D. H., Hull, L. A., Luca, D. C. D., Davis, G. T., Weglein, R. C., Williams, H. K. R., Oxidations of amines. II. Substituent effects in chlorine dioxide oxidations, *J. Am. Chem. Soc.*, **1967**, 89, 1158–1163.
- [223] Wijker, R. S., Adamczyk, P., Bolotin, J., Paneth, P., Hofstetter, T. B., Isotopic analysis of oxidative pollutant degradation pathways exhibiting large H isotope fractionation, *Environ. Sci. Technol.*, **2013**, 47, 13459–13468.
- [224] Rishavy, M. A., Cleland, W. W.,  $^{13}\text{C}$ ,  $^{15}\text{N}$ , and  $^{18}\text{O}$  equilibrium isotope effects and fractionation factors, *Can. J. Chem.*, **1999**, 77, 967–977.
- [225] Tanaka, N., Hosoya, K., Nomura, K., Yoshimura, T., Ohki, T., Yamaoka, R., Kimata, K., Araki, M., Separation of nitrogen and oxygen isotopes by liquid chromatography, *Nature*, **1989**, 341, 727–728.
- [226] Marlier, J. F., Haptonstall, B. A., Johnson, A. J., Sacksteder, K. A., Heavy-atom isotope effects on the hydrazinolysis of methyl formate, *J. Am. Chem. Soc.*, **1997**, 119, 8838–8842.
- [227] Marlier, J. F., Cleland, W. W., Multiple isotope effect study of the hydrolysis of formamide by urease from Jack Bean (*Canavalia ensiformis*), *Biochemistry*, **2006**, 45, 9940–9948.
- [228] Cetó, X., Saint, C. P., Chow, C. W., Voelcker, N. H., Prieto-Simón, B., Electrochemical detection of *N*-nitrosodimethylamine using a molecular imprinted polymer, *Sens. Actuator B-Chem.*, **2016**, 237, 613–620.
- [229] Xia, Y., McGuffey, J. E., Bhattacharyya, S., Selligren, B., Yilmaz, E., Wang, L., Bernert, J. T., Analysis of the tobacco-specific nitrosamine 4-(methylnitrosamino)-1-(3-pyridyl)-1-butanol in urine by extraction on a molecularly imprinted polymer column and liquid chromatography/atmospheric pressure ionization tandem mass spectrometry, *Anal. Chem.*, **2005**, 77, 7639–7645.
- [230] Richardson, S. D., Fasano, F., Ellington, J. J., Crumley, F. G., Buettner, K. M., Evans, J. J., Blount, B. C., Silva, L. K., Waite, T. J., Luther, G. W., McKague, A. B., Miltner, R. J., Wagner, E. D., Plewa, M. J., Occurrence and mammalian cell toxicity of iodinated disinfection byproducts in drinking water, *Environ. Sci. Technol.*, **2008**, 42, 8330–8338.

- [231] Plewa, M. J., Muellner, M. G., Richardson, S. D., Fasano, F., Buettner, K. M., Woo, Y.-T., McKague, A. B., Wagner, E. D., Occurrence, synthesis, and mammalian cell cytotoxicity and genotoxicity of haloacetamides: An emerging class of nitrogenous drinking water disinfection byproducts, *Environ. Sci. Technol.*, **2008**, 42, 955–961.



# Curriculum Vitae

**Stephanie Spahr**

Born July 28, 1987 in Ulm, Germany

- 2012 – 2016    **Doctoral Studies in Environmental Chemistry**  
School of Architecture, Civil and Environmental Engineering,  
Swiss Federal Institute of Technology, Lausanne (EPFL, Switzerland)  
&  
Department of Environmental Chemistry,  
Swiss Federal Institute of Aquatic Science and Technology  
(Eawag Dübendorf, Switzerland)
- 2010 – 2012    **Master of Science in Geoecology**  
University of Tübingen, Germany  
Master thesis: "*Carbon and Nitrogen Isotope Analysis of  
Benzotriazoles*" conducted at Eawag Dübendorf, Switzerland
- 2007 – 2010    **Bachelor of Science in Geoecology/Ecosystem Management**  
University of Tübingen, Germany
- 1997 – 2006    **Gymnasium** in Neu-Ulm, Germany
- 1993 – 1997    **Primary school** in Nersingen, Germany